



***Thermophysical Behaviour and
Applications of Crosslinked
Poly(Ionic Liquid)s***

Alexandru Tudor, M. Sc.

Submitted for the degree of Doctor of Philosophy

Principal Supervisors: Professor Dermot Diamond¹
Dr. Larisa Florea¹
Secondary Supervisor: Dr. Aoife Morrin¹

¹Insight Centre for Data Analytics, National Centre for Science Research, School of Chemical Sciences, Dublin City University, Dublin, Ireland

Dublin City University

August 2017

Declaration

I hereby certify that this material, which I now submit for assessment on the programme of study leading to the award of doctor of philosophy is entirely my own work, and that I have exercised reasonable care to ensure that the work is original, and does not to the best of my knowledge breach any law of copyright, and has not been taken from the work of others save and to the extent that such work has been cited and acknowledged within the text of my work.

Signed:  _____

(Alexandru Tudor)

ID No.: 14210042

Date: 28.08.2017

Acknowledgements

October 2013 still seems like it happened yesterday, and I will remember it with the same vividness from now on. Because of this, I would like to thank prof. Dermot Diamond for giving me the opportunity of fulfilling a long-time dream by offering me the chance to come to Ireland to complete my doctoral studies. Thank you for all of your support, understanding, and humour during these last few years. The second person that I would really like to thank is dr. Larisa Florea. Her guidance, advice and help made moving to Ireland a lot smoother and straightforward. Under their guidance I progressed both personally and from a scientific point of view in a rhythm I have never thought possible, and for that I thank them.

I would also want to thank the people that I spent my last four years with: Wayne, Aishling, Jen and Danielle. I've never imagined I would end up having such great workmates. It's been wonderful working with you guys all of these years.

I would also like to thank all of the people that left in the meantime, which also had a hand in helping me with my work: Simon C., Simon G., Deirdre, Giuzy, Tom G., Tom P., Cormac, Paddy, Connor, and Rory. It wouldn't have been the same without you guys. Also, I would like to thank all the people that I lived with in that big house: Zeliha, Eva, Dirk, Hari, Marina, Gabi, Pasquale, David, Jenny, Claire, and everybody else that lived there while I was around. The fact that it was so easy to find somebody to go for a walk to Anderson's or Omni, or just have a nice conversation, made things very pleasant. And to not forget, I would like to thank all my colleagues from the OrgBIO project: Anna-Maria, Ana, Maria, Marcel, Vijay, Gaurav, Amber, Alex, Quentin, Shokoufeh, Krisztina, Isabel and Brigitte. I always had a blast each time we had to meet for the different OrgBIO meetings and workshops.

I would also like to thank my friends from home: Răzvan, Paul, Norbert, Mădălina, Diana, Laura, Darius, Silviu, Anca, Claudia P., Claudia B., Cris, Adelina, Ana, Roxana, Cristina, Iuli, and the list could go on and on. Thank you for all of your support. Whenever the time for me to come would arrive, I was always looking forward to seeing all of you.

Last but not least, I would like to thank my parents, Gabriela and Romulus, my brother, Paul, and my aunts, especially Nina, for all the patience and support they offered me since I left home. You were the anchor that kept me steady whenever the seas got rough. Thank you very much.

Octombrie 2013 pare să fi fost ieri, și probabil în continuare când mă voi gândi la momentul respectiv va reapărea la fel de vivid în mintea mea. Tocmai din această cauză doresc să-i mulțumesc profesorului Dermot Diamond pentru oportunitatea oferită de a-mi trăi unul din visele pe care le-am avut de când eram licean. A doua persoană căruia aș vrea să-i mulțumesc pentru tot ajutorul pe care mi l-a oferit este Larisa Florea. Nu cred că aș fi putut face față la tot ce ma așteptat în Irlanda fără ajutorul, îndrumarea și susținerea ei. Sub tutela lor, am progresat într-un ritm pe care nu mi-l imaginam posibil, atât din punct de vedere personal, cât și științific.

În continuare, trebuie să le mulțumesc oamenilor cu care mi-am împărțit cei aproape patru ani: Wayne, Aishling, Jen, and Danielle. Nu credeam că aș fi putut întâlnii așa oameni faini cu care să-mi pot împart timpul dealungul acestei perioade nici dacă mi-aș fi putut alege eu colegii. M-am distrat de minune cu voi toți acești ani împreună.

Vreau să le transmit mulțumiri și tuturor colegiilor care au plecat între timp și care m-au ajutat atâta vreme cât au fost prin preajma: Simon C, Simon G, Deirdre, Giuzy, Tom G, Tom P, Cormac, Paddy, Connor, Rory. Nu ar fi fost la fel dacă nu ați fi fost și voi prin preajmă. Și apropo de oameni care au fost timpul prin preajmă, vreau să le mulțumesc colegiilor de casă: Zeliha, Eva, Dirk, Hari, Marina, Gabi, Pasquale, și toți ceilalți care au locuit acolo în timp ce eram și eu prin preajmă. Faptul că era foarte ușor să te întâlnești cu cineva și să ai o discuție, să faci un drum până la Anderson's sau până la Omni era de ajuns să transforme o zi monotonă într-una bună. De asemenea, trebuie să-i menționez și pe colegii din proiectul OrgBIO: Anna-Maria, Ana, Maria, Marcel, Vijay, Gaurav, Amber, Alex, Quentin, Shokoufeh, Krisztina, Isabel and Brigitte. A fost o adevărată plăcere să vă cunosc și să vă fiu coleg.

Următorii cărora aș vrea să le mulțumesc pentru tot sprijinul acordat sunt toți prietenii pe care de abia așteptam să îi văd când mă întorceam acasă: Răzvan, Paul V., Norbert, Mădălina, Diana, Laura, Darius, Silviu, Anca, Claudia P., Claudia B., Cris, Adelina, Ana, Roxana, Cristina, Iuli și lista poate continua mult și bine. Vă mulțumesc mult pentru toată susținerea acordată. Oricât de haotice ajungeau să-mi fie vacanțele, deabia așteptam să vă văd pe cât mai mulți dintre voi, mai ales dacă presupunea degustarea unei cafele într-un mediu plin de hazard.

Și nu în ultimul rând aș dori să le mulțumesc părinților mei Gabi și Romi, fratelui meu Paul, și mătușii mele, în special Ninei, pentru toată răbdarea și susținerea care mi-au oferit-o. Voi ați fost punctul de sprijin cel mai important de când m-am mutat în Irlanda. Susținerea voastră m-a făcut să pot să duc totul până la bun sfârșit.

List of Publications

Peer-Reviewed Journal Articles

- [1] **“Poly(Ionic Liquid) Semi-Interpenetrating Network Multi-Responsive Hydrogels”** A. Tudor, L. Florea*, S. Gallagher, J. Burns and D. Diamond, *Sensors*, 16, 219-235, 2016.
- [2] **“Poly(ionic liquid) thermo-responsive hydrogel microfluidic actuators”** A. Tudor†, J. Saez†, L. Florea*, F. Benito-Lopez* and D. Diamond, *Sensors and Actuators B: Chemical*, 267, 749-755, 2017.
- [3] **“Direct Laser Writing Fabrication by Multi-photon Polymerisation of Stimuli-Responsive Poly(ionic liquid) Based Soft Structures with Sub-Micron Resolution”** A. Tudor, C. Delaney, A. Thompson, V. Curto, L. Florea*, G.-Z. Yang, and D. Diamond, *Nature Materials*, submitted.
- [4] **“Driving Flow in Microfluidic Paper-Based Analytical Devices with a Cholinium Based Poly(Ionic Liquid) Hydrogel”** T. Akyazi†, A. Tudor†, D. Diamond, L. Basabe-Desmonts, L. Florea*, and F. Benito-Lopez*, *Sensors and Actuators B: Chemical*, accepted.
- [5] **“Superabsorbent Biocompatible poly(Ionic Liquid) Crosslinked Hydrogels”** A. Tudor†, L. Florea, and D. Diamond, submitted for a patent application with the United States Patent and Trade Office as a provisional filing, application number 62405314.

Peer-Reviewed Book Chapters

- [1] **“Application of Ionic Liquid Materials in Microfluidic Devices”** T. Akyazi, A. Tudor, C. Delaney, W. Francis, D. Diamond, L. Basabe-Desmonts, L. Florea*, F. Benito-Lopez*, *Ionic liquid devices*, 978-1-78801-181-5, 2017, in press.

Peer-Reviewed Conference Proceedings

- [1] **“Temperature-Controlled Poly(Ionic Liquid) Microfluidic Valves”** Alexandru Tudor, Janire Saez, Larisa Florea, Fernando Benito-Lopez and Dermot Diamond, 20th

International Conference on Miniaturized Systems for Chemistry and Life Sciences, Dublin, Ireland, 9-13 October 2016.

[2] **“Cholinium Based Poly Ionic Liquid Hydrogel as Negative Flow Passive Pump in Paper-Based Analytical Devices”** Tuğçe Akyazi†, Alexandru Tudor†, Dermot Diamond, Lourdes Basabe-Desmonts, Larisa Florea and Fernando Benito-Lopez, 20th International Conference on Miniaturized Systems for Chemistry and Life Sciences, Dublin, Ireland, 9-13 October 2016.

[3] **“Poly(ionic liquid) based dual responsive smart hydrogels,”** Alexandru Tudor, Simon Gallagher, Larisa Florea* and Dermot Diamond, 19th International Conference on Miniaturized Systems for Chemistry and Life Sciences, Gyeongju, Korea, 25-29 October 2015 .

Conference Contributions

The presenting author has been underlined

Oral Presentations

[1] **“Cholinium Based Poly(Ionic Liquid) Hydrogels as Negative Flow Passive Pumps in Paper-Based Analytical Devices”** Fernando Benito-Lopez, Tuğçe Akyazi†, Alexandru Tudor†, Larisa Florea and Dermot Diamond, 20th International Conference on Miniaturized Systems for Chemistry and Life Sciences, Dublin, Ireland, 9-13 October 2016.

[2] **“Solvent Sensing Fluorescent poly(Ionic Liquid) Ionogels”**, Alexandru Tudor, Colm Delaney, Wayne Francis, Adam McColgan, Larisa Florea and Dermot Diamond, 4th Edition of the International Conference on Analytical and Nanoanalytical Methods for Biomedical and Environmental Sciences, Universitatea Transilvania, Brasov, Romania, 29th June – 1st July 2016,

[3] **“Thermo-responsive Poly(Ionic Liquid) Hydrogel Microfluidic Valves”**, Alexandru Tudor, Janire Saez, Larisa Florea*, Fernando Benito-Lopez and Dermot Diamond, 8th Conference on Analytical Sciences Ireland 2016, The Helix, Dublin City University, Dublin, Ireland, 14-15 April 2016 (Flash presentation).

[4] **“Thermo-responsive Poly(Ionic Liquid) Valves for Microfluidic Devices”**, Alexandru Tudor, Janire Saez, Larisa Florea*, Fernando Benito-Lopez and Dermot

Diamond, 3rd OrgBIO Training School, 3rd International Winterschool on Bioelectronics, Kirchberg in Tirol, Austria, 12-19 March 2016.

[5] **“From molecules to devices: can we create disruptive technologies based on 3D functionality at multiple dimensions to solve global challenges?”** Dermot Diamond, Larisa Florea, Aishling Dunne, Alexandru Tudor, Aymen Ben Azouz and Simon Coleman, Henkel Invited Research Seminar Series, Henkel R&D, Tallaght, Dublin, 26 January 2016.

[6] **“Can biomimetic principles coupled with advanced fabrication technologies and stimuli-responsive materials drive revolutionary advances in wearable and implantable biochemical sensors?”** Dermot Diamond, Larisa Florea, Aishling Dunne, Alexandru Tudor, Aymen Ben Azouz and Simon Coleman, Invited Seminar, Tyndall National Institute, Tyndall National Institute, Cork, Ireland, 21 January 2016.

[7] **“Biomimetic microfluidics – the key to revolutionising autonomous chem/bio-sensing platforms”** Dermot Diamond, Larisa Florea, Aishling Dunne, Alexandru Tudor, Aymen Ben Azouz and Simon Coleman, Hamlyn Distinguished Lecture Series, Imperial College London, London, UK, 5 November 2015.

[8] **“Next generation autonomous sensing platforms based on biomimetic principles”** Larisa Florea, Aisling Dunne, Alexandru Tudor, Simon Coleman, Aymen Ben Azouz and Dermot Diamond, NANONET2015, University of Limerick, 21-22 October 2015.

[9] **“Biomimetic microfluidics and stimuli-responsive materials: the key to realising chemical sensing platforms with revolutionary capabilities,”** Larisa Florea, Wayne Francis, Aisling Dunne, Alexandru Tudor and Dermot Diamond, *Royal Society of Chemistry Analytical Research Forum 2015*, London, UK, 3rd July 2015

[10] **“Bio-inspired active fluidic systems based on stimuli-responsive materials.”** Dermot Diamond, Larisa Florea, Wayne Francis, Alexandru Tudor and Danielle Bruen, 67th Irish Universities Chemistry Research Colloquium, Maynooth University, Ireland, 25-26 June 2015.

[11] **“Using molecular photoswitches to build functionality for microfluidic systems”** Dermot Diamond, Larisa Florea, Wayne Francis, Aisling Dunne and Alexandru Tudor COST Action MP 1205 Advances in Optofluidics: Integration of Optical Control and Photonics with Microfluidics, Dublin Institute of Technology, 24-25 Apr 2014.

[12] **“Synthesis and use of novel functionalised materials”** Larisa Florea, Alexandru Tudor and Dermot Diamond, OrgBIO kick-off meeting, 10-11 April 2014, Gardanne, France.

Poster Presentations

[1] **“Temperature-Controlled Poly(Ionic Liquid) Microfluidic Valves”** Alexandru Tudor, Janire Saez, Larisa Florea, Fernando Benito-Lopez and Dermot Diamond, 20th International Conference on Miniaturized Systems for Chemistry and Life Sciences, Dublin, Ireland, 9-13 October 2016.

[2] **“Thermo-responsive Poly(Ionic Liquid) Hydrogel Microvalves,”** Alexandru Tudor, Janire Saez, Larisa Florea*, Fernando Benito-Lopez and Dermot Diamond, 8th Conference on Analytical Sciences Ireland 2016, The Helix, Dublin City University, Dublin, Ireland, 14-15 April 2016.

[2] **“Tuning the Stimuli-Responsive Properties of Poly(Ionic Liquids),”** Alexandru Tudor, Larisa Florea* and Dermot Diamond, 2nd Insight Student Conference, National University of Ireland Galway, Galway, Ireland, 30 October 2015.

[4] **“Phosphonium Based Dual Responsive Hydrogels,”** Alexandru Tudor, Larisa Florea*, Simon Gallagher and Dermot Diamond, 19th International Conference on Miniaturized Systems for Chemistry and Life Sciences – MicroTAS 2015, Gyeongju-si, Republic of Korea, 26-30 October 2014

[5] **“Dual-Responsive Poly(Ionic Liquid) Hydrogels,”** Alexandru Tudor, Simon Gallagher, Larisa Florea* and Dermot Diamond, 12th International Conference on Materials Chemistry – MC12, University of York, York, UK, 20-23 July 2015.

[6] **“Multi-responsive Semi-Interpenetrating Network Hydrogels,”** Alexandru Tudor, Larisa Florea* and Dermot Diamond, 2nd OrgBIO Training School, Nanotechnology 2015/ISSON15, Thessaloniki, Greece, 4-11 July 2015.

[7] **“Thermo and Salt Responsive Poly(Ionic Liquids),”** Alexandru Tudor, Simon Gallagher, Larisa Florea*, Wayne Francis and Dermot Diamond, 67th Irish Universities Chemistry Research Colloquium, Maynooth, Ireland, 25-26 June 2015.

[8] **“Semi-Interpenetrating Network Photo-Responsive Hydrogels Containing Poly(Ionic Liquids)”** Alexandru Tudor, Simon Gallagher, Larisa Florea* and Dermot Diamond, 1st Brazil-Ireland Science Week, Dublin, Ireland, 23-26 February 2015.

- [9] **“Photo-responsive Semi-Interpenetrating Network Hydrogels Based on Poly(Ionic Liquids) and a Poly(N-Isopropylacrylamide-Spiropyran-Acrylic Acid) Copolymer”** Alexandru Tudor, Simon Gallagher, Larisa Florea* and Dermot Diamond, 1st Insight Student Conference, UCD, Dublin, 12 September 2014.
- [10] **“Novel Semi-Interpenetrated Networks Based on Poly(Ionic Liquids) and Dual Responsive Polymers,”** Alexandru Tudor, Simon Gallagher, Larisa Florea* and Dermot Diamond, 13th International Symposium on Advancing the Chemical Sciences (ISACS13) – Challenges in Inorganic and Materials Chemistry, Chartered Accountants House, Dublin, Ireland, 1-4 July 2014.
- [11] **“Characterization of Linear Poly(N-Isopropyl Acrylamide – Spiropyran – Acrylic Acid) Copolymer by DSC and UV-Vis spectroscopy,”** Alexandru Tudor, Larisa Florea* and Dermot Diamond, 49th Thermal Analysis and Calorimetry Conference (TAC 2014) – The use of thermal analysis and calorimetry to support product development, David Jack Research Center, GSK R&D, Ware, UK, 1-2 April 2014.

Overall Aim and Thesis Structure

Overall Aim

The aim of this work was to synthesize new stimuli-responsive and functional crosslinked poly(ionic liquid) (xPIL) materials. A first example is described in Chapter 3 of this report and was achieved by creating xPIL semi-interpenetrating networks (sIPNs) with photo-responsive polymers. The response of this novel xPIL sIPN to photo-stimulus and ionic strength was investigated and characterised. Another example is presented in Chapters 4 of this report, where phosphonium sulfopropylacrylate xPIL hydrogels are investigated for their thermo-response and incorporated in microfluidic devices as thermo-responsive valves. The 3D printing of this material by Direct Laser Writing (DLW) by Two-photon Polymerisation (2-PP) is described in Chapter 5. Chapter 6 details the synthesis, and superabsorbent properties of a novel cholinium-based xPIL, while Chapter 7 proposes its inclusion in paper-based microfluidic devices as a passive pump. In the first part of Chapter 8, the focus shifts towards the synthesis of a fluorescein containing ionic liquid which was further incorporated into an xPIL matrix for the fabrication of a xPIL solvent sensor. The

second part of Chapter 8 discusses the synthesis of a cholinium-based xPIL to be used in the formulation of photocurable resists for 2-PP 3D printing, which could be further used as a biocompatible hydrogel electrode for the monitoring of cell activity.

Selected Publications and Author Contribution

This thesis includes the following chapters: one introduction chapter (Chapter 1), one published book chapter (Chapter 2), followed by two original papers published in peer reviewed journals (Chapter 3 and 4), two original papers submitted for publication (Chapter 5 and 7), one provisional patent (Chapter 6), and one chapter that focuses on the future direction of this research, respectively (Chapter 8).

The leading motivation for this work was to increase the understanding of how ionic liquid monomers and crosslinked poly(ionic liquid) hydrogels can be used in interdisciplinary studies, such as microfluidics and 3D printing. All of the ideas, experiment designs and article writing were the principal responsibility of myself and my supervisors: Dr. Larisa Florea and Prof. Dermot Diamond, while working within the Insight Centre for Data Analytics, National Centre for Sensor Research, School of Chemical Sciences at Dublin City University. The presence of co-authors reflects that collaborations with other research groups were highly prized and encouraged.

My involvement in Chapters 2 to 7 is detailed in the following table:

Thesis Chapter	Publication title	Publication status¹	Nature and extent of candidate's contribution
2	Application of Ionic Liquid Materials in Microfluidic Devices	Published <i>Ionic liquid devices</i> , 978-1-78801-181-5, 2017	Author and writing up.
3	Poly(Ionic Liquid) Semi-Interpenetrating Network Multi-Responsive Hydrogels	Published <i>Sensors</i> , 16, 219-235, 2016	Main-author, key ideas, experimental design, data generation and analysis, patent development and writing up.
4	Poly(ionic liquid) thermo-responsive hydrogel microfluidic actuators	Published <i>Sensors and Actuators B: Chemical</i> , 267, 749-755, 2017	Shared first author, key ideas, experimental design, material synthesis and characterization, manuscript development and writing up.
5	Direct Laser Writing Fabrication by Multi-photon Polymerisation of Stimuli-Responsive Poly(ionic liquid) Based Soft Structures with	Submitted <i>Nature Materials</i>	Main-author, key ideas, experimental design, data generation and analysis.

¹For example, 'published'/ 'in press'/ 'accepted'/ 'returned for revision'/ 'submitted'

in this chapter are ionogels, which are crosslinked polymers solvated by ionic liquids. Several applications, including the use of ILs and IL materials as microvalves, delaying pumps, chemical and physical sensors are presented and discussed.

Chapter 3: Poly(Ionic Liquid) Semi-interpenetrating Network Multi-Responsive Hydrogels

This study was published as an original article in *Sensors*. The motivation of this chapter is to describe the behaviour of stimuli-responsive hydrogels based on phosphonium sulfopropylacrylate xPIL sIPNs. The materials synthesized in this chapter shows shrinking behaviours when exposed to three different stimuli: light, temperature and salt concentration. The response to light is given by the linear poly(N-isopropylacrylamide-co-spiropyran-co-acrylic acid) polymer that is added to the phosphonium ionic liquid monomer mixture. The temperature and salt concentration response is dominated by the xPIL matrix. The photo-response of the linear polymer, the rheological properties of the xPIL sIPNs, and their conformation changes are thoroughly investigated.

Chapter 4: Poly(ionic liquid) thermo-responsive hydrogel microfluidic actuators

The basis of the work presented in this chapter, which was published in *Sensors and Actuators B: Chemical*, was derived from the results obtained for the phosphonium sulfopropylacrylate xPIL hydrogels without any additional linear polymer, presented in the previous chapter. Due to their repeatable shrinking and swelling capabilities, they were integrated into a microfluidic device to be used as temperature-controlled actuators that can control flow through a microfluidic channel. This study details the fabrication of the microfluidic device, further shrinking and swelling tests on the xPIL hydrogels, and the flow characterization through the microfluidic chip when the integrated hydrogel is being actuated by a temperature controller. This work was performed in collaboration with Janire Saez and Fernando Benito-Lopez, from the Analytical Microsystems & Materials for Lab-on-a-Chip Group (AMMa-LOAC), Microfluidics Cluster at the University of the Basque Country, Spain, who were responsible for the flow characterization of the microfluidic chip.

Chapter 5: Direct Laser Writing Fabrication by Multi-photon Polymerisation of Stimuli-Responsive Poly(ionic liquid) Based Soft Structures with Sub-Micron Resolution

This work, which is submitted as an original article to *Nature Materials*, describes the development of multiphoton 3D printed stimuli-responsive hydrogel microstructures. These microstructures exhibit the same type of temperature response as the ones presented in the previous two chapters. The novel approach in this study is given by taking advantage of the ionic liquid monomer's solvation properties, which makes for facile development of a photocurable resin for the multiphoton 3D printing system. The structures printed with the help of this system consisted of different geometric shapes, such as cylinders, twisted vases and hexagons. Moreover, the addition of a rhodamine B-derived polymerisable dye permitted the observation of the swelling effect of the hydrogels by using a STED microscope. The use of a temperature-controlled heating element permitted the characterization of the microstructure's temperature response. This work was performed in collaboration with Vincenzo F. Curto, Alexander Thompson, and Guang-Zhong Yang from Imperial College London.

Chapter 6: Superabsorbent Biocompatible poly(Ionic Liquid) Crosslinked Hydrogels

In this chapter, the synthesis of a novel cholinium-based ionic liquid monomer is detailed, together with its polymerisation protocol to form a superabsorbent xPIL hydrogel. Thermogravimetric analysis was employed to characterize the water intake capabilities of the xPIL hydrogel and its decomposition temperature. Due to its water absorption capabilities coupled with its biocompatibility, the material together with its synthesis procedure formed the basis of a patent submitted to the United States Patent and Trade Office.

Chapter 7: Driving Flow in Microfluidic Paper-Based Analytical Devices with a Cholinium Based Poly(Ionic Liquid) Hydrogel

Based on the water absorption capabilities of the cholinium hydrogels presented in the previous chapter, they were used in the construction of paper-based microfluidic devices (μ PADs). These devices feature a printed channel with two outlets and one inlet. The cholinium hydrogel was polymerised at one of the channel's outlets. Following this, the μ PAD was laminated and had its flow characteristics examined.

The presence of the cholinium xPIL at one of the outlets acted as a passive pump that would draw fluid towards itself, after the μ PAD was initially wetted. This work was performed in collaboration with Tuğçe Akyazi and Fernando Benito-Lopez, from the Analytical Microsystems & Materials for Lab-on-a-Chip Group (AMMa-LOAC), Microfluidics Cluster at the University of the Basque Country, Spain, who were responsible for the device fabrication and flow characterization of the microfluidic device.

Chapter 8: **Future Work**

The last chapter of the thesis focuses on the future work that can be derived from the studies already presented here. The first part of the chapter focuses on the synthesis of a fluorescein containing ionic liquid which was incorporated into an xPIL matrix for the development of xPIL gels with solvent sensing capabilities, based on the solvatochromic effect. In the second part of the chapter, the focus shifts towards the development of new photocurable resists based on cholinium ionic liquid monomer derivatives, and their 3D printing by means of multiphoton polymerization, for the fabrication of microstructured electrodes for future use in cell monitoring.

Table of Contents

	<i>Page</i>
General Declaration	ii
Acknowledgements	iii
List of Publications	v
Conference Contributions	vi
Overall Aim and Thesis Structure	ix
Chapter Overview	xi
Table of Contents	xv
List of Abbreviations	1
List of Figures	3
Thesis Abstract	14
<u>Chapter 1</u>	<u>15</u>
Literature Overview: Crosslinked Poly(Ionic Liquid)s as Building Blocks for Stimuli-Responsive and Functional Materials	
1.1 Introduction to ionic liquids and poly(ionic liquid)s	17
1.2 Application overview of poly(ionic liquid)s	17
1.2.1 Ionic conductors	19
1.2.2 Nanoparticles	22
1.2.3 Temperature – responsive materials	24
1.3 References	27
<u>Chapter 2</u>	<u>29</u>
Application of Ionic Liquid Materials in Microfluidic Devices	
2.1 Abstract	31
2.2 Introduction	31
2.3 Ionic Liquids for Actuators	33

2.3.1 Microvalves	33
2.3.2 Delaying pumps	42
2.4 Ionic Liquids for Sensing	43
2.4.1. Chemical sensing	44
2.4.2. Physical sensing	49
2.5 Other Applications in Microfluidics	52
2.5.1. Ionic liquids for nanoparticle synthesis in microfluidics	52
2.5.2. Ionic liquids for building a microfluidics-based power generator	54
2.5.3. Ionic liquids for precise temperature control in microfluidics	54
2.6 Conclusions	55
2.7 References	55
<u>Chapter 3</u>	60
Poly(Ionic Liquid) Semi-interpenetrating Network Multi-Responsive Hydrogels	
3.1 Abstract	62
3.2 Introduction	62
3.3 Experimental	64
3.3.1 Materials and methods	64
3.3.2 Synthesis of tributylhexyl phosphonium 3-sulfopropylacrylate ionic liquid monomer	65
3.3.3 Synthesis of the linear poly(<i>N</i> -isopropylacrylamide-co-Spiropyran-co-Acrylic Acid) p(NiPAAm-BSP-AA) copolymer	66
3.3.4 Synthesis of the semi-interpenetrating network hydrogels	67
3.3.5 Thermal behaviour of the linear p(NiPAAm-BSP-AA) copolymer	67
3.3.6 White light curing studies of the sIPN hydrogels using rheometry	67

3.3.7 Measurement of the stimuli-induced shrinking	68
3.4 Results and discussion	69
3.4.1 White light and temperature response of the linear p(NiPAAm-BSP-AA) copolymer solutions	69
3.4.2 Photo-induced curing studies and mechanical properties of the hydrogels	74
3.4.3 White light induced shrinking	77
3.4.4 Ionic radius dependent shrinking	80
3.4.5 Temperature induced shrinking	81
3.5 Conclusions	83
3.6 References	83
<u>Chapter 4</u>	86
Poly(ionic liquid) thermo-responsive hydrogel microfluidic valves	
4.1 Abstract	88
4.2 Introduction	88
4.3 Experimental	89
4.3.1 Materials	89
4.3.2 Synthesis of the tributylhexyl sulfopropyl acrylate (PSPA) ionic liquid monomer	90
4.3.3 Crosslinked PSPA hydrogel disk polymerization	91
4.3.4 Characterization of the temperature-induced shrinking and reswelling of the hydrogel disks	91
4.3.5 Microfluidic chip fabrication	92
4.3.6 Thermo-responsive hydrogel valve characterization	93
4.4 Results and discussion	95
4.4.1 Temperature-induced shrinking of the PILc hydrogel disks	95

4.4.2 Temperature-induced flow control in the microfluidic device	85
4.5 Conclusions	100
4.6 References	100
Appendix for Chapter 4	104
<u>Chapter 5</u>	<u>108</u>
Direct Laser Writing Fabrication by Multi-photon Polymerisation of Stimuli-Responsive Poly(ionic liquid) Based Soft Structures with Sub-Micron Resolution	
5.1 Abstract	110
5.2 Introduction	110
5.3 Experimental	113
5.3.1 Materials	113
5.3.2 Photoresists: monomeric cocktails for direct laser writing fabrication	113
5.3.3 Direct laser writing fabrication	114
5.3.4 DLW live-observation	115
5.3.5 Microscopy and quantification	115
5.4 Results and Discussion	115
5.4.1 Microstructure printing	115
5.4.2 Microstructure temperature-induced shrinking	119
5.5 Conclusions	121
5.6 References	121
Appendix for Chapter 5	125
<u>Chapter 6</u>	<u>133</u>
Superabsorbent Biocompatible poly(Ionic Liquid) Crosslinked Hydrogels	
6.1 Abstract	135

6.2 Introduction	135
6.3 Experimental	
6.2.1 Materials	138
6.2.2 Synthesis of the cholinium sulfopropyl acrylate ionic liquid monomer	138
6.2.3 Synthesis of the cholinium PIL hydrogels	139
6.4 Results and Discussion	139
6.3.1 Thermal Characterization of the PIL hydrogels	139
6.5 Problems addressed by the invention	143
6.6 Existing solutions to the problem(s) that you are aware and consider to be closest to the new invention	144
6.7 Key aspects of the invention which make it novel and demonstrate its advantages over the existing solutions	144
6.8 Potential commercial application (products, processes, services, or research tools) based on the invention.	145
6.9 References	145
Chapter 7	148
<hr/>	
Driving Flow in Microfluidic Paper-Based Analytical Devices with a Cholinium Based Poly(Ionic Liquid) Hydrogel	
7.1 Abstract	150
7.2 Introduction	150
7.3 Experimental	153
7.3.1 Materials	153
7.3.2 μ Pad fabrication	154
7.3.3 Synthesis of the cholinium sulfopropyl acrylate ionic liquid monomer	154
7.3.4 Synthesis of the cholinium PIL hydrogels	155
7.3.5 Thermal characterization method of the cholinium hydrogels	155

7.4 Results and Discussion	156
7.4.1 Thermal characterization of the swollen PIL hydrogels	156
7.4.2 μ Pad microfluidic behaviour characterization	158
7.5 Conclusions	161
7.6 References	162
Appendix for Chapter 7	166

Chapter 8: Future Work **169**

Expanding the Application Profile of Crosslinked Poly(Ionic Liquid)s: Fluorescent Ionogels and Biocompatible Hydrogels

8.1 The synthesis and spectrophotometric characterization of crosslinked poly(ionic liquid) – fluorescein ionogels.

8.1.1 Introduction	171
8.1.2 Materials	173
8.1.3 Tetrabutyl phosphonium sulfopropyl methacrylate synthesis	174
8.1.4 Di(Trihexyltetradecyl phosphonium) fluorescein ionic liquid synthesis	174
8.1.5 Synthesis of the crosslinked poly(ionic liquid)(PIL) ionogels	176
8.1.6 UV-Vis and Fluorescence Spectroscopy characterization of the PIL Ionogels	176

8.2 The synthesis of cholinium – based biocompatible crosslinked poly(ionic liquid) hydrogels

8.2.1 Introduction	181
8.2.2 Materials	184
8.2.3 Synthesis of the cholinium acrylate ionic liquid monomer	184
8.2.4 Ionic liquid monomer mixtures to be used as photoresists	184
8.2.5 2-Photon polymerization of the monomer mixtures	185
8.2.6 Silanisation of the glass substrates	186

8.2.7 Fabrication of the electrode arrays	186
8.3 Conclusion	190
8.4 References	192
Appendix for Chapter 8	195

List of Abbreviations

P ₄₄₄₆ SPA/PSPA	Tributylhexylphosphonium Sulfopropylacrylate
P ₄₄₄₆ SPMA/PSPMA	Tributylhexylphosphonium Sulfopropylmethacrylate
P ₄₄₄₄ SPA/PSPA	Tetrabutylphosphonium Sulfopropylacrylate
KSPA	Potassium Sulfopropylacrylate
KSPMA	Potassium Sulfopropylmethacrylate
ChoCl	Cholinium Chloride
ChoSPA	Cholinium Sulfopropylacrylate
ChoAc	Cholinium Acrylate
P ₆₆₆₁₄ Cl/PCl	Trihexyltetradecylphosphonium Chloride
PFI	Trihexyltetradecylphosphonium Fluorescein
Na ₂ FI	Disodium Fluorescein
PEG258	Poly(ethyleneglycol) diacrylate, $M_w \sim 320 \text{ g}\cdot\text{mol}^{-1}$
PPO800/PPG800	Poly(propyleneglycol) diacrylate, $M_w \sim 900 \text{ g}\cdot\text{mol}^{-1}$
MeOH	Methanol
EtOH	Ethanol
DCM	Dichloromethane
DI Water	Deionized water with a resistivity of $18.2 \text{ M}\Omega\cdot\text{cm}^{-1}$
DMSO	Dimethylsulfoxide
IL	Ionic liquid
ILM	Ionic liquid monomer
PIL	Poly(ionic liquid)
xPIL	Crosslinked poly(ionic liquid)
NiPAAm	N-isopropylacrylamide

pNiPAAm	Poly(N-isopropylacrylamide)
AA	Acrylic acid
BSP	Trimethyl-6-hydroxyspiro-(2H-1-benzopyran-2,2'-indoline) acrylate
PBPO	Phenyl-bis(2,4,6-trimethylbenzoyl) phosphine oxide
HMPP	2-hydroxy-2-methylpropiophenone
DMPA	Dimethoxy-2-phenylacetophenone
LCST	Lower critical solution temperature
DSC	Differential scanning calorimetry
TGA	Thermogravimetric analysis
NMR	Nuclear magnetic resonance
UV-Vis	Ultraviolet-visible spectrophotometry
2PP	2-photon polymerization

List of Figures

- Figure 1.1** Chemical structures of the most common cations and anions used in ILs (from left to right): (A) pyrrolidinium, imidazolium, 2-methylimidazolium, phosphonium, ammonium, piperidinium, pyridinium; (B) tetrafluoroborate, hexafluorophosphate, dicyanamide, bis(trifluoromethane)sulfonimide, chloride, bromide, iodide, trifluoromethanesulfonate, methanesulfonate, acetate, formate and lactate, respectively. **18**
- Figure 1.2** The structure of the most common cationic and anionic ILM: (from left to right) vinylimidazolium, vinylpyridinium, vinylphosphonium, vinylammonium, sulfopropylacrylate, acrylate. **19**
- Figure 1.3** Chemical structure of the ILMs used by Yoshizawa et al. in [14] **20**
- Scheme 1.1** Synthetic route for the preparation of monomers 9, 10 and 11. Reagents and conditions: (i) SOCl_2 , THF/DMF, $0^\circ\text{C} \rightarrow \text{RT}$; (ii) $\text{NH}_2\text{SO}_2\text{CF}_3$, THF, NEt_3 , $0^\circ\text{C} \rightarrow \text{RT}$; (iib) $\text{CH}_2(\text{CN})_2$, THF, NEt_3 , $0^\circ\text{C} \rightarrow \text{RT}$; (iic) NH_2CN , THF, NEt_3 , $0^\circ\text{C} \rightarrow \text{RT}$; (iii) LiH , THF, $10^\circ\text{C} \rightarrow \text{RT}$; (iv) 1.4 [1-Bu-1-Me Pyr]Br, H_2O , RT. Reproduced from [19] **21**
- Figure 1.4** Chemical structures of the ILMs used by Koebe et al. in [23] **22**
- Figure 1.5** TEM (top) and cryo-TEM (bottom) characterization of the synthesized poly(ILM-C14Br/C) (A&D), poly(ILM-C16Br/C) (B&E), poly(ILM-C18Br/C) (C&F) poly(ionic liquid) nanoparticles via dispersion polymerization of the corresponding ionic liquid monomers with 10% of divinylimidazolium bromide crosslinker. The insets in A and F show the close view of individual nanoparticles. The above mentioned PILs represent the bromide salts of the tetradecyl, hexadecyl and octadecyl vinylimidazolium derivatives. Reproduced from [23]. **23**
- Figure 1.6** Chemical structures of the ILs and ILMs that were found to possess a lower critical solution temperature. **25**

- Figure 2.1** Image of the microfluidic manifold showing the performance of the ionogelmicrofluidic valves: (a) all microvalves are closed under the applied vacuum. White light is applied for the time specified in each picture (b) Hydrogel (no IL present) valve is first to actuate followed by ionogels incorporating [DCA]- (c), [Tos]- (d), [DBSA]- (e), [NTf₂]- (f). Numbers and arrows indicate when the channel is filled with the dye due to microvalve actuation. Reproduced from Benito-Lopez et al. [30]. **35**
- Figure 2.2** Microscope images of ionogel discs made of: (a) [P_{6,6,6,14}][NTf₂], (b) [P_{6,6,6,14}][DCA] and (c) [P_{6,6,6,14}][Cl] after photopolymerisation (left); swelling in 1mM HCl solution for 2h (middle) and shrinking upon white light irradiation (right). Reproduced from Czugała et al. [31]. **37**
- Figure 2.3** Picture of the microfluidic device fabricated in PMMA: (a) PSA polymer by CO₂ laser ablation (left). Followed by (b) a schematic (top) and images (bottom) of the photoresponsive microvalve in closed (middle) and opened (right) state. Reproduced from Czugała et al. [32]. **38**
- Figure 2.4** Flow profile during three full actuation cycles (left) and photo of the microfluidic device containing the thermo-actuated valve and the microfluidic holder with integrated heaters at the bottom. High flow spikes are due to the stabilisation of the microflow sensor after opening of the valve. Reproduced from Benito-Lopez et al. [33]. **40**
- Figure 2.5** (a) BGA bending motion as a result of ion transfer between layers; direction of bending can be reversed by changing the polarity of the applied potential; (b) BGA strip bended (10 V, 0.1 Hz); (c) Base part and (d) 3D view of the flow regulator assembly. Reprinted with permission from Ghamsari et al. [35]. **41**
- Figure 2.6** A Y-shaped μPAD with photopolymerised [P_{6,6,6,14}][DCA] ionogel in the left side inlet after 5 min (A), 17 min (B), 25 min (C), 33 min (D), while injecting NaOH solution (pH=13) into the left inlet (purple arrow) and phenol red pH indicator and H₂SO₄ solution (pH = 2) (yellow arrow) into the right inlet. Phenol red gives a pink colour change in a basic environment. (E) A Y-shaped μPAD with no ionogel. Reproduced from Akyazi et al. [36]. **43**

Figure 2.7	(a) Chemical structure of [P1,4,4,4][Tos]. (b) Schematic of the OECT. (c) Image of the OECT with a drop of glucose solution added. Reproduced from Yang et al. [39].	45
Figure 2.8	a) Normalised response vs. lactate concentration for the OECT and b) Flexible OECT on the forearm. Adapted from Khodagholy et. al [43].	46
Figure 2.9	Chemical structures of A) N-Isopropyl-acrylamide and N,N-methylene-bis(acrylamide) crosslinked polymer; (B) ionic liquid tetrabutylphosphonium dicyanamide[P _{4,4,4,4}][DCA] and (C) Bromocresol Purple, showing colour changes in acidic and basic environments. Reproduced from Czugala et. al [45].	47
Figure 2.10	(a) Calibration curve of the sensing area of the microfluidic device using pH buffer solutions; (b) Image of the CD platform with the sensing area. Reproduced from Czugala et. al [45].	47
Figure 2.11	(a) Chemical structures of the pH sensitive dyes: Bromophenyl Blue (BPB), Bromocresol Green (BCG), Bromocresol Purple (BCP) and Bromothymol Blue (BTB); (b) Fabricated micro-fluidic device; (c) Smartphone application imaging on-body device. Reproduced from Curto et. al [46].	48
Figure 2.12	(a) Representation of simple linear microfluidic strain sensor with platinum electrodes. Red represents the ionic liquid filling the microfluidic channel; (b) Two-dimensional representation of the geometric deformation of the microfluidic channel when pressure is applied.	50
Figure 2.13	(a) Representation of the PDMS microfluidic device showing the microfluidic channel and electrofluidic circuit layers. (b) Conversion of mechanical pressure to electrical resistance. (c) Wheatstone bridge electrofluidic circuit. Reproduced from Wu et al. [50].	51
Figure 2.14	(a) Representation of the microfluidic cell culture showing electrofluidic circuit layer and a microfluidic cell culture layer and glass substrate. (b) Image of the fabricated device showing: the electrofluidic circuit channels (blue) and microfluidic cell culture channels (red). Reproduced from Liu et al. [51].	52
Scheme 3.1	The PSPA synthesis reaction.	65
Figure 3.1	The photopolymerized hydrogels after swelling in DI water at	66

20°C for 24h.	
Scheme 3.2 Equilibrium of the p(NiPAAm-BSP-AA) copolymer in DI water under different illumination conditions.	70
Figure 3.2 UV-Vis absorbance spectra of the non-irradiated 0.1 % w/w p(NiPAAm-BSP-AA) linear copolymer solution in DI water.	71
Figure 3.3 UV-Vis absorbance spectra of the white light irradiated 0.1 % w/w p(NiPAAm-BSP-AA) linear copolymer solution in DI water.	71
Figure 3.4 Comparison of the absorbance values at 700 nm between the non-irradiated and white light irradiated 0.1% w/w p(NiPAAm-BSP-AA) linear copolymer solutions at different temperatures.	72
Figure 3.5 DSC curve excerpt showing the LCST transition of a 2.5% w/w p(NiPAAm-BSP-AA) linear copolymer solution. The full DSC curve follows a heating program from 14 °C to 70 °C at a heating rate of 10 °C/min.	73
Figure 3.6 Time-dependent variation of the storage modulus of the monomer cocktail during polymerization. The white light is turned on at t = 60s.	74
Figure 3.7 The effect of increasing the mass of linear p(NiPAAm-BSP-AA) copolymer on the fully hydrated hydrogel area (error bars are standard deviations for n=3 replicate measurements).	76
Figure 3.8 (a) – (d) White-light and ionic strength induced shrinking of the hydrogels.	77
Figure 3.9 Area of the hydrogels in DI water and NaCl solutions of different concentrations: 0.5%, 1% and 5%, respectively, in the absence of light.	78
Figure 3.10 The shrinking effect of 1% w/w NaF, NaCl, NaBr and NaI solutions on the area of the hydrogels compared to DI water.	80
Figure 3.11 Graphical representation of the temperature induced shrinking profiles of the hydrogels.	81
Figure 3.12 The shrinking profile of the PILc hydrogel in DI Water and 0.5% w/w NaCl solution.	82
Scheme 4.1 Reaction scheme for PSPA synthesis.	90
Figure 4.1 Schematic illustration of PSPA hydrogel disk polymerization protocol (left) and photo of the PSPA hydrogel disk (right).	91

Figure 4.2	The PMMA and PSA layers of the microfluidic chip before assembly.	93
Figure 4.3	The assembled microfluidic chip containing the thermo-responsive hydrogel actuator.	93
Scheme 4.2	Setup used for the characterization of DI water flow through the chip.	94
Figure 4.4	PSPA hydrogel shrinking in 5 °C steps from 20 to 70 °C, followed by reswelling when the temperature is lowered back to 20 °C.	96
Figure 4.5	Temperature-induced area shrinking of the PSPA hydrogels at 20 °C and at 50 °C.	96
Figure 4.6	PSPA hydrogel actuator at 50 °C allowing a flow rate of ~ 140 nL·min ⁻¹ to pass through the microfluidic channel, and, at 20 °C, restricting flow rate to ~ 20 nL·min ⁻¹ . Small fluctuations on the signal (10 ± 5 nL·min ⁻¹) were observed due to ambient conditions (e.g. vibration of the pumping system) and the ionic liquid polymer network internal reorganisation before and after temperature actuation, which is extended after the stimulus is removed due to the hydration or dehydration processes that continue to happen in the polymer.	97
Figure A.4.1	Shrinking kinetics of the PILc hydrogel valve when the temperature was raised from 20 °C to 50 °C. The blue line represents the experimental flow rate, while the red line represents the modelled flow rate.	105
Figure A.4.2	Swelling kinetics of the PILc hydrogel valve when the temperature was lowered from 50 °C to 20 °C. The blue line represents the experimental flow rate, while the red line represents the modelled flow rate.	106
Figure A.4.3	Determination of the burst-pressure of the integrated actuator via incremental increases in pressure. At pressures above 250 mbar failure in the actuator was induced, resulting in an increase in flow rate through the micro-channel (time: 1860 s). Complete failure of the actuator was achieved at an applied pressure of 400 mbar.	107

- Figure 5.1** 3D microscopy image of 2 micro-pillars arrays (cylinders and spirals) fabricated by 2-PP in PILs using cocktail formulations described in Table 1, in the polymerization cocktail (B, E), during washing in acetone (C, F), and during drying (D, G). It can be observed that in the case of the treated substrates (B-D), the structures maintained their position and structural integrity during the washing process, and no delamination occurs. 117
- Figure 5.2** Structure of the PIL hydrogel (A); Relative area measurements of a micro-cylinder at different height (z) values in hydrated and dehydrated state. The relative area changes in both hydrated and dehydrated states are calculated relative to the printed area (circular structures of 20 μm in diameter). Inset shows a cartoon representation of the micro-cylinder structures in the hydrated and dehydrated states and confocal microscopy images of the micro-cylinder in the hydrated and dehydrated state at the same z value (B). Confocal microscopy images of micro-cylinders (C, E) and micro-spirals (C, F) array fabricated by 2-PP in PILs using cocktail formulations described in Table 1, in air (C, D) and in DI water (E, F). The concentric circles composing the cylinders (contour slicing) become visible in the hydrated structures (E, F). 118
- Figure 5.3** Design, white light microscopy and AFM images of a micro-grid printed at $80 \times 80 \mu\text{m}$ and $1 \mu\text{m}$ in height after hydration and delamination. 119
- Figure 5.4** Schematic of the in-house made cell used to study the thermo-response of the gel structures; After removing of the excess photo-resist and washing of the structures, a $25 \mu\text{m}$ PSA spacer was placed on the cover slide containing the structures and covered with another thing cover slide. DI water was introduced in the cell by capillary forces and the cell was placed on the micro-heater. Schematic representation of the thermo-actuation of the PIL hydrogel structures (B). Structures are exposed to a temperature program and their thermo-response is recorded using white light microscopy. The area of the micro-cylinders is measured from the recorded video (1 frame/2s) using ImageJ software. 120
- Figure A.5.1** ^1H NMR of Acryl-Rhod B in deuterated chloroform. 126

- Figure A.5.2** Excitation and emission spectra of Acryl-Rhod B solution (10⁻⁶ M in pH 7.4 phosphate buffer solution), where the excitation wavelength was 555 nm and the corresponding emission was at 578 nm. Fluorometer parameters; medium sensitivity; 2.5 nm bandwidth. **127**
- Figure A.5.3** Selection of images following the printing of one cylinder (marked) in an array. All cylinders are 20 μm in diameter and 40 μm in height; A) Image taken before the printing of the marked cylinder; B) image taken after 5 s of DLW: the first concentric horizontal circles of the marked cylinder are printed; C) image taken after 20s of printing and D) image taken after the marked cylinder has been fully printed. **127**
- Figure A.5.4** Selection of images showing the swelling of the PIL pillars in the polymerisation cocktail during the printing process. **128**
- Figure A.5.5** Side and top views of the A) cylinder and B) spiral structures. **129**
- Figure A.5.6** 3D preview of the 3x3 array of spiral structures from different perspectives. **129**
- Figure A.5.7** 3D microscopy image of micro-pillars array fabricated by 2-PP in PILs using cocktail formulations described in Table 1, before washing of the unpolymerised photoresist. The focus is on the top of the structures. **129**
- Figure A.5.8** 3D microscopy Image of micro-pillars array fabricated by 2-PP in PILs using cocktail formulations described in Table 5.1, before (left) and after (right) washing of the unpolymerised photoresist. Structure delamination and movement occurs during washing. **130**
- Figure A.5.9** 3D microscopy images of micro-spirals (left) and cylinder (right) array fabricated by 2-PP in PILs using cocktail formulations described in Table 1, in DI water. **130**
- Figure A.5.10** Confocal microscopy images showing z slicing through a micro-cylinder array fabricated by 2-PP in PILs using cocktail formulations described in Table 1, in DI water. The swelling of the structures increases as we move away from the surface, as the structures are restricted by the covalent immobilisation to the glass surface. **131**

Figure A.5.11	Set temperature program (blue) starting with 20s at 25°C (initial) followed by 3 cycles composed of the following steps: 20s at 30°C (step 1), 20s at 50°C (step 2) and 20s at 70°C (step 3), and ending with 20s at 30°C (final) and measured temperature on the micro-heater (black).	132
Scheme 6.1	Chemical structures of the most important chemical derivatives of choline: Phosphatidylcholine, Sphingomyelin and Acetylcholine (X = undefined anion).	136
Scheme 6.2	Reaction scheme for the synthesis of ChoSPA.	139
Figure 6.1	Comparison between the sizes of the ChoSPA hydrogel before swelling (A), swelling in DI water for 12h (B) and after dehydration by drying at room temperature (C), respectively.	140
Figure 6.2	Thermogravimetric curve showing the behaviour of type A hydrogels (right after polymerisation).	141
Figure 6.3	Thermogravimetric curve showing the behaviour of type B hydrogels (after hydration in DI water for 12h)	142
Figure 6.4	Thermogravimetric curve showing the behaviour of type C hydrogels (dehydration)	143
Scheme 7.1	Reaction scheme for the synthesis of ChoSPA	154
Figure 7.1	(A) Chemical structure of the components of hydrogel: trimethylhydroxyethyl ammonium (cholinium) sulfopropyl acrylate ionic liquid (top), poly(ethylene glycol) diacrylate (middle) and poly(cholinium sulfopropyl acrylate) hydrogel (bottom); (B) Comparison between the sizes of the ChoSPA hydrogel before swelling (1), swelling in DI water for 2h (2) and after dehydration by drying at room temperature (3).	156
Figure 7.2	(A) Scheme of the different layers forming the μ PAD. (B) Picture of the final sealed μ PAD after integration of the cholinium PIL hydrogel pump.	159
Figure 7.3	Performance of the hydrogel passive pump in the μ PAD when photopolymerised at the bottom outlet. 0s (A), 2.5 min (B), 25 min (C), 55 min (D), 60 min (E), 65 min (F), 70 min (G), 75 min (H), 90 min (I) after injecting 50 μ L yellow dye, 60 μ L red dye and 70 μ L blue dye into the inlet respectively at different aliquots of 10 μ L over time.	161

Figure A.7.1	Thermogravimetric curve showing the behaviour of the hydrogel 1 (right after polymerisation) from a 2.44 mg disc, initial weight.	167
Figure A.7.2	Thermogravimetric curve showing the behaviour of the hydrogel 2 (after hydration in DI water for 12h) from a 28.71 mg disc, initial weight.	167
Figure A.7.3	Thermogravimetric curve showing the behaviour of hydrogel 3 (dehydrated) from a 3.08 mg disc, initial weight.	168
Scheme 8.1	Structure of 1-ethyl-4-(methoxy-carbonyl) pyridinium iodide.	171
Scheme 8.2	Structure of 2,6-diphenyl-4-(2,4,6-triphenyl-1-pyridinio)phenolate, which is commonly known as Reichardt's dye.	172
Scheme 8.3	Resonance structures of fluorescein.	172
Scheme 8.4	Chemical structures showing the different ionization states of fluorescein.	173
Scheme 8.5	Synthesis reaction of PSPMA.	174
Scheme 8.6	Synthesis reaction of PFI.	175
Figure 8.1	Absorption spectra of the solvents used to swell the ionogels.	177
Figure 8.2	Absorption spectra of the different solvents used for the swelling of the ionogels after the 1st swelling process. Insert shows a zoom in of the 350-600nm region.	177
Figure 8.3	Absorption spectra of PIL ionogels after being swollen in different solvents.	178
Figure 8.4	Excitation (left) and emission (right) spectra of the different solvents used for the swelling of the ionogels after the 1st swelling process.	179
Figure 8.5	Excitation (left) and emission (right) spectra of the different solvents used for the swelling of the ionogels after the 2nd swelling process.	180
Figure 8.6	Excitation (left) and emission (right) spectra of the PFI ionogels when hydrated in PBS buffer (pH 7.4).	181
Scheme 8.7	Reaction scheme for the synthesis of cholinium acrylate.	184
Figure 8.7	The different types of cone matrixes that will be used as templates for the PIL -PEDOT structures.	186
Scheme 8.8	The polymerization of EDOT by immersion in molten iron chloride hexahydrate.	187

- Figure 8.8** (Top) Side view of the glass slide showing: (a) the sputter-coated gold layer, (b) the printed flat square with the conical structures, and (c) the area which will be used to grow cells on; (Bottom) Top view of the final micro-electrode array platform after 3D printing, showing the gold sputter coated areas, and the hydrogel platform featuring the conical microelectrode array. **188**
- Figure 8.9** (Top) Side view of the ITO glass slide showing: (a) the ITO layer, (b) the printed hydrogel platform with the conical microstructured electrodes printed on top, also showing the channel where the ITO was etched away, and (c) which is the exposed space that will be used to grow cells on; (Bottom) Top view of the final 3D printed micro-electrode array platform, showing the region where the ITO covered areas, the area where the ITO was stripped away, and the hydrogel platform featuring the microstructured cone array. **189**
- Figure A.8.1** The NMR spectra of the tetrabutylphosphonium sulfopropylmethacrylate **196**
- Figure A.8.2** The NMR spectrum of the fluorescein salt of trihexyltetradecylphosphonium **197**
- Figure A.8.3** Absorption spectra of the different solvents used for the swelling of the ionogels after the 2nd swelling process. **198**
- Figure A.8.4** Absorption spectra of the different solvents used for the swelling of the ionogels after the 3rd swelling process. **198**

List of Tables

Table 2.1	Ionic liquid names and abbreviations	33
Table 3.1	Surface tension measurements of solutions used in the study, with and without the IL surfactant added.	66
Table 3.2	Loss and storage modulus of the hydrogels at 25 °C after 180 s of white light irradiation	75
Table 3.3	The effect of increasing amount of linear p(NiPAAm-BSP-AA) copolymer on the hydration properties of the hydrogels.	75
Table 3.4	Salt-induced shrinking of the hydrogels in area % compared to DI water.	79
Table 3.5	Temperature induced shrinking of the sIPNs in DI Water.	81
Table 4.1	Experimental shrinking and swelling rate constants.	99
Table 5.1	Monomeric cocktail composition.	113
Table 8.1	Cholinium acrylate monomer mixtures.	185

Alexandru Tudor

Thermophysical Behaviour and Applications of Crosslinked Poly(ionic liquid)s

Thesis abstract:

Ionic liquids (ILs) were discovered in 1914 by Paul Walden when he synthesized ethylammonium nitrate, which was the first salt to be liquid at room temperature. After this point the field of ILs enjoyed a surge in popularity. The main reasons for this interest came from the physical and chemical properties of ionic liquids, including high chemical, thermal and electric stability, negligible vapour pressure, very good dissolution properties and highly tunable configuration, respectively. Based on these properties, ILs with applications in catalysis, solvation, and electrochemistry were developed. At the turn of the 20th century, the first paper published on polymerizable ILs (PILs) appeared. This opened up a new research direction that has just recently started getting more attention.

This thesis focuses on presenting the synthesis, characterisation and potential applications of novel stimuli-responsive materials based on PILs and crosslinked PILs. Chapter 1 will offer a brief overview of the field of ILs and PILs in particular, and Chapter 2 will discuss possible application of such materials in microfluidic devices. Chapter 3 will describe the synthesis of temperature-responsive crosslinked PIL hydrogels which serve as a host matrix for a linear photo-responsive poly(N-isopropylacrylamide) based polymer. Moreover, the resulting composite stimuli-responsive material will be characterized to determine its response to temperature, light and salt concentration, respectively. Chapter 4 focuses on the integration of the temperature-responsive PIL matrix in a microfluidic device as a temperature controlled valve, and Chapter 5 will demonstrate the printing of such materials using Direct Laser Writing technologies. Chapter 6 and 7 will focus on the synthesis and thermal characterization of a novel crosslinked cholinium PIL hydrogel and its integration in paper-based microfluidic devices as passive pumps (Chapter 7). Chapter 8 describes future work in the area of PILs and PIL hydrogels.

Chapter 1: Literature Overview

Crosslinked Poly(Ionic Liquid)s as Building Blocks for Stimuli-Responsive and Functional Materials

1.1 Introduction to ionic liquids and poly(ionic liquid)s

1.2 Application overview of poly(ionic liquid)s

1.2.1 Ionic conductors

1.2.2 Nanoparticles

1.2.3 Temperature – responsive materials

1.3 Aims of this work

1.4 References

Chapter 1

Literature Overview

Crosslinked Poly(Ionic Liquid)s as Building Blocks for Stimuli-Responsive and Functional Materials

1.1 Introduction to Ionic Liquids and Poly(Ionic Liquid)s

Ionic liquids (ILs) are defined as salts that have a melting point lower than 100 °C [1-10]. The first such material was synthesised in 1914 by Paul Walden [1,3,8]. He discovered that ethylammonium nitrate (EAN) has a melting point of 12 °C and is composed of anions and cations [1,3,8]. Since then until the beginning of the nineties, the number of journal articles published on the subject of ILs was below 20 per year [1]. Since the early '90 however, the rates at which journal articles on ILs were published grew steeper than an exponential growth, until it started showing signs of plateauing in the last couple of years [1]. This outstanding increase in the number of outputs published on ILs resulted due to their physical and chemical properties, such as negligible vapour pressure, ionic conductivity, high thermal and chemical stability, their ability to be very good solvents for a wide range of compounds and their inherent structural and synthetic versatility [1-3,8,11]. The enthusiasm regarding ILs as solvents was summarised in 1997 by Kenneth R. Seddon who described ILs as being able to be designed by scientists in such a way as to control and optimize a chemical reaction, both in its yield as well as in its selectivity, according to the needs of the scientist. For this reason, ionic liquids have been termed "designer solvents" [11]. This statement still holds true, just by taking into account that the approximate number of possible ILs is estimated to be in the range of $\sim 10^{18}$ [1,8]. Even so, ILs still have not been widely adopted in industry, mainly due to their price, which relegates them to be used in niche applications, while in academia they still represent one of the most researched groups of materials [1-3].

ILs are typically categorized in two subgroups: protic and aprotic [2,3,8]. The first subgroup features ILs that are synthesised by a neutralization reaction between a Brønsted acid and a Brønsted base [2]. Such an example is EAN, which is synthesised by reacting ethylamine with nitric acid [3,8]. Aprotic ILs are usually synthesised either by a quaternization reaction or a metathesis reaction between an IL that contains a halide salt and an alkaline, typically a silver or an ammonium salt that features the desired anion [3,8].

The most commonly used ionic liquids are based on imidazolium, ammonium, pyridinium, pyrrolidinium and phosphonium cations, respectively (Figure 1.1) [3]. Common anions are halides, organic sulphates, carboxylic acid derivatives, cyanide compounds such as dicyanamide (DCA) and fluoride compounds such as:

hexafluorophosphate, tetrafluoroborate and bis(trifluoromethane)sulfonimide (TFSI), respectively (Scheme 1.1) [3].

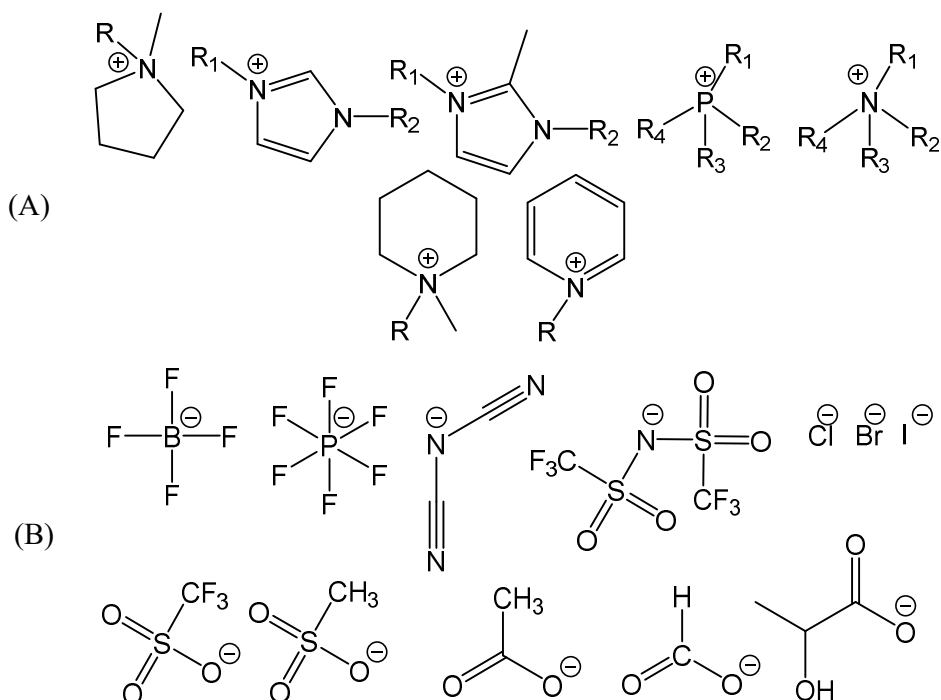


Figure 1.1 Chemical structures of the most common cations and anions used in ILs (from left to right): (A) pyrrolidinium, imidazolium, 2-methyl-imidazolium, phosphonium, ammonium, piperidinium, pyridinium; (B) tetrafluoroborate, hexafluorophosphate, dicyanamide, bis(trifluoromethane)sulfonimide, chloride, bromide, iodide, trifluoromethanesulfonate, methanesulfonate, acetate, formate and lactate, respectively.

If either the anion, the cation or both feature a polymerizable group, then that ionic liquid is classified as an ionic liquid monomer (ILM), which can be polymerized to synthesize a poly(ionic liquid) (PIL) [4-7,9,10,12-17]. This subset of ILs has just recently started gathering more and more interest, but can still be considered just a niche subclass of ILs. If publications for ILs can reach a number of a 120 per week [1], the number for PIL publications in the whole year of 2012 was ~80, but even so the rate of publication is growing [10]. To put this into perspective, in 2008 the number of published articles on PILs was ~20, in 2011 there were ~40 published, while from 2013 till 2016 there were ~400 peer-reviewed studies published. The data for 2011 and 2013-2016 was based on a search performed on the Thompson-Reuters

webofknowledge.com citation search engine using “poly(ionic liquid)” as the search term.

PILs can be categorized based on different criteria, but most commonly two criteria are used. The first criterion is based on which ion possesses the polymerizable group – meaning that there are cationic and anionic PILs (Figure 1.2) [6]. The second criterion is based on the presence or absence of a crosslinking agent used during the polymerization phase of the PILs, which leads to either crosslinked or linear PILs. Crosslinked PILs (xPILs) are commonly featured in review publications together with PILs without necessary having them treated as a separate category of materials [4,6,9,10].

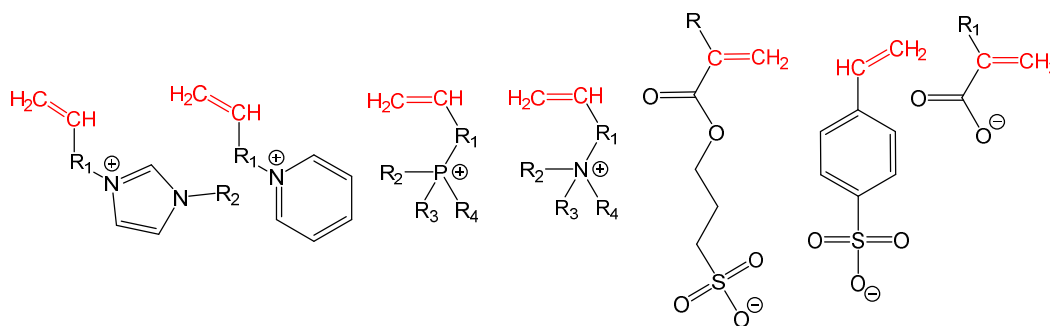


Figure 1.2 The structure of the most common cationic and anionic ILM: (from left to right) vinylimidazolium, vinylpyridinium, vinylphosphonium, vinylammonium, sulfopropylacrylate, acrylate.

The aim of the following section is to address the xPIL category of materials separately by describing some of the already synthesized xPILs and their possible applications and, following this, to try to expand the current application profile of this category of materials.

1.2 Application overview of crosslinked Poly(Ionic Liquid)s

1.2.1 Ionic Conductors

Radical polymerization is the most common method of polymerization for both linear and crosslinked PILs[4-6,9,10,18,19]. In the first paper ever published on xPILs by Yoshizawa *et al.*, two ILMs that featured polymerizable groups in both the

anion and the cation were synthesized by neutralizing vinylimidazole with sulfonic acid derivatives that featured vinyl groups (Figure 1.3)[14].

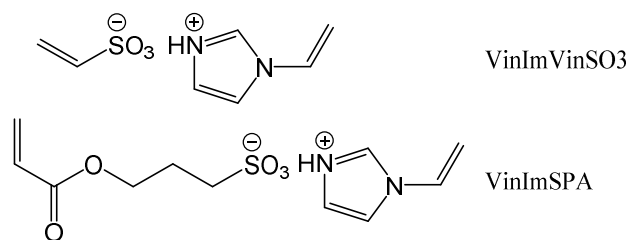
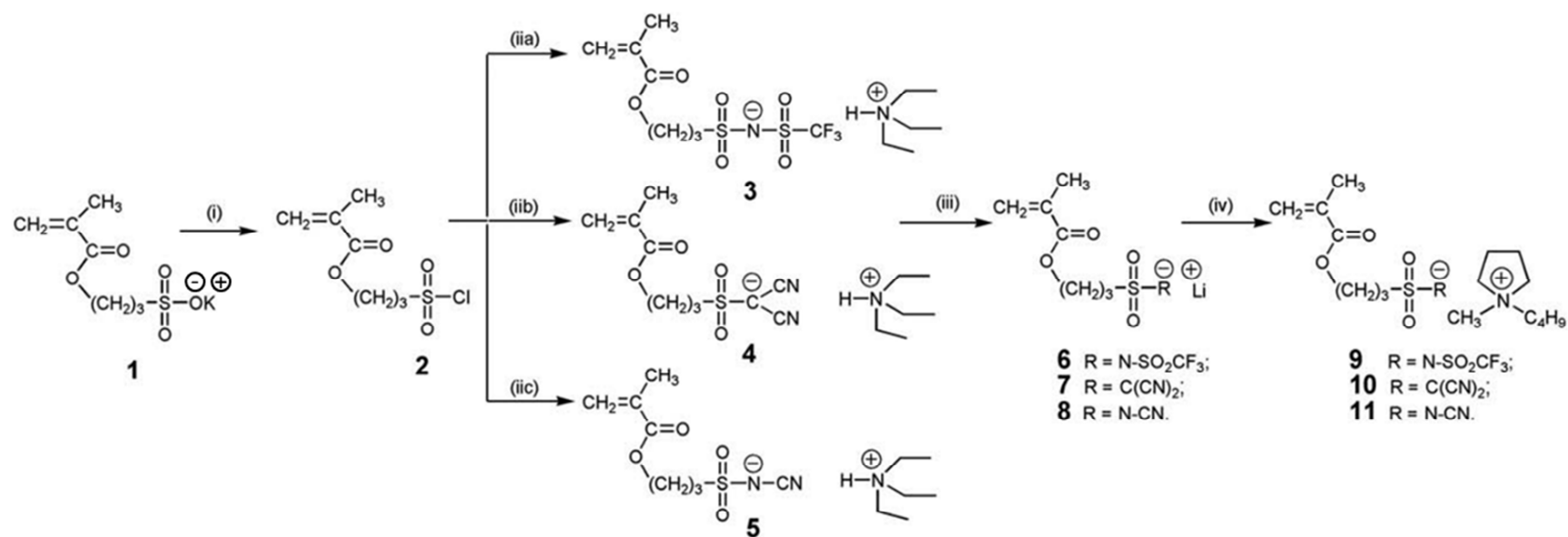


Figure 1.3 Chemical structure of the ILMs used by Yoshizawa *et al.* in [14].

Based on this synthetic method, the ionic liquid polymers can be classified as protic ILs. The scope of the study was to synthesize novel polymer electrolytes by radical polymerization of the two aforementioned ILMs. In monomeric form, they feature high ionic conductivity ($\sim 10^{-6} \text{ S}\cdot\text{cm}^{-1}$). The results indicated that poly(VinImVinSO₃), which was obtained by a 24h polymerization process, had a conductivity in the region of $10^{-9} \text{ S}\cdot\text{cm}^{-1}$. This value was found to be improved by the addition of lithium bis(trifluoromethane)sulfonimide (LiTFSI) to $10^{-6} \text{ S}\cdot\text{cm}^{-1}$, when an equimolar amount to the VinImVinSO₃ ILM was added. After polymerizing VinImSPA, the same value for the ionic conductivity was obtained as for the poly(VinImSPA):LiTFSI = 1:1 molar mixture. The differences between the two xPILs appeared when the amount of LiTFSI was increased above the 1:1 molar ratio: in the case of poly(VinImVinSO₃) the ionic conductivity remained $\sim 10^{-6} \text{ S}\cdot\text{cm}^{-1}$, while for poly(VinImSPA) it was increased to $10^{-5} \text{ S}\cdot\text{cm}^{-1}$. This increase in conductivity was attributed to the spacer that appears between the vinyl group and the sulfonium group in the VinImSPA monomer, which increases the amount of freedom that exists between the polymer chains, enabling the LiTFSI ions to have more freedom.

Using the same sulfopropylacrylate (SPA) anion, Shaplov *et al.* published a study on the design and synthesis of a new classes of SPA-derived anionic xPILs that would feature conductivities similar to ionic liquids which possess TFSI, DCA and tricyanomethanide anions, respectively, which are known to exhibit high conductivities[19]. The synthesis routes for these materials can be seen in Scheme 1.1.

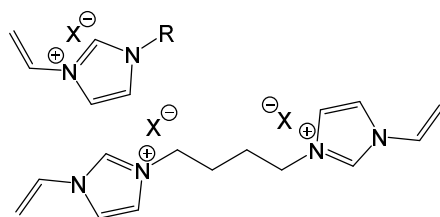


Scheme 1.1. Synthetic route for the preparation of monomers 9, 10 and 11. Reagents and conditions: (i) SOCl₂, THF/DMF, 0 °C→RT; (iia) NH₂SO₂CF₃, THF, NEt₃, 0°C→RT; (iib) CH₂(CN)₂, THF, NEt₃, 0°C→RT; (iic) NH₂CN, THF, NEt₃, 0°C→RT; (iii) LiH, THF, 10°C→RT; (iv) 1.4 [1-Bu-1-Me Pyr]Br, H₂O, RT. Reproduced from [19].

The polymerization reaction was performed by using temperature-induced radical polymerization with azobisisobutyronitrile (AIBN), just as described previously by Yoshizawa *et al.* [14]. The crosslinking was performed using long chain poly(ethylene glycol) dimethacrylates (PEGDM) and methyl ethyl dimethacrylates (PEGM). The resulting polymers featured an ionic conductivity of $\sim 10^{-6} \text{ S}\cdot\text{cm}^{-1}$ when cross-linked using 20% w/w PEGDM and 10% w/w PEGM, and an ionic conductivity of $\sim 10^{-7} \text{ S}\cdot\text{cm}^{-1}$ when 30% w/w PEGDM was used as crosslinker. These results indicate that having an anionic xPIL that features a delocalized charge on its anion together with a free imidazolium cation can produce a material with an ionic conductivity three orders of magnitude higher compared with the first published results on this type of material [14], without the need of adding an external salt to act as a charge carrier.

1.2.2 Nanoparticles

Imidazolium-based ionic liquids were the new class of ILs discovered at the start of the nineties that triggered a massive surge in interest towards this research field [20]. Based on their popularity, ILMs based on vinyl-imidazolium are also common and represent the focus of extensive studies [6,9,10,19,21,22]. One way of determining the nanoscale properties of imidazolium PILs would be to make use of the radical polymerization in emulsion, due to its ability to obtain polymer nanoparticles with low polydispersity. In the case of xPILs, a study was performed by Koebe *et al.* to determine the inner structure and morphology of nanoparticles based on such ILMs [23]. They used long chain vinyl imidazolium ILMs and di-vinyl imidazolium crosslinkers (Figure 1.4) to create nanoparticles by dispersion polymerization using temperature-induced radical polymerization with 2,20-azobis[2-methyl-N-(2-hydroxyethyl)propionamide] (VA86) as the initiator.



R = tetradecyl, hexadecyl or octadecyl
X = bromide or dicyanamide

Figure 1.4. Chemical structures of the ILMs used by Koebe et al. in [23].

The nanoparticles were obtained by stirring an aqueous suspension of the monomer mixtures with 3% w/w VA86 thermal initiator for 24h at 70 °C in an oil bath. The resulting xPILs remained suspended in the aqueous medium. By using cryo-TEM, the morphology and the inner structure of the xPILs were determined (Figure 1.5).

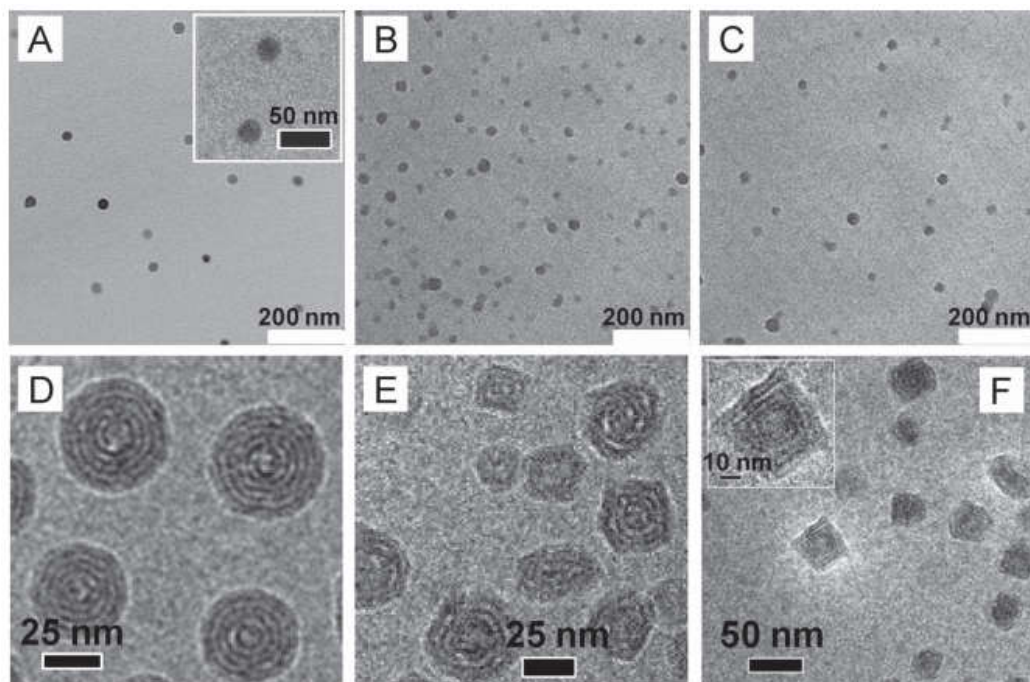


Figure 1.5. TEM (top) and cryo-TEM (bottom) characterization of the synthesized poly(ILM-C14Br/C) (A&D), poly(ILM-C16Br/C) (B&E), poly(ILM-C18Br/C) (C&F) poly(ionic liquid) nanoparticles via dispersion polymerization of the corresponding ionic liquid monomers with 10% of divinylimidazolium bromide crosslinker. The abovementioned PILs represent the bromide salts of the tetradecyl, hexadecyl and octadecyl vinylimidazolium derivatives. Reproduced from [23].

Regardless of the ILM and crosslinker used, all nanoparticles feature a very ordered multilamellar inner structure, which presents dark bands that appear due to the charged nature of the imidazolium and bromide ions. This ordered structure appears due to the simultaneous events of self-assembly and polymerization that take

place in the monomer mixture. The ILMs have an amphiphilic nature, thus they self-assemble into micelles. After the temperature is raised, the initiator starts creating polymerization nuclei that are stabilized by the ILMs into a closed shell. Following this, the shell is polymerized along with the crosslinkers and is again stabilized by a new shell of ILMs [23]. Following the explanation of this effect, the authors determine that the size of the nanoparticles can be increased and the morphology of the nanoparticles tuned, by increasing the amount of tetradecyl monomer used or crosslinker used, or by the addition of a foreign bromide salt, or by increasing the amount of DCA anion present in the monomer mixture, respectively. The applications of these nanoparticles were envisioned to be as templates or carrier systems for different purposes.

1.2.3 Thermo – Responsive materials

One particular class of stimuli-responsive systems that received a lot of attention in the last two decades are polymeric materials that feature a lower critical solution temperature (LCST). One of the most studied polymers possessing this property is poly(N-isopropylacrylamide) (pNiPAAm) [24,25]. At ambient pressure, an aqueous solution of this polymer precipitates at temperatures around 32 °C [26].

ILs and PILs that feature the same property in an aqueous medium were synthesized and extensively characterized by Kohno *et al.* in 2011 [27] and 2012 [28]. They found that the tetrabutyl phosphonium cation, together with 4-methylbenzenesulfonate; 2,4-dimethylbenzenesulfonate; 2,4,6-trimethylbenzenesulfonate and trifluoroacetate anions (Figure 1.6, A, B, C, D) display an LCST when dissolved in water and heated up to 54 °C, 36 °C, 30 °C and 30 °C, respectively [27]. By exchanging the anion to styrenesulfonate (Scheme 1.6, E), an anionic ILM, namely tetrabutyl phosphonium styrenesulfonate (P_{4,4,4,4}SS) was synthesized and further characterized [28]. It was discovered that a 50% w/w aqueous solution of P_{4,4,4,4}SS displays an LCST at 34 °C. Polymerization of P_{4,4,4,4}SS in suspension together with AIBN at 80 °C for 3h, followed by purification, resulted in a PIL that formed a transparent solution when dissolved in water in a 10% w/w ratio at RT. By heating the solution to 57 °C a white precipitate started forming, and the

processed stopped at 59 °C, when the solution was completely opaque. By cooling the solution down to 56 °C, the solution became clear again. The research group also determined that by increasing the length of one of the alkyl chains found on the phosphonium cation, the LCST of the monomer and the resulting polymer can be lowered. In their example, it was found that a 10% w/w aqueous solution of a copolymer synthesised by the copolymerisation of 70% w/w tetrabutylphosphonium styrenesulfonate ($P_{4,4,4,4}SS$) with 30% w/w tributylhexyl styrenesulfonate ($P_{4,4,4,6}SS$) has an LCST lowered to 39 °C from 57 °C in the absence of $P_{4,4,4,6}SS$.

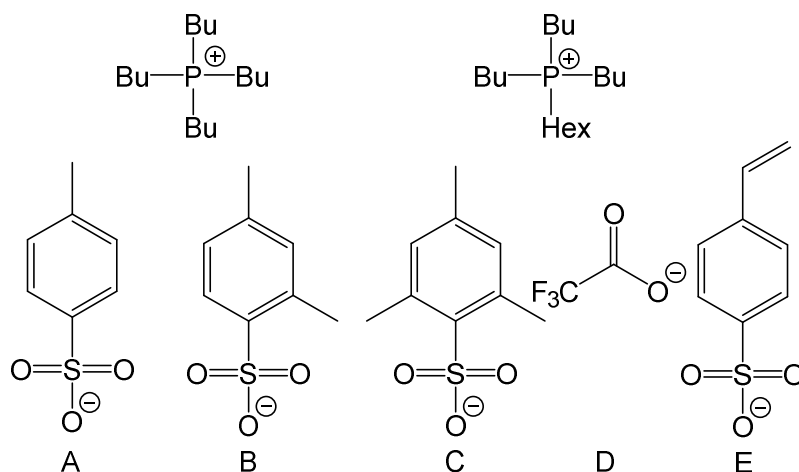


Figure 1.6. Chemical structures of the ILs and ILMs that were found to possess a lower critical solution temperature.

Following up on this study, in our group, Ziółkowski *et al.* were the first to synthesize an xPIL that featured a phosphonium ILM which possessed a LCST [29]. The study focused on synthesizing an xPIL based on the $P_{4,4,4,4}SS$ ILM and a new ILM, namely tributylhexyl sulfopropylacrylate ($P_{4,4,4,6}SPA$). These two ILMs were combined with several crosslinkers of varying length and composition: N,N'-methylenebisacrylamide (MBIS), poly(ethylene glycol) diacrylate ($M_w \sim 300 \text{ g}\cdot\text{mol}^{-1}$ and $\sim 800 \text{ g}\cdot\text{mol}^{-1}$, PEG256 and PEG700) and poly(propylene glycol) diacrylate ($M_w \sim 900 \text{ g}\cdot\text{mol}^{-1}$, PPO800). By adding a photoinitiator to the monomer mix, several types of xPILs were photopolymerized. The resulting crosslinked polymers were swollen in deionized water with different results: the polymers using 5 mol% and 10 mol% MBIS or 5 mol% PEG256, respectively did not crosslink properly and ended up disintegrating into small fragments upon hydration. However, polymers

crosslinked using 5 mol% PEG700 or PPO800 formed stable, transparent swollen polymers – xPIL hydrogels. Following this, their LCST was determined using differential scanning calorimetry. The results indicated that instead of having a sharp peak at a precise temperature value, which is typical for pNiPAAm[26] or for the ILMs and linear PILs previously discussed [27,28], a ~40 °C wide temperature interval was observed in which the xPIL hydrogels shrunk continuously until they reach their minimum size. The results were similar for both the styrenesulfonate and the sulfopropylacrylate based xPILs. Based on the different hydrophobicity of the two xPILs, the styrenesulfonate polymer started its transition at a higher temperature compared to the sulfopropylacrylate one.

Gallagher *et al.* continued researching the topic of thermo-responsive xPILs and explored to improve the thermo-response of aforementioned phosphonium sulfopropylacrylate xPIL hydrogels by adding a linear pNiPAAm polymer in the xPIL matrix, thus creating a semi-interpenetrating network (sIPN) [30]. The resulting hydrogels were characterized by differential scanning calorimetry (DSC) and digital microscopy. The results indicated that the hydrogels containing an amount of 1.2 molar units of linear pNiPAAm compared to the amount of phosphonium sulfopropyl acrylate tended to shrink overall to a greater extent when heated to 70 °C, while also displaying a more pronounced endothermic peak in the DSC analysis. The addition of linear pNiPAAm to the xPIL matrix also increased the hydrogels' swelling capacity.

Another research article that deals with thermo-responsive materials was published by Zhou *et al.* and it describes the synthesis of a crosslinked poly[oligo(ethyleneglycol)methacrylate-vinyl imidazolium) copolymer that was crosslinked by an in-situ quaternization reaction with 1,4-dibromobutane [31]. The aim of this study was to use conventional FTIR and perturbation correlation moving window FTIR together with two-dimensional correlation analysis, to determine the transition mechanism between the hydrated hydrogels and the dehydrated hydrogels. In the case of low crosslinked hydrogels, there is a sharp volume transition due to a cooperative response of the C-H, C=O and the C-O-C groups. In the case of the highly crosslinked hydrogels, there is a broad volume transition that appears due to C=O and C-O-C hydrogen bond breakage, together with the dehydration of the C-H groups. This study offers valuable insights about the mechanism behind the temperature-response of hydrogels that are crosslinked using an ionic liquid, which, in extension, could be used to understand the mechanism present in xPIL systems.

1.3 References

1. Deetlefs, M.; Faselow, M.; Seddon, K.R. Ionic liquids: The view from mount improbable. *RSC Advances* **2016**, *6*, 4280-4288.
2. Greaves, T.L.; Drummond, C.J. Protic ionic liquids: Evolving structure–property relationships and expanding applications. *Chemical Reviews* **2015**, *115*, 11379-11448.
3. Hayes, R.; Warr, G.G.; Atkin, R. Structure and nanostructure in ionic liquids. *Chemical Reviews* **2015**, *115*, 6357-6426.
4. Kohno, Y.; Saita, S.; Men, Y.; Yuan, J.; Ohno, H. Thermoresponsive polyelectrolytes derived from ionic liquids. *Polymer Chemistry* **2015**.
5. Lu, J.; Yan, F.; Texter, J. Advanced applications of ionic liquids in polymer science. *Progress in Polymer Science* **2009**, *34*, 431448.
6. Mecerreyes, D. Polymeric ionic liquids: Broadening the properties and applications of polyelectrolytes. *Progress in Polymer Science* **2011**, *36*, 1629-1648.
7. Vygodskii, Y.S.; Mel'nik, O.A.; Shaplov, A.S.; Lozinskaya, E.I.; Malyshkina, I.A.; Gavrilova, N.D. Synthesis and ionic conductivity of polymer ionic liquids. *Polymer Science Series A* **2007**, *49*, 256-261.
8. Welton, T. Room-temperature ionic liquids. Solvents for synthesis and catalysis. *Chemical reviews* **1999**.
9. Yuan, J.; Antonietti, M. Poly(ionic liquid)s: Polymers expanding classical property profiles. *Polymer* **2011**, *52*.
10. Yuan, J.; Mecerreyes, D.; Antonietti, M. Poly(ionic liquid)s: An update. *Progress in Polymer Science* **2013**.
11. Seddon, K.R. Ionic liquids for clean technology. *Journal of Chemical Technology and Biotechnology* **1997**, *68*, 351-356.
12. Hirao, M.; Ito-Akita, K.; Ohno, H. Polymerization of molten salt monomers having a phenylimidazolium group. *Polymers for Advanced Technologies* **2000**, *11*, 534-538.
13. Hirao, M.; Ito, K.; Ohno, H. Preparation and polymerization of new organic molten salts; n-alkylimidazolium salt derivatives. *Electrochimica Acta* **2000**, *45*, 1291-1294.
14. Yoshizawa, M.; Ohno, H. Synthesis of molten salt-type polymer brush and effect of brush structure on the ionic conductivity. *Electrochimica Acta* **2001**, *46*, 1723-1728.
15. Zhao, F.; Meng, Y.; Anderson, J.L. Polymeric ionic liquids as selective coatings for the extraction of esters using solid-phase microextraction. *Journal of Chromatography A* **2008**, *1208*, 1-9.
16. Zhao, Q.; Wajert, J.C.; Anderson, J.L. Polymeric ionic liquids as co₂ selective sorbent coatings for solid-phase microextraction. *Analytical Chemistry* **2009**, *82*, 707-713.
17. Green, O.; Grubjesic, S.; Lee, S.; Firestone, M.A. The design of polymeric ionic liquids for the preparation of functional materials. *Polymer Reviews* **2009**, *49*, 339-360.

18. Hsieh, Y.-N.; Kuei, C.-H.; Chou, Y.-K.; Liu, C.-C.; Leu, K.-L.; Yang, T.-H.; Wang, M.-Y.; Ho, W.-Y. Facile synthesis of polymerized ionic liquids with high thermal stability. *Tetrahedron Letters* **2010**, *51*, 3666-3669.
19. Shaplov, A.S.; Lozinskaya, E.I.; Ponkratov, D.O.; Malyshkina, I.A.; Vidal, F.; Aubert, P.-H.; Okatova, O.g.V.; Pavlov, G.M.; Komarova, L.I.; Wandrey, C., *et al.* Bis(trifluoromethylsulfonyl)amide based “polymeric ionic liquids”: Synthesis, purification and peculiarities of structure–properties relationships. *Electrochimica Acta* **2011**, *57*, 74-90.
20. Wilkes, J.S.; Zaworotko, M.J. Air and water stable 1-ethyl-3-methylimidazolium based ionic liquids. *Journal of the Chemical Society, Chemical Communications* **1992**, *0*, 965-967.
21. Yoshizawa, M.; Narita, A.; Ohno, H. Design of ionic liquids for electrochemical applications. *Australian Journal of Chemistry* **2004**, *57*, 139.
22. Ogihara, W.; Washiro, S.; Nakajima, H.; Ohno, H. Effect of cation structure on the electrochemical and thermal properties of ion conductive polymers obtained from polymerizable ionic liquids. *Electrochimica Acta* **2006**, *51*, 2614-2619.
23. Koebe, M.; Drechsler, M.; Weber, J.; Yuan, J. Crosslinked poly(ionic liquid) nanoparticles: Inner structure, size, and morphology. *Macromolecular Rapid Communications* **2012**, *33*, 646-651.
24. Rzaev, Z.M.O.; Dinçer, S.; Pişkin, E. Functional copolymers of n-isopropylacrylamide for bioengineering applications. *Progress in Polymer Science* **2007**, *32*, 534595.
25. Ionov, L. Hydrogel-based actuators: Possibilities and limitations. *Materials Today* **2014**, *17*, 494-503.
26. Maeda, Y.; Higuchi, T.; Ikeda, I. Ftir spectroscopic and calorimetric studies of the phase transitions of n-isopropylacrylamide copolymers in water. *Langmuir* **2001**, *17*, 7535-7539.
27. Kohno, Y.; Arai, H.; Saita, S.; Ohno, H. Material design of ionic liquids to show temperature-sensitive lcst-type phase transition after mixing with water. *Australian Journal of Chemistry* **2011**, *64*, 1560.
28. Kohno, Y.; Deguchi, Y.; Ohno, H. Ionic liquid -derived charged polymers to show highly thermoresponsive lcst-type transition with water at desired temperatures. *Chemical Communications* **2012**, *48*, 11883-11885.
29. Ziółkowski, B.; Diamond, D. Thermoresponsive poly(ionic liquid) hydrogels. *Chemical Communications* **2013**, *49*, 10308.
30. Gallagher, S.; Florea, L.; Fraser, K.; Diamond, D. Swelling and shrinking properties of thermo-responsive polymeric ionic liquid hydrogels with embedded linear pnipaaam. *International Journal of Molecular Sciences* **2014**, *15*, 53375349.
31. Zhou, Y.; Tang, H.; Wu, P. Volume phase transition mechanism of poly[oligo(ethylene glycol)methacrylate] based thermo-responsive microgels with poly(ionic liquid) cross-linkers. *Physical Chemistry Chemical Physics* **2015**, *17*, 25525-25535.

Chapter 2: Application of Ionic Liquid Materials in Microfluidic Devices

2.1 Abstract

2.2 Introduction

2.3 Ionic Liquids for Actuators

2.3.1 Microvalves

2.3.2 Delaying Pumps

2.4 Ionic Liquids for Sensing

2.4.1. Chemical Sensing

2.4.2. Physical Sensing

2.5 Other Applications in Microfluidics

2.5.1. Ionic Liquids for Nanoparticle Synthesis in Microfluidics

2.5.2. Ionic Liquids for Building a Microfluidics-based Power Generator

2.5.3. Ionic Liquids for Precise Temperature Control in Microfluidics

2.6 Conclusions

2.7 References

Chapter 2

Application of Ionic Liquid Materials in Microfluidic Devices^{*}

*Application of Ionic Liquid Materials in Microfluidic Devices, T. Akyazi, J. Saez, A. Tudor, C. Delaney, W. Francis, D. Diamond, L. Basabe-Desmonts, L. Florea, F. Benito-Lopez, submitted as a chapter for the *Smart Ionic Liquid* book set, RSC Publishing, ISBN 978-1-78801-181-5, 2017.

2.1 Abstract

The following chapter focuses on the application of ionic liquids and ionic liquid derived materials in microfluidics. Ionic liquids have several attractive physical and chemical properties that would recommend them for use in this type of devices. These properties include: good chemical and physical stability, ionic conductivity and negligible vapour pressure. Moreover, most of these properties can be finely tuned by changing one of the constituent ions. Due to this high structural and synthetic versatility, the following study is split into different subchapters, each of which focuses in detail on the use of these ILs for different applications in microfluidics, such as: chemical and physical sensing, microfluidic control mechanisms (valves and pumps), and in more niche applications, such as in-situ synthesis of nanomaterials.

2.2 Introduction

Ionic liquids are drawing an increasing interest both in academia and in industry as confirmed by the growing number of publications and patents in the area [1,2]. Ionic liquids (ILs) are salts, completely constituted of ions with melting temperatures below 100 °C, which is a result of their low-charge density and low symmetry ions [1,3-5]. ILs are categorised as “green” solvents since they are, potentially, green alternatives to volatile organic compounds due to mainly their two outstanding properties: negligible volatility and conventional non flammability [4-7]. Their unique properties are not limited to non-volatility and non-flammability; they have an excellent solvation ability for organic, inorganic and organometallic compounds with improved selectivity, high thermal stability (decomposition temperatures around 300–500 °C), high chemical stabilities (extremely redox robust), and lastly, high ionic conductivity all of which highly extends the variety of their applications [1-3,8-15]. Nevertheless, other properties, such as biodegradability and toxicity are not yet successfully overtaken, and they should be considered in ILs applications [6].

One of the main advantages concerning the applicability of ILs is the ability tailor their physical and chemical properties (such as their polarities and affinities, their thermo-physical properties, biodegradation ability or toxicological features, as well as their hydrophobicity and solution behaviours) by a proper manipulation of the cation/anion chemical structure [16-21]. This feature gives them the name of

'designer solvent' and favours their use, particularly in the extraction, separation and analysis of value-added compounds from biomass [1-3,17,22]. Moreover, these tuneable properties are enabling rapid advances in devices and processes for the production, storage and efficient use of energy[1,23].

In many applications, the immobilisation of ILs in a solid or semisolid substrate, while keeping their specific properties, is a main requirement in order to generate useful devices. This is possible by the introduction of a new class of hybrid materials, ionogels. Ionogels preserve the important properties of the ILs (liquid-like dynamics and ion mobility) in a solid or a gel like structure, enabling easy shaping, manipulation and integration, increasing remarkably the potential application of ILs in fundamental areas such as energy, environment and analysis [24,25].

In recent years, researchers decided to make use of the exceptional features of ILs and ionogels in the microfluidics area and many papers which include the incorporation of ILs materials in microfluidic systems have been published. "Lab-on-a-chip" (LOC) / "micro-Total Analysis Systems" (μ TAS) or microfluidic (continuous flow, microarray and droplet-based) analysis systems empower the manipulation of fluids at small scales (from a few micrometres up to a millimetre) and small volumes (nanoliters to picoliters). Microfluidic devices run a series of fluidic unit operations on a platform which is designed with a well-defined fabrication technology and provide a consistent approach for miniaturisation, integration, automation and parallelisation of biochemical processes [26,27]. They have the greatest capability of integration of multiple functional elements into a small structure to produce absolute sample-in/answer-out systems [26]. The incorporation of functionalities such liquid handling, temperature control and detection components for sensing allows fast analysis and improves selectivity compared to conventional devices [26,27]. Nevertheless, the development of fully integrated microfluidic devices is still facing some compelling obstacles, including fluidic control, miniaturisation and high costs [26,28]. Considering the critical requirement of fluid control and fluid transport processes and high detection performance within these platforms, microfluidic devices have adopted a wide range of passively or actively controlled, high performance components, such as microfluidic separators, actuators (valves and pumps), reactors, sample/biomolecule storage, sensing elements which are although sophisticated and achieve their tasks efficiently, are as well costly, highly increasing the price and so decreasing the final market possibilities of microfluidic devices.

Ionic liquids have excellent properties that could be used to improve microfluidic devices, since they are low-cost, easily obtainable materials. Their features make them very good and multifunctional candidates for improving the capabilities of microfluidic devices by building miniaturised / passive microfluidic elements for fluid control, sensing, sample storage, microfluidic separation, microreactors (nanoparticle synthesis), power generators, temperature controllers, electrowetting of surface, etc., whereas decreasing the manufacturing costs compared with conventional devices and widens the market possibilities. In this chapter we will look over the fundamental applications of ionic liquids within microfluidic devices.

Table 2.1 Ionic liquid names and abbreviations

Ionic liquid name	Abbreviation
triisobutyl(methyl) phosphonium tosylate	[P _{1,4,4,4}][Tos]
tetrabutylphosphonium dicyanamide	[P _{4,4,4,4}][DCA]
trihexyltetradecyl phosphonium dicyanamide	[P _{6,6,6,14}][DCA]
trihexyltetradecyl phosphonium bis(trifluoromethanesulfonyl) imide	[P _{6,6,6,14}][Ntf ₂]
trihexyltetradecyl phosphonium dodecylbenzenesulfonate	[P _{6,6,6,14}][DBSA]
trihexyltetradecyl phosphonium chloride	[P _{6,6,6,14}][Cl]
1-Methyl-3-octylimidazolium tetrafluoroborate	[OMIM][BF ₄]
1-ethyl-3-methylimidazolium methyl sulphate	[EMIM][MeSO ₄]
1-ethyl-3-methyl imidazolium ethyl sulphate	[EMIM][EtSO ₄]
1-butyl-3-methylimidazolium hydrogen sulphate	[BMIM][HSO ₄]
1-ethyl-3-methyl imidazolium tetrafluoroborate	[EMIM][BF ₄]
1-ethyl-3-methylimidazolium dicyanamide	[EMIM][DCA]
1-Butyl-3-methylimidazolium tetrafluoroborate	[BMIM][BF ₄]
1-Butyl-3-methylimidazolium hexafluorophosphate	[BMIM][PF ₆]
1-Butyl-3-methylimidazolium dodecanesulphonate	[BMIM][DoS]
1-Butyl-3-methylimidazolium bis(trifluoromethanesulfonyl)imide	[BMIM][NTf ₂]
1-Hexyl-3-methylimidazolium bis(trifluoromethanesulfonyl)imide	[HMIM][NTf ₂]
1-Butyl-butyl-4-methylpyridinium tetrafluoroborate	[BMPy][BF ₄]

2.3 Ionic Liquids for Actuators

2.3.1 Microvalves

In 2007 Sugiura *et. al* [29] proposed photo-responsive microfluidic hydrogel valves by copolymerising N-isopropylacrylamide (NiPAAm) with a photochromic acrylic

benzospiropyran ester (BSP) moiety. Prior to photo-polymerisation, the cocktail mixture of the monomer and the photochromic unit was dissolved in 1-butanol, together with a UV initiator and crosslinker. The photoresponse mechanism of these hydrogels comes as a result of the benzospiropyran moiety present in the copolymer matrix. When the copolymer had been kept in the dark and exposed to an aqueous solution of HCl, the benzospiropyran moiety protonates, changing its conformation to the protonated merocyanine form. When in this conformation, the presence of charges on its backbone contributes to it being more hydrophilic than the closed benzospiropyran conformation. Thus, it absorbs more water and, by irradiating it with white light, it can be reversed to the more hydrophobic benzospiropyran form, together with the release of water. The authors have shown that valves obtained from this material can perform, if preconditioned overnight in acidic conditions, to open and stop the flow inside a poly(dimethyl siloxane) (PDMS) microfluidic device.

Building on this work, Benito-Lopez *et. al* [30] synthesised photo-responsive ionogel valves in microfluidic channels by copolymerising NiPAAm and BSP using a mixture of 1-butanol and phosphonium ionic liquids as the solvent. Four different ILs were used, namely triisobutyl(methyl) phosphonium tosylate ([P_{1,4,4,4}][Tos]), trihexyltetradecyl phosphonium dicyanamide ([P_{6,6,6,14}][DCA]), trihexyltetradecyl phosphonium bis(trifluoromethanesulfonyl) imide ([P_{6,6,6,14}][Ntf₂]), and trihexyltetradecyl phosphonium dodecylbenzenesulfonate ([P_{6,6,6,14}][DBSA]), respectively. The resulting crosslinked polymers were left to swell in 1 mM HCl solution for 2 h to reach their maximum swelling capabilities. Following this, they were irradiated with a white light LED until they shrank to their minimum size. In all cases, the time needed for this operation was 100 s. The hydrogel which exhibited maximum shrinking was the control hydrogel, followed by the [P_{6,6,6,14}][DCA], [P_{1,4,4,4}][Tos], [P_{6,6,6,14}][DBSA], and [P_{6,6,6,14}][Ntf₂], respectively. Following this, the monomer mixtures were polymerised in microfluidic devices that featured inlet ports connected to five microchannels which converged into a single microchannel with an outlet port. In each of the five microchannels there was a circular reservoir with a diameter of 500 µm and a height of 175 µm where the monomer mixtures were photopolymerised. The microchannels were 500 µm in width and 50 µm in height. After photopolymerisation, the microfluidic device was flushed with 1 mM HCl to swell the hydrogels. After the hydrogels were swollen and were blocking the channels, a vacuum was applied to the outlet to facilitate the flow and water

containing different coloured dyes was placed at each of the inlets. The valves were actuated using a white light LED with a power output of $1 \text{ mW} \cdot \text{cm}^{-2}$. Actuation times were 2 s for the control hydrogel, 4 s for the $[\text{P}_{6,6,6,14}][\text{DCA}]$, 18s for the $[\text{P}_{1,4,4,4}][\text{Tos}]$, 44 s for the $[\text{P}_{6,6,6,14}][\text{DBSA}]$, and 49 s for the $[\text{P}_{6,6,6,14}][\text{NTf}_2]$ ionogel, respectively (Figure 2.1). This example shows that through the incorporation of different ionic liquids of varying hydrophilic/hydrophobic character, inside ionogel matrices, actuation times can be modulated on demand. The time for the hydrogels to revert back to their original size is approximately 30 min, which lead the researchers to conclude that this type of valve would be best suited for single-use devices.

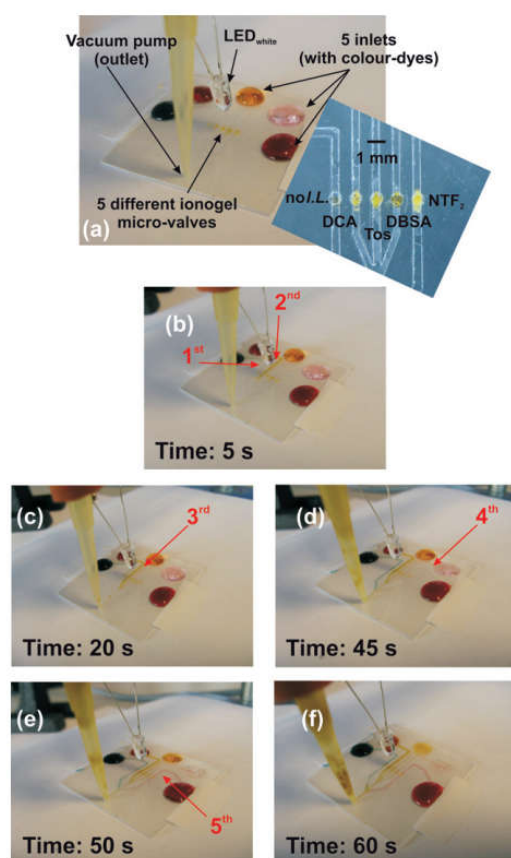


Figure 2.1 Image of the microfluidic manifold showing the performance of the ionogel microfluidic valves: (a) all microvalves are closed under the applied vacuum. White light is applied for the time specified in each picture (b) Hydrogel (no IL present) valve is first to actuate followed by ionogels incorporating $[\text{DCA}]$ - (c), $[\text{Tos}]$ (d), $[\text{DBSA}]$ (e), $[\text{NTf}_2]$ (f). Numbers and arrows indicate when the channel is filled with the dye due to microvalve actuation. Reproduced from Benito-Lopez et al. [30].

A more comprehensive study of such photo-responsive ionogel materials was later performed by Czugala *et. al* [31] who studied the photo-responsive behaviour of pNiPAAm-*co*-BSP ionogels made using phosphonium ILs as solvents. Three different phosphonium ILs were chosen for this study: trihexyltetradecyl phosphonium chloride [P_{6,6,6,14}][Cl], [P_{6,6,6,14}][DCA] and [P_{6,6,6,14}][Ntf₂], respectively, and ionogel actuators were photo-polymerised in four different shapes of varying surface area to volume ratios (SA/V): rings, 250 μm discs, 500 μm discs, and lines, respectively. Their change in size was determined by the change in height, as measured using digital microscopy. By measuring the amount of hydration for each ionogel shape, it was determined that the [P_{6,6,6,14}][Ntf₂] swelled the most, at a value of 109-180 % of the initial gel height (right after photo-polymerisation), followed by [P_{6,6,6,14}][DCA] ionogels (40-58 %), and lastly the [P_{6,6,6,14}][Cl] ionogels (20-27 %). Following this, the shrinking behaviour of the ionogels was analysed and it was determined that after 30 min of white light irradiation, the [P_{6,6,6,14}][Ntf₂] ionogels shrunk by 108 %, 15% of their initial height, followed by the [P_{6,6,6,14}][DCA] ionogels shrunk by 42 %, reaching also 15 % of their initial height, while the [P_{6,6,6,14}][Cl] ionogels shrunk only by 16 %, reaching 4 % of their initial height (Figure 2.2). The kinetics of the swelling and shrinking behaviours were also determined and in each case the [P_{6,6,6,14}][Ntf₂] ionogels exhibited the highest rates of swelling and shrinking at $(5.3 \pm 0.1) \cdot 10^{-2}$ s and $(29 \pm 4) \cdot 10^{-2}$ s, followed by [P_{6,6,6,14}][DCA] at $(4.5 \pm 0.3) \cdot 10^{-2}$ s and $(8.3 \pm 0.9) \cdot 10^{-2}$ s, and [P_{6,6,6,14}][Cl] at $(3.9 \pm 0.2) \cdot 10^{-2}$ s and $(9 \pm 2) \cdot 10^{-2}$ s, respectively. The high swelling and shrinking values attributed to the [P_{6,6,6,14}][Ntf₂] are believed to stem from the fact that this ionic liquid possesses a highly delocalised charge on the S-N-S backbone of the Ntf₂⁻ anion, which makes it interact less with the charged moieties of the polymer. This leads to more freedom for the polymer backbone to interact with the hydration medium. In the case of the [P_{6,6,6,14}][Cl], this effect is inhibited by the localised charge on the chloride ion, thus associating more strongly to the polymer backbone. The [P_{6,6,6,14}][DCA] ionogels would have an intermediate behaviour between these two states. Based on these results, the [P_{6,6,6,14}][Ntf₂] ionogels were incorporated in a glass-poly(dimethyl siloxane) microfluidic device as light actuated valves. Using a fiber optic to irradiate with white light, the ionogel valve opened after 180 s, allowing liquid to pass through the microfluidic channel [31].

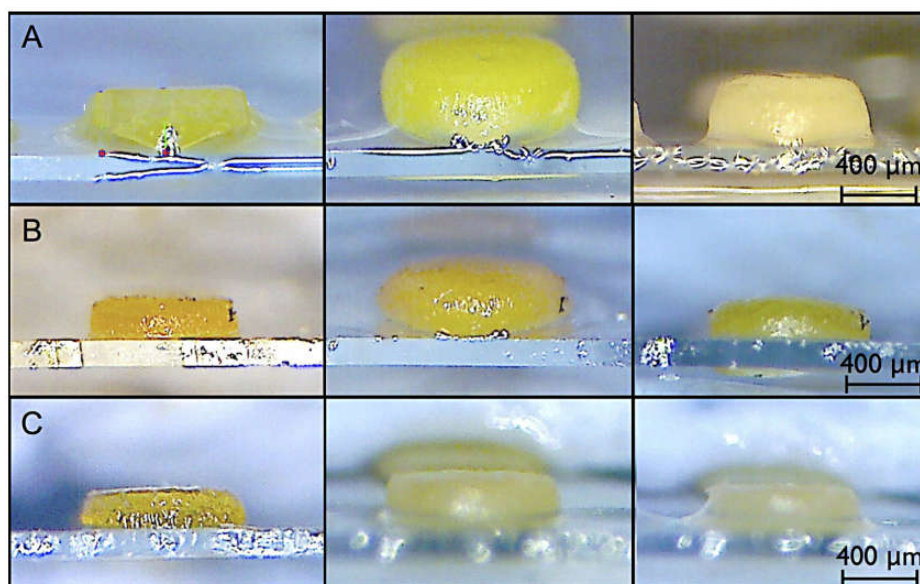


Figure 2.2 Microscope images of ionogel discs made of: (a) $[P_{6,6,6,14}][NTf_2]$, (b) $[P_{6,6,6,14}][DCA]$ and (c) $[P_{6,6,6,14}][Cl]$ after photopolymerisation (left); swelling in 1mM HCl solution for 2h (middle) and shrinking upon white light irradiation (right). Reproduced from Czugała *et. al* [31].

An application of these materials was demonstrated by Czugała *et. al* [32] by using the $[P_{6,6,6,14}][DCA]$ ionogels as photo-responsive valves in a microfluidic analysis platform for the detection of nitrite anions in water. The nitrite assay was performed using the Griess reagent and the change in colour was determined using a Paired Emitter Detector Diode (PEDD) arrangement integrated in the microfluidic holder. The emitter diode has a wavelength of 540 nm, while the detector diode has its maximum absorption at 660 nm. Part of the light produced by the emitter diode is absorbed by the Griess-nitrite complex, which has its maximum absorption at 547 nm, while the rest reaches the detector diode and is transformed into a photo current. The amount of photo current generated is proportional to the concentration of nitrite within the sample. By connecting the PEDD setup to a microcontroller fitted with a wireless radio antenna, the data was sent to a PC, where it was stored and analysed. The monomer mixture was photopolymerised using UV light in a circular reservoir with a radius of 500 μm and a height of 225 μm . The reservoir sat at the junction of a Y-shaped microchannel that separated the sample from the Griess reagent (Figure 2.3a). To operate the valve, the microchannel was filled with 1 mM HCl and left to

swell for 2h in the dark. The opening of the valve was performed with irradiation from a white light LED that was also mounted on the microfluidic device holder. By irradiating with a power of $1 \text{ mW}\cdot\text{cm}^{-2}$, the ionogel valve opened after $30 \pm 5 \text{ s}$ ($n=3$) (Figure 2.3b) and was operated at a pressure of 25 mbar; pressures higher than $31 \pm 4 \text{ mbar}$ ($n=3$) deformed the materials and the valves failed. After the ionogel shrank, the reagent mixture was pumped through the microchannel where it mixed and moved to the detection area for analysis. The calibration curve was made using concentrations of nitrite from $0.2 \text{ mg}\cdot\text{L}^{-1}$ to $1.2 \text{ mg}\cdot\text{L}^{-1}$, in $0.2 \text{ mg}\cdot\text{L}^{-1}$ steps and performed in triplicate. This yielded a R^2 value of 0.98, a level of detection (LOD) of $34.0 \pm 0.1 \text{ }\mu\text{g}\cdot\text{L}^{-1}$ and a level of quantification (LOQ) of $115 \pm 3 \text{ }\mu\text{g}\cdot\text{L}^{-1}$, compared to a R^2 value of 0.99, LOD value of $1.50 \pm 0.02 \text{ }\mu\text{g}\cdot\text{L}^{-1}$, and a LOQ of $14.8 \pm 0.2 \text{ }\mu\text{g}\cdot\text{L}^{-1}$ for a UV-Vis spectrophotometer. The results obtained for the microfluidic platform are lower than the detection limits set by the World Health Organisation. Following this, freshwater samples from the Tolka River in Dublin, Ireland were analysed with both the portable platform and the UV-Vis spectrometer. The close nature of both sets of results proved the suitability of such a microfluidic device and detector for the accurate monitoring of nitrates in real-life samples.

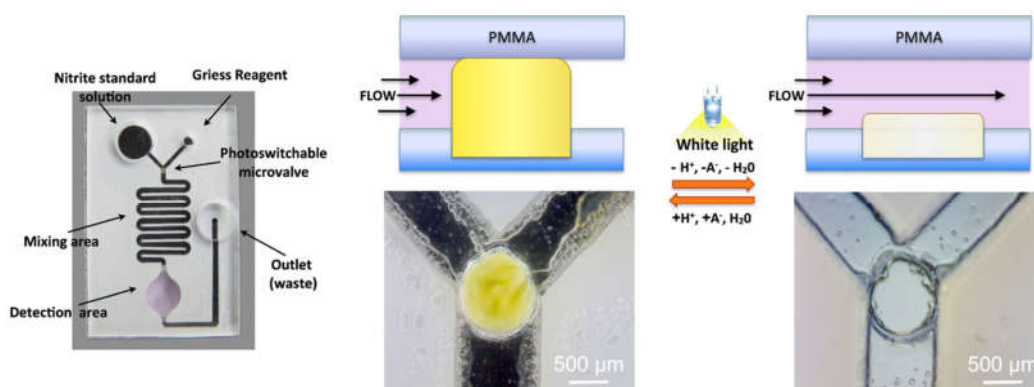


Figure 2.3 Picture of the microfluidic device fabricated in PMMA: (a) PSA polymer by CO_2 laser ablation (left). Followed by (b) a schematic (top) and images (bottom) of the photoresponsive microvalve in closed (middle) and opened (right) state. Reproduced from Czugala *et. al* [32].

Thermo-responsive actuation was also proposed for microvalves fabricated using poly(*N*-isopropylacrylamide) polymer (pNiPAAm) gels [33] by Benito-Lopez *et. al*.

To synthesise these materials, all the components for the monomer mixture were dissolved in 1-ethyl-3-methyl imidazolium ethyl sulphate [EMIM][EtSO₄]. The addition of this IL, as demonstrated prior by Gallagher *et. al* [34], improves the swelling and shrinking capabilities of the pNiPAAm materials, together with lowering the LCST. The microfluidic devices in this study were fabricated using a cutting plotter to cut 100 µm thick layers of cyclic olefin polymer (COP) and thermally bonded, to obtain and microfluidic device with a total area of 1 mm² and a total maximum thickness of 1 mm. The resulting microfluidic devices possessed a circular reservoir, which was filled with the monomeric mixture and photopolymerised using UV light. Following this, the resulting microfluidic devices were mounted in a microfluidic holder with an incorporated heating element which could thermally actuate the ionogel valve. The characterisation of the ionogel valves was performed by connecting the inlet of the microfluidic device to a syringe pump with a set flow rate of 1000 nL·min⁻¹, while the outlet was connected to a flow microsensor. Using this experimental setup, the failure pressure of the valves was determined to be 1100 ± 100 mbar ($n = 5$) and they successfully operated at 200 mbar after being exposed to pressures higher than 1100 mbar. Setting the heating element of the microfluidic holder at a temperature higher than 50 °C, the valves opened 4 ± 1s ($n = 5$), after the temperature of the ionogel passed its LCST. Recovery was achieved in 32 ± 2s ($n = 5$), after the temperature dropped below the LCST of the ionogel valves (Figure 2.4). Furthermore, after 10 repetitions, there was no discernible drop in valve performance, showing the potential of these materials as cost-effective reversible valves.

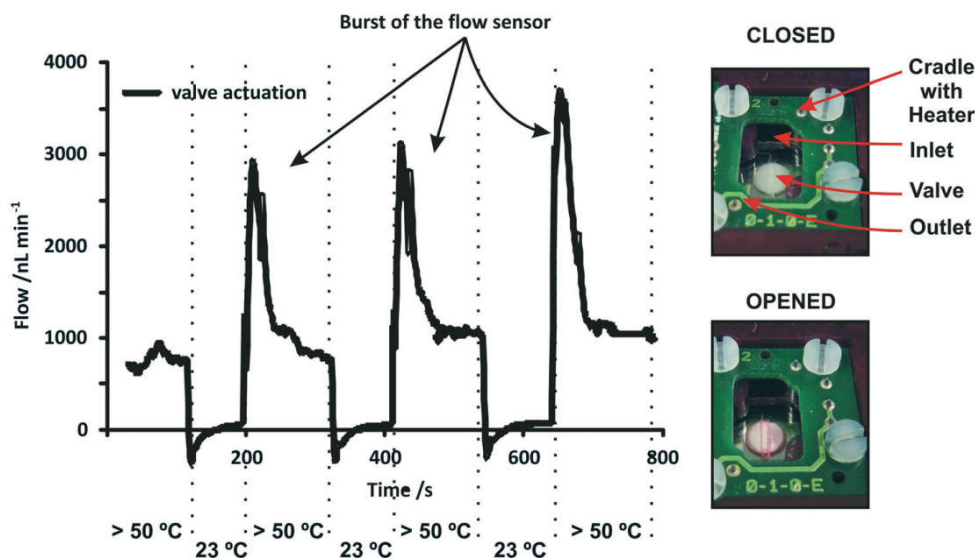


Figure 2.4 Flow profile during three full actuation cycles (left) and photo of the microfluidic device containing the thermo-actuated valve and the microfluidic holder with integrated heaters at the bottom. High flow spikes are due to the stabilisation of the microflow sensor after opening of the valve. Reproduced from Benito-Lopez *et. al* [33].

Electro-actuation of IL based microvalves has also been studied. Ghamsari *et. al* [35] demonstrated the use of bucky gels based on the 1-ethyl-3-methyl imidazolium tetrafluoroborate ionic liquid ([EMIM][BF₄]), poly(vinylidene fluoride) (PVDF), and single-walled carbon nanotubes (SWCNT), respectively, as low-voltage microvalve actuators. Bucky gels are gel-like mixtures of carbon nanotubes and ILs which benefit from both the high electrical conductivity associated with carbon nanotubes and the properties of ILs, such as high temperature and electrochemical stability. Bucky gel actuators (BGA) are composite materials which feature a polymer electrolyte core, in this case an ionogel of [EMIM][BF₄] and PVDF, inserted between two layers of electrodes made out of bucky gels. Applying voltage to this composite will make it bend in the direction of the applied voltage (Figure 2.5a and b). The electrode components composite was made by mixing all the aforementioned constituents with dimethylacetamide (DMAC) in a ball mill until a black gel mass was obtained. The resulting gel was cast in PDMS moulds and dried until all the DMAC had evaporated. The ionogel layer was fabricated in the same way, without the addition of SWCNT to the constituent mixture. The resulting layers were then hot-pressed together and covered in a layer of PDMS to increase the adhesion of the resulting BGA to the walls

of the microfluidic device, which would ensure better sealing during operation. The actuation properties of the BGA are dependent on the total thickness of the device and on the ratio between the electrolyte layers. Three devices were tested to determine which generates the maximum amount of force by application of a voltage sweep between 4 and 10 V. The devices had thicknesses of 281.9 μm (BGA1), 322.6 μm (BGA2), and 393.7 μm (BGA3), and thickness ratios of 0.73, 1.20, and 0.87, respectively. The results indicated that BGA3 generated a force of 80 mN, which was the highest generated force of the three BGAs. BGA1 and BGA2 generated forces of 38 and 41 mN, respectively. By enclosing the BGAs in a PDMS layer, the forces generated when a voltage is applied are increased between 14 to 23 %. Taking into account that the BGAs will be used in an aqueous medium, a voltage sweep between 2 and 10 V confirmed that there are no bubbles formed due to the hydrolysis. All three BGAs were fitted to microfluidic devices to cover an inlet channel that was fabricated from a tube (Figure 2.5c and d). The tests consisted of using three different operating voltages, namely 5, 8 and 10 V and six different frequencies: 250, 125, 100, 50, 25, and 0 mHz respectively. For all the BGAs, the results indicated that the higher the voltages and the lower the frequency, the better they are suited for use as microfluidic valves. The best results were obtained at 10 V and 0 mHz, at which the flow rate was reduced by 93 %. In all experiments, a leakage flow was present, which led the researchers to determine that the design of the device can be improved to minimise the reoccurrence of this phenomenon.

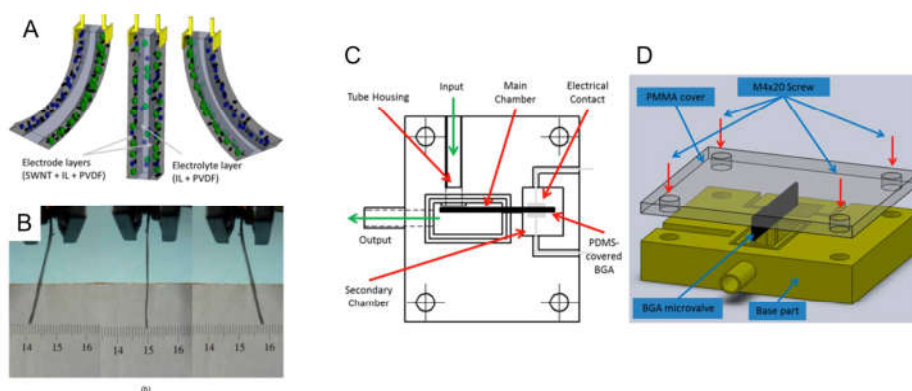


Figure 2.5 (a) BGA bending motion as a result of ion transfer between layers; direction of bending can be reversed by changing the polarity of the applied potential; (b) BGA strip bended (10 V, 0.1 Hz); (c) Base part and (d) 3D view of the flow regulator assembly. Reprinted with permission from Ghamsari et. al [35].

2.3.2 Delaying Pumps

Another application of ILs and ionogels in microfluidic devices include passive pumps where several examples have been proposed in the recent years. In the area of paper-based microfluidic devices, Akyazi *et. al* [36] demonstrated the use of pNiPAAm based ionogels as delaying pumps. Paper is becoming a material of choice in microfluidics due to its ubiquity and low cost, together with attractive physical properties, such as good flexibility, low thickness, low weight, and ability to wick fluids. Its fibrous nature also presents additional challenges with isotropic wicking. The study conducted by Akyazi *et. al* discusses the use of ionogels integrated in paper microfluidic devices to manipulate the wicking properties of these devices. These ionogels were made by dissolving NiPAAm and a crosslinker unit in two different ILs, [EMIM][EtSO₄] and [P_{6,6,6,14}][DCA], respectively. The paper microfluidic devices (μ PADs) were fabricated by ink stamping in triplicate the channels on Whatman Filter paper. After the designs were stamped and dried, the ink provided hydrophobic barriers, which kept the flow of liquid between its limits. The ionogels were photopolymerised at the ends of the microfluidic devices immediately after application, so that most of the ionogel was formed at the surface of the μ PAD. This ensures that the swelling is uniform and the hydrogel will not deteriorate during swelling, while also still being attached to the μ PAD. The swelling results indicate that the ionogel synthesised with [P_{6,6,6,14}][DCA] absorbed the most water compared to the [EMIM][EtSO₄] ionogel and the μ PAD with no ionogel. Following this, investigations were made to explore the effect of adding an ionogel to one of the channels of a Y-shaped μ PAD. The solutions used for this test consisted of a pH = 13 NaOH solution and a pH = 2 H₂SO₄ solution which had methyl red dissolved in it. The pH = 2 solution was added to the right branch of the μ PAD, with no ionogel, while the pH = 13 solution was added to the left branch, with the [P_{6,6,6,14}][DCA] ionogel (Figure 2.6). Another Y-shaped μ pad without any hydrogels was used as the control. In the case of the control μ PAD, the meeting point of the solutions was determined to be in the centre branch of the μ PAD, where the colour of the yellow pH = 2 solution changed to purple when it interfaced with the pH = 13 solution. In the case of the μ PAD that had the ionogel, the interface between the two solutions formed in the left branch of the μ PAD, close to where the [P_{6,6,6,14}][DCA] ionogel resided. After the initial formation of the interface between the two solutions, the interface

moved towards the centre branch of the μ PAD, due to the constant flow of solution coming from the $[P_{6,6,6,14}][DCA]$ ionogel, after it reached its swelling equilibrium. The use of high and low pH solutions emphasises the fact that the ionogels maintain their function even in harsh conditions. The addition of these materials to paper microfluidic devices increases the usefulness of these devices by decreasing the complexity associated with fluid manipulation, while also being cheap enough to keep costs low.

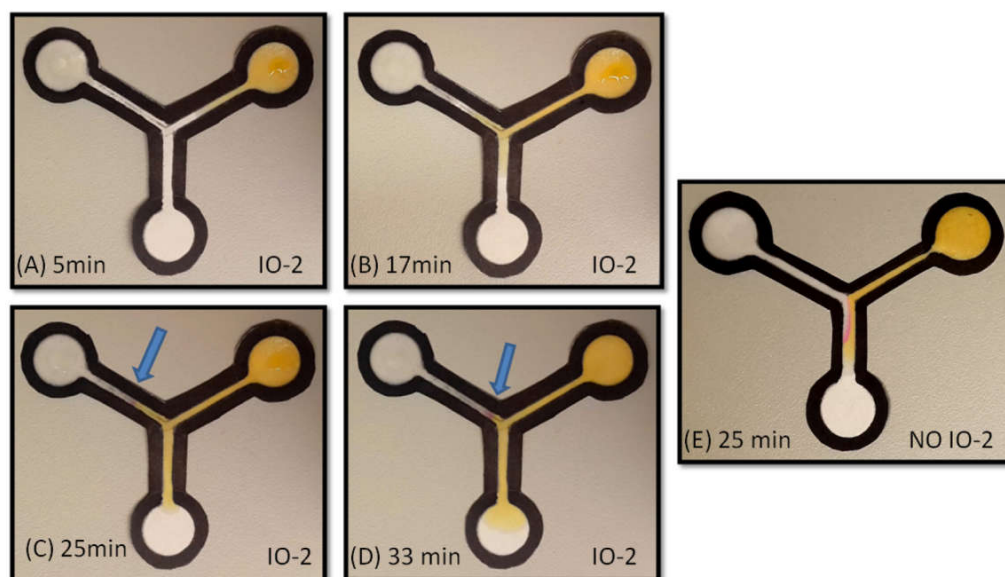


Figure 2.6 A Y-shaped μ PAD with photopolymerised $[P_{6,6,6,14}][DCA]$ ionogel in the left side inlet after 5 min (A), 17 min (B), 25 min (C), 33 min (D), while injecting NaOH solution ($pH=13$) in to the left inlet (purple arrow) and phenol red pH indicator and H_2SO_4 solution ($pH = 2$) (yellow arrow) into the right inlet. Phenol red gives a pink colour change in a basic environment. (E) A Y-shaped μ PAD with no ionogel. Reproduced from Akyazi et al. [36].

2.4 Ionic Liquids for Sensing

The use of ionic liquids (ILs) for sensing in microfluidic devices continues to gain traction, owed primarily to the ability of these materials to offer a matrix which is capable of responding to chemical and physical stimuli. The wide electrochemical windows, high conductivity, propensity to stabilise enzymes and liquid state at room temperature have carved a particular niche for these exciting new materials in the

field of sensing chemical and physical changes [37]. Their ability to immobilise molecules for use in pH analysis, catalysis and electrochemistry have also brought additional application as biomolecular sensors [38].

2.4.1 Chemical Sensing

The serendipitous growth of point-of-care (POC) technologies, in particular through organic electronics, has buttressed the development of these compounds with a tangible need for efficient protein solubilisation in specific pH and temperature ranges. One such example, by Yang *et al.* [39][39], shows the recent inroads being made in the field of Organic Electrochemical Transistors (OECTs), which have found application in the sensing of ions and antibodies. These simple transistors operate through migration of ions from an electrolyte into a semiconductor, which is often fabricated from a doped polymer, such as poly(3,4-ethylenedioxythiophene) doped with poly(styrene sulfonate) (PEDOT : PSS). By using redox enzymes, such as glucose oxidase in Phosphate Buffer Solution (PBS), it has been possible to achieve micromolar limits of detection [39][39]. Recent endeavours to use RTILs as a suitable replacement for aqueous electrolytes has brought Yang *et al.* to an IL, namely triisobutyl-(methyl)-phosphonium tosylate [$P_{1,4,4,4}$][Tos], for the fabrication of a new generation of OECTs (Figure 2.7). The hydrophilic nature of the IL, attributed to the tosylate anion, ensures that when patterned over the active area of the OECT, the material subsequently acts as a reservoir for the enzyme and mediator. Upon mixing, the mediator (ferrocene in this case) dissolves, while the enzyme remains dispersed. The presence of this dispersion can have a positive impact on the lifetime of the device by inhibiting a change in the secondary enzyme structure [40]. Figure 2.7c shows that the analyte, in this case a glucose solution forms directly over the area pre-defined by tridecafluoro-1,1,2,2-tetra-hydrooctyl trichlorosilane (FOTS) template. The device, which operates in the 10^{-7} - 10^{-2} M range, well within clinical ranges found in the blood (2–30 mM) and saliva (0.008–0.21 mM) [41]. This shows great potential for being used as a low cost, disposable, POC device.

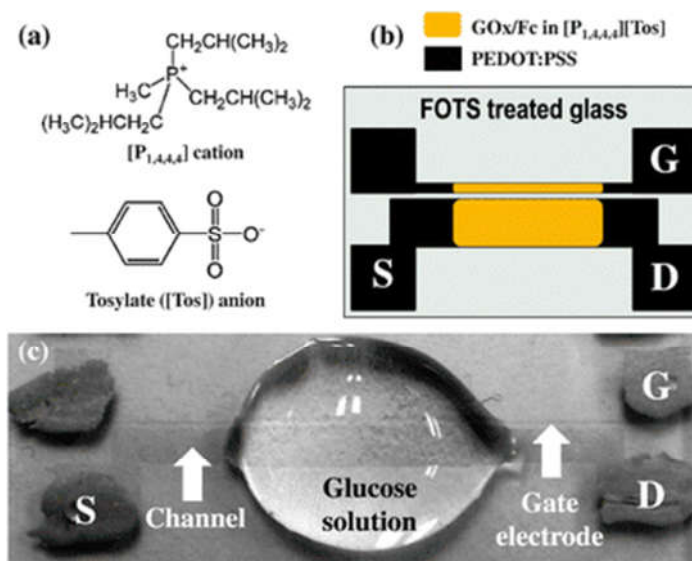


Figure 2.7 (a) Chemical structure of $[P_{1,4,4,4}][Tos]$. (b) Schematic of the OEET. (c) Image of the OEET with a drop of glucose solution added. Reproduced from Yang et al. [39].

This work has also been developed to sense for other clinically relevant analytes, such as lactate, through incorporation of lactate oxidase (LOx) into an OEET device [42]. In this instance a flexible ionogel based NIPAAm, N,N-methylene-bis(acrylamide) (MBAAm) and $[EMIM][EtSO_4]$ incorporating the LOx enzyme was polymerised on the OEET device. As in the case for the glucose sensor, introduction of the specific analyte (in this case lactate), results in an increase in the drain current, which can be directly correlated to lactate concentration, as seen in Figure 2.8(a). Figure 2.8(b) shows a prototype fabricated from parylene worn on the forearm [42]. Such a flexible prototype, coupled with detection levels suitable for use in the clinical range, prove extremely exciting potential in the fields of sport science and patient care. The conformability of an ionogel incorporated into the OEET device, offers flexibility not previously possible with more rigid conjugated polymers.

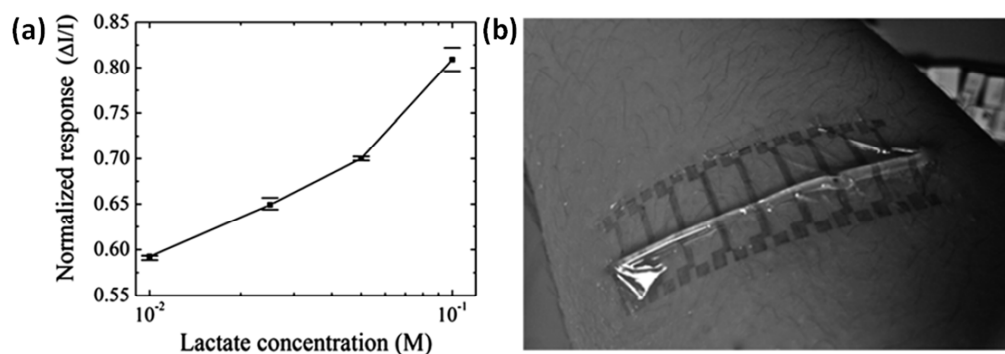


Figure 2.8 a) Normalised response vs. lactate concentration for the OECT and b) Flexible OECT on the forearm. Adapted from Khodagholy *et. al* [42].

A true understanding of the effect that ILs have on enzymes, has recently been developed by Curto *et. al* [43], in particular for choline-based ILs containing LOx enzyme. They conclude that hydrated ILs can provide the necessary hydrogen bonding for necessary stabilisation of proteins, in addition to controlling the proton buffering within the medium. Interestingly, when stored in choline chloride, over a 140 day period at 5 °C, 80 % of the initial activity of LOx.

In a similar fashion to the immobilisation of enzymes, ionic liquids can also be used to stabilise other sensing molecules such as dyes. Through ion-pair interactions, a charged dye molecule can be held in the IL or ionogel matrix without leaching. Czugała *et al.* have developed a direct application of such a system, through the use of a centrifugal disc with functionalised ionogel sensing areas [44][45]. The ionogel, based on poly(N-isopropyl-acrylamide) and N,N'-methylene-bis(acrylamide) and shown Figure 9(a) is used to entrap the ionic liquid, tetrabutylphosphonium dicyanamide [P_{4,4,4,4}][DCA], and the dye molecule, bromocresol purple (BCP), shown in Figure 2.9(b) and (c), respectively. Photopolymerisation yielded an ionogel, which responds to a variation in pH with the colour change shown in Figure 9.

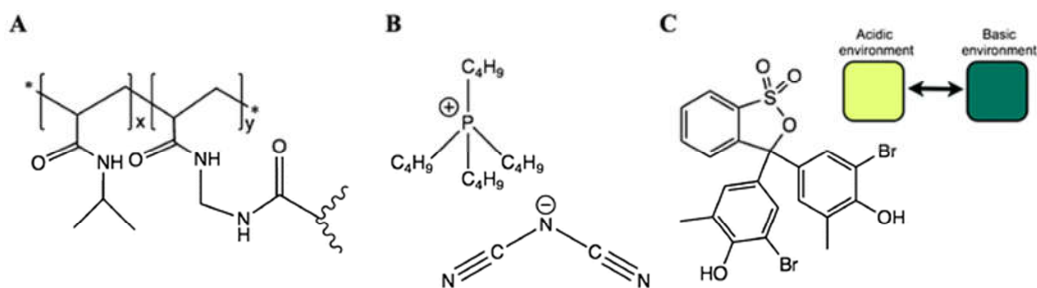


Figure 2.9 Chemical structures of A) *N*-Isopropyl-acrylamide and *N,N*-methylenebis(acrylamide) crosslinked polymer; B) ionic liquid tetrabutylphosphonium dicyanamide [P_{4,4,4,4}][DCA] and C) Bromocresol Purple, showing colour changes in acidic and basic environments. Reproduced from Czugała et. al [44].

By development of a light emitting diode (LED) based detector it is possible to generate a colorimetric assay. Optimisation of the concentration of BCP concluded with a $6 \cdot 10^{-3}$ M concentration which was used to generate calibration curves across a range of pH values, as shown in Figure 2.10. Moreover, through incorporation of these ionogel materials into a centrifugal disc device, it was possible to include a full colorimetric assay in a CD platform.

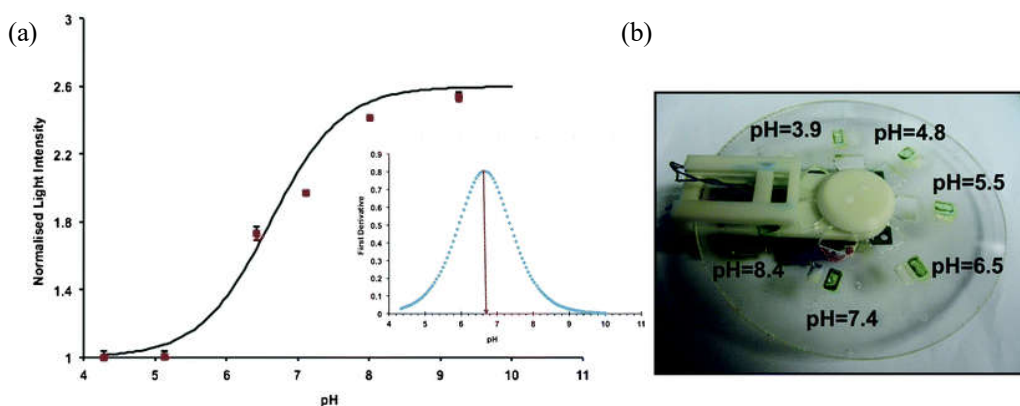


Figure 2.10 (a) Calibration curve of the sensing area of the microfluidic device using pH buffer solutions; (b) Image of the CD platform with the sensing area. Reproduced from Czugała et. al [44].

In a similar fashion, Curto et. al [45] have extended the use of IL encapsulated pH responsive dyes to yield a simple barcode device which is capable of measuring sweat

pH in real time, using colorimetric imaging through a mobile phone application (Figure 2.11). In a bid to further extend the lifetime of the microfluidic device, immobilisation of the ionogel on a polymethylmethacrylate (PMMA) substrate was achieved through the use of water plasma treatment, followed by silanisation. The ionogel containing the various dye molecules could then be directly bonded to the functionalised surface, through covalent attachment. By applying an algorithm which mapped to the hue saturation value (HSV) colour space it was then possible to use the mobile phone application to generate calibration curves with R^2 value greater than 0.995.

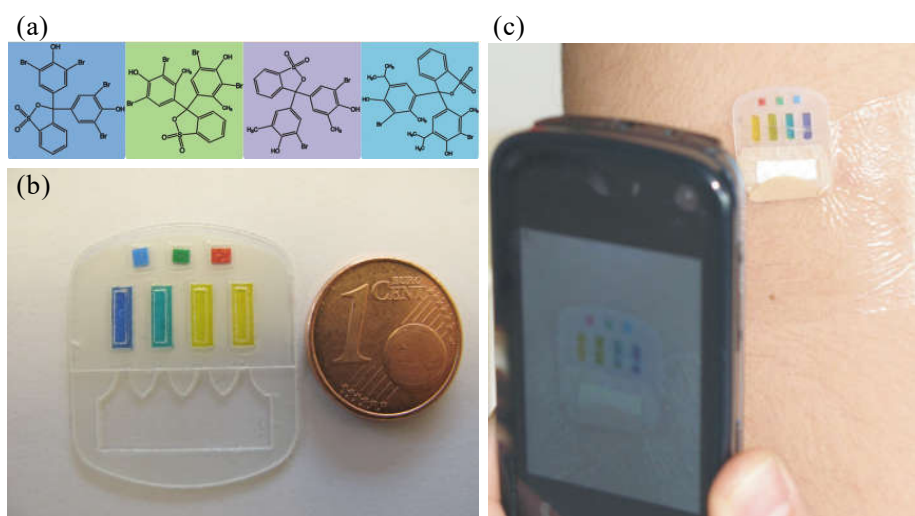


Figure 2.11 (a) Chemical structures of the pH sensitive dyes: Bromophenyl Blue (BPB), Bromocresol Green (BCG), Bromocresol Purple (BCP) and Bromothymol Blue (BTB); (b) Fabricated micro-fluidic device; (c) Smartphone application imaging on-body device. Reproduced from Curto *et. al* [45].

Not only can ionic liquids be used as vehicles for entrapping, immobilising and stabilising sensing materials, such as enzymes, dyes and stimuli responsive materials, they too can be used for their direct interactions with target molecules, most notably in the fields of capillary and microfluidic device electrophoresis. Using ILs as the supporting electrolyte or as additives to the running buffer can dramatically increase the speed and efficiency of operation, in addition to broadening the range of compounds which can be separated using electrophoresis. When used as background

electrolytes, in a similar fashion to alkylammonium salts, ILs based on the 1-alkyl-3-methylimidazolium cation were seen to behave as electroosmotic flow modifiers through interaction of the cation either by coating the capillary wall or by migrating into the bulk solution [46]. For the separation of polyphenol compounds in grape extracts the method proved reliable and reproducible. Similarly, for microfluidic device electrophoresis, the use of dynamic coating can prove to be a viable solution to counteract the adsorption of compounds on the hydrophobic polymer materials commonly used for microfluidic fabrication. In the analysis of proteins, for example, surface modification of PDMS channels with ILs, such as 1-butyl-3-methylimidazolium dodecanesulfonate ([BMIM][DoS]) and [EMIM][BF₄], can serve to inhibit adsorption of analytes [47].

2.4.2 Physical Sensing

Attributes of ILs, such as good electrical conductivity, high ion density and non-volatility which form the basis for new generations of chemical sensors can also form the basis for much novel work being carried out in the field of physical sensing. Confinement of these conductive liquid materials within a microfluidic channel can generate cheap, pliable and accurate strain-sensors for monitoring motion. These sensors, previously fabricated by casting conductive materials such as silver nanowire, graphene films and carbon nanotubes or through the use of liquid metals within microfluidic channels have generated much recent attention, with the advent of the ubiquitous wearable device. Previous iterations, however, have suffered from complicated fabrication techniques which can result in large hysteresis, resulting in the inability to undergo multiple deformations.

Fabrication of a flexible PDMS channel, filled with a single IL or binary mixture thereof can be used to fabricate thin wearable strain sensors. Matching refractive indices of the binary mixture can generate a transparent strain sensor, used to measure stretching, bending and other motions. When pressure is applied to the flexible membrane a geometric change within the channel results in an increase of pressure within the channel, thereby leading to a measurable variation in the electrical properties of the ionic liquid (Figure 2.12). These devices can therefore be considered as constant electrofluidic resistors.

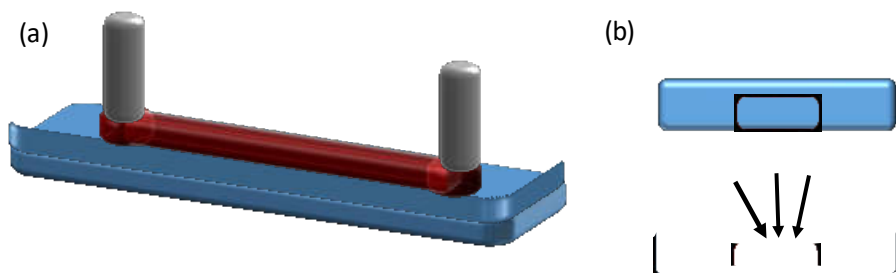


Figure 2.12 (a) Representation of simple linear microfluidic strain sensor with platinum electrodes. Red represents the ionic liquid filling the microfluidic channel; (b) Two-dimensional representation of the geometric deformation of the microfluidic channel when pressure is applied.

Yoon *et al.* [48] described a simple linear channel system of 400 μm width and 70 μm height, filled with a binary mixture (51:49 molar ratio) of 1-butyl-3-methylimidazolium bis-(trifluoromethanesulfonyl)imide ([BMIM][Ntf2]) and 1-butyl-3-methylimidazolium acetate ([BMIM][Ac]). Using platinum electrodes at a constant voltage of 1V (DC) it was possible to monitor current under a range of tensile strain from 10-25 % for multiple cycles. At low strain speeds minimal hysteresis was observed, attributed to the dynamic nature of the IL, thereby eliminating and possible disconnection in the circuit.

This concept has been extended upon in publications such as that by Wu *et al.* [49][50] to fabricate novel pressure sensors using ILs in similar flexible PDMS channels. Through the use of a bilayer microfluidic device it is possible to use one microfluidic channel as a pressure sensor at a specific location in the second. This change in pressure in the channel filled with 1-ethyl-3-methylimidazolium dicyanamide [EMIM][DCA] can be directly related to electrical resistance within the circuit. This change in resistance can be accurately measured through the design of a Wheatstone bridge, as shown in Figure 2.13. Using pressurised gas and liquid in the microfluidic channel it was possible to characterise the sensor, which exhibited impressive thermal stability over extended periods of time. These results displayed much promise for the application of such a device in LOC devices.

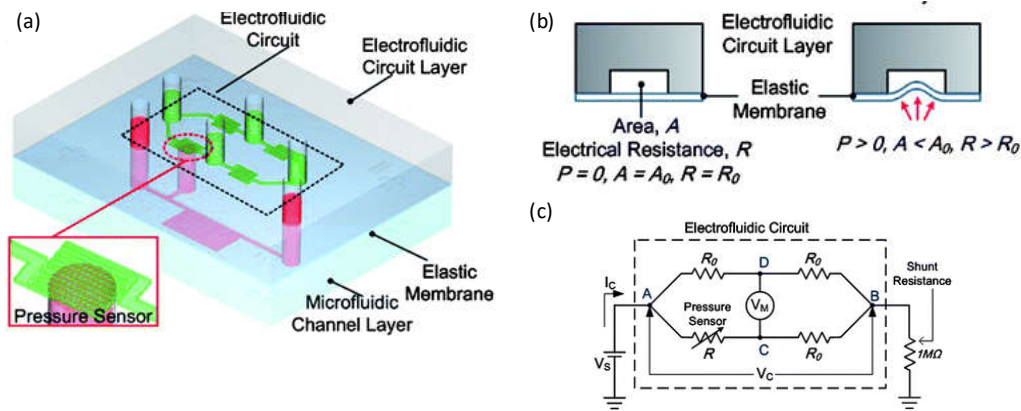


Figure 2.13 (a) Representation of the PDMS microfluidic device showing the microfluidic channel and electrofluidic circuit layers. (b) Conversion of mechanical pressure to electrical resistance. (c) Wheatstone bridge electrofluidic circuit. Reproduced from Wu *et al.* [49].

The ability to develop these systems to measure stretch and shear within microfluidic devices has extended their application to devices for microfluidic cell culture, such as Organ-on-a-Chip. These devices can provide a greater understanding of analogous biological processes by monitoring cells *in vitro*, through real time flow monitoring. Liu *et. al* [50] have developed a microfluidic device for endothelial cell culturing with an embedded pressure sensor (Figure 2.14). Again, by measuring the variation in electrical properties generated from a change in the geometry of the soft-polymer channel filled with [EMIM][DCA], it is possible to determine the pressure within the microfluidic device (Figure 2.14). Such a measurement is critical for the understanding of the surrounding environment of endothelial cells which are commonly exposed to stress, stretch and hydrostatic pressure.

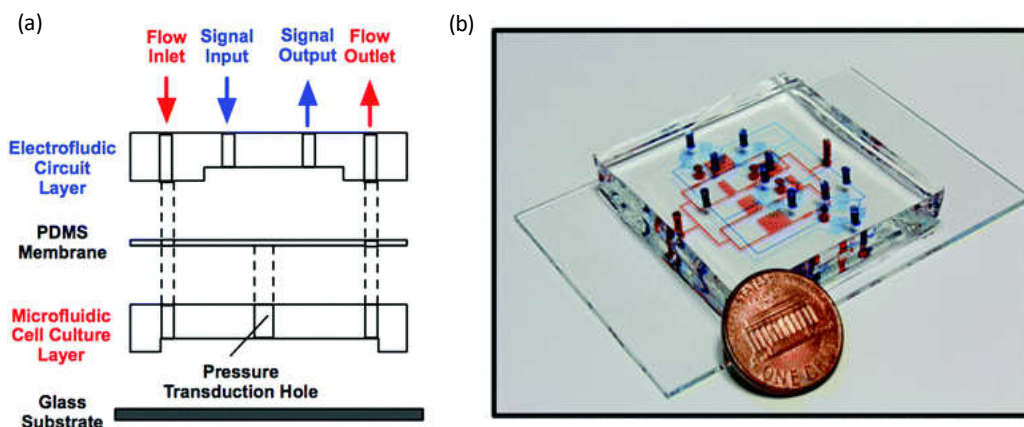


Figure 2.14 (a) Representation of the microfluidic cell culture showing electrofluidic circuit layer and a microfluidic cell culture layer and glass substrate. (b) Image of the fabricated device showing: the electrofluidic circuit channels (blue) and microfluidic cell culture channels (red). Reproduced from Liu et al. [50].

2.5 Other Applications in Microfluidics

The broad nature of applications using ILs in microfluidic devices makes it difficult to efficiently categorize them independently. The following section presents a compendium of publications, which have not been covered hitherto, in which ILs play an important role for the development and application of microfluidic devices.

2.5.1. Ionic Liquids for Nanoparticle Synthesis in Microfluidics

A particular use for the incorporation of ionic liquids in microfluidic devices is the synthesis of metallic nanoparticles and inorganic nanomaterials. As nanoparticles are an emerging tool in many biomedical applications there is an increasing demand for low cost, rapid, and reproducible nanomanufacturing methods for these materials [47,51]. Microfluidic devices are considered an advantageous option for manufacturing nanoparticles, through continuous flow synthesis. In addition, improved heat and mass transport, fast reagent mixing, continuous throughput, greater reaction control, and minimal solvent waste serve as extremely beneficial attributes [52,53]. These features result in tailor-made nanoparticles of controlled size distribution [54-58]. Recently, ionic liquids, such as those based on

dialkylimidazolium cations, have demonstrated promise as both excellent solvents and stabilising ligands for metal nanoparticles while also exhibiting compatibility with PDMS microfluidic devices [59-61]. Their high ionic charge, high dielectric constant, low interfacial tension and ability to form supramolecular hydrogen-bonded networks in the condensed phase make them ideal solvents for the synthesis and stabilization of metal nanoparticles [59-64].

Malmstadt *et al.* [65] presented the synthesis of small monodisperse AuNPs using imidazolium-based ILs in a simple PDMS device. It was reported that the nanoparticles owed their high quality to the particle stabilisation effects of the IL solvent working cooperatively with the controlled and fast mixing from the microfluidic device. This technology was used for the fabrication of other high quality nanoparticles through control of reaction parameters, mixing rate and anion of imidazolium IL. The same group fabricated gold and silver nanoparticles in an ionic liquid solvent using a simple droplet-based microfluidic device [66]. They presented a microfluidic platform which brings together a controlled microfluidic mixing with ionic solvents as in their previous work, but this time involving a simplified two-phase droplet flow for the continuous synthesis of high quality, small, monodisperse gold and silver nanoparticles (AuNPs and AgNPs, respectively). This method is reported as an inexpensive, rapid, and reproducible approach which has minimal impact on the environment and opens the possibility of utilising such platforms for high scale nanomanufacturing of nanoparticles.

After the synthesis of metal nanoparticles, the synergistic combination of ionic liquid and droplet microfluidic process was once again adopted for nanomanufacturing of various inorganic materials by Kim and his co-workers [67]. Inorganic nanomaterials with unique properties and functions received much recent interest due to their wide variety of applications [68-70]. Despite the many efforts to achieve efficient, fast and continuous synthesis of nanostructured inorganic materials with uniform structure, shape and narrow size distribution, the synthetic process has always been a big challenge. This can be attributed to unmanageable mass and heat transfer and the harsh experimental conditions of high temperature and pressure [62,66,71]. Kim and his team presented a novel droplet-ionic liquid cooperated microfluidic (DIM) synthetic method, which reaps the benefits of both ionic liquids and droplet-assisted microreaction systems, enabling ultrafast, delicate and continuous synthesis of inorganic nanomaterials [67]. This method significantly reduced the reaction time

from days to tens of minutes and produced a narrow size distribution and excellent crystalline qualities. As a proof of concept, three nanomaterials ZSM-5, γ -AlOOH, and β -FeOOH were synthesised with the DIM system with excellent quality.

2.5.2. Ionic Liquids for Building a Microfluidics-based Power Generator

Kong *et al.* introduced another outstanding application of ionic liquid in microfluidics by building an electrets-based microfluidic power generator (MPG) for harvesting vibrational energy using ionic liquids [72]. It was demonstrated that the MPG with different ILs can generate varying amounts of power, depending on the different variation magnitude of the top contact area. An MPG using IL over water can operate for longer times in air over a wider range of operating temperatures. This power generator demonstrated the significant potential applications in harvesting low-frequency mechanical vibrations.

2.5.3 Ionic Liquids for Precise Temperature Control in Microfluidics

A novel application, to generate precise and accurate temperature control in microfluidic devices using Joule heating of ionic liquids was presented by Mello *et al.* [73]. The relationship between the temperature and conductivity of ionic liquids allows for an internal temperature measurement, with the possibility for application within a thermocouple system. Microfluidic platforms with such fluidic heaters can be easily manufactured, using small amounts of ionic liquid and require no manipulation or replenishment of the heating medium once introduced into the heating microchannel. They also offer extremely long operational lifetimes (estimated order of hundreds of hours). This concept could be used in thermocycling applications, where integration of multiple heating channels along a co-running reaction microchannel should favour efficient and localised temperature control. Ongoing studies are focusing on the use of these heaters in microfluidic systems for small molecule synthesis within a temperature-controlled environment.

2.6 Conclusions

Lab-on-a-Chip and micro-Total Analysis Systems show great potential for the integration of multiple functional elements, to produce sample-in/answer-out systems. However, due to the critical need for fluid control, fluid transport, separation and sensing, the need for high performance microfluidic components can provide significant obstacles for the development of low-cost, miniaturised microfluidic devices. The examples presented in this chapter show the capabilities of ionic liquids for the fabrication of low cost and high performance microfluidic elements which can improve the potential of low-cost microfluidic devices.

2.7 References

1. Petkovic, M.; Seddon, K.R.; Rebelo, L.P.N.; Pereira, C.S. Ionic liquids: A pathway to environmental acceptability. *Chemical Society Reviews* **2011**, *40*, 1383-1403.
2. S. Zhang, J.W., X. Lu, Q. Zhou *Structures and interactions of ionic liquids* Springer-Verlag: Berlin-Heidelberg, 2014; p 197.
3. Passos, H.; Freire, M.G.; Coutinho, J.A. Ionic liquid solutions as extractive solvents for value-added compounds from biomass. *Green Chemistry* **2014**, *16*, 4786-4815.
4. Stark, A.; Seddon, K.R. Ionic liquids. *Kirk-Othmer encyclopedia of chemical technology* **2007**.
5. Seddon, K.R. Ionic liquids for clean technology. *Journal of Chemical Technology and Biotechnology* **1997**, *68*, 351-356.
6. Soares, B.; Passos, H.; Freire, C.S.; Coutinho, J.A.; Silvestre, A.J.; Freire, M.G. Ionic liquids in chromatographic and electrophoretic techniques: Toward additional improvements in the separation of natural compounds. *Green Chemistry* **2016**, *18*, 4582-4604.
7. Dupont, J.; Suarez, P.A.; Umpierre, A.P.; Souza, R.F.d. Pd (ii)-dissolved in ionic liquids: A recyclable catalytic system for the selective biphasic hydrogenation of dienes to monoenes. *Journal of the Brazilian Chemical Society* **2000**, *11*, 293-297.
8. Earle, M.J.; Esperança, J.M.; Gilea, M.A.; Lopes, J.N.C.; Rebelo, L.P.; Magee, J.W.; Seddon, K.R.; Widegren, J.A. The distillation and volatility of ionic liquids. *Nature* **2006**, *439*, 831.
9. Guo, F.; Zhang, S.; Wang, J.; Teng, B.; Zhang, T.; Fan, M. Synthesis and applications of ionic liquids in clean energy and environment: A review. *Current Organic Chemistry* **2015**, *19*, 455-468.
10. MSS Esperança, J.; Canongia Lopes, J.N.; Tariq, M.; Santos, L.s.M.; Magee, J.W.; Rebelo, L.s.P.N. Volatility of aprotic ionic liquids□ a review. *Journal of Chemical & Engineering Data* **2009**, *55*, 3-12.

11. Plechkova, N.V.; Seddon, K.R. Applications of ionic liquids in the chemical industry. *Chemical Society Reviews* **2008**, *37*, 123-150.
12. Weber, C.C.; Masters, A.F.; Maschmeyer, T. Structural features of ionic liquids: Consequences for material preparation and organic reactivity. *Green Chemistry* **2013**, *15*, 2655-2679.
13. Wilkes, J.S. A short history of ionic liquids—from molten salts to neoteric solvents. *Green Chemistry* **2002**, *4*, 73-80.
14. Zhang, J.; Bond, A.M. Practical considerations associated with voltammetric studies in room temperature ionic liquids. *Analyst* **2005**, *130*, 1132-1147.
15. Rogers, R.D.; Seddon, K.R. Ionic liquids--solvents of the future? *Science* **2003**, *302*, 792-793.
16. Earle, M.J.; Seddon, K.R. Ionic liquids. Green solvents for the future. *Pure and applied chemistry* **2000**, *72*, 1391-1398.
17. Freire, M.G.; Claudio, A.F.M.; Araujo, J.M.; Coutinho, J.A.; Marrucho, I.M.; Lopes, J.N.C.; Rebelo, L.P.N. Aqueous biphasic systems: A boost brought about by using ionic liquids. *Chemical Society Reviews* **2012**, *41*, 4966-4995.
18. Ranke, J.; Stolte, S.; Störmann, R.; Arning, J.; Jastorff, B. Design of sustainable chemical products the example of ionic liquids. *Chemical Reviews* **2007**, *107*, 2183-2206.
19. Rebelo, L.P.N.; Lopes, J.N.C.; Esperanca, J.M.; Guedes, H.J.; Łachwa, J.; Najdanovic-Visak, V.; Visak, Z.P. Accounting for the unique, doubly dual nature of ionic liquids from a molecular thermodynamic and modeling standpoint. *Accounts of chemical research* **2007**, *40*, 1114-1121.
20. Rogers, R.D.; Seddon, K.R. *Ionic liquids iii a: Fundamentals, progress, challenges, and opportunities: Properties and structure*. ACS Publications: 2005.
21. Welton, T. Room-temperature ionic liquids. Solvents for synthesis and catalysis. *Chemical reviews* **1999**, *99*, 2071-2084.
22. Freire, M.G.; Teles, A.R.R.; Rocha, M.A.; Schröder, B.; Neves, C.M.; Carvalho, P.J.; Evtuguin, D.V.; Santos, L.M.; Coutinho, J.A. Thermophysical characterization of ionic liquids able to dissolve biomass. *Journal of Chemical & Engineering Data* **2011**, *56*, 4813-4822.
23. Wishart, J.F. Energy applications of ionic liquids. *Energy & Environmental Science* **2009**, *2*, 956-961.
24. Le Bideau, J.; Viau, L.; Vioux, A. Ionogels, ionic liquid based hybrid materials. *Chemical Society Reviews* **2011**, *40*, 907-925.
25. Marr, P.C.; Marr, A.C. Ionic liquid gel materials: Applications in green and sustainable chemistry. *Green Chemistry* **2016**, *18*, 105-128.
26. Culbertson, C.T.; Mickleburgh, T.G.; Stewart-James, S.A.; Sellens, K.A.; Pressnall, M. Micro total analysis systems: Fundamental advances and biological applications. *Analytical chemistry* **2013**, *86*, 95-118.
27. Livak-Dahl, E.; Sinn, I.; Burns, M. Microfluidic chemical analysis systems. **2011**.
28. Byrne, R.; Benito-Lopez, F.; Diamond, D. Materials science and the sensor revolution. *Materials Today* **2010**, *13*, 16-23.
29. Sugiura, S.; Sumaru, K.; Ohi, K.; Hiroki, K.; Takagi, T.; Kanamori, T. Photoresponsive polymer gel microvalves controlled by local light irradiation. *Sensors and Actuators A: Physical* **2007**, *140*, 176-184.

30. Benito-Lopez, F.; Byrne, R.; Răduță, A.M.; Vrana, N.E.; McGuinness, G.; Diamond, D. Ionogel-based light-actuated valves for controlling liquid flow in micro-fluidic manifolds. *Lab on a Chip* **2010**, *10*, 195-201.
31. Czugala, M.; O'Connell, C.; McKeon, A.; Sánchez, C.F.; Munoz-Berbel, X.; Llobera, A.; Diamond, D.; Benito-Lopez, F. In *Photo-patterning of ionogel microstructures for on-chip microvalve applications controlled by fiber optics*, Solid-State Sensors, Actuators and Microsystems (TRANSDUCERS & EUROSENSORS XXVII), 2013 Transducers & Eurosensors XXVII: The 17th International Conference on, 2013; IEEE: pp 1695-1698.
32. Czugala, M.; Fay, C.; O'Connor, N.E.; Corcoran, B.; Benito-Lopez, F.; Diamond, D. Portable integrated microfluidic analytical platform for the monitoring and detection of nitrite. *Talanta* **2013**, *116*, 997-1004.
33. Benito-Lopez, F.; Antoñana-Díez, M.; Curto, V.F.; Diamond, D.; Castro-López, V. Modular microfluidic valve structures based on reversible thermoresponsive ionogel actuators. *Lab on a Chip* **2014**, *14*, 3530-3538.
34. Gallagher, S.; Kavanagh, A.; Ziołkowski, B.; Florea, L.; MacFarlane, D.R.; Fraser, K.; Diamond, D. Ionic liquid modulation of swelling and lcst behavior of n-isopropylacrylamide polymer gels. *Physical Chemistry Chemical Physics* **2014**, *16*, 3610-3616.
35. K. Ghamsari, A.; Zegeye, E.; Jin, Y.; Woldesenbet, E. Application of bucky gel in fabrication of a low-voltage rapid microvalve for flow regulation. *ACS applied materials & interfaces* **2013**, *5*, 5408-5412.
36. Akyazi, T.; Saez, J.; Elizalde, J.; Benito-Lopez, F. Fluidic flow delay by ionogel passive pumps in microfluidic paper-based analytical devices. *Sensors and Actuators B: Chemical* **2016**, *233*, 402-408.
37. Kavanagh, A.; Byrne, R.; Diamond, D.; Fraser, K.J. Stimuli responsive ionogels for sensing applications—an overview. *Membranes* **2012**, *2*, 16-39.
38. Behera, K.; Pandey, S.; Kadyan, A.; Pandey, S. Ionic liquid-based optical and electrochemical carbon dioxide sensors. *Sensors* **2015**, *15*, 30487-30503.
39. Yang, S.Y.; Ciccoira, F.; Byrne, R.; Benito-Lopez, F.; Diamond, D.; Owens, R.M.; Malliaras, G.G. Electrochemical transistors with ionic liquids for enzymatic sensing. *Chemical Communications* **2010**, *46*, 7972-7974.
40. Lau, R.M.; Sorgedraeger, M.J.; Carrea, G.; van Rantwijk, F.; Secundo, F.; Sheldon, R.A. Dissolution of candida antarctica lipase b in ionic liquids: Effects on structure and activity. *Green Chemistry* **2004**, *6*, 483-487.
41. Yamaguchi, M.; Mitsumori, M.; Kano, Y. Noninvasively measuring blood glucose using saliva. *IEEE Engineering in Medicine and Biology Magazine* **1998**, *17*, 59-63.
42. Khodagholy, D.; Curto, V.F.; Fraser, K.J.; Gurfinkel, M.; Byrne, R.; Diamond, D.; Malliaras, G.G.; Benito-Lopez, F.; Owens, R.M. Organic electrochemical transistor incorporating an ionogel as a solid state electrolyte for lactate sensing. *Journal of Materials Chemistry* **2012**, *22*, 4440-4443.
43. Curto, V.F.; Scheuermann, S.; Owens, R.M.; Ranganathan, V.; MacFarlane, D.R.; Benito-Lopez, F.; Diamond, D. Probing the specific ion effects of biocompatible hydrated choline ionic liquids on lactate oxidase biofunctionality in sensor applications. *Physical Chemistry Chemical Physics* **2014**, *16*, 1841-1849.
44. Czugala, M.; Gorkin III, R.; Phelan, T.; Gaughran, J.; Curto, V.F.; Ducrée, J.; Diamond, D.; Benito-Lopez, F. Optical sensing system based on wireless

- paired emitter detector diode device and ionogels for lab-on-a-disc water quality analysis. *Lab on a Chip* **2012**, *12*, 5069-5078.
45. Fraser, K.J.; Curto, V.F.; Coyle, S.; Schazmann, B.; Byrne, R.; Benito-Lopez, F.; Owens, R.M.; Malliaras, G.G.; Diamond, D. In *Wearable electrochemical sensors for monitoring performance athletes*, SPIE Photonic Devices+ Applications, 2011; International Society for Optics and Photonics: pp 81180C-81180C-81112.
 46. Yanes, E.G.; Gratz, S.R.; Baldwin, M.J.; Robison, S.E.; Stalcup, A.M. Capillary electrophoretic application of 1-alkyl-3-methylimidazolium-based ionic liquids. *Analytical chemistry* **2001**, *73*, 3838-3844.
 47. Xu, Y.; Wang, E. Ionic liquids used in and analyzed by capillary and microchip electrophoresis. *Journal of Chromatography A* **2009**, *1216*, 4817-4823.
 48. Choi, D.Y.; Kim, M.H.; Oh, Y.S.; Jung, S.-H.; Jung, J.H.; Sung, H.J.; Lee, H.W.; Lee, H.M. Highly stretchable, hysteresis-free ionic liquid-based strain sensor for precise human motion monitoring. *ACS applied materials & interfaces* **2017**, *9*, 1770-1780.
 49. Wu, C.-Y.; Liao, W.-H.; Tung, Y.-C. Integrated ionic liquid-based electrofluidic circuits for pressure sensing within polydimethylsiloxane microfluidic systems. *Lab on a Chip* **2011**, *11*, 1740-1746.
 50. Liu, M.-C.; Shih, H.-C.; Wu, J.-G.; Weng, T.-W.; Wu, C.-Y.; Lu, J.-C.; Tung, Y.-C. Electrofluidic pressure sensor embedded microfluidic device: A study of endothelial cells under hydrostatic pressure and shear stress combinations. *Lab on a Chip* **2013**, *13*, 1743-1753.
 51. Chang, C.-H.; Paul, B.K.; Remcho, V.T.; Atre, S.; Hutchison, J.E. Synthesis and post-processing of nanomaterials using microreaction technology. *Journal of Nanoparticle Research* **2008**, *10*, 965-980.
 52. Demello, A.J. Control and detection of chemical reactions in microfluidic systems. *Nature* **2006**, *442*, 394-402.
 53. Song, Y.; Hormes, J.; Kumar, C.S. Microfluidic synthesis of nanomaterials. *Small* **2008**, *4*, 698-711.
 54. Chan, E.M.; Mathies, R.A.; Alivisatos, A.P. Size-controlled growth of cdse nanocrystals in microfluidic reactors. *Nano Letters* **2003**, *3*, 199-201.
 55. Khan, S.A.; Günther, A.; Schmidt, M.A.; Jensen, K.F. Microfluidic synthesis of colloidal silica. *Langmuir* **2004**, *20*, 8604-8611.
 56. Song, H.; Chen, D.L.; Ismagilov, R.F. Reactions in droplets in microfluidic channels. *Angewandte chemie international edition* **2006**, *45*, 7336-7356.
 57. Song, Y.; Modrow, H.; Henry, L.L.; Saw, C.K.; Doomes, E.; Palshin, V.; Hormes, J.; Kumar, C.S. Microfluidic synthesis of cobalt nanoparticles. *Chemistry of materials* **2006**, *18*, 2817-2827.
 58. Wagner, J.; Köhler, J. Continuous synthesis of gold nanoparticles in a microreactor. *Nano letters* **2005**, *5*, 685-691.
 59. Dupont, J.; Scholten, J.D. On the structural and surface properties of transition-metal nanoparticles in ionic liquids. *Chemical Society Reviews* **2010**, *39*, 1780-1804.
 60. Krishnadasan, S.; Brown, R. Intelligent routes to the controlled synthesis of nanoparticles. *Lab on a Chip* **2007**, *7*, 1434-1441.
 61. Neouze, M.-A. About the interactions between nanoparticles and imidazolium moieties: Emergence of original hybrid materials. *Journal of Materials Chemistry* **2010**, *20*, 9593-9607.

62. Abou-Hassan, A.; Sandre, O.; Cabuil, V. Microfluidics in inorganic chemistry. *Angewandte Chemie International Edition* **2010**, *49*, 6268-6286.
63. Ma, Z.; Yu, J.; Dai, S. Preparation of inorganic materials using ionic liquids. *Advanced Materials* **2010**, *22*, 261-285.
64. Marquardt, D.; Xie, Z.; Taubert, A.; Thomann, R.; Janiak, C. Microwave synthesis and inherent stabilization of metal nanoparticles in 1-methyl-3-(3-carboxyethyl)-imidazolium tetrafluoroborate. *Dalton Transactions* **2011**, *40*, 8290-8293.
65. Lazarus, L.L.; Yang, A.S.-J.; Chu, S.; Brutchey, R.L.; Malmstadt, N. Flow-focused synthesis of monodisperse gold nanoparticles using ionic liquids on a microfluidic platform. *Lab on a Chip* **2010**, *10*, 3377-3379.
66. Lazarus, L.L.; Riche, C.T.; Marin, B.C.; Gupta, M.; Malmstadt, N.; Brutchey, R.L. Two-phase microfluidic droplet flows of ionic liquids for the synthesis of gold and silver nanoparticles. *ACS applied materials & interfaces* **2012**, *4*, 3077-3083.
67. Hoang, P.H.; Park, H.; Kim, D.-P. Ultrafast and continuous synthesis of unaccommodating inorganic nanomaterials in droplet-and ionic liquid-assisted microfluidic system. *Journal of the American Chemical Society* **2011**, *133*, 14765-14770.
68. Cushing, B.L.; Kolesnichenko, V.L.; O'Connor, C.J. Recent advances in the liquid-phase syntheses of inorganic nanoparticles. *Chemical reviews* **2004**, *104*, 3893-3946.
69. Jun, Y.w.; Choi, J.s.; Cheon, J. Shape control of semiconductor and metal oxide nanocrystals through nonhydrolytic colloidal routes. *Angewandte Chemie International Edition* **2006**, *45*, 3414-3439.
70. van Bommel, K.J.; Friggeri, A.; Shinkai, S. Organic templates for the generation of inorganic materials. *Angewandte Chemie International Edition* **2003**, *42*, 980-999.
71. Duraiswamy, S.; Khan, S.A. Droplet-based microfluidic synthesis of anisotropic metal nanocrystals. *Small* **2009**, *5*, 2828-2834.
72. Kong, W.; Cheng, L.; He, X.; Xu, Z.; Ma, X.; He, Y.; Lu, L.; Zhang, X.; Deng, Y. Electret-based microfluidic power generator for harvesting vibrational energy by using ionic liquids. *Microfluidics and Nanofluidics* **2015**, *18*, 1299-1307.
73. De Mello, A.J.; Habgood, M.; Lancaster, N.L.; Welton, T.; Wootton, R.C. Precise temperature control in microfluidic devices using joule heating of ionic liquids. *Lab on a Chip* **2004**, *4*, 417-419.

Chapter 3: Poly(Ionic Liquid) Semi-interpenetrating Network Multi-Responsive Hydrogels

3.1 Abstract

3.2 Introduction

3.3 Experimental

3.3.1 Materials and Reagents

3.3.2 Synthesis of Tributylhexyl Phosphonium 3-Sulfopropyl Acrylate Ionic Liquid Monomer

3.3.3 Synthesis of the Linear Poly(N-isopropylacrylamide-co-Spiropyran-co-Acrylic Acid) p(NiPAAm-BSP-AA) Copolymer

3.3.4 Synthesis of the Semi-Interpenetrating Network Hydrogels

3.3.5 Thermal Behaviour of Linear p(NiPAAm-SPA-AA) Copolymer

3.3.6 White-Light Curing Studies of the sIPN Hydrogels Using Rheometry

3.3.7 Measurement of Stimuli-Induced Shrinking

3.4 Results and Discussion

3.4.1 White Light and Temperature Response of the Linear p(NiPAAm-BSP-AA) Copolymer Solutions

3.4.2 Photo-Induced Curing Studies and Mechanical Properties of the Hydrogels

3.4.3 White Light Induced Shrinking

3.4.4 Ionic Radius Dependent Shrinking

3.4.5 Temperature Induced Shrinking

3.5 Conclusions

3.6 References

Chapter 3

Poly(Ionic Liquid) Semi-Interpenetrating Network Multi-Responsive Hydrogels^{*}

*Poly(Ionic Liquid) Semi-Interpenetrating Network Multi-Responsive Hydrogels, A. Tudor, L. Florea, S. Gallagher, J. Burns, D. Diamond, *Sensors*, **16**, 219 – 235, 2016.

3.1 Abstract

Herein we describe poly(ionic liquid) hydrogel actuators that are capable of responding to multiple stimuli, namely temperature, ionic strength and white light irradiation. Using two starting materials, a crosslinked poly ionic liquid (PIL) and a linear poly(N-isopropylacrylamide-co-spiropyran-co-acrylic acid), several semi-interpenetrating (sIPN) hydrogels were synthesised. The dimensions of hydrogel discs were measured before and after applying the stimuli, to quantify their response. Samples composed of 100% crosslinked PIL alone showed an average area reduction value of ~53% when the temperature was raised from 20 °C to 70 °C, ~24% when immersed in 1% w/w NaF salt solution and no observable photo-response. In comparison, sIPNs containing 300% w/w linear polymer showed an average area reduction of ~45% when the temperature was raised from 20 °C to 70 °C, ~36% when immersed in 1% NaF w/w salt solution and ~10% after 30 min exposure to white light irradiation, respectively. Moreover, by varying the content of the linear component, fine-control over the photo-, thermo- and salt response, swelling-deswelling rate and mechanical properties of the resulting sIPN was achieved.

This type of triggered surfactant release through external stimulation aims to achieve new means for controlling droplet movement within microfluidic devices, as well as developing biomimetic synthetic vehicles with integrated functionalities such as detection of chemoattractant gradients, signaling, sensing and repair.

3.2 Introduction

Stimuli-responsive polymers are defined as polymers that exhibit a conformation change in a reliable, reproducible and useful manner when exposed to a variation in their external environment [1,2]. Many types of stimuli can be employed, including temperature, pressure, magnetic and electric field, lighting conditions, pH and the presence of other chemical species in their local medium [1,3-20]. Hydrogels comprise a particularly interesting class of stimuli-responsive materials due to their biomimetic nature [6]. These materials are crosslinked polymer networks that absorb large quantities of water and, when under the influence of specific stimuli, change their water absorption properties, which in turn translate into a hydrogel volume variation [7,14]. Extensively studied examples of such materials include N-isopropylacrylamide (NiPAAm) hydrogels, which possess a well-documented

thermally induced shrinking behaviour associated with a lower critical solution temperature (LCST) at ca. 32-35 °C [4,5,9,12-15,21-24]. This behaviour is a result of a thermodynamically driven equilibrium shift from the strongly hydrated form defined by solution-polymer interactions to a much more compact form dominated by polymer-polymer interactions. Copolymerization of NiPAAm with other stimuli-responsive units, such as photochromic dyes, offers the possibility of creating hydrogels that respond to additional stimuli such as light [4,12,25].

Ziołkowski et al. recently described the synthesis and characterization of a photo/thermo-responsive hydrogel material consisting of NiPAAm-co-spiropyran-co-acrylic acid (p(NiPAAm-BSP-AA)) copolymer [4]. The additional photo-response is conferred by the presence of the spiropyran photochromic monomer that reversibly changes its conformation from a hydrophilic protonated merocyanine form (Mc-H⁺) to a hydrophobic spiropyran form (SP) under different illumination conditions. When immersed in DI water, the acrylic acid comonomer dissociates and the spiropyran is protonated to form the Mc-H⁺ form. In this conformation, the molecule is more hydrophilic compared to the closed SP form, triggering hydrogel expansion. Upon white light irradiation, the reverse process happens, and the Mc-H⁺ is converted back to the closed SP form. Thus, based on this photo-induced transition of the polymer from a more hydrophilic to a more hydrophobic conformation, water is expelled from the hydrogel matrix. This effect caused some of the hydrogels to shrink by ~49%, compared to their maximum shrinking capability, after a 20 min exposure to white-light. The gels subsequently revert back to ~97% of their original size after 1 h in the dark.

A new class of polymeric materials that feature LCST behaviour are a series of phosphonium-based poly(ionic liquids) (PILs) [3,8,10,11,15,26-28]. These materials represent a subgroup of ionic liquids that include polymerizable groups in the cation, the anion or both, respectively. The PILs inherit the properties of ionic liquids, such as very low vapour pressure, thermal stability and high ionic conductivity [29-31], while they can also be polymerized, thus can be used in the production of membranes, hydrogels, coatings and films. A recent paper by Gallagher et. al. discusses the improved thermal response of a semi-interpenetrating network (sIPN) synthesized by polymerizing a phosphonium PIL in the presence of linear pNiPAAm chains [15]. The addition of linear pNiPAAm chains to the crosslinked PIL matrix improved the

temperature-induced shrinking at 75 °C of the PIL hydrogels by ~13% when compared to the crosslinked PIL without any linear pNiPAAm chains.

In this context, the focus of the following study was the synthesis of multi-responsive sIPN hydrogels using a tributylhexyl phosphonium 3-sulfopropyl acrylate PIL crosslinked matrix and controlled amounts of linear p(NiPAAm-BSP-AA) copolymer chains. The shrinking properties of these hydrogels under the influence of temperature, white light irradiation and salt solutions were described. Further characterization of the linear copolymer was performed using Differential Scanning Calorimetry (DSC) and UV-Vis spectroscopy, while the curing properties of the sIPNs were analysed using rheometry.

3.3 Experimental

3.3.1 Materials and methods

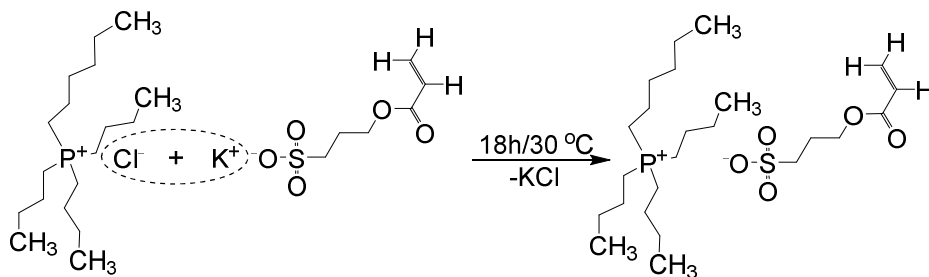
N-isopropylacrylamide 97% (NiPAAm) (100 ppm MEHQ as inhibitor), phenyl-bis(2,4,6-trimethylbenzoyl) phosphine oxide 97% (PBPO), potassium 3-sulfopropyl acrylate (KSPA), polypropylene glycol diacrylate (Mw ~800, 100 ppm MEHQ and 100 ppm BHT as inhibitors) (PPG800), sodium fluoride >99%, sodium chloride >99%, sodium iodide >99% were bought from Sigma Aldrich® and used as received, sodium bromide >99% and HPLC grade acetonitrile (ACN) were bought from Riedel de Hæn® and used as received. The tributylhexyl phosphonium chloride (P4446Cl) was kindly donated by Cytec® Industries. Trimethyl-6-hydroxyspiro-(2H-1-benzopyran-2,2'-indoline) acrylate (BSP) was synthesized according to a previous procedure [4]. Deionized water (18.2 MΩ·cm⁻¹) (DI water) was made using a Merck Millipore Milli-Q Water Purification System.

3.3.2 Synthesis of tributylhexyl phosphonium 3-sulfopropyl acrylate ionic liquid monomer

The synthesis of tributylhexyl phosphonium 3-sulfopropyl acrylate (PSPA) was carried out by dissolving 5 g of P₄₄₄₆Cl and 4.628 g of KSPA (1.3 molar equivalents) in 25 ml of deionized water, followed by stirring at 30 °C for 18 h (Scheme 2.1). The reaction product was extracted three times with 25 ml of dichloromethane (DCM).

The resulting organic phase was washed with deionized water to extract any unreacted products. Following this final separation, anhydrous MgSO_4 was added and the resulting solution was filtrated. The PSPA organic solution was concentrated using a rotary evaporator, followed by extracting the final solvent traces using a high vacuum pump (0.5 mBar). The yield of the synthesis and purification method was around ~65%.

PSPA – ^1H NMR, δH (400 MHz): 0.84-0.95 (m, 12H, CH_3), 1.26-1.29 (m, 4H, CH_2), 1.47-1.50 (m, 16H, CH_2), 2.14-2.32 (m, 10H, CH_2), 2.84-2.87 (t, 2H, CH_2), 4.22-4.25 (t, 2H, CH_2), 5.74-5.77 (dd, 1H, CH), 6.01-6.08 (m, 1H, CH), 6.31-6.36 (dd, 1H, CH) ppm.



Scheme 3.1. The PSPA synthesis reaction.

3.3.3 Synthesis of the linear poly(N-isopropylacrylamide-co-spiropyran-co-acrylic acid) p(NiPAAm-BSP-AA) copolymer

For the synthesis of linear p(NiPAAm-BSP-AA) copolymer, 1.13g of NiPAAm was dissolved in 5 ml of THF, along with 1 mol% eq. of PBPO, 1 mol% eq. BSP and 5 mol% eq. acrylic acid. The mixture was stirred until all of the components were completely dissolved. The resulting solution was then photopolymerized for 20 min with the help of a Dolan Jenner Industries LMI-6000 Fiber-Lite white light source (~200 kLux). Finally, after the polymerization was finished, the resulting dissolved polymer was precipitated in cold diethyl ether. Afterwards, the precipitate was vacuum-filtered and dried in a vacuum oven at 40 °C for one hour to yield the p(NiPAAm-BSP-AA) copolymer.

3.3.4 Synthesis of the semi-interpenetrating network hydrogels

The semi-interpenetrating networks (sIPNs) were synthesized by adding the required amount of PSPA to a series of linear p(NiPAAm-BSP-AA) copolymer solutions in 1:1 w/w mixture of ACN and DI water, together with 2 mol % eq. PBPO and 5 mol % eq. PPG800 with regard to PSPA (Table 3.1). The amount of linear copolymer was calculated so that the molar ratio between the PSPA and the NiPAAm co-monomer increases from 1:1 in sIPN 1 to 1:4 in sIPN 4 (Figure 3.1). This was performed to provide some insights into how the increasing amounts of linear p(NiPAAm-BSP-AA) affects the thermo- and photo- induced shrinking capabilities of the resulting sIPN hydrogel.

Table 3.1. Surface tension measurements of solutions used in the study, with and without the IL surfactant added.

	PILc	sIPN 1	sIPN 2	sIPN 3	sIPN 4
P_{4,4,4,6}-SPA (g)	0.1935	0.1935	0.1935	0.1935	0.1935
Linear polymer (g)	0	0.0453	0.0905	0.1308	0.1810
P_{4,4,4,6}-SPA:NiPAAm (molar ratio)	1:0	1:1	1:2	1:3	1:4
PPG 800 (g)	0.0160	0.0160	0.0160	0.0160	0.0160
PBPO (g)	0.0034	0.0034	0.0034	0.0034	0.0034
ACN:H₂O (g)	0.1935	0.1935	0.1935	0.1935	0.1935

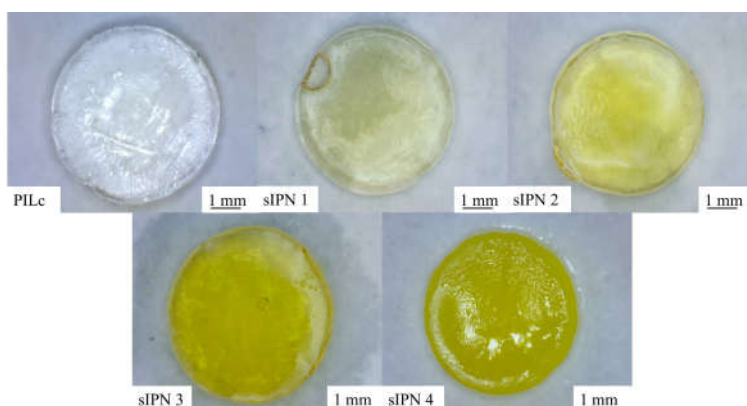


Figure 3.1. The photopolymerized hydrogels after swelling in DI water at 20°C for 24h.

The monomer solutions were mechanically shaken until all of the components were dissolved. Following this, volumes from each mixture were transferred into a

polydimethylsiloxane mould with wells of 3 mm diameter and 1 mm depth, and photopolymerized in the wells using a Dolan Jenner Industries LMI-6000 Fiber-Lite white light source (~200 kLux) for 20 min. After the polymerization was complete, the gels were hydrated in DI Water until they were fully swollen.

3.3.5 Thermal behaviour of linear p(NiPAAm-SPA-AA) copolymer

A Perkin-Elmer Lambda 900 UV-Vis spectrometer was used to determine the presence of the lower critical solution temperature (LCST) in the linear p(NiPAAm-BSP-AA) copolymer. This was achieved by making a 0.1% w/w linear copolymer solution in DI Water, and measuring its absorbance at 2 °C temperature steps between 20 °C and 36 °C. Temperature control was achieved via a Perkin Elmer PTP-1 Peltier Temperature Programmer. The temperature was held constant for 5 min at each temperature step to enable the dynamics of the temperature effect on the polymer to be observed. Two sets of data were gathered, one for the solution kept in the dark and one for the solution after it was irradiated with white light. To confirm the LCST determined using UV-Vis spectrometry, differential scanning calorimetry analysis (DSC) was performed using a Perkin-Elmer Pyris 1 DSC, which was calibrated using an indium standard with a melting point of 156.6 °C. The sample, 14.3 mg of 2.5% w/w linear copolymer solution in DI Water, was analysed using the following thermal program: heating from 14 °C to 70 °C at a heating rate of 10 °C/min followed by cooling from 70 °C to 14 °C at a cooling rate of 10°C/min. This process was repeated three times to ensure that the results were reproducible.

3.3.6 White light curing studies of the sIPN hydrogels using rheometry

An Anton-Paar MCR301 rheometer and was used to analyse the photo-induced curing behaviour of PILc and sIPN mixtures described in Table 3.1. The analysis was performed by fitting the rheometer with the PP15 parallel plate tool and using a strain of 0.1% at a frequency of 1 Hz. Data points were collected every 5 seconds for a total of 480 seconds. The rheometer was fitted with a glass slide base to facilitate the photo-polymerization of the monomer mixtures. The white-light source was mounted

to provide a ~200 kLux illuminance exposure on the monomer mixture. All measurements were taken at a constant temperature of 25 °C.

3.3.7 Measurement of stimuli-induced shrinking

Quantifying the stimuli-induced shrinking of PILc and sIPN hydrogels was achieved by taking area measurements before and after applying the stimulus. Sample images were taken with an Aigo GE-5 digital microscope, fitted with a 60x lens and using Aigo ScopeImage 9.0 imaging software. The resulting images were analysed using ImageJ image analysis software. For each stimulus measurement three gels were used. The %shrinking of each hydrogel was calculated using the formula:

$$\%shrinking = 100 - (A_f/A_i \cdot 100) \quad (1)$$

where A_f is area of the hydrogel after applying a stimulus and A_i is the initial area of the hydrogel.

The stimuli investigated were: white-light irradiation, ionic strength and temperature. For the white-light induced shrinking, the hydrogels were placed in poly(methyl methacrylate) (PMMA) wells filled with DI Water and covered with a glass slide, to prevent evaporation, and irradiated with white light (~200 kLux) for 30 min. In the case of the ionic strength induced shrinking, the gels were swollen in DI water and transferred to 1% w/w solutions of NaF, NaCl, NaBr and NaI, respectively, and left until equilibrium was reached. Temperature measurements were performed using an Anton Paar MCR 301 Rheometer Peltier holder fitted with an aluminium plate. The gels were placed on the plate and covered with either DI Water or 0.5% w/w NaCl solution. A glass plate cover was used to avoid evaporation. The temperature program used covered a temperature interval between 20 °C and 70 °C with a heating step of 5 °C. Between each step, the temperature was kept constant for a period of 5 min to ensure the gels reached equilibrium, after which an image was taken for subsequent analysis.

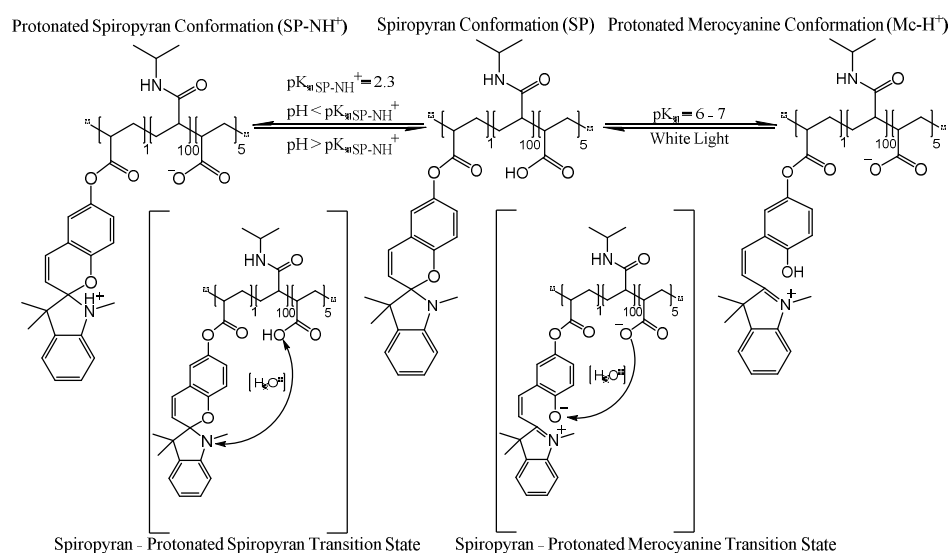
3.4 Results and discussion

3.4.1 White light and temperature response of the linear p(NiPAAm-BSP-AA) copolymer solutions

When p(NiPAAm-BSP-AA) linear copolymer is dissolved in DI Water or in aqueous solutions of pH>4, the following equilibrium takes place (Scheme 3.2): in pH solutions of pH>4 (pKa acrylic acid = 4.2 [4]), the acrylic acid comonomer dissociates and in the transition state, it protonates the merocyanine (Mc) isomer of the spiropyran, forming the yellow-coloured protonated, merocyanine (Mc-H⁺, Scheme 2.2). When the solution is irradiated with white-light the equilibrium shifts towards the closed colourless spiropyran isomer (Scheme 3.2). The Mc-H⁺ form is more hydrophilic, while the closed spiropyran form is more hydrophobic [4,12]. This equilibrium shift has an important impact on the hydrophilic/hydrophobic character of the dissolved polymer, triggering a bulk conversion of the polymer into a more hydrophobic conformation. Poly(NiPAAm) is a thermo-responsive polymer, meaning that it exhibits lower critical solution temperature (LCST) behaviour, which in the case of poly(NiPAAm) is around 32 °C [5,12,21]. The mechanism behind this behaviour is related to how the solubility equilibrium between the linear polymer chains and the hydrating water molecules changes due to an increase in temperature. Below the LCST, the hydrophilic amide part of NiPAAm forms hydrogen bonds with the water molecules, and the polymer adopts a swollen, strongly hydrated extended coil conformation. In contrast, above the LCST, the polymer-solvent hydrogen bonds weaken to the extent that the hydrophobic interactions between the polymer chains become dominant. This makes the polymer adopt a more compact globular form, which precipitates out of the solution [21]. By co-polymerising additional monomeric units in the poly(NiPAAm), like BSP in this instance, this temperature-response can be converted into a photo-response. The creation of hydrophobic units (spiropyran conformation) inside the polymer matrix through irradiation with white light causes a cascade effect, inducing the precipitation of the polymer chain from the hydrated form. As a consequence, an expulsion of water takes place when the equilibrium is shifted by white light irradiation, and the polymer shrinks.

The determination of the LCST of p(NiPAAm-BSP-AA) is a necessary part of this study, because it enables us to gain an insight into how the additional co-

monomers influence the thermo-responsive properties of the linear copolymer [32]. The LCST of the copolymer was determined both qualitatively by UV-Vis spectroscopy and quantitatively by DSC. The UV-Vis LCST analysis was made using a 0.1% w/w copolymer solution in DI Water. This allowed the LCST to be determined qualitatively by observing the temperature-dependent absorbance increase at 700nm. At this wavelength there is no interference from any other peaks present in the absorbance spectrum of the copolymer solution [12]. This means that the increase in absorbance is solely caused by precipitation of linear copolymer in solution. Following the qualitative analysis of the LCST, DSC was chosen to generate quantitative data. During the LCST event there is a change in the hydration energy of the polymer, which appears as an endothermic transition on the DSC curve [5].



Scheme 3.2. Equilibrium of the p(NiPAAm-BSP-AA) copolymer in DI water under different illumination conditions.

The UV-Vis analysis of the non-irradiated sample shows an absorption peak centred at 422 nm, which corresponds to the presence of the protonated merocyanine (Mc-H⁺) conformation in the copolymer solution [12]. This is the dominant species of the SP/Mc/Mc-H⁺ system under these conditions, and it arises due to the dissociation of the AA comonomer and protonation of the MC form to Mc-H⁺ (pK_a = 6-7 [12]). This process happens spontaneously when the p(NiPAAm-BSP-AA) copolymer is hydrated in DI water in the dark [4]. The N-protonated SP form (SP-NH⁺, pK_a = 2.3 [33]) is formed in a competing side equilibrium and the band with the maximum centre around 316 nm can be assigned to this form [33]. From 20 °C to 28 °C the

absorption peak at 422nm continuously rises, because the acrylic acid dissociation equilibrium is shifted towards release of free protons [34], increasing the amount of Mc-H^+ present in the linear copolymer. Between 30 °C and 36 °C the absorbance at 422nm continues to rise, with a concomitant red shift towards 436 nm, which is associated with the formation of Mc-H^+ J-aggregates [35]. Simultaneously, the absorbance at 700 nm starts growing, indicating that precipitation is happening.

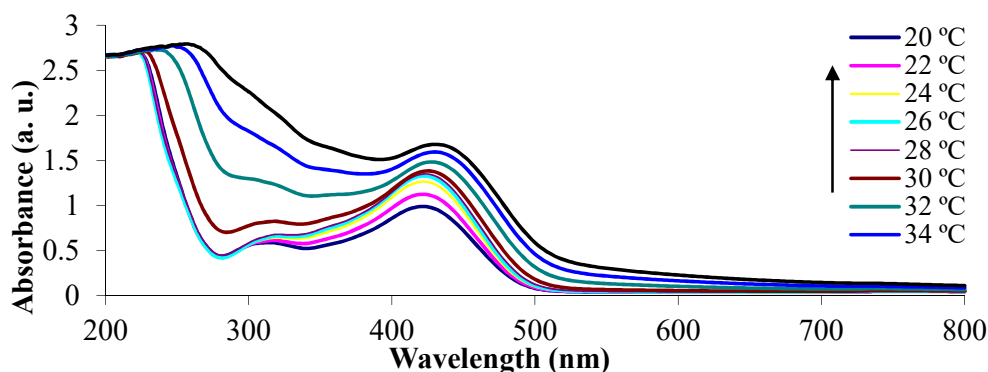


Figure 3.2. UV-Vis absorbance spectra of the non-irradiated 0.1 % w/w *p*(NiPAAm-BSP-AA) linear copolymer solution in DI water.

The same solution was then irradiated with white light (~ 250 kLux) for 5 min before the absorbance spectrum was recorded at each temperature (Figure 3.2). After the solution was irradiated, its colour changed from bright yellow to colourless, due to conversion of Mc-H^+ to the closed SP form (Figure 2.3). This is confirmed by the decrease of the peak at 422 nm. The absorbance peak centred at 294 nm shown in Figure 3.3 due to the presence of the SP isomer, while the shoulder at ~ 316 nm probably indicates the presence of the SP-NH^+ form [33].

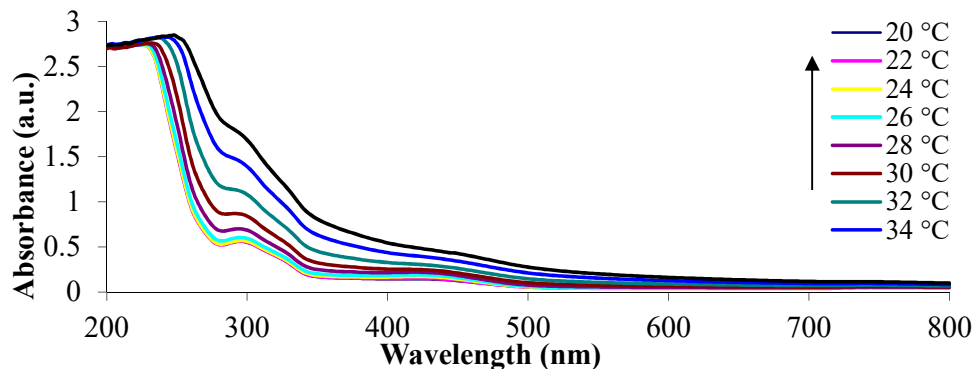


Figure 3.3. UV-Vis absorbance spectra of the white light irradiated 0.1 % w/w *p*(NiPAAm-BSP-AA) linear copolymer solution in DI water.

In Figure 3.4 the rise in absorbance at 700 nm between the non-irradiated and white light irradiated samples is compared. The absorbance at 700 nm for the white light irradiated solution begins to increase at a lower temperature (~ 28 °C) compared to the non-irradiated solution (~ 30 °C), which is in accordance with results reported previously by Sumaru *et. al.* [12]. This phenomenon occurs because of the hydrophobicity increase of the polymer chains when irradiated with white light. The BSP form is more hydrophobic compared to Mc-H^+ , thus promoting the precipitation of the linear p(NiPAAm-BSP-AA) chains at a lower temperature [32]. After 32 °C, the non-irradiated solution absorbance crosses the irradiated solution absorbance, which can be explained by additional formation of J aggregates between the Mc-H^+ molecules in the linear p(NiPAAm-BSP-AA) copolymer chains which facilitates chain precipitation.

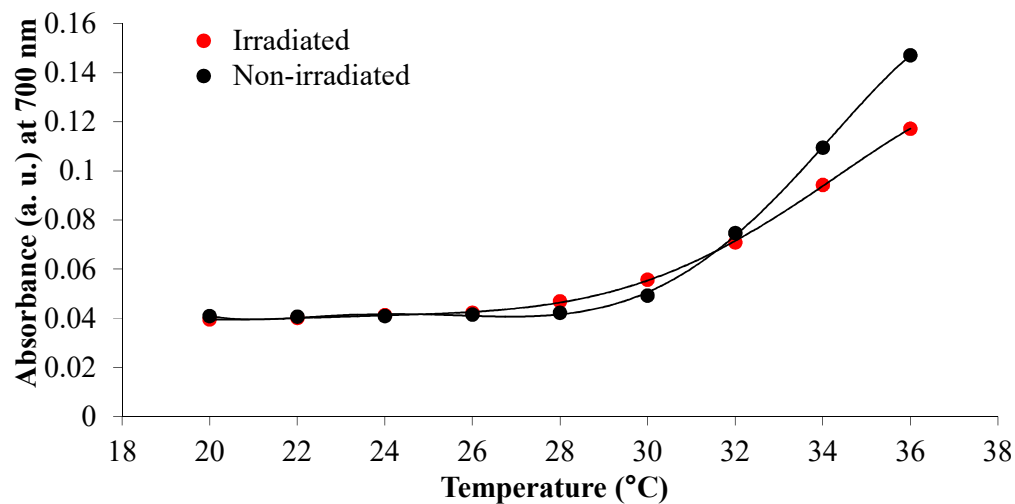


Figure 3.4. Comparison of the absorbance values at 700 nm between the non-irradiated and white light irradiated 0.1% w/w p(NiPAAm-BSP-AA) linear copolymer solutions at different temperatures.

Following the qualitative analysis of the LCST, DSC was used to obtain quantitative data. The DSC analysis of the 2.5% linear copolymer w/w solution determined an onset temperature at 26.29 °C and a maximum peak temperature at 32.33 °C (Figure 3.5). The onset temperature corresponds to the temperature at which the solution starts to undergo the precipitation process, while the peak temperature corresponds to

the temperature at which the system completely precipitates (*i.e.* the LCST). These results correlate with the UV-Vis measurements, showing in both cases that the linear copolymer starts to precipitate between 26-28 °C and continues up to 36 °C. Moreover, the DSC curve gives a very close LCST value to the 32-35 °C value quoted in literature for poly(*N*-isopropylacrylamide), the main component of the p(NiPAAm-BSP-AA) copolymer [5].

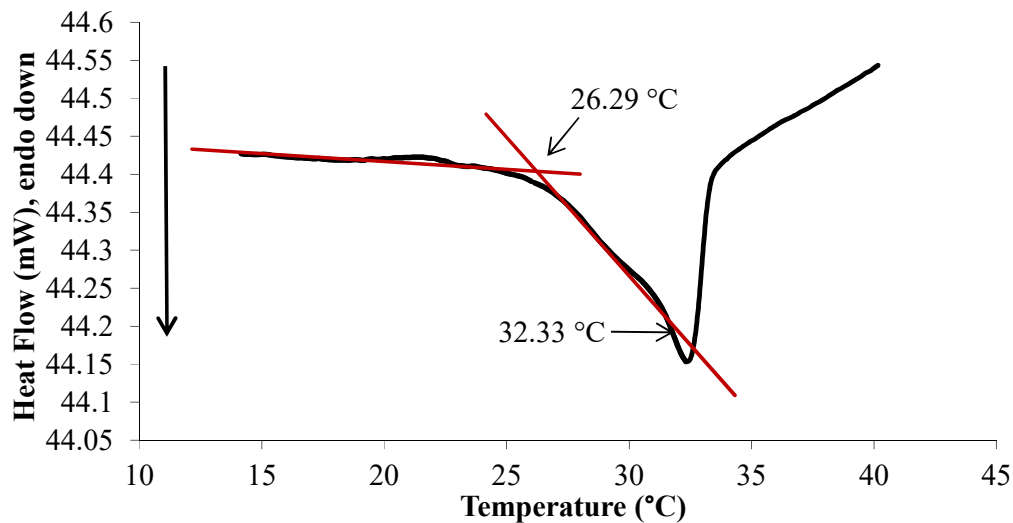


Figure 3.5. DSC curve excerpt showing the LCST transition of a 2.5% w/w p(NiPAAm-BSP-AA) linear copolymer solution. The full DSC curve follows a heating program from 14 °C to 70 °C at a heating rate of 10 °C/min.

3.4.2 Photo-induced curing studies and mechanical properties of the hydrogels

To determine the curing and mechanical properties of the hydrogels, samples of PILc, sIPN 1, sIPN 2, sIPN 3 and sIPN 4 hydrogels were synthesized in triplicate, according to the cocktail compositions given in Table 3.1.

The storage modulus curves in Figure 3.6 show that each mixture features a sharp increase in the storage modulus value after being exposed to white light at $t = 60$ s. This is due to the rapid initiation and propagation of the photo-polymerization reaction. Following this, the storage modulus begins to plateau at approximately the same time for every monomer mixture used, indicating that the storage modulus reached ~95% of its maximum value after ca. 120 s exposure to white-light.

From the same data, additional observations can be made about the mechanical properties of the relationship between the mechanical properties of the resulting IPN hydrogels and the monomer cocktail compositions. By increasing the amount of linear copolymer a decrease in the storage modulus of the hydrogels can be seen (Figure 3.6). For example, when increasing the amount of linear copolymer from 1:1 (P4,4,4,6-SPA:NiPAAm, molar ratio) in sIPN 1 to 1:2 (P4,4,4,6-SPA:NiPAAm) for sIPN 2, the storage modulus decreases from 31.4 kPa to 16.3 kPa. The lower storage modulus indicates that the hydrogels are more brittle and prone to breaking when handled. $\tan\delta$ represents the ratio between the loss and storage modulus of a fluid and is a measure of the viscoelastic behaviour of a material [24]. If the value is below 1, it indicates that the sample has a more elastic-like behaviour, while if the value is greater than 1, then the sample has a more viscous-like behaviour [24].

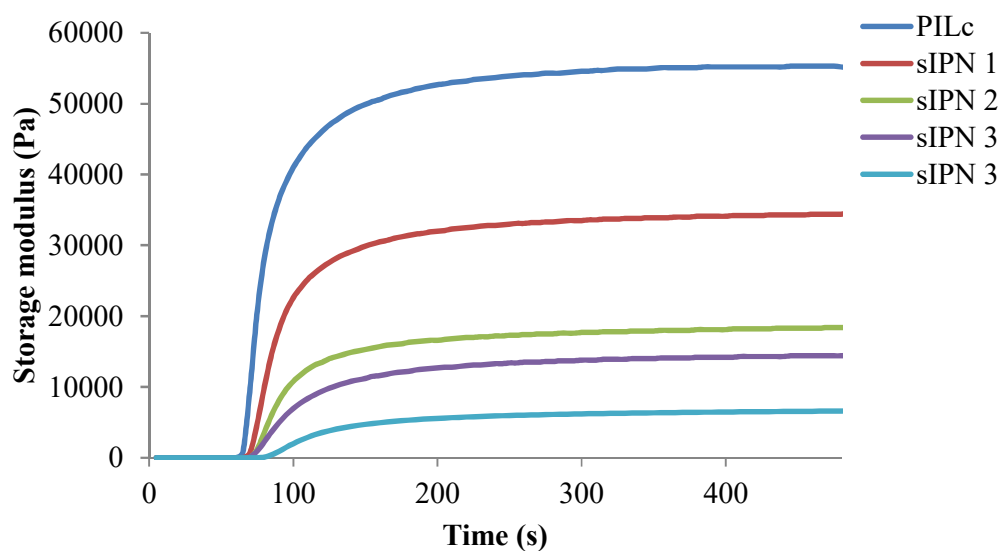


Figure 3.6. Time-dependent variation of the storage modulus of the monomer cocktail during polymerization. The white light is turned on at $t = 60s$.

Based on the $\tan\delta$ values calculated for the PILc and sIPN hydrogels, all of the hydrogels have an elastic-like behaviour (Table 3.2). The increasing value of $\tan\delta$ with increasing amount of the linear p(NiPAAm-BSP-AA) is confirmed by the increased tendency of the hydrogels to become tackier after polymerization, thus making them harder to manipulate.

Table 3.2. Loss and storage modulus of the hydrogels at 25 °C after 180 s of white light irradiation

Hydrogel	NiPAAm (molar % - to PSPA)	Loss modulus (Pa)	Storage modulus (Pa)	Tanδ
PILc	0	76	51800	0.0015
sIPN 1	100	85.7	31400	0.0027
sIPN 2	200	650	16300	0.0400
sIPN 3	300	617	12200	0.0506
sIPN 4	400	832	5310	0.1567

Another effect caused by the increasing quantity of linear copolymer in the PILc matrix is an observable increase in swelling area when the gels are left to hydrate in DI water (Figure 3.7, Table 3.3). The addition of linear p(NiPAAm-BSP-AA) increases the hydrophilic character of the hydrogels, because the co-monomers are hydrophilic molecules at room temperature. The maximum increase in hydrated area ($31.72\% \pm 1.70\%$) is obtained for sIPN 4 relative to the PILc in the absence of copolymer. To calculate this, the following formula was used:

$$\text{Hydrated Area Increase (\%)} = 100 - \left(\frac{\text{sIPN}_x \text{ Hydrated Area}}{\text{PILc Hydrated Area}} * 100 \right) \quad (2)$$

Where sIPN_x is sIPN 1, sIPN 2, sIPN 3 and sIPN 4, respectively.

Table 3.3. The effect of increasing amount of linear p(NiPAAm-BSP-AA) copolymer on the hydration properties of the hydrogels.

Hydrogel	NiPAAm (molar % - to PSPA)	Hydrated Area (mm ²)	Standard Deviation (n=3)	Hydrated Area increase (%)	RSD (%) (n=3)
PILc	0	14.140	0.606	-	4.286
sIPN 1	100	14.851	0.177	5.030	1.193
sIPN 2	200	17.445	1.191	23.375	6.825
sIPN 3	300	18.482	1.242	30.708	6.717
sIPN 4	400	18.625	0.317	31.715	1.703

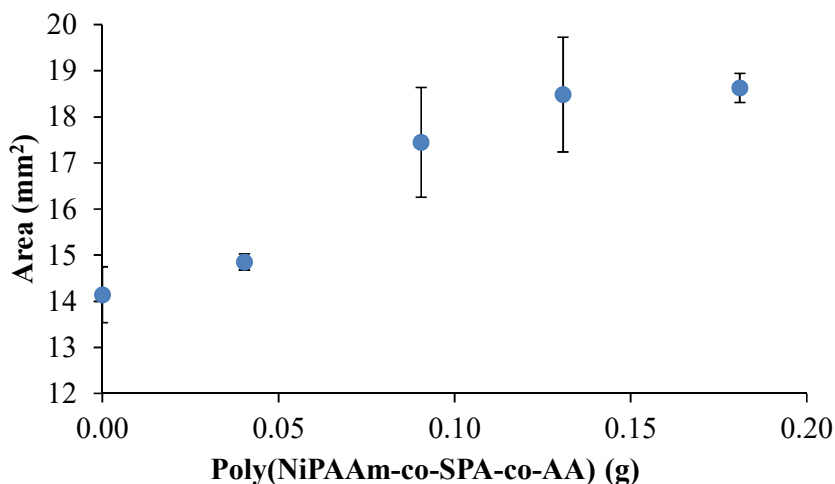
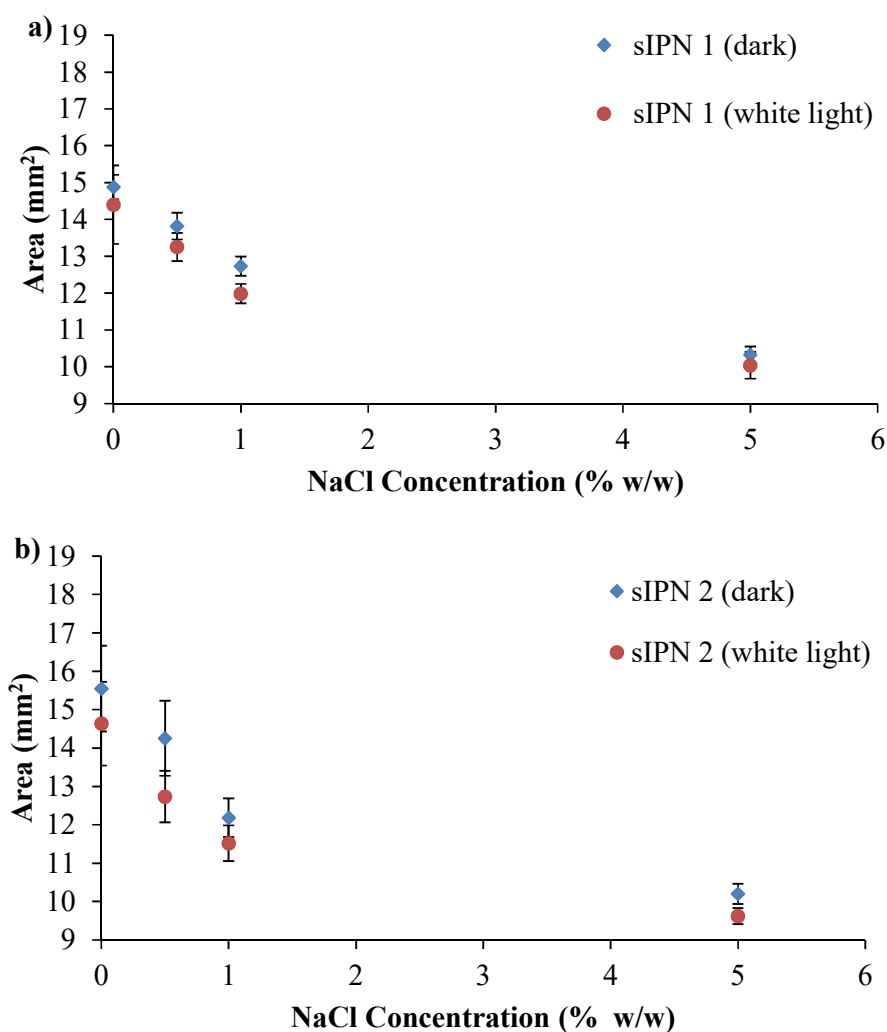


Figure 3.7. The effect of increasing the mass of linear *p*(NiPAAm-BSP-AA) copolymer on the fully hydrated hydrogel area (error bars are standard deviations for *n*=3 replicate measurements).

3.4.3 White light induced shrinking

The inclusion of the white-light sensitive linear copolymer, *p*(NiPAAm-BSP-AA), in the sIPN matrix makes it possible to use the Mc-H⁺->SP photo-induced conformation change to influence the degree of swelling of the hydrogel [4,12]. The photo-induced shrinking of the different sIPN hydrogels was tested in different hydration media: DI water, 0.5% w/w NaCl, 1% w/w NaCl and 5% w/w NaCl, respectively. The effect of salt solutions on NiPAAm-based hydrogels has already been studied, and it was found that at 25 °C and at salt concentrations higher than 4% w/w NaCl, the dissolved linear *p*NiPAAm polymer precipitates out of solution [22]. This is due to the Na⁺ and Cl⁻ ions competing for water with the linear *p*(NiPAAm), enhancing the tendency of *p*(NiPAAm) to form polymer-polymer interactions and to more readily precipitate as the globular form. This is the same phenomenon that appears when salting-out proteins from a solution [7,36]. A similar effect of the salt concentration is expected with the *p*(NiPAAm-BSP-AA) chains when the sIPN is hydrated in aqueous salt solutions. In Figure 3.8 a)-d), the area of sIPN 1, sIPN 2, sIPN 3 and sIPN 4 is plotted against salt concentration. For each hydrogel two area values were plotted for every salt concentration, representing the hydrogel's area before and after being irradiated with white light for 30 min at ~200 kLux. The largest area decreases occur with sIPN 2 and sIPN 3 when immersed 0.5% w/w NaCl

solutions. For sIPN 2 the decrease in area is $10.77\% \pm 5.24\%$ ($n=3$), while for sIPN 3 the decrease is $10.26\% \pm 2.59\%$ ($n=3$). The results indicate that for each hydrogel, the white-light induced shrinking remains roughly constant until the salt concentration exceeds 1% w/w NaCl. At higher salt concentrations, the hydrogels primarily shrink in size due to the interactions that start taking place between the dissolved salt ions and the charged polymer chains, while the white light irradiation shows reduced influence. This shrinking behaviour is known as the polyelectrolyte effect [7,26]. For each hydrogel composition, the shrinking profile is very similar as the salt concentration is increased ($13.95 \pm 0.21 \text{ mm}^2$ in 0.5% w/w NaCl, $12.56 \pm 0.23 \text{ mm}^2$ in 1% w/w NaCl and $10.00 \pm 0.09 \text{ mm}^2$ in 5% NaCl, respectively) (Figure 2.9).



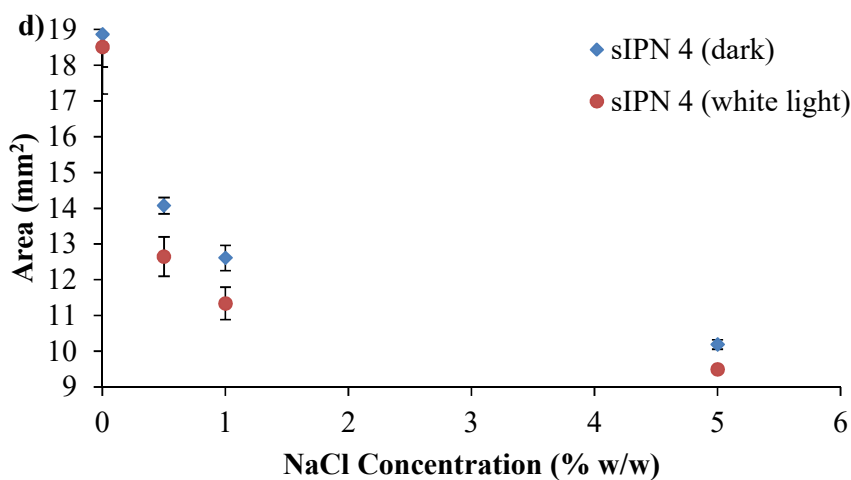
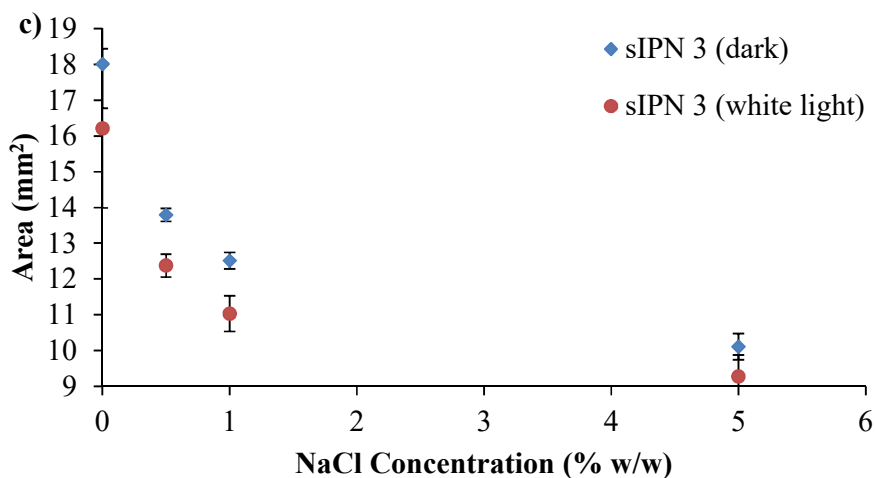


Figure 3.8. (a) – (d) White-light and ionic strength induced shrinking of the hydrogels.

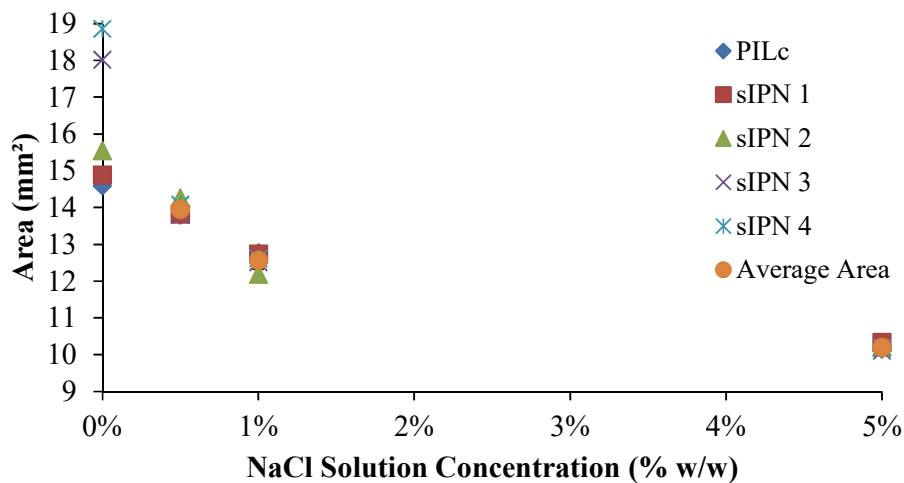


Figure 3.9. Area of the hydrogels in DI water and NaCl solutions of different concentrations: 0.5%, 1% and 5%, respectively, in the absence of light.

3.4.4 Ionic radius dependent shrinking

To better understand the effect of dissolved ions in the hydrating solution on the hydration properties of the hydrogels, a series of 1% w/w solutions were made using NaF, NaCl, NaBr and NaI, respectively. In Figure 3.10, the area of each hydrogel was plotted against the ionic radius of the anions present in the hydrating solutions. The shrinking% was calculated, using formula (1), taking into account that the fully hydrated area was considered the area of the hydrogels swollen in DI water. By plotting the shrinking effect against the ionic radius of the anions, the influence of volume charge density can be explained. Volume charge density is a measure of electric charge per unit of volume. The results indicate that F⁻ induces the maximum area shrinking for every hydrogel, while I⁻ has the least influence (Table 3.4). The reason behind this shrinking effect is two-fold: the dissolved salts have a shrinking effect on the PIL matrix due to the polyelectrolyte effect [7], while also having the same effect on the linear p(NiPAAm-BSP-AA) chains [22,32,36]. The shrinking effect occurs because of an electrostatic screening that appears between the charged PIL chains and the ions present in the solution that affects the way water is distributed around the polymer chains and salt ions, thus directly contributing to the water intake of the hydrogels [37]. The fluoride anion has the highest volume charge density and therefore has the strongest screening effect, making the hydrogels shrink the most. In contrast, iodide has the lowest volume charge density, making the hydrogels shrink the least.

Table 3.4. Salt-induced shrinking of the hydrogels in area % compared to DI water.

	A⁻ Ionic Radius (pm)	PILc (%)	sIPN 1 (%)	sIPN 2 (%)	sIPN 3 (%)	sIPN 4 (%)
NaF	119	82.491	79.760	70.316	68.742	68.912
NaCl	167	82.621	81.791	70.058	70.582	73.098
NaBr	182	90.246	84.833	78.894	81.213	74.110
NaI	206	94.196	94.898	78.703	82.195	80.228

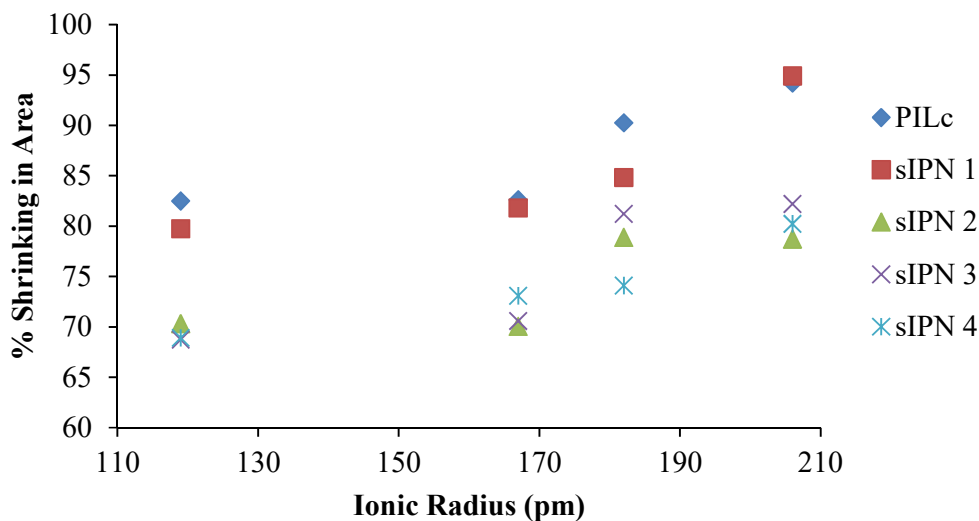


Figure 3.10. The shrinking effect of 1% w/w NaF, NaCl, NaBr and NaI solutions on the area of the hydrogels compared to DI water.

3.4.5 Temperature induced shrinking

In the case of crosslinked PILs, the LCST is a temperature interval, not an exact temperature value as in the case of pNiPAAm or linear PILs. This is due to the PIL polymer chains being crosslinked, with decreased freedom to shrink owing to the highly bulky and charged nature of the ionic liquid monomers [3,15].

As described in the experimental section, the hydrogels were initially allowed to swell in DI Water. For each measurement, three different hydrogels were used, to ensure that the process is reproducible. In Figure 3.11, the area difference at each temperature step is plotted against temperature to determine the influence of the linear p(NiPAAm-BSP-AA) copolymer on the temperature induced shrinking properties of the sIPN hydrogels. Using formula (1), the area difference between the hydrogels at 20 °C and 70 °C was calculated (Table 3.5). PILc showed the highest degree of area shrinking at ~53.3% of its fully hydrated size, followed by sIPN 1, sIPN 2, and sIPN 3, with ~50.6%, ~47.6%, and ~45.5% area shrinking, respectively. These results indicate that the addition of the linear p(NiPAAm-BSP-AA) copolymer doesn't significantly influence the thermally induced shrinking capabilities of the PIL matrix up to a linear copolymer:PILc molar ratio of 3:1. With sIPN 4 however, the shrinkage effect is much reduced at ~11%, suggesting that above a certain concentration of the copolymer, the linear chains inside the PILC matrix inhibit the collapse of the matrix.

The effect of salt in the hydrating medium on the temperature response of the hydrogels was also investigated. In Figure 3.12, the temperature response of the PILc in the presence of 0.5% w/w NaCl was completely prevented. This result is consistent with a previous study performed by Men et. al. which showed that the LCST of different linear poly(ionic liquid)s is influenced by the presence of competing ions in the hydrating solution, to the point that the LCST completely disappears if the competing salt has a chaotropic behaviour [2]. In our experiments a 0.5% w/w NaCl concentration was enough to stabilize the PSPA chains in such a way that they did not collapse at any temperature. Furthermore, the 0.5% w/w NaCl solution had a similar effect with all the sIPNs, completely suppressing the temperature induced swelling in every case.

Table 3.5. Temperature induced shrinking of the sIPNs in DI Water.

Sample	Fully swollen hydrogel area (mm ²)	Standard Deviation (n=3)	Contracted hydrogel area (mm ²)	Standard Deviation (n=3)	% Shrinking
PILc	16.101	1.074	7.524	0.945	53.273
sIPN 1	16.774	0.853	8.295	0.765	50.549
sIPN 2	17.483	0.507	9.172	1.414	47.537
sIPN 3	17.497	0.443	9.537	0.232	45.494
sIPN 4	19.296	0.530	17.174	0.922	10.995

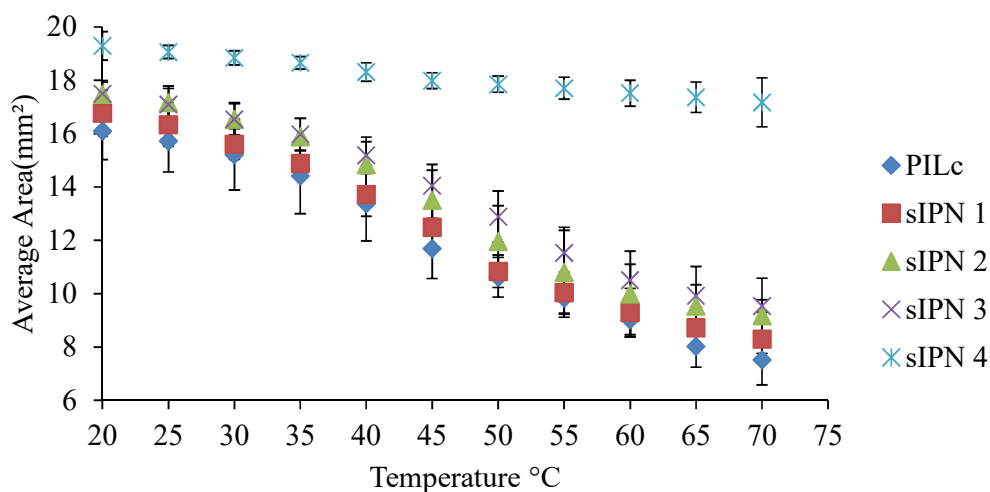


Figure 3.11. Graphical representation of the temperature induced shrinking profiles of the hydrogels.

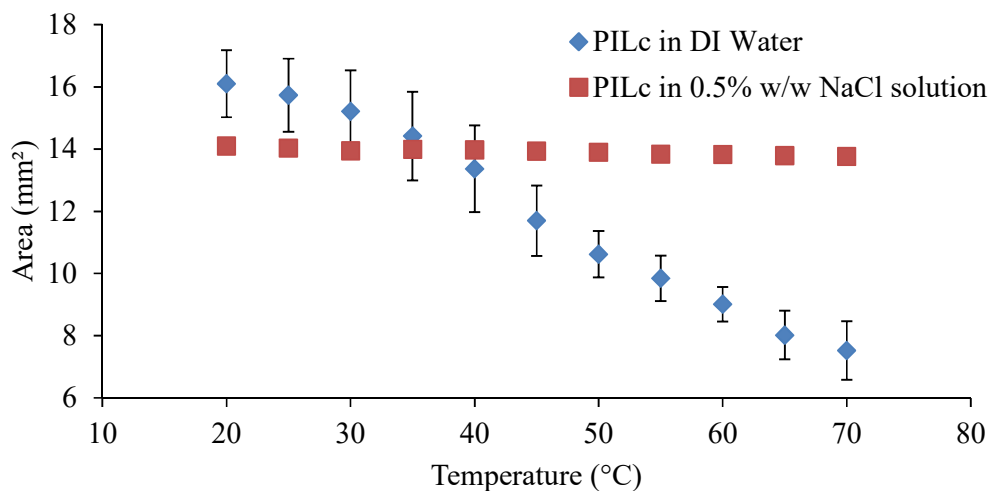


Figure 3.12. The shrinking profile of the PILc hydrogel in DI Water and 0.5% w/w NaCl solution.

3.5 Conclusions

A series of multi-responsive crosslinked sIPN hydrogels were synthesised by adding increasing amounts of linear p(NiPAAm-BSP-AA) copolymer to a crosslinked PIL matrix. UV-Vis spectroscopy and DSC were used to determine how temperature and white light affect the linear copolymer. From the DSC data, it was determined that the LCST of the linear p(NiPAAm-BSP-AA) copolymer was at ca. 32.33 °C, while from the UV-Vis data it was found that white light irradiation promotes the precipitation of the linear copolymer from an aqueous solution at a lower temperature compared to the non-irradiated solution. Digital microscopy was used to determine the influence of white light, temperature, and salt concentration on the shrinking capabilities of sIPN hydrogels. From the gathered rheometry data, all hydrogels polymerized approximately after the same time period of 120s, but have different mechanical properties that are influenced by the amount of linear p(NiPAAm-BSP-AA) copolymer used in their synthesis. The increasing amount of linear p(NiPAAm-BSP-AA) copolymer lowers the storage modulus and increases the loss modulus, thus the sIPNs become more tackier compared to the PILc. By analysing the shrinking response of the hydrogels after being exposed to photo-, thermo-, and salt stimuli, it was determined that sIPN 2 and sIPN 3 would be best suited to consider for use as polymer actuators (e.g. in microfluidic systems), because they can be efficiently

actuated by white light irradiation, salt concentration and an increase in temperature. Furthermore, this study shows that PILs can provide functional building blocks for the synthesis of novel smart materials, and provides an experimental template the examination of other PILs as temperature and ionic strength responsive polymers, either by themselves or as components in composite materials.

3.6 References

1. Bogue, R. Smart materials: A review of recent developments. *Assembly Automation* **2012**, *32*, 37.
2. Men, Y.; Li, X.-H.; Antonietti, M.; Yuan, J. Poly(tetrabutylphosphonium 4-styrenesulfonate): A poly(ionic liquid) stabilizer for graphene being multi-responsive. *Polymer Chemistry* **2012**, *3*, 871.
3. Ziolkowski, B.; Diamond, D. Thermoresponsive poly(ionic liquid) hydrogels. *Chemical Communications* **2013**, *49*, 10308-10310.
4. Ziolkowski, B.; Florea, L.; Theobald, J.; Benito-Lopez, F.; Diamond, D. Self-protonating spiropyran- co -nipam- co -acrylic acid hydrogel photoactuators. *Soft Matter* **2013**, *9*, 8754.
5. Boutris, C.; Chatzi, E.G.; Kiparissides, C. Characterization of the lcst behaviour of aqueous poly(n-isopropylacrylamide) solutions by thermal and cloud point techniques. *Polymer* **1997**, *38*, 2567-2570.
6. Buwalda, S.J.; Boere, K.W.M.; Dijkstra, P.J.; Feijen, J.; Vermonden, T.; Hennink, W.E. Hydrogels in a historical perspective: From simple networks to smart materials. *Journal of Controlled Release* **2014**, *190*, 254-273.
7. Renamayor, C.S.; Pastoriza, A.; Usma, C.L.; Pierola, I.F. Salting-in effect of ionic liquids on poly(n-vinylimidazole) hydrogels. *Colloid and Polymer Science* **2013**, *291*, 2017-2021.
8. Mecerreyes, D. Polymeric ionic liquids: Broadening the properties and applications of polyelectrolytes. *Progress in Polymer Science* **2011**, *36*, 1629-1648.
9. Guilherme, M.R.; da Silva, R.; Rubira, A.F.; Geuskens, G.; Muniz, E.C. Thermo-sensitive hydrogels membranes from paam networks and entangled pnipaam: Effect of temperature, cross-linking and pnipaam contents on the water uptake and permeability. *Reactive & Functional Polymers* **2004**, *61*, 233-243.
10. Yuan, J.; Mecerreyes, D.; Antonietti, M. Poly(ionic liquid)s: An update. *Progress in Polymer Science* **2013**, *38*, 1009-1036.
11. Yuan, J.; Antonietti, M. Poly(ionic liquid)s: Polymers expanding classical property profiles. *Polymer* **2011**, *52*, 1459-1482.
12. Sumaru, K.; Kameda, M.; Kanamori, T.; Shinbo, T. Characteristic phase transition of aqueous solution of poly(n-isopropylacrylamide) functionalized with spirobenzopyran. *Macromolecules* **2004**, *37*, 4949-4955.
13. Schild, H.G. Poly (n-isopropylacrylamide) - experiment, theory and application. *Progress in Polymer Science* **1992**, *17*, 163-249.
14. Gallagher, S.; Kavanagh, A.; Ziolkowski, B.; Florea, L.; R. MacFarlane, D.; Fraser, K.J.; Diamond, D. Ionic liquid modulation of swelling and lcst

- behavior of n -isopropylacrylamide polymer gels. *Physical Chemistry Chemical Physics* **2013**, *16*, 3610-3616.
15. Gallagher, S.; Florea, L.; Fraser, K.J.; Diamond, D. Swelling and shrinking properties of thermo-responsive polymeric ionic liquid hydrogels with embedded linear pnipaam. *International Journal of Molecular Sciences* **2014**, *15*, 5337-5349.
 16. Stuart, M.A.; Huck, W.T.; Genzer, J.; Müller, M.; Ober, C.; Stamm, M.; Sukhorukov, G.B.; Szleifer, I.; Tsukruk, V.V.; Urban, M., *et al.* Emerging applications of stimuli-responsive polymer materials. *Nature materials* **2010**, *9*, 101-113.
 17. Vancoillie, G.; Frank, D.; Hoogenboom, R. Thermoresponsive poly(oligo ethylene glycol acrylates). *Progress in Polymer Science* **2014**, *39*, 1074-1095.
 18. Yuan, C.; Guo, J.; Tan, M.; Guo, M.; Qiu, L.; Yan, F. Multistimuli responsive and electroactive supramolecular gels based on ionic liquid gemini guest. *ACS Macro Letters* **2014**, *3*, 271-275.
 19. Yuan, C.; Guo, J.; Yan, F. Shape memory poly(ionic liquid) gels controlled by host–guest interaction with β -cyclodextrin. *Polymer* **2014**, *55*, 3431-3435.
 20. Zhang, W.; Yuan, C.; Guo, J.; Qiu, L.; Yan, F. Supramolecular ionic liquid gels for quasi-solid-state dye-sensitized solar cells. *ACS Applied Materials & Interfaces* **2014**, *6*, 8723-8728.
 21. Zhang, X.Z.; Yang, Y.Y.; Chung, T.S.; Ma, K.X. Preparation and characterization of fast response macroporous poly(n-isopropylacrylamide) hydrogels. *Langmuir* **2001**, *17*, 6094-6099.
 22. Orlov, Y.; Xu, X.P.; Maurer, G. An experimental and theoretical investigation on the swelling of n-isopropyl acrylamide based ionic hydrogels in aqueous solutions of (sodium chloride or di-sodium hydrogen phosphate). *Fluid Phase Equilibria* **2007**, *254*, 1-10.
 23. Zhang, X.-Z.; Xu, X.-D.; Cheng, S.-X.; Zhuo, R.-X. Strategies to improve the response rate of thermosensitive pnipaam hydrogels. *Soft Matter* **2008**, *4*, 385-391.
 24. Ziółkowski, B.; Ates, Z.; Gallagher, S.; Byrne, R.; Heise, A.; Fraser, K.J.; Diamond, D. Mechanical properties and uv curing behavior of poly(n-isopropylacrylamide) in phosphonium-based ionic liquids. *Macromolecular Chemistry and Physics* **2013**, *214*, 787-796.
 25. Florea, L.; Diamond, D.; Benito-Lopez, F. Photo-responsive polymeric structures based on spiropyran. *Macromolecular Materials and Engineering* **2012**, *297*, 11481159.
 26. Kohno, Y.; Deguchi, Y.; Ohno, H. Ionic liquid -derived charged polymers to show highly thermoresponsive lcst-type transition with water at desired temperatures. *Chemical Communications* **2012**, *48*, 11883-11885.
 27. Kohno, Y.; Saita, S.; Men, Y.; Yuan, J.; Ohno, H. Thermoresponsive polyelectrolytes derived from ionic liquids. *Polymer Chemistry* **2015**, 2163-2178.
 28. Men, Y.; Schlaad, H.; Voelkel, A.; Yuan, J. Thermoresponsive polymerized gemini dicationic ionic liquid. *Polymer Chemistry* **2014**, *5*, 3719-3724.
 29. Welton, T. Room-temperature ionic liquids. Solvents for synthesis and catalysis. *Chemical Reviews* **1999**, *99*, 2071-2083.
 30. Wilkes, J.S.; Zaworotko, M.J. Air and water stable 1-ethyl-3-methylimidazolium based ionic liquids. *Journal of the Chemical Society-Chemical Communications* **1992**, 965-967.

31. Fraser, K.J.; MacFarlane, D.R. Phosphonium-based ionic liquids: An overview. *Australian Journal of Chemistry* **2009**, *62*, 309-321.
32. Maeda, Y.; Higuchi, T.; Ikeda, I. Ftir spectroscopic and calorimetric studies of the phase transitions of n-isopropylacrylamide copolymers in water. *Langmuir* **2001**, *17*, 7535-7539.
33. Hammarson, M.; Nilsson, J.R.; Li, S.; Beke-Somfai, T.; Andréasson, J. Characterization of the thermal and photoinduced reactions of photochromic spiropyrans in aqueous solution. *The Journal of Physical Chemistry B* **2013**, *117*, 13561-13571.
34. Reijenga, J.; Hoof, A.v.; Loon, A.v.; Teunissen, B. Development of methods for the determination of pka values. *Analytical Chemistry Insights* **2013**, *8*, 53-71.
35. Krongauz, V.A.; Fishman, S.N.; Goldburt, E.S. Quasi-crystals. Growth from photochromic spiropyrans on irradiation in a constant electric field. *The Journal of Physical Chemistry* **1978**, *82*, 2469-2474.
36. Baldwin, R.L. How hofmeister ion interactions affect protein stability. *Biophysical Journal* **2009**, *71*, 2056-2063.
37. Odijk, T.; Houwaart, A.C. On the theory of the excluded-volume effect of a polyelectrolyte in a 1-1 electrolyte solution. *Journal of Polymer Science: Polymer Physics Edition* **1978**, *16*, 627-639.

Chapter 4: Poly(ionic liquid) thermo-responsive hydrogel microfluidic actuators

4.1 Abstract

4.2 Introduction

4.3 Experimental

4.3.1 Materials

4.3.2 Synthesis of the tributylhexyl sulfopropyl acrylate (PSPA) ionic liquid monomer

4.3.3 Crosslinked PSPA hydrogel disk polymerization

4.3.4 Characterization of the temperature-induced shrinking and reswelling of hydrogel disks

4.3.5 Microfluidic chip fabrication

4.3.6 Thermo-responsive hydrogel valve characterization

4.4 Results and Discussion

4.4.1 Temperature-induced shrinking of the PILc hydrogel disks

4.4.2 Flow characterization study

4.5 Conclusions

4.6 References

Chapter 4

Poly(ionic liquid) thermo-responsive hydrogel microfluidic actuators*

Poly(ionic liquid) thermo-responsive hydrogel microfluidic valves, A. Tudor, J. Saez, L. Florea, F. Benito-Lopez*, D. Diamond, *Sensors and Actuators B: Chemical*, 267, 749-755, 2017.

4.1 Abstract

In this study we report the synthesis, characterisation and performance of thermo-responsive crosslinked tributylhexyl phosphonium sulfopropylacrylate (PSPA) poly(ionic liquid) (PILc) hydrogels as temperature controlled actuators in microfluidic devices. The hydrogel size is modulated by localised changes in its conformation due to the lower critical solution temperature (LCST) behaviour exhibited by PSPA.

4.2 Introduction

Microfluidics is an interdisciplinary science that focuses on producing devices capable of manipulating small volumes of fluids, ranging from picoliters to microliters [1,2]. The advantages of microfluidics come either directly from the reduction in size compared to conventional laboratory fluidics or as a result of the ability to integrate sequential processes at the micro-scale. The former results in reduced reagent consumption, low waste production, reduced measurement times and improved sensitivity, while the latter offers the benefits of sampling, pre-processing and sample analysis “on-chip”, thereby reducing process time, risk of contamination, and human error[1-10]. Despite many years of research, functioning devices incorporating microfluidics still typically require highly specialised and bulky macroscopic equipment such as pumps, valves and detectors to be located off-chip. Therefore, one of the main challenges in microfluidics is downscaling conventional pumps and valves so they can be fully integrated within the microfluidic device. In this context, one of the approaches that are being explored is the use of soft materials for flow control [11-17]. In recent years, effective fluidic control systems based on soft, polymer gel-type materials fully integrated within the microfluidic device have been demonstrated by several groups. These novel devices are now becoming more reminiscent of biological units than conventional silicon micromachined components. Examples include the microfluidic integration of a variety of stimuli-responsive materials that respond to changes in their external environment, such as temperature, light, pH, or variations in electrical potential and pressure [18-32]. Among them, one of the most studied stimuli-responsive hydrogels is poly(N-isopropyl acrylamide) (pNiPAAm), due to its lower critical solution temperature (LCST) behaviour in the

presence of an aqueous medium [20,33-35]. LCST behaviour arises from changes in the hydration forces between the polymer chains and the aqueous medium, and the attractive forces between the polymer chains themselves. If the temperature of the hydration medium is below the LCST, then the polymer chains are hydrated and swollen by the aqueous medium. When the temperature rises above the LCST, the polymer chains expel the water molecules and attract each other, which leads to the polymer collapsing from solution and contraction of the polymer [20,33-35]. In the case of a linear polymer, the presence of a LCST leads to the appearance of a polymer precipitate, while in the case of a crosslinked polymeric hydrogel, it causes volume contraction [31,34]. This property has made pNiPAAm hydrogels interesting candidates for the realisation of thermo-responsive microfluidic valves and for thermo-, photo-[36], magneto- responsive valving units when ionic liquids [37], photochromic molecules [14,38], or magnetic nanoparticles [39,40], respectively, are included in the polymer matrix.

Similar LCST behaviour has been reported recently in a relatively new class of materials, namely poly(ionic liquid)s (PILs) [22,29-31,41-43]. These materials are polymers formed through the polymerisation of ionic liquid (IL) monomers which feature a polymerisable group in the anion, the cation or both. Although generally the focus remains on linear PILs, there are several reports dealing with crosslinked PIL networks, that are explored either as ion conductors [44,45], templates for multilamellar structured nanoparticles [46] or as actuators [31,47].

The aim of this paper is the integration, for the first time, of the phosphonium-based crosslinked PIL tributylhexylphosphonium sulfopropylacrylate (PSPA), in a microfluidic structure, to provide thermo-actuated flow control functionality.

4.3 Experimental

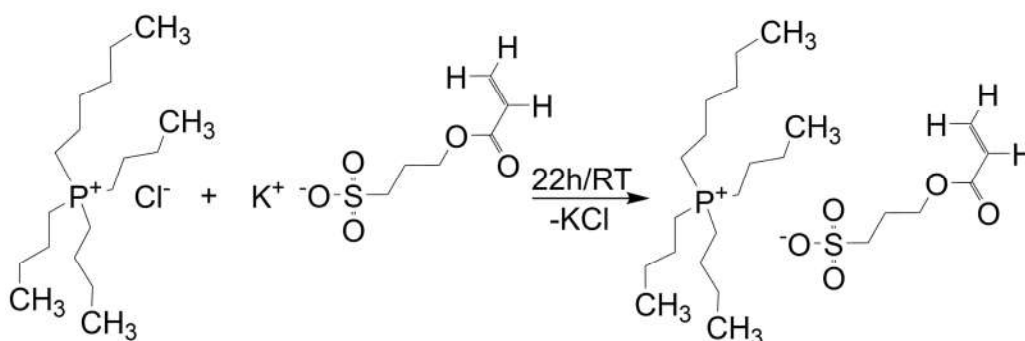
4.3.1 Materials

Potassium 3-sulfopropyl acrylate (KSPA), 2-hydroxy-2-methylpropiophenone 97% (HMPP), phenyl-bis(2,4,6-trimethylbenzoyl) phosphine oxide 97% (PBPO), polypropylene glycol diacrylate (Mw ~800, 100 ppm MEHQ and 100 ppm BHT as inhibitors) (PPG800) and HPLC grade acetonitrile (ACN) were bought from Sigma Aldrich® (Arklow, Ireland) and used as received. Tributylhexyl phosphonium

chloride was kindly donated by Cytec® Industries (Niagara Falls, Canada). Deionized water (DI water), with a resistivity of $18.2 \text{ M}\Omega \cdot \text{cm}^{-1}$, was made using a Milli-Q Water Purification System (Merck Millipore, Darmstadt, Germany).

4.3.2 Synthesis of the tributylhexyl sulfopropyl acrylate (PSPA) ionic liquid monomer

For PSPA synthesis, 15g of tributylhexyl chloride (PCl) and 16.02g of KSPA were dissolved in 25 mL DI water. The amount of KSPA used represents a 50% molar excess compared to the stoichiometric value needed for this reaction. This was performed to ensure that the reaction equilibrium is shifted towards the formation of PSPA. The reaction was maintained at room temperature and atmospheric pressure overnight (Scheme 1). Purification was completed by extracting the PSPA from the aqueous solution with dichloromethane. This process was repeated three times. The resulting mixture was dried over anhydrous magnesium sulphate and gravity filtered. Following this, the extraction solvent was removed by rotary evaporation and the resulting viscous mixture was dried overnight using a high vacuum pump. The obtained product was a clear, colourless viscous liquid. The yield of the synthesis was 85%. The purity of the product was analysed using $^1\text{H-NMR}$, δH (Bruker Advance Ultrashield, 400MHz, deuterated chloroform): 0.86–1 (m, 12H, CH_3), 1.28–1.33 (m, 4H, CH_2), 1.51–1.53 (m, 16H, CH_2), 2.18–2.37 (m, 10H, CH_2), 2.88–2.92 (m, 2H, CH_2), 4.25–4.29 (t, $J=6.46 \text{ Hz}$, 2H, CH_2), 5.77–5.80 (dd, 1H, $J=1.51, 10.42 \text{ Hz}$, CH), 6.04–6.11 (m, 1H, $J=10.44, 17.33 \text{ Hz}$, CH), 6.34–6.39 (dd, 1H, $J=1.51, 17.38 \text{ Hz}$, CH) ppm.



Scheme 4.1. Reaction scheme for PSPA synthesis.

4.3.3 Crosslinked PSPA hydrogel disk polymerization

The crosslinked PILc hydrogel was synthesized by dissolving 0.1935 g (400 μmol) of PSPA in 0.1935 g 1:1 w/w mixture of ACN and DI water together with 0.0160 g (20 μmol) of PPG800 as the crosslinker and 0.0034 g (8 μmol) of PBPO as the white light polymerization initiator. The resulting mixture was mechanically stirred until all the components were completely dissolved. Following this, the monomer solution was pipetted in poly(dimethyl siloxane) moulds 3mm wide and 1mm deep (Figure 3.1). To polymerize the monomer mixture, a Dolan-Jenner LMI-6000 Fiber-Lite (Boxborough, MA, USA) white-light was used at an illumination level of ~ 200 kLux for 30 minutes. The resulting PILc disks were swollen in DI water overnight (Figure 4.1). Based on previously performed studies [48], a polymerisation time of 30 minutes ensures that the monomer mixture is fully polymerised.

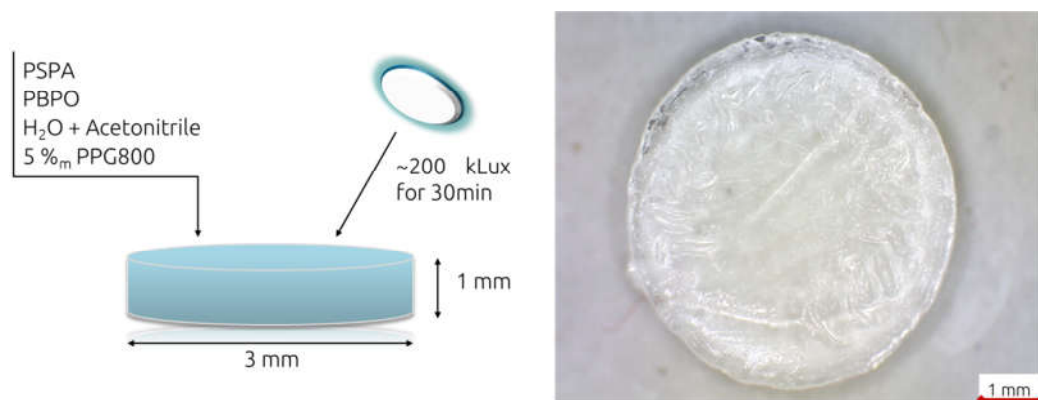


Figure 4.1. Schematic illustration of PSPA hydrogel disk polymerization protocol (left) and photo of the PSPA hydrogel disk (right).

4.3.4 Characterization of the temperature-induced shrinking and reswelling of the hydrogel disks

The resulting hydrogel disks, as seen in Figure 4.1, were transferred to an Anton Paar MCR301 rheometer fitted with a Peltier temperature control holder with an aluminium plate. The hydrogel disks were covered with DI water and the holder was covered with a 5mm glass plate, to ensure that the water will not evaporate when the temperature was raised. Two different experiments were performed: the first

experiment focused on the study of the shrinking and swelling kinetics of the hydrogel disks, while the second experiment focused on the repeatability and the reproducibility of the shrinking and reswelling effect.

The first experiment was carried out by heating the hydrogels from 20 °C to 70 °C in 5 °C steps to analyze the shrinking effect, followed by cooling the gels at the same rate back to 20 °C to analyze the reswelling effect. The hydrogel disks were kept for 8 minutes at each step to ensure that the area of the hydrogel has reached a steady state. At each step an image was taken using an Aigo GE-5 digital microscope having a 60x magnification objective. The hydrogels' %shrinking in area was studied using the ImageJ software. Each image was analyzed using the following formula:

$$\%shrinking = 100 - (A_f/A_i \cdot 100) \quad (\text{Eq. 4.1})$$

Where A_f is the size of the shrunken hydrogel disk at a set temperature and A_i is the initial size of the swollen hydrogel disk.

To further illustrate this behaviour, a time-lapse video of the gel shrinking and reswelling was made by using images taken every 20 seconds for a total of 60 minutes for each shrinking and reswelling cycle (Video A.4.1: Temperature-induced shrinking and reswelling of PILc hydrogels).

The second experiment was completed by alternatively shrinking the hydrogel disks by applying a temperature of 50 °C and reswelling them by applying a temperature of 20 °C. This alternation was repeated six times to ensure that the temperature-induced shrinking behaviour is repeatable. The same formula (Eq. 4.1) was used in this case to calculate %shrinking in area when the hydrogels were heated to 50 °C.

4.3.5 Microfluidic chip fabrication

The microfluidic chip was fabricated from poly(methyl methacrylate) (PMMA) sheets with a height of 250 µm and pressure sensitive adhesive (PSA) sheets with a thickness of 60 µm (Figure 4.2). The bottom parts of the chip, the well layer in which the hydrogel was polymerized and the top part of the chip were cut using an Epilog Zing 16 30W CO₂ laser. These three PMMA layers were bound using two PSA layers, the first of which was used to connect the bottom part of the chip to the

polymer well layer of the chip, while the second PSA layer had the microfluidic channel cut into it and was used to connect the top part of the chip to the polymer well layer of the chip. The PSA layers were cut using a Graphtec Craft Robo-Pro cutting plotter. The total thickness of the chip was 1 mm (Figure 4.3). This dimension was used to ensure the chip will fit in the microfluidic chip holder which will be used to actuate the thermo-responsive hydrogel actuator.

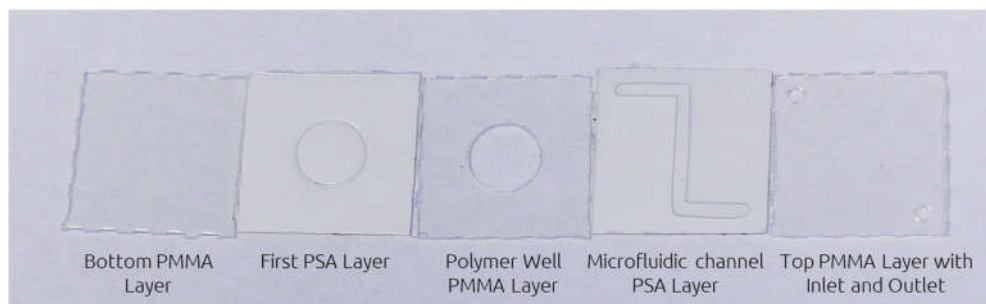


Figure 4.2. The PMMA and PSA layers of the microfluidic chip before assembly.

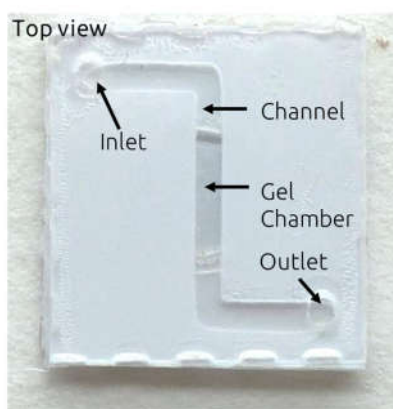


Figure 4.3. The assembled microfluidic chip containing the thermo-responsive hydrogel actuator.

4.3.6 Thermo-responsive hydrogel valve characterization

The hydrogel actuators were fabricated by photo-polymerising 3 μL of monomer mixture for 20 min using a 365nm UV lamp. In this case, the PBPO initiator was substituted, while respecting the same mol ratio, with HMPP to allow UV photopolymerisation. Based on a previously published study [49], the polymerisation time used ensures the full monomer conversion. The characterization

of the hydrogel actuator's thermo-response was performed by inserting the microfluidic chip into a microfluidic holder fitted with a heating element. This heating element sits at the bottom of the microfluidic chip and is capable of homogeneously increasing the temperature at a rate of $7.4\text{ }^{\circ}\text{C}\cdot\text{s}^{-1}$ and decreasing the temperature at a rate of $2.4\text{ }^{\circ}\text{C}\cdot\text{s}^{-1}$. To induce shrinking in the thermo-responsive PILc hydrogel, a temperature of $50\text{ }^{\circ}\text{C}$ was chosen, while to reswell the hydrogel a temperature of $20\text{ }^{\circ}\text{C}$ was chosen. The microfluidic holder also contains the inlet and outlet connections at its sides. After the microfluidic chip was placed in the holder, its inlet was connected to a WPI-Europe SP101IZ syringe pump, while its outlet was connected to a Sensirion CMOSens flow microsensor. The flow rate was set at $500\text{ nL}\cdot\text{min}^{-1}$. The schematic of the setup can be seen in Scheme 3.2.



Scheme 4.2. Setup used for the characterization of DI water flow through the chip.

DI water was chosen as the flow medium to ensure that there are no other effects inhibiting the shrinking behaviour of the PIL hydrogels. The effect of foreign salts dissolved in the hydration medium on the temperature-induced shrinking of both linear and crosslinked PILs were investigated in several other studies [18,28,29,48,50]. For future applications envisioned to work with different kinds of solutions as flow mediums, a configuration in which the hydrogel flow control actuator is separated from the flow medium by a flexible membrane can be used, as demonstrated by Tanaka et. al [51] and Beebe et. al [11]. In both cases they used a flexible membrane to separate an electroactive polymer, and a pH-responsive hydrogel, respectively, from the analyte flow, which ensured that they operated in optimal conditions.

The results exhibited by the ionic liquid polymer flow control actuator followed a sigmoidal fit (Flow rate, Q , versus time, t) (Eq. 4.2). This type of fit is commonly used in chemistry to obtain constant values such as pK_a (acid dissociation constant) and can be used to determine the rate constant of the ionic liquid polymer hydrogel actuator in this case.

$$Q = \frac{a}{1 + e^{kx+b}} + d \quad (\text{Eq. 4.2})$$

Where “a” is the maximum Q value obtained when hydrogel is fully open, “b” correspond to the interception point value, k give us the value of the rate constant, and “d” accounts for a baseline offset, minimum Q.

Using the setup from Scheme 4.2 the flow rates through the chip were analysed. Based on these results, further investigations were made to determine the shrinking and swelling kinetics by using the logistic curve equation and the Solver plug-in for Microsoft Excel (Eq. 4.2). In Figures A.4.1 and A.4.2 detailed views of the flow rate and the modelled flow rate can be seen.

4.4 Results and discussions

4.4.1 Temperature-induced shrinking of the PILc hydrogel disks

In the case of conventional temperature-responsive linear polymers, such as poly(N-isopropylacrylamide), the LCST appears as a sharp transition at a specific temperature value (~ 32 °C for pNiPAAm) [34]. This remains valid also for linear PILs. In contrast, with crosslinked PILs the polymeric volume changes occur over a temperature interval, rather than at a sharp value, suggesting that more gradual changes are occurring in the polymer chains [31]. This phenomenon has been assigned to the decreased level of freedom of the bulky IL in the polymer network and manifests itself in an incremental decrease in size of the PIL hydrogels with increase in temperature (and vice versa). This behaviour also appears to occur in the PSPA hydrogels presented in this study.

Figure 3.4 shows that when the temperature is increased from 20 °C to 70 °C the hydrogels shrink by ~ 39 % at 50 °C and ~ 56 % at 70 °C (Video A.4.1). When the temperature is lowered back from 70 °C to 20 °C, the hydrogels start absorbing water until they return to their original size. The slight difference in area between the heating and the cooling cycle arose from the fact that the heating rate is ~ 10 °C·min⁻¹, while the cooling rate is ~ 13 °C·min⁻¹.

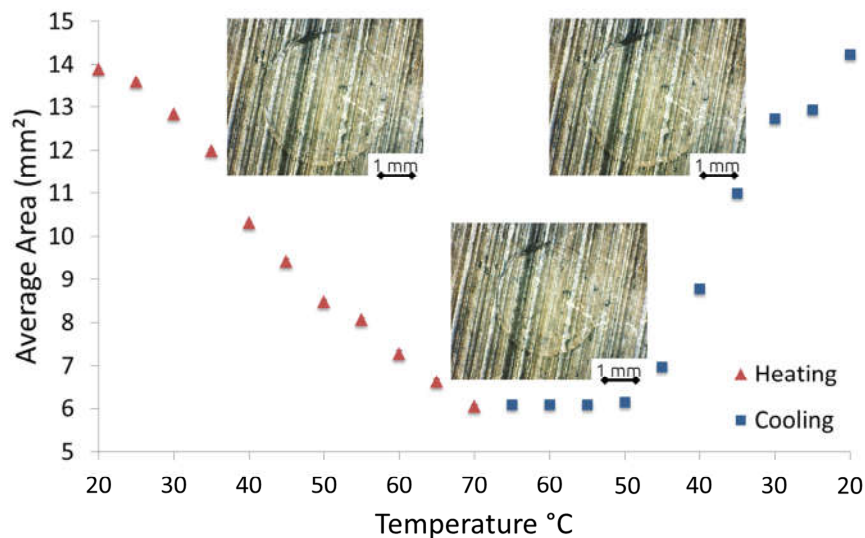


Figure 4.4. PSPA hydrogel shrinking in 5 °C steps from 20 to 70 °C, followed by reswelling when the temperature is lowered back to 20 °C.

Figure 4.5 presents results of reproducibility and repeatability of this behaviour. In these experiments, a set of three gels were analysed by heating their hydration medium to a temperature of 50 °C to make the hydrogels shrink, followed by cooling them to 20 °C to allow for reswelling to their original size. As in the previous test, the hydrogels were kept for 8 min at each temperature, to ensure a steady-state volume was reached. The heating and cooling cycle was repeated six times. In all cases the hydrogels shrank by ~ 44 % (± 3 %, $n = 6$) at 50 °C and reverted back to ~ 97 % (± 2 %, $n = 6$) of their original size when the temperature was lowered to 20 °C.

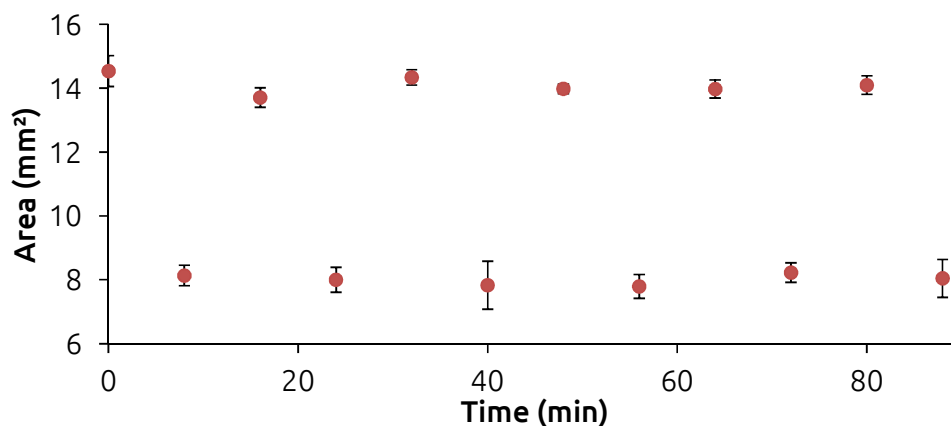


Figure 4.5. Temperature-induced area shrinking of the PSPA hydrogels at 20 °C and at 50 °C.

4.4.2 Flow characterization study

Following this, microfluidic devices were fabricated as described in the experimental section with the necessary configuration for a hydrogel to be photopolymerised and used as a temperature-controlled actuator. The hydrogel actuator was opened and closed six times (Figure 4.6), thus confirming the reproducibility and repeatability of the PIL hydrogel thermo-actuation.

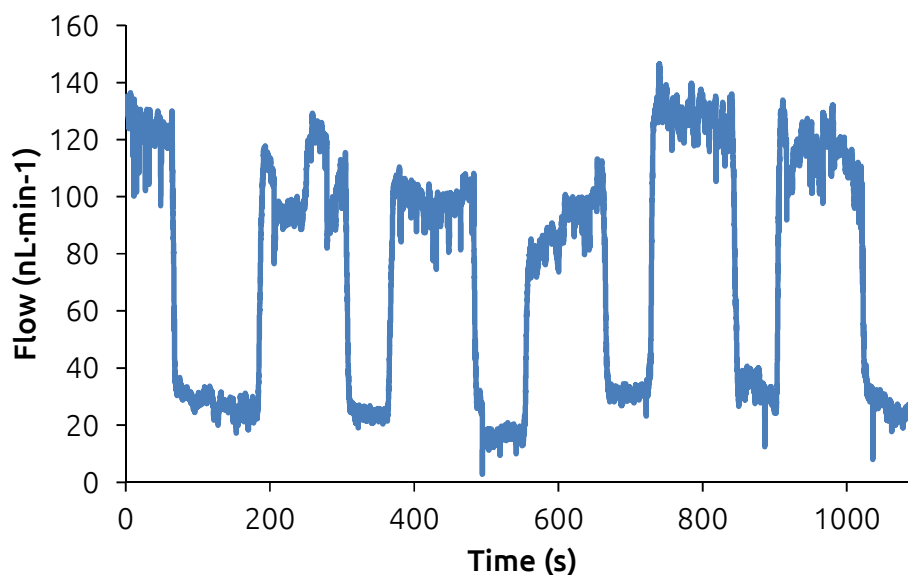


Figure 4.6. PSPA hydrogel actuator at 50 °C allowing a flow rate of $\sim 140 \text{ nL}\cdot\text{min}^{-1}$ to pass through the microfluidic channel, and, at 20 °C, restricting flow rate to $\sim 20 \text{ nL}\cdot\text{min}^{-1}$. Small fluctuations on the signal ($10 \pm 5 \text{ nL}\cdot\text{min}^{-1}$) were observed due to ambient conditions (e.g. vibration of the pumping system) and the ionic liquid polymer network internal reorganisation before and after temperature actuation, which is extended after the stimulus is removed due to the hydration or dehydration processes that continue to happen in the polymer.

In the ‘open’ form, when the actuator is fully contracted, a flow of $\sim 120 \text{ nL}\cdot\text{min}^{-1}$ occurs rather than the $500 \text{ nL}\cdot\text{min}^{-1}$ flow rate obtained with a fully open channel. This means that the PIL actuator is partially occluding the microchannel, impeding the normal flow through the microchannel. In the actuator’s “closed” form, the flow sensor still detects a residual flow of $20 \text{ nL}\cdot\text{min}^{-1}$ rather than 0. The reason

why the flow signal does not reach $0 \text{ nL}\cdot\text{min}^{-1}$ can be attributed to small residual pathways through which the fluid still can pass:

- (1) Either bypassing the swollen gel (e.g. where the gel meets the channel top surface); or
- (2) Through the valve structure (due to pores or inherent liquid transport arising from the open polymeric structure of the hydrated gel).

Both of these effects can be corrected by changing the geometry of the hydrogel actuator, together with design optimizations of the microfluidic device. Moreover, the PIL hydrogel can be placed behind a thin elastic membrane, to ensure that the hydrogel does not come into contact with the liquid flowing through the microfluidic device if the application deems it necessary. Furthermore, with additional optimization, the PIL materials could be used either as valves in simple, low-cost, microfluidic platforms, or as temperature-modulated flow regulators, due to their wide LCST interval. This property can be used to affect the measured flow through a microfluidic device in a repeatable and reproducible way, thus providing enough information for a pulse width modulation feedback loop platform to control the flow through a microfluidic device automatically. In addition, to better understand the ability of this hydrogel actuator to be used in a microfluidic device, its burst pressure was determined. This was performed by applying incremental increases in pressure to the hydrogel actuator starting with 5 mbar up to 400 mbar (Figure A.3). When the pressure reached the value of 250 mbar, the hydrogel actuator started degrading, which resulted in an increase in flow rate (time: 1860s). At 400 mbar, complete failure of the hydrogel actuator was observed. Consequently, based on the results obtained for this particular microchip configuration, the burst pressure was acknowledged to be 250 mbar, while the complete failure pressure was found to be 400 mbar.

The shrinking and swelling rate constants of the hydrogel actuator (Table 4.1) were calculated using the logistic curve equation (Eq. 4.2) based on the flow rate measurements (Figure 4.6).

Table 4.1. Experimental shrinking and swelling rate constants.

Shrinking		Swelling	
Repetition	k	Repetition	k
1	0,9	1	0,9
2	0,4	2	0,9
3	0,5	3	0,8
4	0,8	4	0,4
5	0,7	5	0,5
6	0,6		
Average	0,6	Average	0,7
Standard Deviation	0,2	Standard Deviation	0,3
RSD (%)	29,8	RSD (%)	36,4

The rate constants were found to be $(1.1 \pm 0.3) \cdot 10^{-2} \text{ s}^{-1}$ ($n = 6$) for the shrinking of the hydrogel and $(1.1 \pm 0.5) \cdot 10^{-2} \text{ s}^{-1}$ ($n = 5$) for the swelling of the hydrogel. The close values of the rate constants convey the fact that both effects take place with approximately the same speed, which indicates no perceptible hysteresis between the opening and the closing of the PILc hydrogel flow regulator when the temperature was cycled between 50 °C and 20 °C (Figure A.4.1 and Figure A.4.2). This effect is confirmed by the fact that the closing and opening time of the hydrogel actuator vary between 5 to 8 s. The actuation time values compare favourably with actuation times given for other stimuli-responsive hydrogels actuators based on conventional thermo-responsive polymers[52], or several phase-change mechanical actuators based on paraffin wax [6], while being similar with state of the art in hydrogel valves [37,53]. Compared to other type of actuators, especially vacuum operated or electrically operated hard valves, the response times are slower. Regardless of this, there are several ways in which their response times could be improved, including: fitting a heating element capable of much faster heating and cooling rates, changing the geometry of the hydrogel and the hydrogel positioning to ensure that there is a need for less hydrogel to open and close the microchannel, and the addition of a pore forming agent to the monomer mixture, such as high molecular weight poly(ethylene glycol), which would help the hydrogel absorb and expel its hydration medium faster.

4.5 Conclusions

In conclusion, a tributylhexyl phosphonium sulfopropyl acrylate ionic liquid monomer was synthesised and photopolymerised to produce a poly(ionic liquid) hydrogel that features a lower critical solution temperature. Due of this, the hydrogel is able to shrink by increasing the temperature of its surrounding hydration medium. Based on this thermo-responsive behaviour, the hydrogel actuation behaviour was fully characterised and the hydrogel was incorporated into a microfluidic device with the purpose of being used as temperature-controlled actuator. The characterisation of the hydrogel indicates that the hydrogel shrinks by $\sim 58\%$ of its swollen area when the temperature is raised from 20 to 70 °C and $\sim 39\%$ when the temperature is raised from 20 to 50 °C. Furthermore, the hydrogel is able to shrink and reswell repeatedly when subjected to temperature cycles between 20 °C and 50 °C. Moreover, by including the hydrogel in a microfluidic device as a temperature-controlled actuator, the microfluidic channel was modulated between $\sim 110 \text{ nL}\cdot\text{min}^{-1}$ ($\pm 15 \text{ nL}\cdot\text{min}^{-1}$, $n = 6$) and $\sim 27 \text{ nL}\cdot\text{min}^{-1}$ ($\pm 5 \text{ nL}\cdot\text{min}^{-1}$, $n = 6$) by varying the temperature between 50 °C and 20 °C. This process was repeated six times with no performance loss, thus suggesting the possibility of repeatable use for more than six times. Based on these results and taking into account the vast collection of ionic liquids available and their synthetic versatility, thermo-responsive poly(ionic liquid)s could constitute a new tool box for the generation of simple and low-cost temperature responsive microfluidic actuators.

3.6 References

1. Nge, P.N.; Rogers, C.I.; Woolley, A.T. Advances in microfluidic materials, functions, integration, and applications. *Chemical Reviews* **2013**, *113*, 2550-2583.
2. Whitesides, G.M. The origins and the future of microfluidics. *Nature* **2006**, *442*, 368-373.
3. Dong, L.; Jiang, H. Autonomous microfluidics with stimuli-responsive hydrogels. *Soft Matter* **2007**, *3*, 1223.
4. Araci, I.; Brisk, P. Recent developments in microfluidic large scale integration. *Current Opinion in Biotechnology* **2014**, *25*, 60-68.
5. Mohammed, M.I.; Abraham, E.; Desmulliez, M.P.Y. Rapid laser prototyping of valves for microfluidic autonomous systems. *Journal of Micromechanics and Microengineering* **2013**, *23*, 35034.

6. Ogden, S.; Klintberg, L.; Thornell, G.; Hjort, K.; Bodén, R. Review on miniaturized paraffin phase change actuators, valves, and pumps. *Microfluidics and Nanofluidics* **2014**, *17*, 53-71.
7. Oh, K.W.; Ahn, C.H. A review of microvalves. *Journal of Micromechanics and Microengineering* **2006**, *16*.
8. Selvaganapathy, P.; Carlen, E.T.; Mastrangelo, C.H. Electrothermally actuated inline microfluidic valve. *Sensors and Actuators A: Physical* **2003**, *104*, 275-282.
9. Yang, B.; Lin, Q. A latchable microvalve using phase change of paraffin wax. *Sensors and Actuators A: Physical* **2007**, *134*, 194-200.
10. Zhang, C.; Xing, D.; Li, Y. Micropumps, microvalves, and micromixers within per microfluidic chips: Advances and trends. *Biotechnology Advances* **2007**, *25*, 483-514.
11. Beebe, D.J.; Moore, J.S.; Bauer, J.M.; Yu, Q.; Liu, R.H.; Devadoss, C.; Jo, B.-H. Functional hydrogel structures for autonomous flow control inside microfluidic channels. *Nature* **2000**, *404*, 588-590.
12. Agarwal, A.K.; Dong, L.; Beebe, D.J.; Jiang, H. Autonomously-triggered microfluidic cooling using thermo-responsive hydrogels. *Lab on a Chip* **2007**, *7*, 310-315.
13. Florea, L.; Diamond, D.; Benito-Lopez, F. Opto-smart systems in microfluidics. *Research Perspectives on Functional Micro-and Nanoscale Coatings* **2016**, 265.
14. ter Schiphorst, J.; Coleman, S.; Stumpel, J.E.; Ben Azouz, A.; Diamond, D.; Schenning, A.P. Molecular design of light-responsive hydrogels, for in situ generation of fast and reversible valves for microfluidic applications. *Chemistry of Materials* **2015**, *27*, 5925-5931.
15. Ziółkowski, B.; Czugała, M.; Diamond, D. Integrating stimulus responsive materials and microfluidics: The key to next-generation chemical sensors. *Journal of Intelligent Material Systems and Structures* **2012**, 1045389-12459591.
16. Czugała, M.; O'Connell, C.; Blin, C.; Fischer, P.; Fraser, K.J.; Benito-Lopez, F.; Diamond, D. Swelling and shrinking behaviour of photoresponsive phosphonium-based ionogel microstructures. *Sensors and Actuators B: Chemical* **2014**, *194*, 105-113.
17. Saez, J.; Etxebarria, J.; Antoñana-Diez, M.; Benito-Lopez, F. On-demand generation and removal of alginate biocompatible microvalves for flow control in microfluidics. *Sensors and Actuators B: Chemical* **2016**, *234*, 1-7.
18. Men, Y.; Li, X.-H.; Antonietti, M.; Yuan, J. Poly(tetrabutylphosphonium 4-styrenesulfonate): A poly(ionic liquid) stabilizer for graphene being multi-responsive. *Polymer Chemistry* **2012**, *3*, 871.
19. Bogue, R. Smart materials: A review of recent developments. *Assembly Automation* **2012**, *32*, 37.
20. Boutris, C.; Chatzi, E.G.; Kiparissides, C. Characterization of the lscst behaviour of aqueous poly(n-isopropylacrylamide) solutions by thermal and cloud point techniques. *Polymer* **1997**, *38*, 2567-2570.
21. Florea, L.; Diamond, D.; Benito - Lopez, F. Photo - responsive polymeric structures based on spiropyran. *Macromolecular Materials and Engineering* **2012**, *297*, 11481159.
22. Gallagher, S.; Florea, L.; Fraser, K.J.; Diamond, D. Swelling and shrinking properties of thermo-responsive polymeric ionic liquid hydrogels with

- embedded linear pnipaaam. *International Journal of Molecular Sciences* **2014**, *15*, 5337-5349.
23. Gallagher, S.; Kavanagh, A.; Ziolkowski, B.; Florea, L.; MacFarlane, D.R.; Fraser, K.; Diamond, D. Ionic liquid modulation of swelling and lcst behavior of n -isopropylacrylamide polymer gels. *Physical Chemistry Chemical Physics* **2013**, *16*, 3610.
 24. Guilherme, M.R.; da Silva, R.; Rubira, A.F.; Geuskens, G.; Muniz, E.C. Thermo-sensitive hydrogels membranes from paam networks and entangled pnipaaam: Effect of temperature, cross-linking and pnipaaam contents on the water uptake and permeability. *Reactive & Functional Polymers* **2004**, *61*, 233-243.
 25. Hammarson, M.; Nilsson, J.R.; Li, S.; Beke-Somfai, T.; Andréasson, J. Characterization of the thermal and photoinduced reactions of photochromic spiropyrans in aqueous solution. *The Journal of Physical Chemistry B* **2013**, *117*, 13561-13571.
 26. Ionov, L. Hydrogel-based actuators: Possibilities and limitations. *Materials Today* **2014**, *17*, 494-503.
 27. Kohno, Y.; Deguchi, Y.; Ohno, H. Ionic liquid -derived charged polymers to show highly thermoresponsive lcst-type transition with water at desired temperatures. *Chemical Communications* **2012**, *48*, 11883-11885.
 28. Kohno, Y.; Ohno, H. Key factors to prepare polyelectrolytes showing temperature-sensitive lower critical solution temperature-type phase transitions in water. *Australian Journal of Chemistry* **2012**, *65*, 91-94.
 29. Kohno, Y.; Saita, S.; Men, Y.; Yuan, J.; Ohno, H. Thermoresponsive polyelectrolytes derived from ionic liquids. *Polymer Chemistry* **2015**, 2163-2178.
 30. Yuan, J.; Mecerreyes, D.; Antonietti, M. Poly(ionic liquid)s: An update. *Progress in Polymer Science* **2013**, *38*, 1009-1036.
 31. Ziolkowski, B.; Diamond, D. Thermoresponsive poly(ionic liquid) hydrogels. *Chemical Communications* **2013**, *49*, 10308-10310.
 32. Ziolkowski, B.; Florea, L.; Theobald, J.; Benito-Lopez, F.; Diamond, D. Self-protonating spiropyran- co -nipam- co -acrylic acid hydrogel photoactuators. *Soft Matter* **2013**, *9*, 8754.
 33. Maeda, Y.; Higuchi, T.; Ikeda, I. Ftir spectroscopic and calorimetric studies of the phase transitions of n-isopropylacrylamide copolymers in water. *Langmuir* **2001**, *17*, 7535-7539.
 34. Schild, H.G. Poly (n-isopropylacrylamide) - experiment, theory and application. *Progress in Polymer Science* **1992**, *17*, 163-249.
 35. Zhang, X.Z.; Yang, Y.Y.; Chung, T.S.; Ma, K.X. Preparation and characterization of fast response macroporous poly(n-isopropylacrylamide) hydrogels. *Langmuir* **2001**, *17*, 6094-6099.
 36. Glennon, T.; Saez, J.; Czugała, M.; Florea, L.; McNamara, E.; Fraser, K.J.; Ducree, J.; Diamond, D.; Benito-Lopez, F. Photo-switchable microvalve in a reusable lab-on-a-disc. *iee* **2015**, 109-112.
 37. Benito-Lopez, F.; Byrne, R.; Răduță, A.M.; Vrana, N.E.; McGuinness, G.; Diamond, D. Ionogel-based light-actuated valves for controlling liquid flow in micro-fluidic manifolds. *Lab on a Chip* **2010**, *10*, 195-201.
 38. Sugiura, S.; Sumaru, K.; Ohi, K.; Hiroki, K.; Takagi, T.; Kanamori, T. Photoresponsive polymer gel microvalves controlled by local light irradiation. *Sensors and Actuators A: Physical* **2007**, *140*, 176-184.

39. Satarkar, N.S.; Zhang, W.; Eitel, R.E.; Hilt, J.Z. Magnetic hydrogel nanocomposites as remote controlled microfluidic valves. *Lab on a Chip* **2009**, *9*, 1773-1779.
40. Ghosh, S.; Yang, C.; Cai, T.; Hu, Z.; Neogi, A. Oscillating magnetic field-actuated microvalves for micro-and nanofluidics. *Journal of Physics D: Applied Physics* **2009**, *42*, 135501.
41. Vancoillie, G.; Frank, D.; Hoogenboom, R. Thermoresponsive poly(oligo ethylene glycol acrylates). *Progress in Polymer Science* **2014**, *39*, 1074-1095.
42. Mecerreyes, D. Polymeric ionic liquids: Broadening the properties and applications of polyelectrolytes. *Progress in Polymer Science* **2011**, *36*, 1629-1648.
43. Benito-Lopez, F.; Antoñana-Díez, M.; Curto, V.F.; Diamond, D.; Castro-López, V. Modular microfluidic valve structures based on reversible thermoresponsive ionogel actuators. *Lab on a Chip* **2014**, *14*, 3530-3538.
44. Yoshizawa, M.; Ohno, H. Synthesis of molten salt-type polymer brush and effect of brush structure on the ionic conductivity. *Electrochimica Acta* **2001**, *46*, 1723-1728.
45. Shaplov, A.S.; Lozinskaya, E.I.; Ponkratov, D.O.; Malyshkina, I.A.; Vidal, F.; Aubert, P.-H.; Okatova, O.g.V.; Pavlov, G.M.; Komarova, L.I.; Wandrey, C., *et al.* Bis(trifluoromethylsulfonyl)amide based “polymeric ionic liquids”: Synthesis, purification and peculiarities of structure–properties relationships. *Electrochimica Acta* **2011**, *57*, 74-90.
46. Koebe, M.; Drechsler, M.; Weber, J.; Yuan, J. Crosslinked poly(ionic liquid) nanoparticles: Inner structure, size, and morphology. *Macromolecular Rapid Communications* **2012**, *33*, 646-651.
47. Gallagher, S.; Florea, L.; Fraser, K.; Diamond, D. Swelling and shrinking properties of thermo-responsive polymeric ionic liquid hydrogels with embedded linear pnipaam. *International Journal of Molecular Sciences* **2014**, *15*, 53375349.
48. Tudor, A.; Florea, L.; Gallagher, S.; Burns, J.; Diamond, D. Poly(ionic liquid) semi-interpenetrating network multi-responsive hydrogels. *Sensors* **2016**, *16*, 219.
49. Ziółkowski, B.; Ates, Z.; Gallagher, S.; Byrne, R.; Heise, A.; Fraser, K.J.; Diamond, D. Mechanical properties and uv curing behavior of poly(n - isopropylacrylamide) in phosphonium - based ionic liquids. *Macromolecular Chemistry and Physics* **2013**, *214*, 787796.
50. Men, Y.; Schlaad, H.; Voelkel, A.; Yuan, J. Thermoresponsive polymerized gemini dicationic ionic liquid. *Polymer Chemistry* **2014**, *5*, 3719-3724.
51. Tanaka, Y.; Fujikawa, T.; Kazoe, Y.; Kitamori, T. An active valve incorporated into a microchip using a high strain electroactive polymer. *Sensors and Actuators B: Chemical* **2013**, *184*, 163-169.
52. Zhu, C.H.; Lu, Y.; Peng, J.; Chen, J.F.; Yu, S.H. Photothermally sensitive poly (n - isopropylacrylamide)/graphene oxide nanocomposite hydrogels as remote light - controlled liquid microvalves. *Advanced Functional Materials* **2012**, *22*, 4017-4022.
53. Lee, E.; Lee, H.; Yoo, S.I.; Yoon, J. Photothermally triggered fast responding hydrogels incorporating a hydrophobic moiety for light-controlled microvalves. *ACS applied materials & interfaces* **2014**, *6*, 16949-16955.

Appendix Chapter 4

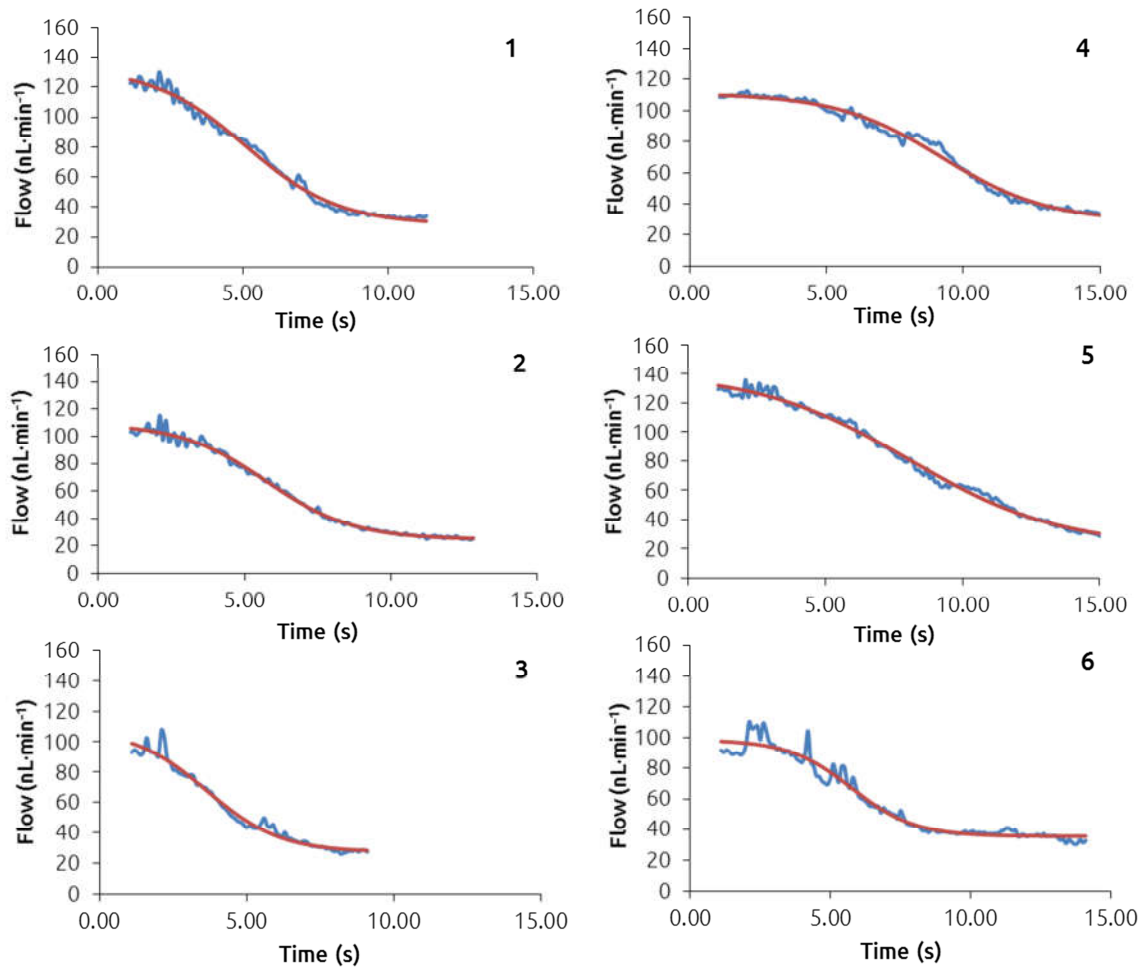


Figure A.4.1. Shrinking kinetics of the PILc hydrogel valve when the temperature was raised from 20 °C to 50 °C. The blue line represents the experimental flow rate, while the red line represents the modelled flow rate.

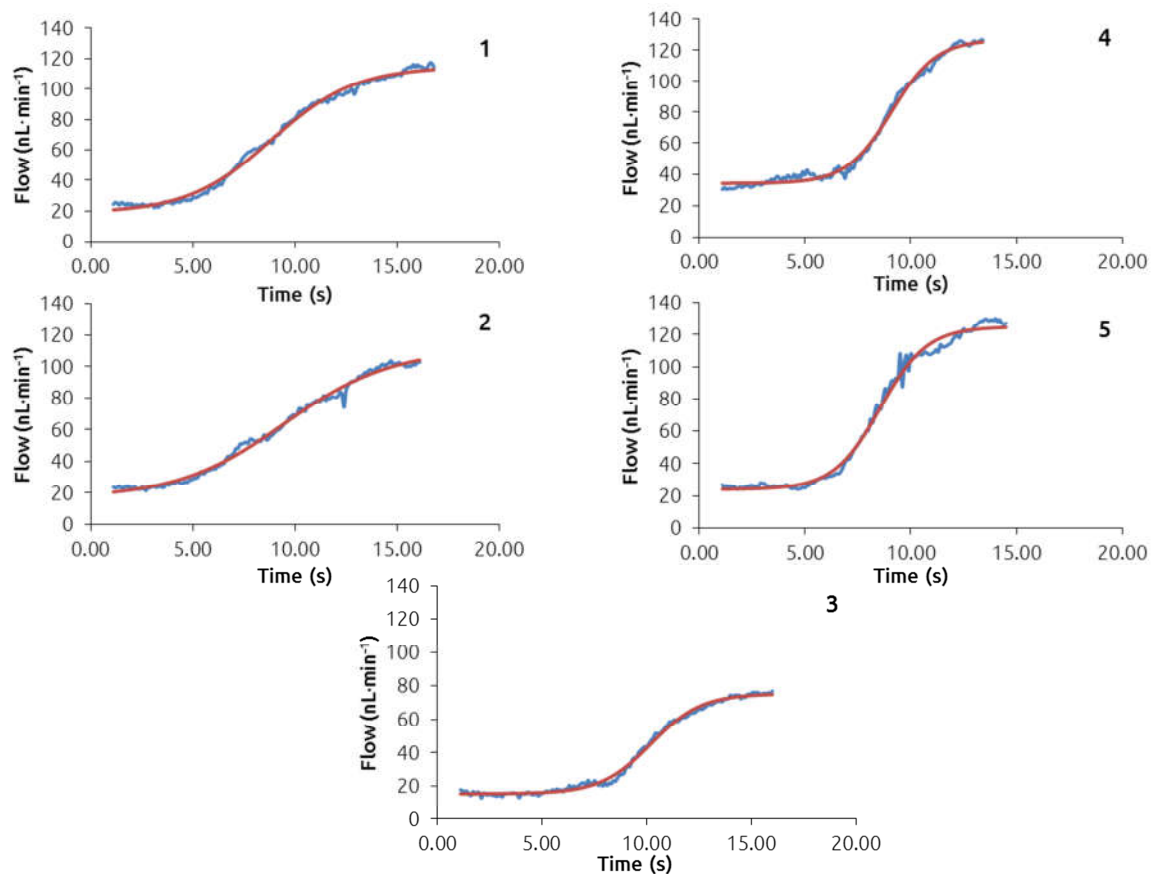


Figure A.4.2. Swelling kinetics of the PILc hydrogel valve when the temperature was lowered from 50 °C to 20 °C. The blue line represents the experimental flow rate, while the red line represents the modelled flow rate.

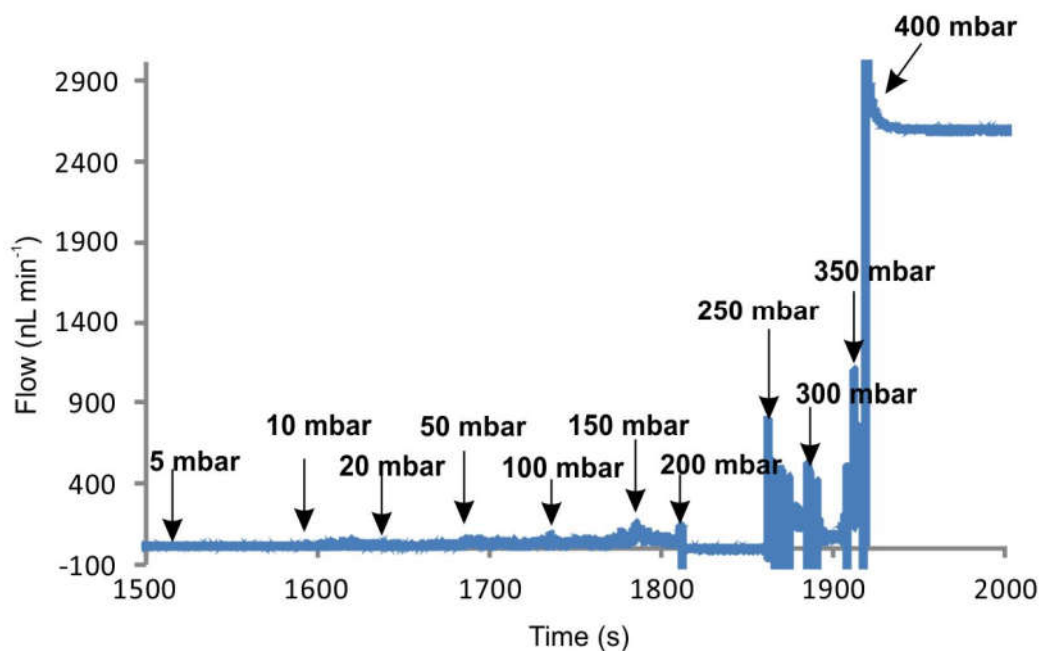


Figure A.4.3. Determination of the burst-pressure of the integrated actuator via incremental increases in pressure. At pressures above 250 mbar failure in the actuator was induced, resulting in an increase in flow rate through the micro-channel (time: 1860 s). Complete failure of the actuator was achieved at an applied pressure of 400 mbar.

Chapter 5: Direct Laser Writing Fabrication by Multi-photon Polymerisation of Stimuli-Responsive Poly(ionic liquid) Based Soft Structures with Sub-Micron Resolution

5.1 Abstract

5.2 Introduction

5.3 Experimental

5.3.1 Materials

5.3.2 Photoresists: Monomeric Cocktails for Direct Laser Writing Fabrication

5.3.3 Direct Laser Writing Fabrication

5.3.4 DLW Live-Observation

5.3.5 Microscopy and Quantification

5.4 Results and Discussion

5.4.1 Microstructure Printing

5.4.2 Microstructure temperature-induced shrinking

5.5 Conclusions

5.6 References

Chapter 5

Direct Laser Writing Fabrication by Multi-photon Polymerisation of Stimuli-Responsive Poly(ionic liquid) Based Soft Structures with Sub- Micron Resolution *

*Direct Laser Writing Fabrication by Multi-photon Polymerisation of Stimuli-Responsive Poly(ionic liquid) Based Soft Structures with Sub-Micron Resolution, A. Tudor, C. Delaney, A. Thompson, V. F. Curto, L. Florea, G.-Z. Yang, D. Diamond, *Nature Materials* (submitted)

5.1 Abstract

Herein, we demonstrate soft, stimuli-responsive 4D structures based on crosslinked poly(ionic liquid)s (PILs), created with unprecedented sub-micron resolution using direct laser-writing (DLW). Up to now, almost all sub-micron resolution DLW 3D structures have been created using proprietary cocktails that result in highly cross-linked, inflexible structures that have no inherent 4D character. In contrast, we demonstrate that, for the first time, it is possible to build soft 3D structures that are more mechanically compatible with biological systems than conventional highly-crosslinked DLW structures. Furthermore, inherited properties of the ionic liquid monomer (ILM) can be conferred on the resulting polymer, as well as advantages arising from the high precision of the technique, such as fast thermal responsiveness and even pre-programmed actuation due to their swelling/contraction behaviour in the presence/absence of water. The broad importance and adaptability of this breakthrough is further emphasised by the vast libraries of available monomeric ILs, which can be used to further fine-control of the resulting polymer characteristics. Various PIL patterns, including cylinders, spirals, hexagonal pillars, and grids of intersecting lines are demonstrated and analysed for their hydration/solvation properties and thermo-actuation behaviour.

5.2 Introduction

Direct laser-writing (DLW) is rapidly emerging as a route for the production of 3D structures with exquisite sub-micron resolution [1]. DLW relies on the simultaneous absorption of two photons of light to excite an initiator molecule from the ground state to a higher energy electronic state [2,3]. During the DLW process, the beam of a near-IR ultra-fast laser (780 nm) is focused on a point at which enough energy is available to initiate polymerisation by absorption of two-photons. This spot can be moved in three dimensions inside a volume of transparent monomeric material, with polymerisation induced by irradiation of one volume element (voxel) at a time, allowing for the construction of structures with ~200 nm resolution [3,4]. In this fashion, complex micromodels of any CAD design can be created [5]. Although, commercialised DLW devices have only recently entered the micro-fabrication technologies portfolio, the technology has already found much application within the

photonics community [6,7]. Even more recently DLW has also found relevance in other fields, such as micro-optics [8], microfluidics [9], clinical microtools [10], biomedical implants [11] and in 3D scaffolds for cell culturing and tissue engineering [4,12]. Despite the wide-ranging applications mentioned, the overwhelming majority of published structures produced by DLW employ vendor-supplied solvent-free photoresists (*e.g.* IP-L 780, IP-G 780, provided by Nanoscribe GmbH, Germany [13]) which produce highly-crosslinked and rigid structures. However, to truly embrace the potential of DLW as a platform and to generate more adaptable structures, the chemist is charged with translating methodologies from existing techniques and novel materials to develop a more flexible route to a much wider array of resources. To make inroads in fields with such biomedical application, the proven ability of soft polymer hydrogels may well hold un-tapped potential. Hydrogels are three-dimensional, hydrophilic, polymer networks capable of large water intake. These characteristics make them a potential candidate for the fabrication of biocompatible systems, which can be used for tailored drug delivery and regenerative medicine. Their ability to modulate their size and shape has been used to much advantage, by harnessing the ability of the hydrogel itself to respond to changes in hydration or temperature but also through the incorporation of co-polymerised stimuli-responsive molecules. Incorporation of responsive units in such polymeric networks allows for their use as micro-machines capable of doing mechanical work in response to the chosen stimulus. The application of smart materials offers tangible solutions in the field of actuators for microfluidic valves, artificial muscles and biomimetic robots [14-18]. Among the broad class of hydrogels, those based on poly(ionic liquid)s have only emerged in recent years [19]. Poly(Ionic Liquid)s (PILs) are a class of ionic liquids which feature polymerizable groups in either the cation, the anion or both [20-31]. PILs maintain the desired properties inherited from ionic liquids (ILs) such as low vapour pressure, high charge density and high thermal/chemical stability while gaining the characteristic properties of polymers such as the ability to form films and self-standing structures. To date, PILs have been used in various applications, including conducting materials for solar cells [32], lithium-ion rechargeable batteries [33], soft polymer actuators [34] and recently they have attracted enormous attention as innovative polyelectrolytes to build up advanced materials and multifunctional devices [35-38]. Crosslinking of several PILs have shown to produce gel-like materials capable of solvent-induced swelling for

ultrasensitive solvent sensing [39] and fast actuation purposes [40]. ILs/PILs comprised of moderately hydrophilic/hydrophobic ions have the potential to show a lower critical solution temperature (LCST)-type phase transition [31,41,42]. Hydrogels made of such PILs inherit this property, with the mention that as opposite to LCST transition in classic thermo-responsive hydrogels such as p(N-isopropyl acrylamide) [43], the LCST doesn't manifest as a step transition process but rather as a gradual volume change over a broad LCST range. Therefore, thermo-responsive PILs offer a great possibility for the development of fine-controlled thermo-actuators. Despite their attractive properties, to our knowledge, PILs have not been used in the creation of 3D structured actuators or sensors.

Herein we demonstrate, for the first time, the DLW of stimuli-responsive 3D structures made of crosslinked PILs, namely tributylhexyl poly(sulfopropylacrylate) ($[P_{4,4,4,6}][SPA]$). These 3D structures can increase their size through the absorption of water or solvent (acetone) molecules by over 300%. Moreover as $[P_{4,4,4,6}][SPA]$ has an LCST, the 3D printed PIL structures are responsive to temperature (4D effect), showing a decrease in area over 25% at 70 °C. Traditionally, the swelling and shrinking of the polymer networks is the dominant mechanism to modulate hydrogel actuators, and this process can be relatively slow as it is limited by the retarded diffusion in the wet state. However, as these soft PIL structures are printed at unprecedented resolutions, the diffusion times are extremely fast, allowing for thermo-response without a noticeable delay. This work not only unlocks the latent potential in DLW methodologies for microfabrication of new soft materials but also presents a roadmap for the inclusion of a large library of polymeric ionic liquid materials with proven application far beyond the boundaries of material science.

5.3 Experimental

5.3.1 Materials

Polypropylene glycol diacrylate ($M_w \sim 800$, 100 ppm MEHQ and 100 ppm BHT as inhibitors) (PPG800) and 3-(trimethoxysilyl) propyl methacrylate were acquired from Sigma Aldrich, Ireland and used as received. 7-Diethylamino-3-thenoylcoumarin (DEATC) was purchased from Exciton (Dayton, Ohio) and used as received. Tributylhexyl sulfopropyl acrylate ($P_{4,4,4,6}SPA$) was synthesised as described

elsewhere[44]. The acrylated derivative of Rhodamine B (Acryl Rhod. B) was synthesised as described in the supporting information. Deionized water (DI water), with a resistivity of $18.2 \text{ M}\Omega\cdot\text{cm}^{-1}$, was made using a Milli-Q Water Purification System (Merck Millipore, Darmstadt, Germany).

5.3.2 Photoresists: Monomeric Cocktails for Direct Laser Writing Fabrication

For the DLW of 3D soft structures based on PILs, the monomer mixture contains an ILM (P_{4,4,4,6}SPA), a long chain crosslinker (PPG800) and photo-initiator, 7-Diethylamino-3-thenoylcoumarin (Table 1). The quantity of the photo-initiator in the monomer mixture was varied between 1-7 mol%, while the concentration of the crosslinker was varied between 4-12.5 mol%. An example of the cocktail used for the fabrication of soft thermo-responsive crosslinked PIL is indicated in Table 1.

Table 5.1. Monomeric cocktail composition.

Cocktail components	Quantity (g)	μmols	mol% to P _{4,4,4,6} SPA
P _{4,4,4,6} SPA	0.3872	800	100
DEATC photoinitiator	0.0052	16	2
PPO800	0.033	60	7.5

For structures prepared for confocal fluorescence imaging, Acryl Rhod. B was added to the monomeric cocktail in a molar ratio to P_{4,4,4,6}SPA of 2-5 mol%, and the PPO800 amount was increased to 100 μmol , which represents a concentration of 12.5 mol%.

5.3.3 Direct Laser Writing Fabrication

Two-photon polymerization was induced by a focused laser beam from a 780 nm femtosecond laser in a commercial DLW workstation (Photonic Professional, Nanoscribe GmbH). Fabrication of the 3D soft structures using cocktails described in Table 1 was performed in an Oil-immersion configuration using a 63x immersion objective (NA=1.4, WD=190 μm) (Zeiss, Plan Aplanachromat). The sample position was controlled by a 3D galvo translation stage.

A drop of the monomeric cocktail was placed in the centre on one side of DiLL glass substrates for high resolution applications^[1] (25x25 mm²; thickness: 0.17 mm; provided by Nanoscribe GmbH) and a drop of oil was placed in the centre of the glass slide on the other side. The laser power and the scan speed for fabrication of the 3D structures was set between 30-50 mW and scan speeds varied between 5000 $\mu\text{m}\cdot\text{s}^{-1}$ and 10000 $\mu\text{m}\cdot\text{s}^{-1}$. After laser writing, the structures were developed by first removing some the unpolymerised cocktail by positioning the slide at a 70° angle and then rinsing carefully 3 times with acetone to remove residual unpolymerised cocktail. The structures were then dried in air for 10 min and prepared for further characterisation. For the substrate-attached structures, in order to enhance the adhesion of the acrylic-based photoresists to the glass substrate, the glass slides were cleaned with acetone, isopropanol, ethanol, methanol and DI water, dried, and exposed to oxygen plasma for 2 min (Harrick Plasma). Following this, the slides were immersed in a solution of 3-(trimethoxysilyl) propyl methacrylate (Sigma Aldrich; 3vol% in EtOH with 0.1vol% Acetic acid) for 1 h, rinsed in EtOH, and dried under nitrogen.

5.3.4 DLW Live-Observation

The DLW process was recorded using the Nanoscribe high-sensitivity microscope camera (1.4 Megapixel). This allows live visualization of the DLW process in order to track the efficiency of the writing process.

5.3.5 Microscopy and Quantification

The 3D structures were analysed in air and DI water using a 3D Digital Microscope VHX 5000 from Keyence (USA) equipped with objectives of adjustable magnification (100x-5000x). For the thermal analysis, 2 pressure sensitive adhesive (PSA) spacers of 60 μm were placed on the slide containing the structures and a clean glass cover was placed on top of the spacers to enclose the 3D printed structures in a cell-type arrangement with two opposite walls (Figure 4A). The custom made cell was then filled with DI water by capillary forces and placed onto the micro-heater and a temperature program was applied (Figure A.5.14). This arrangement ensures that

the level of the water on top of the structures does not change. Videos and images were recorded using the microscope camera (2 Megapixel).

Confocal laser microscopy analysis was performed using a Leica SP8 confocal microscope with an excitation laser chosen at $\sim 550\text{nm}$. For analysis the PIL structures contained Acryl. Rhod. B copolymerized in their structure at 2-5 mol% relative to $\text{P}_{4,4,4,6}\text{SPA}$.

5.4. Results and discussions

5.4.1 Microstructure printing

Polymerisation of a range of soft microscopic 3D motifs was achieved through the use of a polymerisable tributylhexyl phosphonium 3-sulfopropyl acrylate ($\text{P}_{4,4,4,6}\text{SPA}$) ionic-liquid monomer, a long-chain crosslinker (polypropylene glycol diacrylate, Mw ~ 800) and diethylamino-3-thenoylcoumarin (DEATC) photoinitiator. Additionally, through incorporation of a co-polymerised fluorescent dye it has also been possible to truly characterize the effect of external stimuli, such as hydration and thermal changes, on these microscopic structures in real time using stimulated emission depletion (STED) microscopy. Because of suitable matching of viscosity and refractive index, it has been possible to directly substitute commercially available photoresists with our novel monomeric cocktail. Simply by placing a drop of the monomeric cocktail at the centre of glass slide, outlined in Figure 5.1A, optimization of the DLW configuration, such as varied scan speeds and laser power, allowed for the successful creation of a wide variety of micrometre-sized structures. Figure 5.1 outlines such a procedure for the creation of various shaped objects, namely cylindrical columns, spirals (Figure A.5.5) and hexagonal pillars. Upon polymerization, the newly-formed feature can be seen to expand rapidly during washing in acetone owed to the solvation properties of the IL-based cocktail. Removal of residual cocktail, achieved by rinsing the structures with acetone (Video A.5.1 and Video A.5.2), results in the structures shown in Figure 5.1C and Figure 5.1F. In the absence of surface functionalisation to yield covalent attachment, the constructs can re-assemble themselves when solvent is reintroduced (Video A.5.2). Most fascinating is their ability to maintain relative positions and withstand any deformation during washing. In the absence of solvent, the structures contract,

thereby disturbing their superstructures. Through functionalisation of the glass surface with alkoxy silane moieties, the polymerised structures can be covalently attached. This has a profound effect on the behaviour of structures during actuation. Figure 5.2 shows further structures achieved using the same PIL (Figure 5.2A), with a copolymerised fluorescent rhodamine dye. This offers a convenient method for imaging of the structures using confocal/STED microscopy. This technique provided improved means for visualising the micro-patterning achieved during printing of the structures due to higher degrees of cross-linking along the chosen pathway of the laser beam. Upon swelling, these patterns, observed as concentric circles within the pillars (spirals), become more pronounced, as is clearly evident in Figure 5.2 (E) and (F). Once swelling was induced, the resulting behaviour of the structures proved of particular interest. The confinement of the bottom of the columnar structures, owed to the covalent attachment to the surface, generates a frustum-like shape which is caused by a higher degree of swelling at the top of the pillar, where the hydrogel is less restricted. The extent to which hydration induced swelling is increased towards the top extremity of the column can be readily measured using a Z-stacking function of the confocal microscope. Analysis of the 2D images using ImageJ software, at varied Z heights (0.1 μm between slices), allowed for the analysis of the hydrated and dehydrated cylinders (Figure 5.2B) and an increase in the area of the pillar to 169% of the base area was observed for the 8.1 μm slice (from the substrate surface) in the hydrated structure, while a contraction of 81% of the base area was calculated for the same structure in the dehydrated state for the 2.5 μm slice (from the substrate surface). Imaging further away from the surface in the case of both hydrated (above 8.1 μm) and dehydrated (above 2.5 μm) structures were not possible in the given experimental conditions due to strong absorbance of the fluorescent dye.

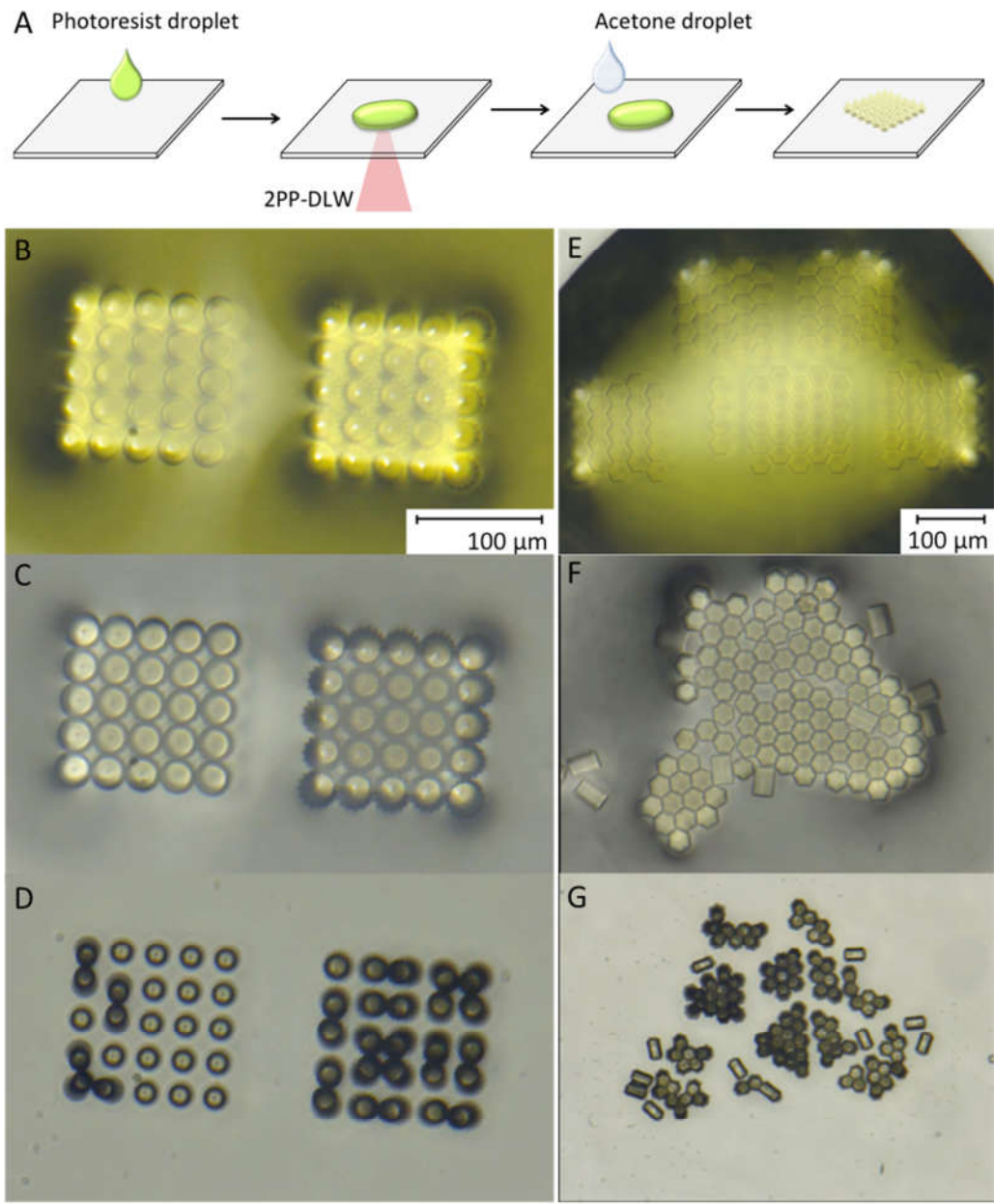


Figure 5.1 3D microscopy image of 2 micro-pillars arrays (cylinders and spirals) fabricated by 2-PP in PILs using cocktail formulations described in Table 1, in the polymerization cocktail (B, E), during washing in acetone (C, F), and during drying (D, G). It can be observed that in the case of the treated substrates (B-D), the structures maintained their position and structural integrity during the washing process, and no delamination occurs.

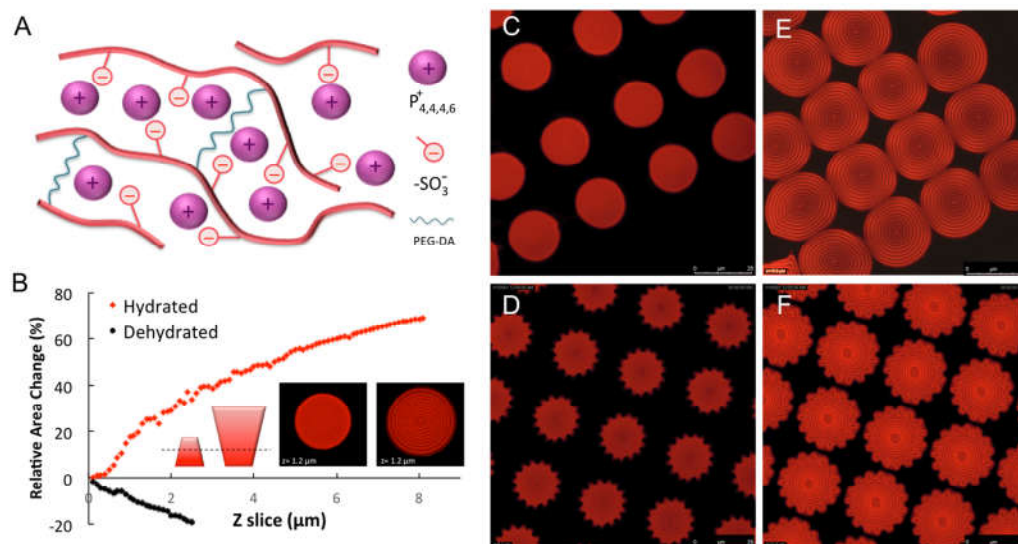


Figure 5.2 Structure of the PIL hydrogel (A); Relative area measurements of a micro-cylinder at different height (z) values in hydrated and dehydrated state. The relative area changes in both hydrated and dehydrated states are calculated relative to the printed area (circular structures of $20\ \mu\text{m}$ in diameter). Inset shows a cartoon representation of the micro-cylinder structures in the hydrated and dehydrated states and confocal microscopy images of the micro-cylinder in the hydrated and dehydrated state at the same z value (B). Confocal microscopy images of micro-cylinders (C, E) and micro-spirals (C, F) array fabricated by 2-PP in PILs using cocktail formulations described in Table 1, in air (C, D) and in DI water (E, F). The concentric circles composing the cylinders (contour slicing) become visible in the hydrated structures (E, F).

The contorted nature of the patterning which forms a spiral endo-skeleton confers directionality on the rotation of the spiral during hydration. When cycling between the states seen in Figure 5.2 (D) and Figure 5.2 (F) respectively, rotation in a counter clockwise motion is achieved upon hydration and subsequently reversed upon dehydration (Video A.5.4).

In contrast to the surface-bound structures, structures printed on non-treated glass slides delaminated during the washing process with acetone. These free-standing structures exhibited homogeneous swelling to produce a larger than original cylindrical form, rather than the frustum shaped structures generated by the surface bound structures. The degree of swelling also depended on the aspect ratio of the printed structure and the hatching/slicing dimensions used during DLW. For

examples, grids printed at $80 \times 80 \mu\text{m}$ and $1 \mu\text{m}$ in height (slicing distance $0.2 \mu\text{m}$; hatching distance $1 \mu\text{m}$; contour count: 4; contour distance: $1 \mu\text{m}$; hatching angle offset: 1) tended to delaminate and increase in area by over 300% during the washing step with acetone (Video A.5.3, Figure 5.3).

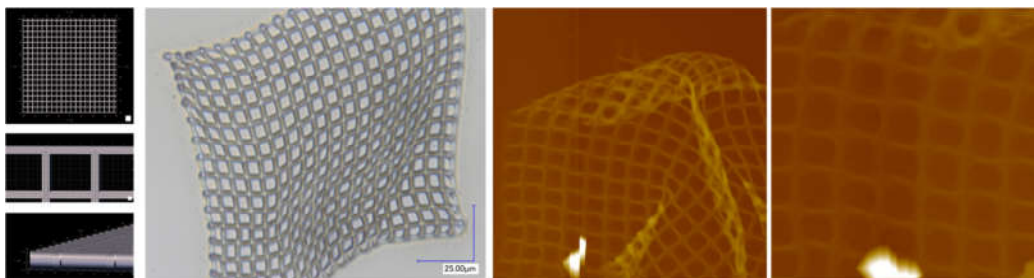


Figure 5.3 Design, white light microscopy and AFM images of a micro-grid printed at $80 \times 80 \mu\text{m}$ and $1 \mu\text{m}$ in height after hydration and delamination.

5.4.2 Microstructure temperature-induced shrinking

Depending on the hydrophobicity/ hydrophilicity balance of the ions constituting the IL, several ILs, ILMs and PILs were found to exhibit lower critical solution temperature (LCST) phase transition behaviour in water. In general, the thermoresponsive IL (ILM/PIL) /water mixtures can be obtained by designing the cations and anions to give a desired hydrophobicity/hydrophilicity balance. The great structural diversity of the ions and enormous amount of possible combinations make thermo-responsive ILMs and PILs an attractive approach for the fabrication of thermo-responsive materials, as the LCST can be tuned with greater ease than classic thermo-responsive polymers such as poly(N-isopropylacrylamide) (pNIPAAm).

To best demonstrate this thermal response for micron-sized structures of this nature, DLW fabricated pillars were formed on a microscope slide. Using a custom-built cell, shown in Figure 5.4 (A), water was introduced leading to complete hydration of the pillars. The cell was then placed into a micro-heater block, described elsewhere[34], which provides a homogeneous heating rate of $7.4 \text{ }^\circ\text{C s}^{-1}$ and a cooling rate of $2.4 \text{ }^\circ\text{C s}^{-1}$. A pre-programmed heating regime was applied, plotted in red in Figure 5.4 (B), and an optical microscope used to video the effect on the cylindrical structures at 15 fps. Subsequently, by analysing the response in 2s increments, using ImageJ, it was

possible to map the area response of the hydrogel structures with varying temperature. Remarkably, the response of the gel structures to temperature cycles at 25 °C, 30 °C, 50 °C, 70 °C is almost instantaneous, with a maximum area change of $30\% \pm 3\%$ ($n=40$ measurement points) at 70 °C, with respect to initial area at 20 °C. Re-expansion of the 3D microstructures, through cooling of the surrounding water from 70 °C to 30 °C (and 25 °C, respectively, for the final step) was also achieved at a rate comparable with the limits of the temperature control device. The ability to cycle such a response over 11 actuation steps with reproducible gel reaction and fast response time offers a fascinating possibility for the creation of responsive soft micro-robots.

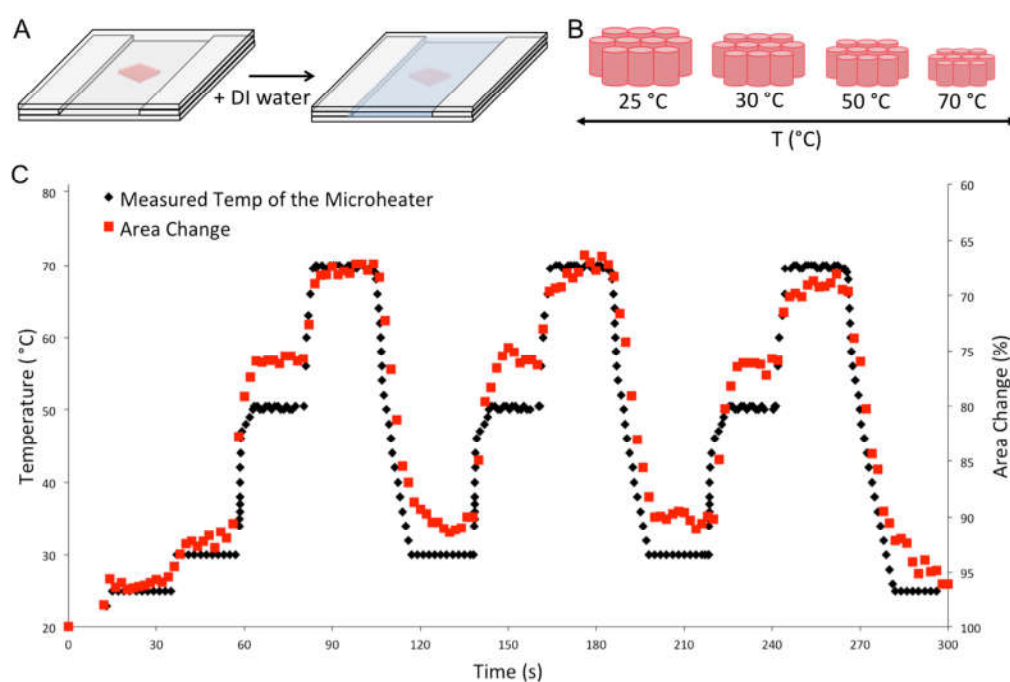


Figure 5.4 Schematic of the in-house made cell used to study the thermo-response of the gel structures; After removing of the excess photo-resist and washing of the structures, a $25\mu\text{m}$ PSA spacer was placed on the cover slide containing the structures and covered with another thing cover slide. DI water was introduced in the cell by capillary forces and the cell was placed on the micro-heater. Schematic representation of the thermo-actuation of the PII hydrogel structures (B). Structures are exposed to a temperature program and their thermo-response is recorded using white light microscopy. The area of the micro-cylinders is measured from the recorded video (1 frame/2s) using ImageJ software.

5.5 Conclusions

A phosphonium sulfopropylacrylate monomer mixture was synthesised that had the right properties to be usable as a photocurable resist in a multiphoton 3D printer. By using this photoresist it was possible to print shapes with simple geometries, such as cylinders, hexagons, grids, and twisted vases on both unsilanised and silanised glass slides. Due to the inherent physical properties of the ionic liquid monomer, the printed structures were able to absorb water, and expand in size up to 300%, in case of the grids printed on unsilanised glass slides. Moreover, due to the PIL possessing a LCST, it was possible to observe the shrinking and reswelling phenomenon with the help of a high-resolution optical microscope and of a temperature controller. It was found that the structure respond very fast to local changes in temperature, both during shrinking and during reswelling, while also maintaining their ability to go through several heating and cooling cycles without a drop in performance. We believe that using ionic liquid monomers to create photocurable resists opens up the possibilities for creating microstructures that display versatile physical and chemical properties that would benefit greatly the field of multiphoton 3D printed microstructures, with further applications in different related fields, such as microrobotics.

5.6 References

1. Bückmann, T.; Stenger, N.; Kadic, M.; Kaschke, J.; Frölich, A.; Kennerknecht, T.; Eberl, C.; Thiel, M.; Wegener, M. Tailored 3d mechanical metamaterials made by dip-in direct-laser-writing optical lithography. *Advanced Materials* **2012**, *24*, 2710-2714.
2. Selimis, A.; Mironov, V.; Farsari, M. Direct laser writing: Principles and materials for scaffold 3d printing. *Microelectronic Engineering* **2015**, *132*, 83-89.
3. Malinauskas, M.; Farsari, M.; Piskarskas, A.; Juodkazis, S. Ultrafast laser nanostructuring of photopolymers: A decade of advances. *Physics Reports* **2013**, *533*, 1-31.
4. Ovsianikov, A.; Mironov, V.; Stampfl, J.; Liska, R. Engineering 3d cell-culture matrices: Multiphoton processing technologies for biological and tissue engineering applications. *Expert review of medical devices* **2012**, *9*, 613-633.
5. Da Sie, Y.; Li, Y.-C.; Chang, N.-S.; Campagnola, P.J.; Chen, S.-J. Fabrication of three-dimensional multi-protein microstructures for cell migration and adhesion enhancement. *Biomedical optics express* **2015**, *6*, 480-490.

6. Hossain, M.M.; Gu, M. Fabrication methods of 3d periodic metallic nano/microstructures for photonics applications. *Laser & Photonics Reviews* **2014**, *8*, 233-249.
7. Juodkazis, S.; Mizeikis, V.; Misawa, H. Three-dimensional microfabrication of materials by femtosecond lasers for photonics applications. *Journal of Applied Physics* **2009**, *106*, 8.
8. Brasselet, E.; Malinauskas, M.; Žukauskas, A.; Juodkazis, S. Photopolymerized microscopic vortex beam generators: Precise delivery of optical orbital angular momentum. *Applied Physics Letters* **2010**, *97*, 211108.
9. Amato, L.; Gu, Y.; Bellini, N.; Eaton, S.M.; Cerullo, G.; Osellame, R. Integrated three-dimensional filter separates nanoscale from microscale elements in a microfluidic chip. *Lab on a Chip* **2012**, *12*, 1135-1142.
10. Villangca, M.J.; Palima, D.; Banas, A.R.; Glückstad, J. Light-driven micro-tool equipped with a syringe function. *Light: Science & Applications* **2016**, *5*.
11. Schizas, C.; Melissinaki, V.; Gaidukeviciute, A.; Reinhardt, C.; Ohrt, C.; Dedoussis, V.; Chichkov, B.N.; Fotakis, C.; Karalekas, D.; Farsari, M. In *3d biomedical implants fabricated using direct laser writing*, 2010; pp 759105-759105-759108.
12. Raimondi, M.T.; Eaton, S.M.; Nava, M.M.; Laganà, M.; Cerullo, G.; Osellame, R. Two-photon laser polymerization: From fundamentals to biomedical application in tissue engineering and regenerative medicine. *J Appl Biomater Biomech* **2012**, *10*, 55-65.
13. <http://www.nanoscribe.de/en/>. <http://www.nanoscribe.de/en/>
14. ter Schiphorst, J.; Coleman, S.; Stumpel, J.E.; Ben Azouz, A.; Diamond, D.; Schenning, A.P. Molecular design of light-responsive hydrogels, for in situ generation of fast and reversible valves for microfluidic applications. *Chemistry of Materials* **2015**, *27*, 5925-5931.
15. Ziółkowski, B.; Florea, L.; Theobald, J.; Benito-Lopez, F.; Diamond, D. Self-protonating spiropyran-co-nipam-co-acrylic acid hydrogel photoactuators. *Soft Matter* **2013**, *9*, 8754-8760.
16. Florea, L.; Hennart, A.; Diamond, D.; Benito-Lopez, F. Synthesis and characterisation of spiropyran-polymer brushes in micro-capillaries: Towards an integrated optical sensor for continuous flow analysis. *Sensors and Actuators B: Chemical* **2012**, *175*, 92-99.
17. Florea, L.; Diamond, D.; Benito - Lopez, F. Photo - responsive polymeric structures based on spiropyran. *Macromolecular Materials and Engineering* **2012**, *297*, 1148-1159.
18. Florea, L.; Diamond, D.; Benito-Lopez, F. Opto-smart systems in microfluidics. *Research Perspectives on Functional Micro-and Nanoscale Coatings* **2016**, 265.
19. Yuan, J.; Mecerreyes, D.; Antonietti, M. Poly(ionic liquid)s: An update. *Progress in Polymer Science* **2013**, *38*, 1009-1036.
20. Hirao, M.; Ito - Akita, K.; Ohno, H. Polymerization of molten salt monomers having a phenylimidazolium group. *Polymers for Advanced Technologies* **2000**, *11*, 534-538.
21. Hirao, M.; Ito, K.; Ohno, H. Preparation and polymerization of new organic molten salts; n-alkylimidazolium salt derivatives. *Electrochimica Acta* **2000**, *45*, 1291-1294.

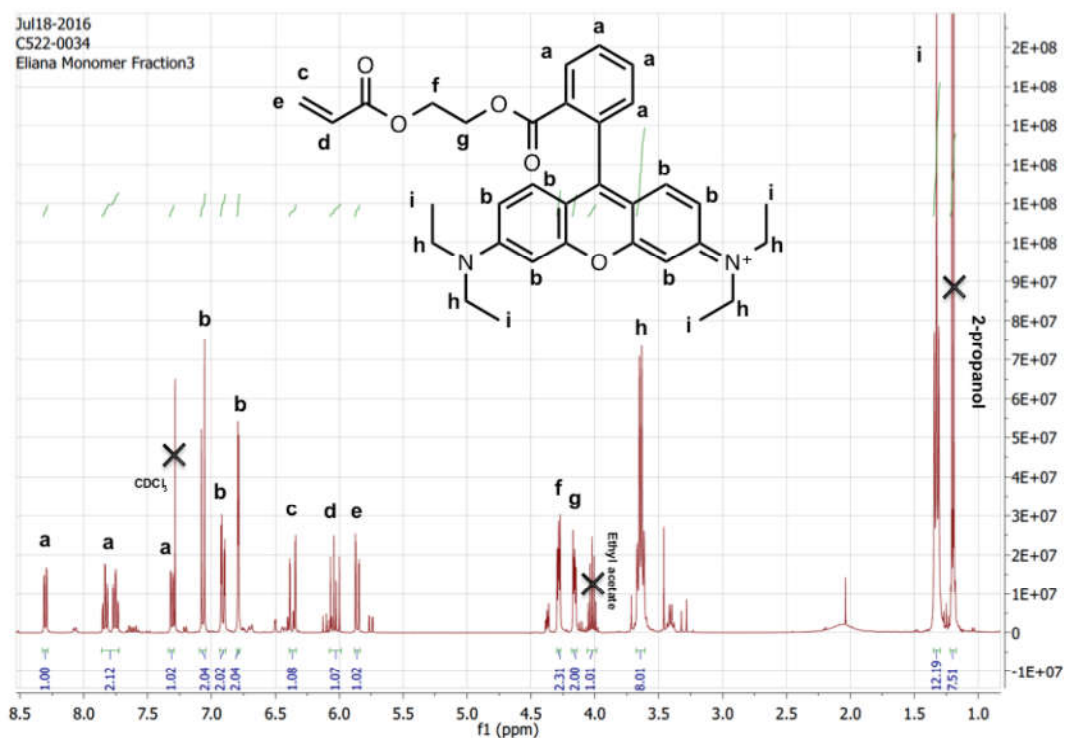
22. Yoshizawa, M.; Ohno, H. Synthesis of molten salt-type polymer brush and effect of brush structure on the ionic conductivity. *Electrochimica Acta* **2001**, *46*, 1723-1728.
23. Vygodskii, Y.S.; Mel'nik, O.A.; Shaplov, A.S.; Lozinskaya, E.I.; Malyshkina, I.A.; Gavrilova, N.D. Synthesis and ionic conductivity of polymer ionic liquids. *Polymer Science Series A* **2007**, *49*, 256-261.
24. Zhao, F.; Meng, Y.; Anderson, J.L. Polymeric ionic liquids as selective coatings for the extraction of esters using solid-phase microextraction. *Journal of Chromatography A* **2008**, *1208*, 1-9.
25. Zhao, Q.; Wajert, J.C.; Anderson, J.L. Polymeric ionic liquids as CO₂ selective sorbent coatings for solid-phase microextraction. *Analytical Chemistry* **2009**, *82*, 707-713.
26. Green, O.; Grubjesic, S.; Lee, S.; Firestone, M.A. The design of polymeric ionic liquids for the preparation of functional materials. *Polymer Reviews* **2009**, *49*, 339-360.
27. Lu, J.; Yan, F.; Texter, J. Advanced applications of ionic liquids in polymer science. *Progress in Polymer Science* **2009**, *34*, 431-448.
28. Mecerreyes, D. Polymeric ionic liquids: Broadening the properties and applications of polyelectrolytes. *Progress in Polymer Science* **2011**, *36*, 1629-1648.
29. Yuan, J.; Antonietti, M. Poly(ionic liquid)s: Polymers expanding classical property profiles. *Polymer* **2011**, *52*.
30. Yuan, J.; Mecerreyes, D.; Antonietti, M. Poly(ionic liquid)s: An update. *Progress in Polymer Science* **2013**.
31. Kohno, Y.; Saita, S.; Men, Y.; Yuan, J.; Ohno, H. Thermoresponsive polyelectrolytes derived from ionic liquids. *Polymer Chemistry* **2015**.
32. Zhao, J.; Shen, X.; Yan, F.; Qiu, L.; Lee, S.; Sun, B. Solvent-free ionic liquid/poly(ionic liquid) electrolytes for quasi-solid-state dye-sensitized solar cells. *Journal of Materials Chemistry* **2011**, *21*, 7326-7330.
33. Balo, L.; Shalu; Gupta, H.; Kumar Singh, V.; Kumar Singh, R. Flexible gel polymer electrolyte based on ionic liquid emimtfsi for rechargeable battery application. *Electrochimica Acta* **2017**, *230*, 123-131.
34. Tudor, A.; Saez, J.; Florea, L.; Benito-Lopez, F.; Diamond, D. Poly(ionic liquid) thermo-responsive hydrogel microfluidic actuators. *Sensors and Actuators B: Chemical* **2017**, *247*, 749-755.
35. Zhang, K.; Feng, X.; Sui, X.; Hempenius, M.A.; Vancso, G.J. Breathing pores on command: Redox-responsive spongy membranes from poly(ferrocenylsilane)s. *Angewandte Chemie International Edition* **2014**, *53*, 13789-13793.
36. Schüler, F.; Kersch, B.; Beckert, F.; Thomann, R.; Mülhaupt, R. Hyperbranched polymeric ionic liquids with onion-like topology as transporters and compartmentalized systems. *Angewandte Chemie International Edition* **2013**, *52*, 455-458.
37. Zhao, Q.; Zhang, P.; Antonietti, M.; Yuan, J. Poly(ionic liquid) complex with spontaneous micro-/mesoporosity: Template-free synthesis and application as catalyst support. *Journal of the American Chemical Society* **2012**, *134*, 11852-11855.
38. Cui, J.; Zhu, W.; Gao, N.; Li, J.; Yang, H.; Jiang, Y.; Seidel, P.; Ravoo, B.J.; Li, G. Inverse opal spheres based on polyionic liquids as functional

- microspheres with tunable optical properties and molecular recognition capabilities. *Angewandte Chemie International Edition* **2014**, *53*, 3844-3848.
39. Zhao, Q.; Heyda, J.; Dzubiella, J.; Täuber, K.; Dunlop, J.W.C.; Yuan, J. Sensing solvents with ultrasensitive porous poly(ionic liquid) actuators. *Advanced Materials* **2015**, *27*, 2913-2917.
 40. Zhao, Q.; Dunlop, J.W.C.; Qiu, X.; Huang, F.; Zhang, Z.; Heyda, J.; Dzubiella, J.; Antonietti, M.; Yuan, J. An instant multi-responsive porous polymer actuator driven by solvent molecule sorption. *Nature Communications* **2014**, *5*, 4293.
 41. Kohno, Y.; Arai, H.; Saita, S.; Ohno, H. Material design of ionic liquids to show temperature-sensitive lcst-type phase transition after mixing with water. *Australian Journal of Chemistry* **2011**, *64*, 1560.
 42. Kohno, Y.; Deguchi, Y.; Ohno, H. Ionic liquid -derived charged polymers to show highly thermoresponsive lcst-type transition with water at desired temperatures. *Chemical Communications* **2012**, *48*, 11883-11885.
 43. Maeda, Y.; Higuchi, T.; Ikeda, I. Ftir spectroscopic and calorimetric studies of the phase transitions of n-isopropylacrylamide copolymers in water. *Langmuir* **2001**, *17*, 7535-7539.
 44. Tudor, A.; Florea, L.; Gallagher, S.; Burns, J.; Diamond, D. Poly(ionic liquid) semi-interpenetrating network multi-responsive hydrogels. *Sensors* **2016**, *16*, 219.

Appendix Chapter 5

The synthesis of the acrylated Rhodamine B derivative

The acrylated derivative of Rhodamine B (Acryl-Rhod B) was synthesised using a modified procedure from that previously reported method in *J. Mater. Chem. B*, 2015,3, 440-448. Briefly, a solution containing 20 mmol *N,N'*-Dicyclohexylcarbodiimide (DCC) (Sigma-Aldrich) and 2 mmol 4-(dimethylamino)pyridine (DMAP) (Sigma-Aldrich) dissolved in DCM (75 mL) was added dropwise to a solution composed of 5 mmol of Rhodamine B and 20 mmol 2-hydroxyethyl acrylate in DCM (25 mL). The reaction was stirred under nitrogen at room temperature overnight. The white byproduct was then removed by vacuum filtration. The reaction mixture was concentrated *in vacuo* and purified by column chromatography on silica, using 1:9 (isopropanol: ethyl acetate). The product was collected and analysed by ^1H NMR on a 400 MHz Bruker NMR spectrometer (Figure S1).



^1H NMR (CDCl₃, 400MHz): 8.30 (1H, d, CH - a), 7.80 (2H, m, CH - a), 7.29 (1H, d, CH - a), 7.07 (2H, d, CH - b), 6.92 (2H, d, CH - b), 6.79 (2H, d, CH - b), 6.35 (1H, dd, CH₂ - c), 6.05 (1H, dd, CH₂ - d), 5.86 (1H, dd, CH₂ - e), 4.28 (2H, dd, CH₂ - f), 4.16 (2H, m, CH₂ - g), 3.64 (8H, dd, CH₂ - h), 1.32 (12H, t, CH₃ - h)

Figure A.5.1 ^1H NMR of Acryl-Rhod B in deuterated chloroform.

Spectral measurements

Fluorescence spectroscopy for the Acryl-Rhod B solution (10^{-6} M in Phosphate buffer) was performed using a JASCO Spectrofluorometer FP-8300 (Figure S2).

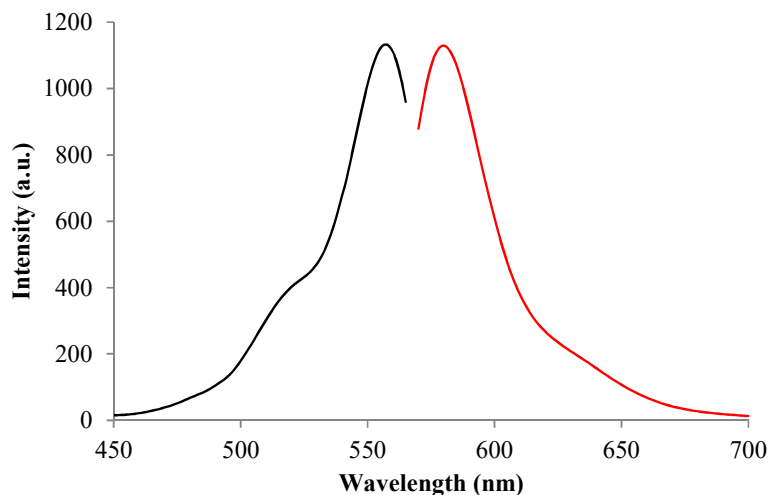


Figure A.5.2 Excitation and emission spectra of Acryl-Rhod B solution (10^{-6} M in pH 7.4 phosphate buffer solution), where the excitation wavelength was 555 nm and the corresponding emission was at 578 nm. Fluorometer parameters; medium sensitivity; 2.5 nm bandwidth.

DLW Live-Observation

The .stl file comprised an array of pillars, wherein each pillar is a cylinder of 20 μm in diameter and 40 μm in height.

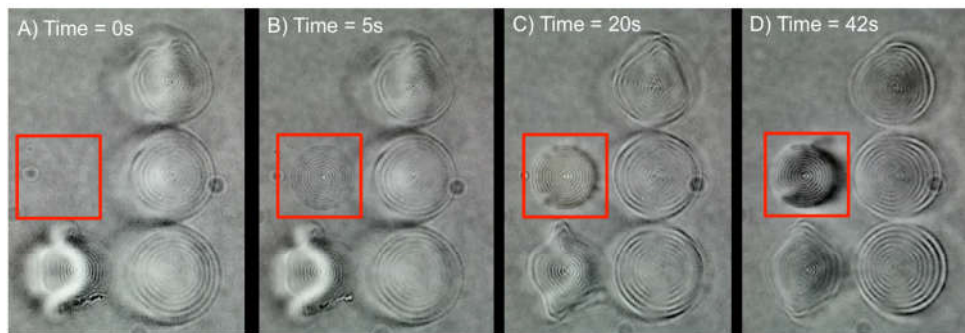


Figure A.5.3 Selection of images following the printing of one cylinder (marked) in an array. All cylinders are 20 μm in diameter and 40 μm in height; A) Image taken before the printing

of the marked cylinder; B) image taken after 5 s of DLW: the first concentric horizontal circles of the marked cylinder are printed; C) image taken after 20s of printing and D) image taken after the marked cylinder has been fully printed.

It can be observed that at 5mol% concentration of the crosslinker (Table 1), the PILs structures swell significantly in the polymerisation cocktail (Figure A.5.3 and Figure A.5.4), resulting in pillars that have a diameter up to 40 μm , in comparison with the .stl file where the pillar diameter was fixed at 20 μm . However, despite this significant swelling, the structures maintain their geometry.

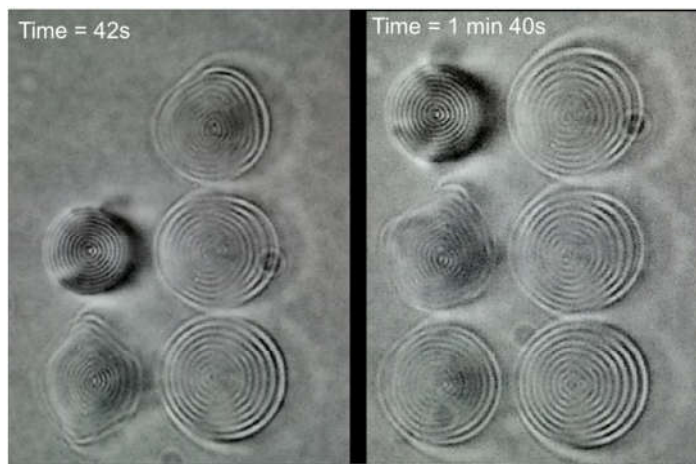


Figure A.5.4 Selection of images showing the swelling of the PIL pillars in the polymerisation cocktail during the printing process.

Structure Design.

In the fabrication process, arrays of 3x3, 4x4, and 5x5, of cylinders (40 μm in height, 20 μm in diameter) (Figure A.5.5A) and spirals (50 μm in height, 20 μm in diameter) (Figure A.5.5B and Figure A.5.6), respectively, were fabricated by DLW using cocktail formulations tabulated in Table 1 (Experimental section). The writing parameters were; slicing distance 0.2 μm ;; hatching distance 1 μm ;; contour count: 8; contour distance: 1 μm ;; hatching angle offset: 1.

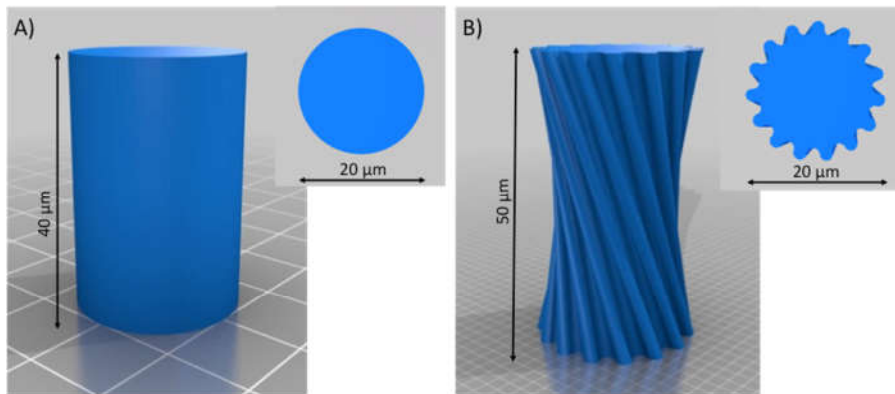


Figure A.5.5 Side and top views of the A) cylinder and B) spiral structures.

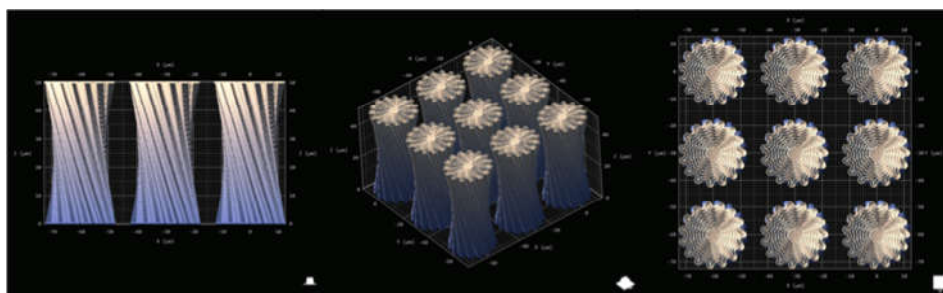


Figure A.5.6 3D preview of the 3x3 array of spiral structures from different perspectives.

Structure development. Following DLW, the structures are visible in the polymerisation cocktail (Figure S7):

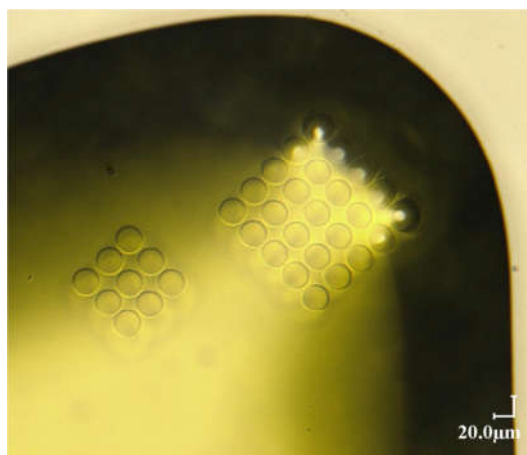


Figure A.5.7 3D microscopy image of micro-pillars array fabricated by 2-PP in PILs using cocktail formulations described in Table 1, before washing of the unpolymerised photoresist. The focus is on the top of the structures.

Following DLW, the structures are carefully washed with acetone as indicated in the experimental section. It was observed that if the glass substrate has not been chemically pre-treated to allow for covalent attachment of the structures to the substrate, then delamination of the structures arises during washing (Figure S8) and the micro structures move location.

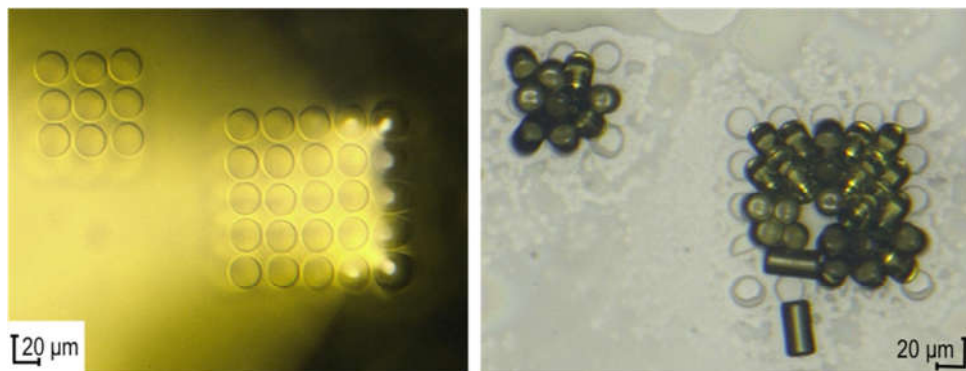


Figure A.5.8 3D microscopy Image of micro-pillars array fabricated by 2-PP in PILs using cocktail formulations described in Table 5.1, before (left) and after (right) washing of the unpolymerised photoresist. Structure delamination and movement occurs during washing.

However, in the case when the glass slides were treated with 3-(trimethoxysilyl) propyl methacrylate, good adhesion of the structures to the substrate was observed during washing.

Another example of free-standing Structures:

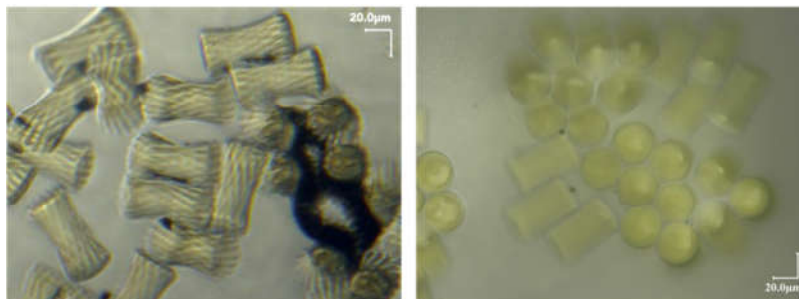


Figure A.5.9 3D microscopy images of micro-spirals (left) and cylinder (right) array fabricated by 2-PP in PILs using cocktail formulations described in Table 1, in DI water.

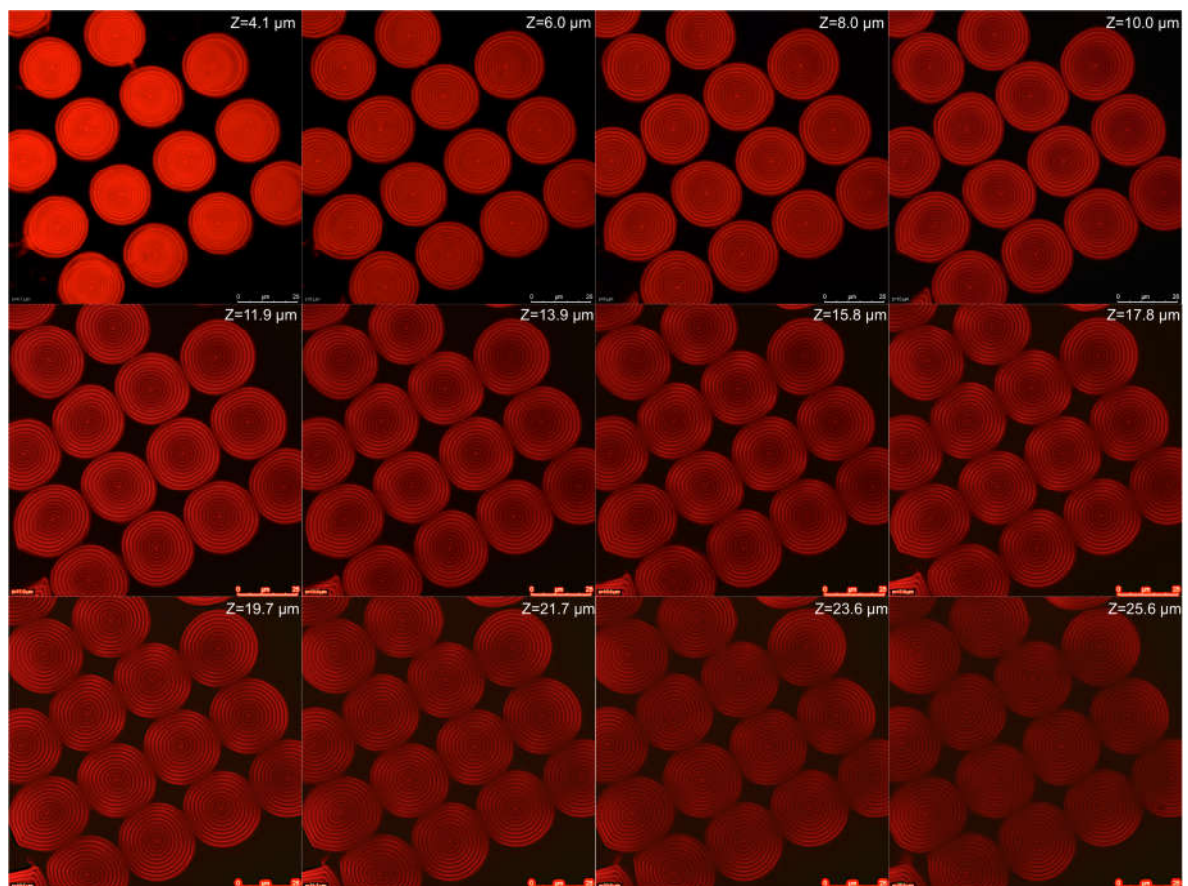


Figure A.5.10 Confocal microscopy images showing z slicing through a micro-cylinder array fabricated by 2-PP in PILs using cocktail formulations described in Table 1, in DI water. The swelling of the structures increases as we move away from the surface, as the structures are restricted by the covalent immobilisation to the glass surface.

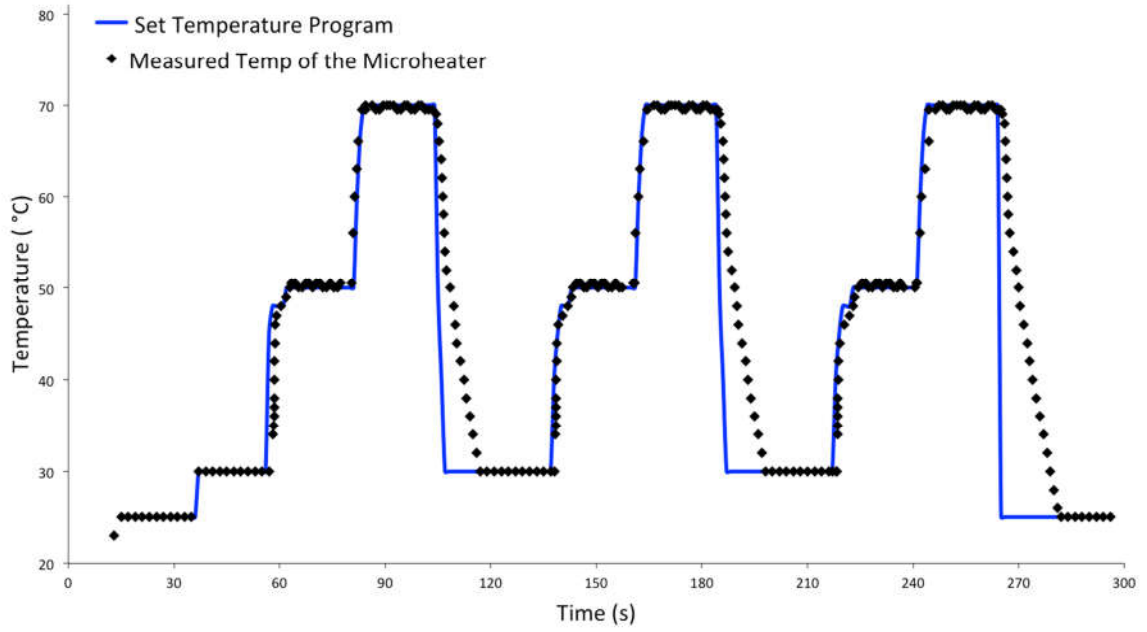


Figure A.5.11 Set temperature program (blue) starting with 20s at 25°C (initial) followed by 3 cycles composed of the following steps: 20s at 30°C (step 1), 20s at 50°C (step 2) and 20s at 70°C (step 3), and ending with 20s at 30°C (final) and measured temperature on the microheater (black).

Chapter 6: Superabsorbent Biocompatible poly(Ionic Liquid) Crosslinked Hydrogels

6.1 Abstract

6.2. Introduction

6.2.1 Materials and Reagents

6.2.2 Synthesis of the cholinium sulfopropyl acrylate ionic liquid monomer

6.2.3 Synthesis of the cholinium PIL hydrogels

6.3. Results and Discussion

6.3.1 Thermal Characterization of the PIL hydrogels

6.4. Problems addressed by the invention

6.5. Existing solutions to the problem(s) that you are aware and consider to be closest to the new invention

6.6. Key aspects of the invention which make it novel and demonstrate its advantages over the existing solutions

6.7. Potential commercial application (*products, processes, services, or research tools*) based on the invention.

Chapter 6

Superabsorbent Biocompatible poly(Ionic Liquid) Crosslinked Hydrogels^{*}

^{*}Submitted for a patent application with the United States Patent and Trade Office as a provisional filing, application number 62405314.

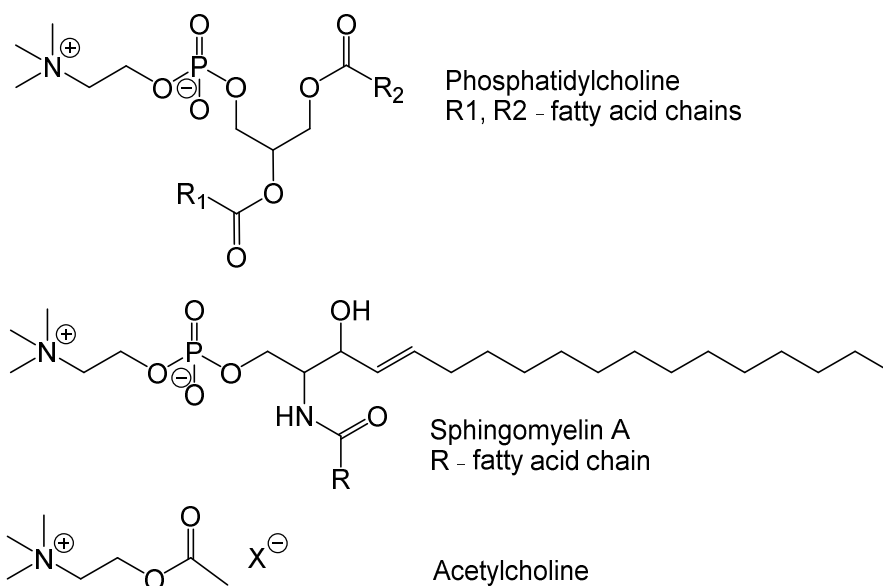
6.1 Abstract

Superabsorbent polymers are defined as polymers that are able to absorb between 10 and 1000 times their original weight when immersed in water or water-based solutions. There are two types of superabsorbent materials, namely superabsorbent polymers and superporous hydrogels. Both of these materials rely on an equilibrium between diffusion and capillary forces to absorb water. In superabsorbent polymers, the main driving force for absorption is diffusion, which makes the process of swelling in these materials dependent on their size, i.e. in their applications they are mainly used as fine powders. In comparison, superporous hydrogels rely on capillary forces for their absorption mechanism, which translates into an independent relationship between their size and rate of aqueous solution absorption. Herein we describe the synthesis of a superabsorbent biocompatible crosslinked poly(ionic liquid) hydrogel material. The monomer used in this study is (2-hydroxyethyl)trimethylammonium (also known as cholinium) sulfopropylacrylate, which when polymerized together with a poly(ethylene glycol) diacrylate crosslinker forms a hydrogel capable of absorbing ~35 times its own weight when immersed in DI water. This behaviour was characterized using thermogravimetric analysis. Following this, based on the fact that choline is a ubiquitous biomolecule, tests were done on L929 mouse fibroblast cells to determine if the resulting hydrogels are biocompatible.

6.2 Introduction

In 1850, a pharmacist named Theodore Gobley from Paris discovered a molecule that he named 'lecithine'. The origin of this word comes from the Greek word 'lekithos' which means egg yolk. He chose this word, because the molecule he isolated came from carp fish eggs and brain tissue [1]. Following this discovery, in 1862, Adolph Strecker discovers a new nitrogen containing compound by heating up lecithin extracted from pig and ox bile. He names it 'choline' based on the Greek word 'chole', which means bile [1]. More than a decade later, in 1874, Theodore Gobley, chemically characterizes lecithin and realizes that the compound is actually phosphatidylcholine. This molecule together with lysophosphatidylcholine, choline plasmalogen and sphingomyelin are essential components found in the structure of all

cell membranes (Scheme 4.7) [2]. Choline also plays an important role in the synthesis of acetylcholine, which is an important neurotransmitter molecule in humans, and in the methyl group metabolism, by participating in the reduction of homocysteine [2].



Scheme 6.1. Chemical structures of the most important chemical derivatives of choline: Phosphatidylcholine, Sphingomyelin and Acetylcholine (X = undefined anion).

Continuous studies on the role of choline in the human body determined that it can be classified as an essential micronutrient [1,2]. Its absence from a person's diet can lead to muscle and liver damage. This damage is reversed when choline is administered at normal levels [2]. Choline also plays a very important role in the development of human foetuses, by ensuring that the risk of neural tube damage is minimized [3], and it also positively influences memory development [2].

Taking into account all these important roles that choline fulfils together with the fact that it is an asymmetric quaternary tetraalkylammonium cation make choline a remarkable prospect for being used as a building block for biocompatible ionic liquids (ILs).

ILs are salts that have their melting point at a temperature lower than 100 °C [4]. They possess numerous properties including negligible vapour pressure, high chemical and thermal stability, ionic conductivity, excellent dissolution properties and highly tunable structures [4-10].

Due to the massive and ever-growing library of ILs, ecotoxicological data for most of them is unavailable. One way to circumvent this problem is to design ILs using known naturally occurring precursors. This increases the chance of synthesizing an IL that would be biocompatible.

Biocompatibility research has been performed on several choline derived ILs to assess their toxicity[4-7,9-15] and their potential applications, including for batteries, catalysis, electrodeposition and smart-materials [8,16-24]. These toxicity studies underline the fact that the biggest contribution towards ensuring biocompatibility comes from the IL's cation. If the cation remains the same, the length of the anion's carbon chain will be the determining factor, with shorter chains being more biocompatible [5-7]. In the studies previously mentioned, it was found that choline ILs were less toxic than imidazolium ILs [6,13] and pyrrolidinium ILs [13].

The next step that can be taken to further enhance the versatility of choline ILs is to use choline ILs as precursor IL monomers (ILMs) used in the synthesis of poly(ionic liquid)s (PILs). ILMs are ILs that feature a polymerizable group in either the cation, the anion, or both. By synthesizing PILs, part of the typical properties of ILs are moved towards polymeric materials, including high chemical and thermal stability, ionic conductivity, and highly tunable structures [25-27]. A summary search of cholinium poly(ionic liquid) articles on the Thompson-Reuters webofscience.com database returns only three articles published using these materials [28-30]. Considering this fact and taking into account the extensive possibilities of synthesizing novel cholinium based ILMs, this research direction offers very exciting possibilities towards developing novel compounds with a wide application spectrum.

The aim of this study is to synthesize a cholinium ionic liquid monomer that features a polymerizable group in its anion. This is in direct contrast with the cholinium PILs that were described in the aforementioned papers, which feature the polymerizable group attached on the cholinium moiety. The current study focuses on the synthesis of the ionic liquid monomer, its characterization by ¹H-NMR spectroscopy, followed by the synthesis of the crosslinked cholinium PILs and their thermal characterization using thermogravimetric analysis. Investigations on the hydration capabilities of the resulting cholinium crosslinked PIL were also performed.

6.3 Experimental

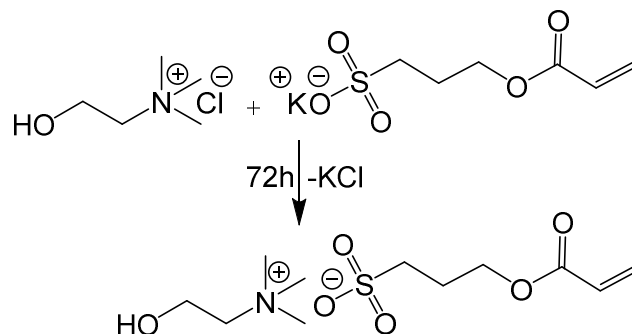
6.3.1 Materials

Choline chloride $\geq 98\%$ (ChoCl, BioReagent, suitable for cell culture, suitable for insect cell culture), Potassium 3-sulfopropyl acrylate (KSPA), polyethylene glycol diacrylate ($M_w \sim 320$, 100 ppm MEHQ as inhibitor) (PEG256), 2-Hydroxy-2-methylpropiophenone 97% (HMPP), ethanol (Chormasolv[®], HPLC grade, $\geq 99.8\%$) were bought from Sigma Aldrich[®] and used as received. Deionized water ($18.2 \text{ M}\Omega \cdot \text{cm}^{-1}$) (DI water) was purified using a Merck Millipore Milli-Q Water Purification System.

6.3.2 Synthesis of the cholinium sulfopropyl acrylate ionic liquid monomer

The synthesis of the cholinium sulfopropyl acrylate (ChoSPA) was performed by dissolving 7.5 g of ChoCl together with 16.2 g of KSPA (1.3 molar equivalents) in 20 mL of DI water. The mixture was magnetically stirred at room temperature for 5 days. Following this, the reaction mixture was poured in a beaker and the reaction mixture was moved to a vacuum oven which was kept at 45 °C and 200 mBar for 32 h. This resulted in a crystalline deposit forming at the bottom of the beaker. To finalize the crystallization process, the beaker was kept for further 48 h in a vacuum oven at normal conditions of temperature and pressure. This resulted in a crystalline product formed at the bottom of the beaker. To extract the ChoSPA, absolute ethanol was poured in the beaker followed by magnetic stirring and gravity filtration of the resulting heterogeneous mixture. The resulting solution was concentrated by rotary evaporation at 40 °C, followed by complete overnight drying using a high vacuum line (0.5 mBar). The resulting product was obtained with a yield of $\sim 60\%$ and had a translucent white colour and was viscous.

ChoSPA – ¹H-NMR, δ_H (400 MHz): 1.98-2.05 (m, 2H, CH₂), 2.88-2.92 (p, 2H, CH₂), 3.08 (s, 9H, CH₃), 3.38-3.41 (p, 2H, CH₂), 3.91-3.95 (m, 2H, CH₂), 4.15-4.19 (t, 2H, CH₂), 5.84-5.87 (dd, 1H, CH), 6.05-6.12 (dd, 1H, CH), 6.29-6.34 (dd, 1H, CH).



Scheme 6.2. Reaction scheme for the synthesis of ChoSPA.

6.3.3 Synthesis of the cholinium PIL hydrogels

The monomer cocktail that was used for the synthesis of the cholinium hydrogels consisted of 0.238 g of ChoSPA (800 μmol s) that were mixed with 0.238 g of ethanol:DI water 1:1 mixture, 3.2 μL of HMPP (20 μmol s) and 6 μL of PEG256 (16 μmol s), respectively. The resulting monomer mixture was mechanically stirred until every component was completely dissolved. Following this, ~ 5 μL aliquots of monomer mixture were pipetted in circular poly(dimethylsiloxane) moulds with a diameter of 3 mm and a depth of 1 mm. The polymerization was performed in a UVP CL-1000 Ultraviolet Crosslinker curing chamber using a wavelength of 365nm at a power level of $3.5 \text{ mW} \cdot \text{cm}^{-2}$ for 30 minutes.

6.4 Results and discussion

6.4.1 Thermal characterization of the cholinium hydrogels

The resulting circular polymers were immersed in DI water and left overnight to swell. This ensured that they reached their maximum swelling capacity (Fig. 4.8).



Figure 6.1. Comparison between the sizes of the ChoSPA hydrogel before swelling (A), swelling in DI water for 12h (B) and after dehydration by drying at room temperature (C), respectively.

The thermal characterization of the hydrogel was performed to determine the amount of DI water that can be absorbed by the ionogel. For this, each gel presented in Figure 4.8 was analysed using a TA Instruments Q50 Thermogravimetric Analysis instrument. The temperature program used consisted of a temperature ramp between room temperature and 500 °C in 10 °C·min⁻¹. The measurement was performed in a N₂ atmosphere at a flow rate of 50 ml·min⁻¹.

The first hydrogel to get analysed was the type A hydrogel. The sample had a weight of 2.44 mg. The analysis was performed to determine the amount of solvent still present inside the hydrogel right after polymerisation and to determine its decomposition temperature, respectively. In Figure 4.9 the type A hydrogel starts eliminating water/solvent as soon as the temperature is raised from room temperature. This trend continues up to ~200 °C when all the water has been removed. This corresponds to a weight loss of 12.97% (0.3164 mg) of the original weight of the sample. At this point the weight of the hydrogel starts plateauing until ~250 °C when it starts dropping, due to the decomposition phase starting. The onset temperature of this process is at 350.49 °C and it continues at the same rate up to ~375 °C, where it starts slowing down and continues until the final temperature of 500 °C. At this point, a further 66.84% (1.63 mg) of the initial weight is lost. This leaves the hydrogel at ~20% of its original weight. This represents the undecomposed residue of the hydrogel at 500 °C.

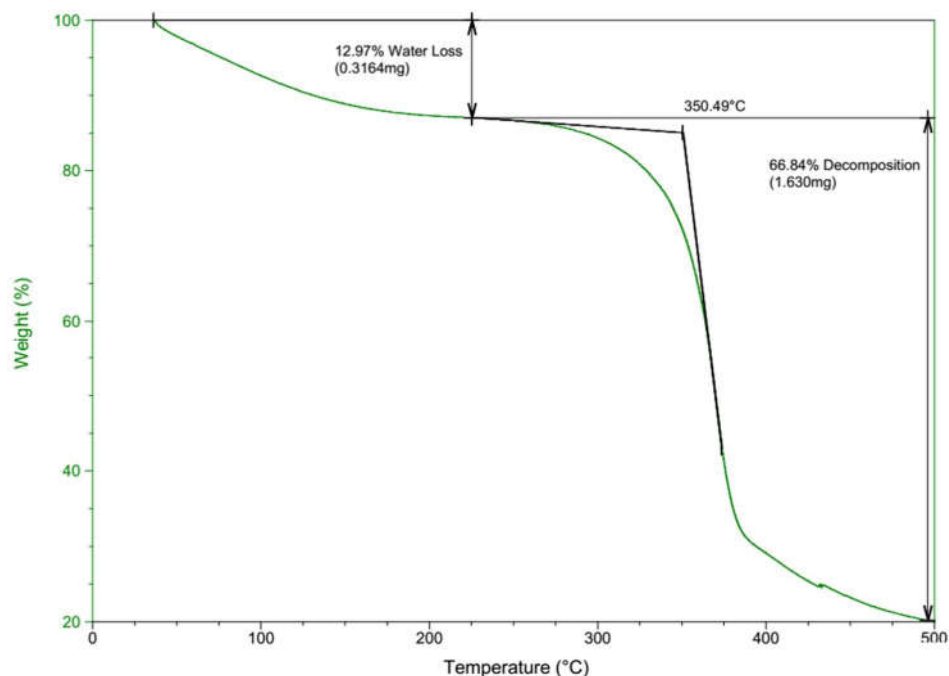


Figure 6.2. Thermogravimetric curve showing the behaviour of type A hydrogels (right after polymerisation).

The second hydrogel to get analysed was the type B hydrogel (after complete swelling in DI water for 12h). In this case, the initial weight of sample was 28.71 mg. Like in the case of the type A hydrogel, the weight loss due to water leaving the hydrogel starts immediately after the temperature starts increasing and it continues up to ~160 °C. At this point 96.91% (27.82 mg) of the hydrogel's mass is lost. From this temperature up to ~320 °C the hydrogel's mass doesn't suffer any notable change. At ~340 °C the decomposition phase begins. During this process, the hydrogel's mass continues to drop by 2.60% (0.75 mg) until a temperature of ~390 °C is reached and after that it starts plateauing. This signals the end of the decomposition phase.

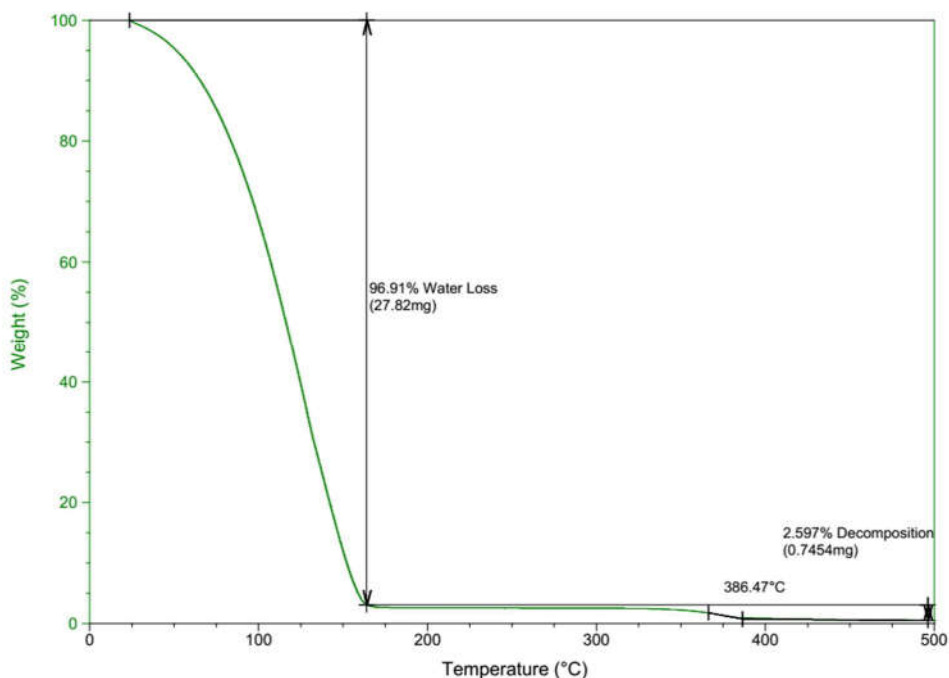


Figure 6.3. Thermogravimetric curve showing the behaviour of type B hydrogels (after hydration in DI water for 12h)

The final hydrogel to get analysed was the type C hydrogel, which has a very similar TGA curve to the type A hydrogel. The weight of the type C hydrogel samples was 2.08 mg. The weight loss due to the hydration water evaporating from the hydrogel starts from room temperature and continues until close to ~ 200 °C. The weight loss during this phase is 14.47%, which is equal to 0.30 mg of water lost. Following this, there is negligible weight loss until ~ 280 °C, at which point the decomposition phase starts. The onset temperature for this process is 349.05 °C, which is very close to the onset temperature seen for both type B hydrogels and for type A hydrogels. During this phase, the hydrogel loses 69% of its weight, which is equal to 1.44 mg of its original weight. This process starts slowing down after ~ 375 °C, but continues until 500 °C where it plateaus, and just like in the case of the type A hydrogel, 20% of the initial weight of the hydrogel is left. This represents the undecomposed part of the hydrogel. In all cases, the hydrogels started losing water as soon as the temperature was raised above room temperature. Also, their decomposition onset temperatures were very similar. Based on this, it can be concluded that in all cases – freshly polymerized, hydrated and dehydrated, the hydrogels maintain their thermal characteristics.

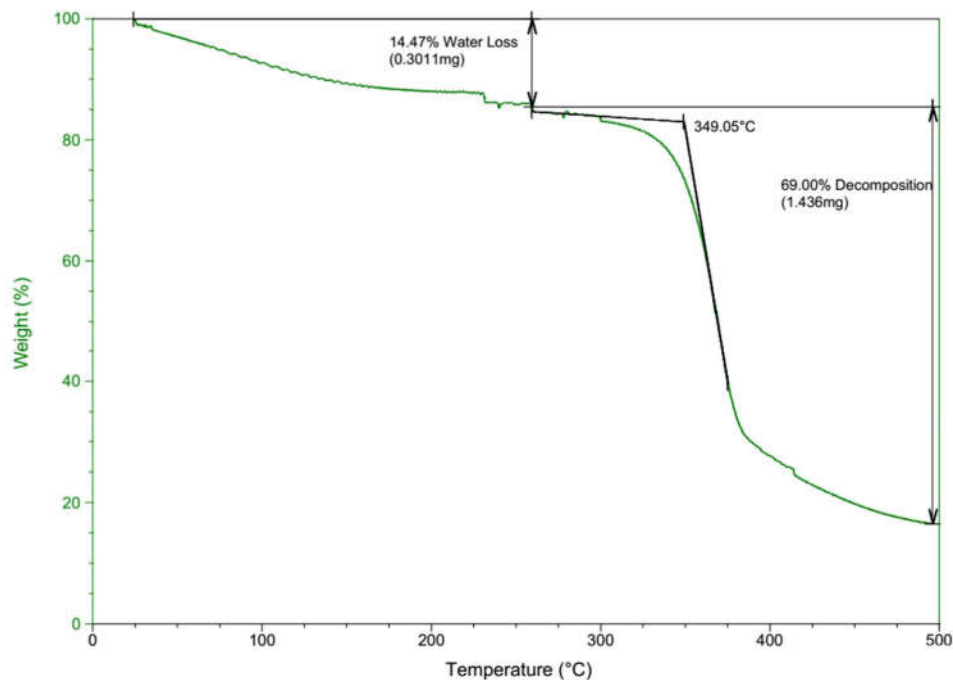


Figure 6.4. Thermogravimetric curve showing the behaviour of type C hydrogels (dehydration)

The hydrogels' ability to absorb such large quantities of water compared with its weight should be emphasized, because it represents an important factor in using these ionogels as a biocompatible polymeric matrices cell culturing media.

A water uptake of ~3250% compared to the initial polymer weight can be calculated based on the results obtained in graph B for the swollen hydrogels. This is performed by dividing the mass of the hydration water to the mass of the hydrogel before the decomposition step.

6.5 Problems addressed by the invention

This invention creates novel hydrophilic poly(ionic liquid)s, that could be further used to create cross-linked hydrogel type materials that incorporate large quantities of water (~97% of the mass of the hydrogel is water). This hydrogel (and similar derivatives) is biocompatible due to the biocompatibility of the cholinium cation (Table 1) and also due to the large quantities of water they can absorb, similar to other materials found in nature. Possible applications for this material include: passive flow control in printed microfluidic devices and in wearable microfluidic

devices, incorporation in burn dressings to help keep the tissue hydrated, wound dressings, and hydrated scaffolds for cell culture, respectively.

6.6. Existing solutions to the problem(s) that you are aware of and consider to the new invention

Several hydrogel materials based on polyacrylates (e.g. poly-2-hydroxyethylmethacrylate (PHEMA), poly(acrylic acid), polyacrylamide, poly(acrylic acid-co-acrylamide)), other polymers (e.g. poly(vinyl alcohol), poly(vinyl-pyrrolidone), poly(ethylene glycol), poly(ethylene oxide), poly(propylene fumarate-co-ethylene glycol)), some polysaccharides and polypeptides or naturally derived polymers (e.g. agarose, alginate, chitosan, collagen, fibrin, gelatin, hyaluronic acid) are currently used for the production of biocompatible hydrogel materials that can absorb large quantities of water. These hydrogel materials are widely used in particular for biomedical applications such as materials for contact lenses, wound dressing, drug delivery systems, scaffolds for tissue engineering or hygiene products (e.g. disposable diapers, sanitary napkins, etc).

The proposed invention opens up a new class of hydrogel materials based on biocompatible poly(ionic liquids). The advantages of poly(ionic liquids) versus classic polymers is that they are liquid at room temperature, meaning that, unlike the above materials, they are not subject to cracking and physical degradation in the dry state.

6.7. Key aspects of the invention which make it novel and demonstrate its advantages of the existing solutions

This invention describes for the first time an anionic ionic liquid monomer (polymerisable group as part of the anion) that incorporates a cholinium cation. The invention further describes the polymerisation of this ionic liquid monomer and the generation of a crosslinked matrix that can incorporate large amount of water with fast absorption kinetics. A summary search of cholinium poly(ionic liquid) articles on the Thompson-Reuters webofscience.com database returns only three articles published using cholinium based ions. The current invention is distinct from the cholinium PILs that were described in the aforementioned papers, which feature the

polymerizable group attached on the cholinium moiety. This approach is therefore not obvious, similar or incremental to the existing cholinium based poly(ionic liquids) present in the literature.

6.8. Potential commercial application (*products, processes, services, or research tools*) based on the invention

It is expected that the current invention would have numerous applications including in the biomedical field (e.g. wound dressing, contact lenses materials, super absorbent materials, tissue engineering) and microfluidic field (passive pumps for microfluidic devices).

6.9. References

1. Zeisel, S.H. A brief history of choline. *Annals of Nutrition and Metabolism* **2012**, *61*, 254-258.
2. Zeisel, S.H.; Costa, K.A. Choline: An essential nutrient for public health. *Nutrition Reviews* **2009**, *67*, 615-623.
3. Shaw, G.M.; Carmichael, S.L.; Yang, W.; Selvin, S.; Schaffer, D.M. Periconceptional dietary intake of choline and betaine and neural tube defects in offspring. *American journal of epidemiology* **2004**, *160*, 102-109.
4. Vrikkis, R.M.; Fraser, K.J.; Fujita, K.; Macfarlane, D.R.; Elliott, G.D. Biocompatible ionic liquids: A new approach for stabilizing proteins in liquid formulation. *Journal of biomechanical engineering* **2009**, *131*, 74514.
5. Dias, A.M.A.; Cortez, A.R.; Barsan, M.M.; Santos, J.B.; Brett, C.M.A.; de Sousa, H.C. Development of greener multi-responsive chitosan biomaterials doped with biocompatible ammonium ionic liquids. *ACS Sustainable Chemistry & Engineering* **2013**, *1*, 14801492.
6. Gouveia, W.; Jorge, T.F.; Martins, S.; Meireles, M.; Carolino, M.; Cruz, C.; Almeida, T.V.; Araújo, M.E.M. Toxicity of ionic liquids prepared from biomaterials. *Chemosphere* **2014**, *104*, 51-56.
7. Petkovic, M.; Ferguson, J.L.; Gunaratne, N.H.Q.; Ferreira, R.; Leitão, M.C.; Seddon, K.R.; Rebelo, L.N.; Pereira, C. Novel biocompatible cholinium-based ionic liquids—toxicity and biodegradability. *Green Chemistry* **2010**, *12*, 643-649.
8. Quental, M.V.; Caban, M.; Pereira, M.M.; Stepnowski, P.; Coutinho, J.A.P.; Freire, M.G. Enhanced extraction of proteins using cholinium-based ionic liquids as phase-forming components of aqueous biphasic systems. *Biotechnology Journal* **2015**, *10*, 1457-1466.
9. Tao, D.-J.; Cheng, Z.; Chen, F.-F.; Li, Z.-M.; Hu, N.; Chen, X.-S. Synthesis and thermophysical properties of biocompatible cholinium-based amino acid ionic liquids. *Journal of Chemical & Engineering Data* **2013**, *58*, 1542-1548.

10. Weaver, K.D.; Kim, H.; Sun, J.; MacFarlane, D.R.; Elliott, G.D. Cyto-toxicity and biocompatibility of a family of choline phosphate ionic liquids designed for pharmaceutical applications. *Green Chemistry* **2010**, *12*, 507-513.
11. Deive, F.J.; Ruivo, D.; Rodrigues, J.V.; Gomes, C.M.; Sanromán, Á.M.; Rebelo, L.N.; Esperança, J.M.S.S.; Rodríguez, A. On the hunt for truly biocompatible ionic liquids for lipase-catalyzed reactions. *RSC Advances* **2014**, *5*, 3386-3389.
12. Liu, L.; Hu, Y.; Wen, P.; Li, N.; Zong, M.; Ou-Yang, B.; Wu, H. Evaluating the effects of biocompatible cholinium ionic liquids on microbial lipid production by trichosporon fermentans. *Biotechnology for Biofuels* **2015**, *8*, 1-9.
13. Rebros, M.; Gunaratne, H.Q.; Ferguson, J.; Seddon, K.R.; Stephens, G. A high throughput screen to test the biocompatibility of water-miscible ionic liquids. *Green Chemistry* **2009**, *11*, 402-408.
14. Rengstl, D.; Kraus, B.; Vorst, M.; Elliott, G.D.; Kunz, W. Effect of choline carboxylate ionic liquids on biological membranes. *Colloids and Surfaces B: Biointerfaces* **2014**, *123*, 575-581.
15. Taha, M.; Almeida, M.R.; Silva, F.A.; Domingues, P.; Ventura, S.P.M.; Coutinho, J.A.P.; Freire, M.G. Novel biocompatible and self-buffering ionic liquids for biopharmaceutical applications. *Chemistry - A European Journal* **2015**, *21*, 4781-4788.
16. Cojocar, A.; Mares, M.; Prioteasa, P.; Anicai, L.; Visan, T. Study of electrode processes and deposition of cobalt thin films from ionic liquid analogues based on choline chloride. *Journal of Solid State Electrochemistry* **2015**, *19*, 1001-1014.
17. Correia, P.B. Pharmaceutical product useful for e.G. Eliminating antibiotic resistant bacteria, and treating cancer, comprises ionic liquid with anions based on e.G. Penicillin, ampicillin and meticillin, and cations based on e.G. Cetylpyridinium. US2015174145-A1, US2015174145-A1 25 Jun 2015 A61K-031/66 201551.
18. Costa, A.J.L.; Soromenho, M.R.C.; Shimizu, K.; Esperança, J.M.S.S.; Lopes, J.N.; Rebelo, L.N. Unusual lct-type behaviour found in binary mixtures of choline-based ionic liquids with ethers. *RSC Advances* **2013**, *3*, 10262-10271.
19. Jia, X.; Yang, Y.; Wang, C.; Zhao, C.; Vijayaraghavan, R.; MacFarlane, D.R.; Forsyth, M.; Wallace, G.G. Biocompatible ionic liquid-biopolymer electrolyte-enabled thin and compact magnesium-air batteries. *ACS Applied Materials & Interfaces* **2014**, *6*, 21110-21117.
20. Kobayashi, T.; Yoshino, M.; Miyagawa, Y.; Adachi, S. Production of 5-hydroxymethylfurfural in a eutectic mixture of citric acid and choline chloride and its extractive recovery. *Separation and Purification Technology* **2015**, *155*, 26-31.
21. Lopes, J.M.; Paninho, A.B.; Mólho, M.F.; Nunes, A.; Rocha, A.; Lourenço, N.; Najdanovic-Visak, V. Biocompatible choline based ionic salts: Solubility in short-chain alcohols. *The Journal of Chemical Thermodynamics* **2013**, *67*, 99-105.
22. Peng, H.; Sun, S.; Hu, Y.; Xing, R.; Fang, D. Clean procedure for the synthesis of α -aminophosphonates catalyzed by choline-based ionic liquid. *Heteroatom Chemistry* **2015**, *26*, 215-223.
23. Zakrewsky, M.; Mitragotri, S.; Fox, D.T.; Koppisch, A.; Del Sesto, R.; Lovejoy, K. Liquid transdermal composition, e.G. Used for treating skin

- bacterial infection and skin disease, comprises ionic drug, and ionic liquid including anionic component, e.G. Geraniol, and a cationic component, e.G. Choline. WO2015066647-A2; WO2015066647-A3; WO2015066647-A9, WO2015066647-A2 07 May 2015 A61K-045/08 201535.
24. Zhu, A.; Bai, S.; Li, L.; Wang, M.; Wang, J. Choline hydroxide: An efficient and biocompatible basic catalyst for the synthesis of biscoumarins under mild conditions. *Catalysis Letters* **2015**, *145*, 1089-1093.
 25. Mecerreyes, D. Polymeric ionic liquids: Broadening the properties and applications of polyelectrolytes. *Progress in Polymer Science* **2011**, *36*, 1629-1648.
 26. Koebe, M.; Drechsler, M.; Weber, J.; Yuan, J. Crosslinked poly(ionic liquid) nanoparticles: Inner structure, size, and morphology. *Macromolecular Rapid Communications* **2012**, *33*, 646-651.
 27. Yuan, J.; Mecerreyes, D.; Antonietti, M. Poly(ionic liquid)s: An update. *Progress in Polymer Science* **2013**, *38*, 1009-1036.
 28. Isik, M.; Sardon, H.; Saenz, M.; Mecerreyes, D. New amphiphilic block copolymers from lactic acid and cholinium building units. *RSC Advances* **2014**, *4*, 53407-53410.
 29. Isik, M.; Gracia, R.; Kollnus, L.C.; Tome, L.C.; Marrucho, I.M.; Mecerreyes, D. Cholinium lactate methacrylate: Ionic liquid monomer for cellulose composites and biocompatible ion gels. *Macromolecular Symposia* **2014**, *342*, 21-24.
 30. Isik, M.; Lonjaret, T.; Sardon, H.; Marcilla, R.; Herve, T.; Malliaras, G.G.; Ismailova, E.; Mecerreyes, D. Cholinium-based ion gels as solid electrolytes for long-term cutaneous electrophysiology. *Journal of Materials Chemistry C* **2015**, *3*, 8942-8948.

Chapter 7: Driving Flow in Microfluidic Paper-Based Analytical Devices with a Cholinium Based Poly(Ionic Liquid) Hydrogel

7.1 Abstract

7.2 Introduction

7.3 Experimental

7.3.1 Materials

7.3.2 μ Pad fabrication

7.3.3 Synthesis of the cholinium sulfopropyl acrylate ionic liquid monomer

7.3.4 Synthesis of the cholinium PIL hydrogels

7.3.5 Thermal characterization method of the cholinium hydrogels

7.4 Results and Discussion

7.4.1 Thermal characterization of the swollen PIL hydrogels

7.4.2 μ Pad microfluidic behaviour characterization

7.5 Conclusions

7.6 References

Chapter 7

Driving Flow in Microfluidic Paper-Based Analytical Devices with a Cholinium Based Poly(Ionic Liquid) Hydrogel*

Driving Flow in Microfluidic Paper-Based Analytical Devices with a Cholinium Based poly(Ionic Liquid) Hydrogel, T. Akyazi[†], A. Tudor[†], D. Diamond, L. Basabe-Desmonts, L. Florea, F. Benito-Lopez*, *Sensors and Actuators B: Chemical* (accepted).

7.1 Abstract

Paper microfluidics technology requires effective handling and control of fluids, and this remains a significant obstacle for their accessibility by end-users, inhibiting their transition from the laboratory into the market. This work presents a new concept for fluid flow manipulation in microfluidic paper-based analytical devices by introducing cholinium based poly(ionic liquid) hydrogel as an absorbent material to be used to draw liquid towards itself without requiring an external power source.

7.2 Introduction

The field of “Lab-on-a-Chip” (LOC) has an inherently interdisciplinary nature that requires input from widely differing knowledge domains to develop novel analytical platforms. The greatest potential of these systems is the integration of multiple functional elements into a small platform to generate truly sample-in/answer-out systems [1]. The design, fabrication, fluid control, sample handling, integration and analysis techniques are under continuous development and significant research is still needed to improve the capabilities of these platforms [2].

The critical need of a large variety of high performance components for fluid control and transport such as mixers, actuators, separators, valves and pumps leads to high production costs for these microfluidic devices. Therefore, despite the significant advances achieved in the microfluidics field, the number of commercially available products based on microfluidics devices and components remains quite low regardless of few exceptions like the home pregnancy test kit, microarrays and some medical diagnostics devices with very particular applications [3]. In other words, the increase in production cost of a device results in the decrease of their market adoption possibilities, where penetration of microfluidics into applications with significant socio-economic impact has been restricted almost entirely to single use devices (disposables) rather than applications that require continuous long-term monitoring approaches.

Consequently, “Lab on a paper” has been developed to provide an answer to the need of simple, cheap and autonomous devices, which could be able to reach the end users easily [4]. They exhibit not only most of the same properties as classical microfluidics, but also the strength of a well-focused commercialisation path [5]. Paper is considered as a highly attractive and promising substrate material for microfluidics due to its extremely low cost and

ubiquity, as well as its great mechanical properties comprising flexibility, lightness, variable thickness, and liquid transport and separation capabilities [4]. Microfluidic paper-based analytical devices (μ PADs) are a new group of analytical instruments that demonstrate an innovative low-cost platform technology for fluid handling and analysis, providing simple fabrication and operation, thus enabling a wide range of applications. For instance, the possibility of analysing complex biochemical samples within one analytical run was recently demonstrated with the incorporation of several fluidic operations like transportation, sorting, mixing and separation, performed in the device [6].

Paper is made of cellulose fibres, which are the driving force for the wicking of fluids by capillary action. Therefore, there is no need for external pumps to provide fluid transport through the paper, unlike the traditional microfluidic devices. However, this advantage comes with a drawback. Isotropic wicking behaviour of paper and fluid transportation by any exposed surface area makes accurate control of the fluid transport together with flow control to be highly challenging and complicated [7,8]. As a result, μ PADs need ways to implement effective handling and controlling of fluid movement. Because of this, significant obstacles are generated in the reproducibility during device fabrication, and performance precluding their production in large volumes. Hence, fluid control in paper microfluidic devices is currently one of the main investigation paths for researchers interested in developing new capabilities in μ PADs.

In order to achieve better flow control in microfluidic paper devices, several patterning processes such as photolithography [9], ink jet printing [10] and wax printing [11], using hydrophobic materials, were adopted. They were developed as the first step to generate operative μ PADs but they are not sufficiently proficient to provide proper fluidic control in the device. Therefore, fluidic switches, microvalves, timers and micropumps integrated into μ PADs can provide fluid control in the channels, as well as minimising dead volumes. The first microfluidic switch in a μ PAD was introduced by Li *et al.* [12] by applying pressure, manually, to allow or block the fluid flow. Later, Whitesides' group developed a pressure sensitive valve with a more complex mechanism in a three dimensional paper based microfluidic device [13]. Fu and her team [14] demonstrated that the time to deliver multiple fluids can be partially controlled and modified by designing different path lengths from each inlet and by drop-casting different fluid volumes to each inlet. Houghtaling *et al.* [15] developed an innovative shut-off valve in the form of a dissolvable bridge structure enabling self-delivery of different fluid volumes from a common inlet to different pathways in a paper-based device. Other dissolvable fluidic restrictors, made of sugar, were introduced by Lutz *el*

al. [16] and by Jahanshahi-Anbuhi *et al.* [17] using a dissolving polymer. More recently, Toley *et al.* [18] developed a toolkit of paper microfluidic valves using movable paper strips and fluid-triggered expanding elements.

In this regard, stimuli-responsive gels are receiving considerable attention in microfluidic devices, due to their autonomous response towards changes in their local environment [19,20]. They are considered smart materials since they are able to carry out functions by weak changes in their surroundings without the need of any human intervention [21]. Owing to their physical or chemical characteristics, these gels can endure controlled and reversible shape changes in response to external stimuli (magnetic, electric field, temperature, light, pH, solvent composition, etc.) [22-24].

Smart hydrogels consist of three-dimensional hydrophilic polymer networks capable of absorbing or releasing large amount of water in response to an external stimulus, mainly pH, light or temperature, generating an abrupt change in their volume. When the stimulus is removed, the gel returns back to its original configuration, which means that the volume change is usually reversible [25]. These properties have inspired scientists to integrate hydrogels within microfluidic systems in order to achieve fluidic control and manipulation [26-28]. Niedl *et al.* [19] made the use of stored chemicals possible by utilising responsive hydrogels as fluid reservoirs in μ PADs. The controlled release of the hydrogel fluid was achieved by an external stimulus, temperature, enabling multi-step sequences of chemical reaction on a μ PAD. Another example of the use of hydrogels on a μ PAD to manipulate the fluidic flow is the study of Yang *et al.* [20]. They used target-responsive hydrogels to mediate fluidic flow and signal readout in a paper-based point of care assay designed for simultaneous detection of multiple targets.

Recently, ionogels have been used within microfluidic devices as actuators [29-31]. They are a new class of stimuli-responsive polymer gels with an ionic liquid (IL) within their polymer matrixes where the ionic liquid can enhance the mechanical strength and the physical robustness of the gel [30-32]. Moreover, the possibility of tuning the chemical and physical properties of the ionogel by changing the ILs enables precise control of the actuation in the microfluidic devices [2,33]. In our previous work, we integrated ionogels into μ PADs for fluidic flow manipulation as passive pumps [34] and later as negative passive pumps to drive the liquid flow towards the direction of the pump [35]. These types of configurations open the possibility to detect multiple analytes sequentially by circumventing the main μ PAD channel's wicking force, without the need to design complicated device configurations.

Despite the great potential of ionogels as smart materials for fluid control in μ PADs, other materials could also improve μ PAD performance, such as superabsorbent polymers, namely superabsorbent poly(ionic liquid)s (PILs). PILs are ILs that features a polymerisable group in the cation, the anion, or both. Due to their hydrophilic nature and large water uptake, several PILs have been studied for their biocompatibility and low toxicity character. Biocompatibility studies realised on several choline derived ILs [36-46], underlined the fact that the larger contribution towards ensuring biocompatibility comes from the IL cation, where choline is an omnipresent biomolecule in nature. If the cation remains the same, the size of the anion, more so the number of carbon atoms present in it will be the determining factor, with anions that possess shorter carbon chains being more biocompatible. This is due to the fact that ILs that are lipophilic tend to accumulate in the body, while ILs that are hydrophilic are eliminated more easily [37,38,40]. In the studies previously mentioned, it was found that choline ILs were less toxic compared to imidazolium ILs [36,38-41,44,46] and pyrrolidinium ILs. By synthesizing PILs, the typical properties of ILs are transferred to the polymeric material, including high chemical and thermal stability, ionic conductivity, and highly tunable structures [47-51].

Here, we report the synthesis and thermal characterisation of a novel cholinium based crosslinked poly(ionic liquid) hydrogel, the integration of the hydrogel in a μ PAD and the performance of the hydrogel as a negative passive pump to control liquid flow and storage of fluids in the μ PAD.

7.3 Experimental

7.3.1 Materials

Choline chloride $\geq 98\%$ (ChoCl, BioReagent, suitable for cell culture, suitable for insect cell culture), Potassium 3-sulfopropyl acrylate (KSPA), polyethylene glycol diacrylate ($M_w \sim 320$, 100 ppm MEHQ as inhibitor) (PEG256), 2-Hydroxy-2-methylpropiophenone 97% (HMPP), ethanol (Chormasolv[®], HPLC grade, $\geq 99.8\%$) were bought from Sigma Aldrich[®] and used as received. Deionised water ($18.2\text{ M}\Omega\cdot\text{cm}^{-1}$) (DI water) was purified using a Merck Millipore Milli-Q Water Purification System.

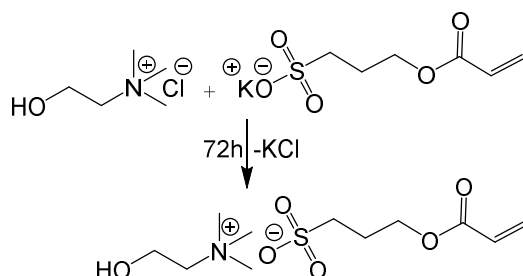
7.3.2 μ Pad fabrication

Whatman Filter paper Grade 1, wax printer XEROX ColourQube8580 and a hot plate (Labnet International Inc., USA) were used in order to fabricate the μ PADs. The design of the devices was carried out with the software application AutoCADTM. Adhesive Research, Ireland, generously provided the pressure sensitive adhesive layers. The μ PAD consists of a single channel (32 mm length and 1.5 mm width) with the inlet at the middle of the channel (6 mm radius dimension) and two outlets (10 mm radius dimension) situated at the same distance from the inlet.

7.3.3 Synthesis of the cholinium sulfopropyl acrylate ionic liquid monomer

Cholinium sulfopropyl acrylate (ChoSPA) was synthesised by dissolving 7.5 g of ChoCl together with 16.2 g of KSPA (1.3 molar equivalents) in 20 mL of DI water. The reaction mixture was magnetically stirred at room temperature for 5 days. Following this, it was poured into a beaker and moved to a vacuum oven which was kept at 45 °C and 200 mBar for 32 h. This resulted in a crystalline deposit forming at the bottom of the beaker. To finalize the crystallization process, the beaker was kept for further 48 h in a vacuum oven under normal conditions of temperature and pressure. The resulting ChoSPA crystalline product was extracted using absolute ethanol which was poured into the beaker, followed by magnetic stirring and gravity filtration of the resulting heterogeneous mixture. The extracted solution was concentrated by rotary evaporation at 40 °C, followed by complete overnight drying using a high vacuum line (0.5 mBar). The resulting viscous, translucent white coloured product was obtained with a yield of ~60%.

ChoSPA – ¹H-NMR (Figure A.7.3), δ_{H} (400 MHz): 1.98-2.05 (m, 2H, CH₂), 2.88-2.92 (p, 2H, CH₂), 3.08 (s, 9H, CH₃), 3.38-3.41 (p, 2H, CH₂), 3.91-3.95 (m, 2H, CH₂), 4.15-4.19 (t, 2H, CH₂), 5.84-5.87 (dd, 1H, CH), 6.05-6.12 (dd, 1H, CH), 6.29-6.34 (dd, 1H, CH).



Scheme 7.1. Reaction scheme for the synthesis of ChoSPA.

7.3.4 Synthesis of the cholinium PIL hydrogels

The monomer cocktail used for the synthesis of the cholinium hydrogels consisted of 0.238 g of ChoSPA (800 μmol) that were mixed with 0.238 g of ethanol:DI water 1:1 w/w mixture, 3.2 μL of HMPP (20 μmol) and 6 μL of PEG256 (16 μmol), respectively. The resulting monomer mixture was mechanically stirred until every component was completely dissolved. Following this, ~ 5 μL aliquots of monomer mixture were pipetted in circular poly(dimethylsiloxane) moulds with a diameter of 3 mm and a depth of 1 mm. For real time observation of the hydration process, a 500 μm diameter film was produced by allowing the monomeric cocktail to migrate by capillary force into a house-made cell formed between a glass slide (bottom) and a top layer made of poly(methyl methacrylate) separated by 500 μm pressure-sensitive adhesive (PSA) spacers. The polymerization was completed in a UVP CL-1000 Ultraviolet Crosslinker curing chamber using a wavelength of 365nm at a power level of $3.5 \text{ mW}\cdot\text{cm}^{-2}$ for 30 minutes.

7.3.5 Thermogravimetric analysis of the cholinium hydrogels

The thermogravimetric analysis was made using a TA Instruments Q50 Thermogravimetric Analysis instrument. The temperature program used consisted of a temperature ramp between room temperature and 500 $^{\circ}\text{C}$ in $10 \text{ }^{\circ}\text{C}\cdot\text{min}^{-1}$. The measurement was performed in a N_2 atmosphere at a flow rate of $50 \text{ mL}\cdot\text{min}^{-1}$. This ensured that oxidation events did not occur during the decomposition phase.

7.4 Results and Discussion

7.4.1 Thermal characterization of the swollen PIL hydrogels

The cholinium PIL hydrogel was synthesised following the protocol described in the experimental section. Using the cholinium sulfopropyl acrylate ionic liquid monomer (ChoSPA) and polyethylene glycol diacrylate (PEG256), a crosslinked polymer network was generated; see Figure 7.1(a). The hydrogel was photopolymerised in 3 mm disc shapes (Figure 1(b)) or as 500 μm thin films (Video 7.1) that can absorb large quantities of water. The resulting hydrogel discs are shown in Figure 7.1(b) before swelling (1), after immersion

in DI water for 2 h to ensure that the disc has reached its maximum swelling capacity (2) and after complete dehydration at room temperature (3).

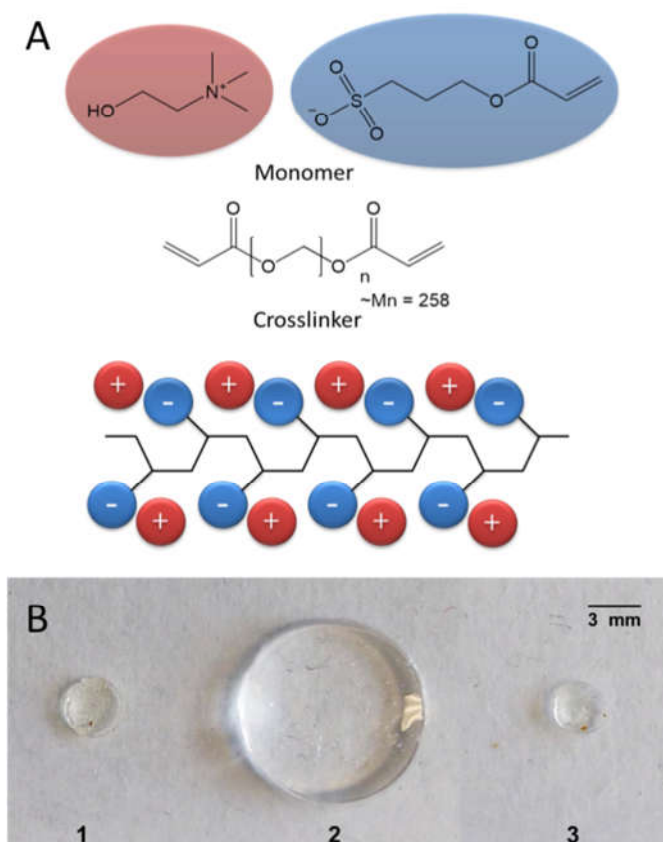


Figure 7.1. (A) Chemical structure of the components of hydrogel: trimethylhydroxyethyl ammonium (cholinium) sulfopropyl acrylate ionic liquid (top), poly(ethylene glycol) diacrylate (middle) and poly(cholinium sulfopropyl acrylate) hydrogel (bottom); (B) Comparison between the sizes of the ChoSPA hydrogel before swelling (1), swelling in DI water for 2h (2) and after dehydration by drying at room temperature (3).

Thermal characterisation of the hydrogel was performed using thermogravimetric analysis to determine the amount of DI water that can be absorbed by the material, see experimental section. For hydrogel (1) (Figure 7.1), results showed the amount of water still present inside the hydrogel immediately after polymerisation and the decomposition temperature, respectively. Hydrogel 1 started eliminating water/solvent as soon as the temperature increased. This trend continued up to ~ 200 °C, when all the water was evaporated, corresponding to a weight loss of 13.0% compared to the original weight. At this point, the weight of the hydrogel started plateauing until ~ 280 °C when it started dropping again, due to the start of the decomposition phase of the hydrogel. The onset temperature of this process is

351 °C and it continued at the same rate up to ~375 °C, where it started slowing down until 500 °C. At this point, a further 66.8 % of the initial weight was lost. This left hydrogel (1) at ~20.0 % of its original weight. This represents the non-decomposed residue of hydrogel (1) at 500 °C; see Figure A.7.1.

Hydrogel (2) (Figure 7.1), after complete swelling in DI water for 2h, presented similar behaviour to hydrogel 1, with differences appearing in the magnitude of the heating-induced weight loss events (Figure A.7.2). The weight loss due to water evaporation started immediately after temperature increased, up to ~160 °C. At this point 96.9 % of the initial mass of the hydrogel was lost. From this temperature up to ~320 °C the hydrogel mass did not undergo any notable change. At ~340 °C the decomposition phase began. During this process, the hydrogel mass dropped by 2.6 % of its initial weight until a temperature of ~390 °C was reached, after which the mass reached a plateau. This signalled the end of the decomposition phase.

From Figure A.7.3 it can be observed that hydrogel (3) (Figure 7.1) presented a similar thermogravimetric analysis curve to hydrogel (1). The weight loss started just after the temperature started increasing and it stopped when the temperature was at ~200 °C. The weight loss during this phase was 14.5 %. Following this, there was negligible weight loss until ~280 °C, at which point the decomposition phase started. The onset temperature for this process was 349 °C, which was very close to the onset temperature observed in 1 and 2. During this phase, the hydrogel lost 69% of its weight. This process started slowing down after ~375 °C, but continued until ~500 °C at which point it reached a plateau. As in the case of hydrogel (1), ~20 % of the initial weight of the hydrogel was left, representing the non-decomposed part of the hydrogel. In all cases, the hydrogels started losing water as soon as the temperature rose above room temperature. Moreover, their decomposition onset temperatures were very similar at ~350 °C. Based on this, it can be concluded that in all three cases, the freshly polymerized, hydrated and dehydrated hydrogels essentially retain their thermogravimetric characteristics. The equilibrium water uptake % was obtained from thermogravimetric data for hydrogel (2) (Figure A.7.2) using the formula:

$$\text{Water uptake \%} = \frac{W_{h.water}}{W_{swollen} - W_{h.water}} \times 100 \quad \text{Eq. 7.1}$$

where $W_{swollen}$ is the weight of the swollen hydrogel and $W_{h.water}$ is the weight of hydration water lost during thermal decomposition. The calculations show that for hydrogel (2) the

water uptake was $\sim 3150\%$ of the residual polymer mass ($W_{swollen} - W_{h.water}$). Therefore, the absorbency, calculated as grams of water per gram of residual dried polymer (g/g) is ~ 31.5 , which is comparable to other superabsorbent crosslinked polymers based on polyacrylates[52]. This is an important value to be considered for the envisaged application of this hydrogel as passive pump in μ PADs.

7.3.2 μ Pad microfluidic behaviour characterization

After thermal characterisation of the hydrogel, the μ PADs were fabricated using the wax printing method on standard laboratory filter paper. The wax printing method for μ PAD fabrication is based on (1) designing the shape of the device, (2) patterning hydrophobic wax barriers on the paper surface using a commercially available printer and (3) penetration of wax through all the paper thickness by heating the device on a hot plate to form a complete hydrophobic barrier. The final dimensions of the microfluidic structure, borders and flow channels, are addressed only after a post-heating process at $125\text{ }^{\circ}\text{C}$ for 7 min, as reported previously [35]. The post-heating treatment ensures that there is very little variation between the dimensions of all μ PADs. The hydrogel was photopolymerised in a defined disc format over an $80\text{ }\mu\text{m}$ diameter pressure sensitive adhesive (PSA) layer. This configuration ensures the hydrogel can be neatly fixed on top of one of the two μ PAD outlets as shown in Figure 7.2A. Then, the fluid flow behaviour towards the outlets (with hydrogel: outlet-1 and without hydrogel: outlet-2) was compared. Finally, the back of the μ PAD was covered with another layer of PSA to protect the μ PAD and to diminish the effect of solvent evaporation over time during testing. Moreover, this sandwich configuration improved the robustness of the entire device, see Figure 7.2B.

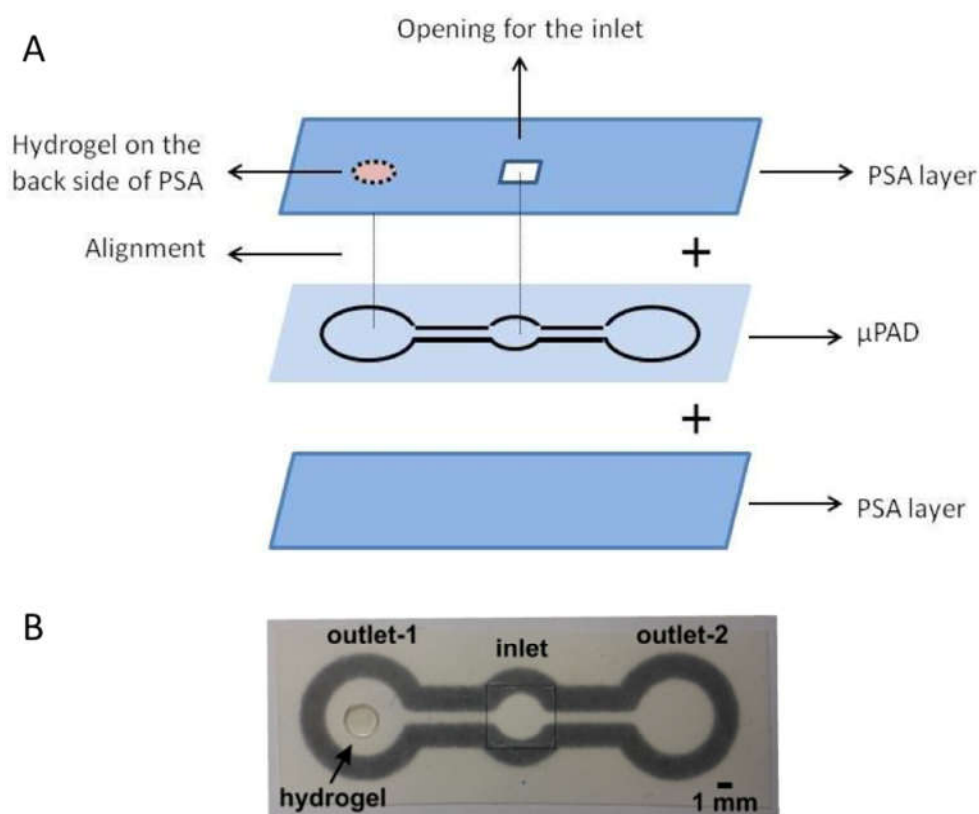


Figure 7.2. (A) Scheme of the different layers forming the μ PAD. (B) Picture of the final sealed μ PAD after integration of the cholinium PIL hydrogel pump.

Different amounts of cholinium PIL hydrogel (5, 10, 15, 20, 25, 30 μ L) were photopolymerised in a disc shape form and placed in the μ PADs at outlet-1. It was found that 20 μ L of monomer mixture was the maximum that could be applied, as higher amounts damaged the microfluidic device due to bending of the paper at the outlet during the hydration process. However, this is true only for this configuration, as other μ PAD configurations may be able to hold higher amounts of hydrogel and so promote longer use models. Therefore, 20 μ L of cholinium PIL monomer mixture was chosen to investigate the performance of the hydrogel as a passive pump in μ PADs.

Figure 7.3A shows the μ PAD when a 20 μ L cholinium PIL hydrogel disc was integrated in the device. In Figure 7.3B, 50 μ L of a yellow dye solution was dropped at the inlet of the μ PAD in order to wet the paper channels. Yellow liquid equally flowed through both channels, reaching the outlets at the same time, as can be seen in Figure 7.3C. In a conventional μ PAD, when all the channels are hydrated, the wicking property of paper no longer has any effect and the device stops working. In this case, the hydrogel passive pump

dominates the capillary forces of the paper and all liquid added to the μ PAD moves towards the hydrogel, in preference to outlet-2.

In order to investigate hydrogel passive pumping capacity of the gel, 60 μ L of a red dye solution, Figure 7.3D, was added to the inlet. The liquid flows almost exclusively towards the hydrogel at outlet-1. A small amount of red dye is visible in the channel going to the outlet-2, but no liquid flow was observed. The reason for this behaviour is slow diffusion of dye molecules through the already hydrated paper fibres. In fact no flow was observed towards outlet-2, even after 10 min, as can be seen in Figure 7.3E and 7.3F. Conversely, the vast majority of the red dye solution is been absorbed by the hydrogel at outlet-1 (Figure 7.3G). Subsequently, 70 μ L of a blue dye solution were added the inlet of the μ PAD, in several aliquots of 10 μ L. The hydrogel continues pulling the liquid flow towards outlet-1 and accumulating the solution (Figure 7.3H). The final 2 μ L of the blue solution were not absorbed by the hydrogel, as at this point, the hydrogel had reached its full wicking capacity in this configuration, as it can be seen in Figure 7.3I.

In both of the above cases, the dye was continuously drawn towards the outlet containing the hydrogel, due to the cholinium PIL hydrogel hydration capacity. The hydrogel was therefore able to direct the fluid flow preferentially towards one of the μ PAD outlets, and prevent fluid flow to the other outlet. This clearly opens the way for fluid flow manipulation and retention in μ PADs. This hydrogel 'passive pump' increased the water intake capability of the μ PAD by a factor of 9 compared to the bare μ PAD (178 μ L of liquid), for just 20 μ L of hydrogel monomer mixture. Obviously, the water retention capacity, and the flow rate, can be increased or reduced by changing the amount of the hydrogel used and the configuration of the μ PAD. Moreover, the operational lifetime of this μ PAD configuration over time was impressive, at over 90 min of continuous use before reaching saturation of the gel.

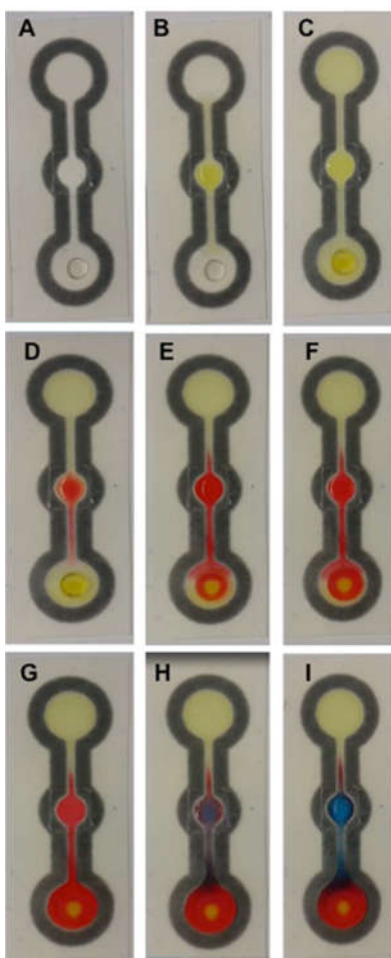


Figure 7.3. Performance of the hydrogel passive pump in the μ PAD when photopolymerised at the bottom outlet. 0s (A), 2.5 min (B), 25 min (C), 55 min (D), 60 min (E), 65 min (F), 70 min (G), 75 min (H), 90 min (I) after injecting 50 μ L yellow dye, 60 μ L red dye and 70 μ L blue dye into the inlet respectively at different aliquots of 10 μ L over time.

7.5 Conclusion

In conclusion we achieved a highly effective fluid flow manipulation method in μ PADs by introducing cholinium – based crosslinked poly(ionic liquid) hydrogel pumps which have a very high water intake capability and thus excellent control on directing the fluid flow on the paper device. To our knowledge, these hydrogel passive pumps have the highest capacity demonstrated in μ PADs up to now.

These high capacity negative flow pumps open the possibility for sequential multi-step analysis enabling several different tests running in the same small-scale device owing to their high degree of water absorption and fluid control ability. Moreover, due to their influence on

flow direction, they also open possibilities for developing μ PADs with no valves or external pumps. The biocompatibility of the material should also open possibilities for point-of-care measurements, and potentially many other applications. This study demonstrates the feasibility of using cholinium – based poly(ionic liquid) hydrogels as a passive pump material for many future microfluidic applications.

7.6 References

1. Culbertson, C.T.; Mickleburgh, T.G.; Stewart-James, S.A.; Sellens, K.A.; Pressnall, M. Micro total analysis systems: Fundamental advances and biological applications. *Analytical chemistry* **2013**, *86*, 95-118.
2. Czugala, M.; Ziolkowski, B.; Byrne, R.; Diamond, D.; Benito-Lopez, F. In *Materials science: The key to revolutionary breakthroughs in micro-fluidic devices*, SPIE NanoScience+ Engineering, 2011; International Society for Optics and Photonics: pp 81070C-81070C-81010.
3. Mohammed, M.I.; Haswell, S.; Gibson, I. Lab-on-a-chip or chip-in-a-lab: Challenges of commercialization lost in translation. *Procedia Technology* **2015**, *20*, 54-59.
4. Fu, E.; Liang, T.; Spicar-Mihalic, P.; Houghtaling, J.; Ramachandran, S.; Yager, P. Two-dimensional paper network format that enables simple multistep assays for use in low-resource settings in the context of malaria antigen detection. *Analytical chemistry* **2012**, *84*, 4574-4579.
5. Livak-Dahl, E.; Sinn, I.; Burns, M. Microfluidic chemical analysis systems. *Annual review of chemical and biomolecular engineering* **2011**, *2*, 325-353.
6. Lisowski, P.; Zarzycki, P.K. Microfluidic paper-based analytical devices (μ pads) and micro total analysis systems (μ tas): Development, applications and future trends. *Chromatographia* **2013**, *76*, 1201-1214.
7. Mace, C.R.; Deraney, R.N. Manufacturing prototypes for paper-based diagnostic devices. *Microfluidics and nanofluidics* **2014**, *16*, 801-809.
8. Böhm, A.; Carstens, F.; Trieb, C.; Schabel, S.; Biesalski, M. Engineering microfluidic papers: Effect of fiber source and paper sheet properties on capillary-driven fluid flow. *Microfluidics and nanofluidics* **2014**, *16*, 789-799.
9. He, Y.; Wu, Y.; Fu, J.-Z.; Wu, W.-B. Fabrication of paper-based microfluidic analysis devices: A review. *RSC Advances* **2015**, *5*, 78109-78127.
10. Xu, C.; Cai, L.; Zhong, M.; Zheng, S. Low-cost and rapid prototyping of microfluidic paper-based analytical devices by inkjet printing of permanent marker ink. *Rsc Advances* **2015**, *5*, 4770-4773.
11. Jeong, S.-G.; Lee, S.-H.; Choi, C.-H.; Kim, J.; Lee, C.-S. Toward instrument-free digital measurements: A three-dimensional microfluidic device fabricated in a single sheet of paper by double-sided printing and lamination. *Lab on a Chip* **2015**, *15*, 1188-1194.
12. Albatal, R.; Mulhem, P.; Chiamarella, Y.; Chin, T.-J. In *Comparing image segmentation algorithms for content based image retrieval systems*, Singaporean-French Symposia SinFra 2009, 2008; p 66.
13. Martinez, A.W.; Phillips, S.T.; Nie, Z.; Cheng, C.-M.; Carrilho, E.; Wiley, B.J.; Whitesides, G.M. Programmable diagnostic devices made from paper and tape. *Lab on a Chip* **2010**, *10*, 2499-2504.

14. Fu, E.; Lutz, B.; Kauffman, P.; Yager, P. Controlled reagent transport in disposable 2d paper networks. *Lab on a Chip* **2010**, *10*, 918-920.
15. Houghtaling, J.; Liang, T.; Thiessen, G.; Fu, E. Dissolvable bridges for manipulating fluid volumes in paper networks. *Analytical chemistry* **2013**, *85*, 11201-11204.
16. Lutz, B.; Liang, T.; Fu, E.; Ramachandran, S.; Kauffman, P.; Yager, P. Dissolvable fluidic time delays for programming multi-step assays in instrument-free paper diagnostics. *Lab on a Chip* **2013**, *13*, 2840-2847.
17. Jahanshahi-Anbuhi, S.; Henry, A.; Leung, V.; Sicard, C.; Pennings, K.; Pelton, R.; Brennan, J.D.; Filipe, C.D. Paper-based microfluidics with an erodible polymeric bridge giving controlled release and timed flow shutoff. *Lab on a Chip* **2014**, *14*, 229-236.
18. Toley, B.J.; Wang, J.A.; Gupta, M.; Buser, J.R.; Lafleur, L.K.; Lutz, B.R.; Fu, E.; Yager, P. A versatile valving toolkit for automating fluidic operations in paper microfluidic devices. *Lab on a Chip* **2015**, *15*, 1432-1444.
19. Niedl, R.R.; Beta, C. Hydrogel-driven paper-based microfluidics. *Lab on a Chip* **2015**, *15*, 2452-2459.
20. Wei, X.; Tian, T.; Jia, S.; Zhu, Z.; Ma, Y.; Sun, J.; Lin, Z.; Yang, C.J. Target-responsive DNA hydrogel mediated "stop-flow" microfluidic paper-based analytic device for rapid, portable and visual detection of multiple targets. *Analytical chemistry* **2015**, *87*, 4275-4282.
21. Ziółkowski, B.; Florea, L.; Theobald, J.; Benito-Lopez, F.; Diamond, D. Self-protonating spiropyran-co-nipam-co-acrylic acid hydrogel photoactuators. *Soft Matter* **2013**, *9*, 8754-8760.
22. Ahn, S.-k.; Kasi, R.M.; Kim, S.-C.; Sharma, N.; Zhou, Y. Stimuli-responsive polymer gels. *Soft Matter* **2008**, *4*, 1151-1157.
23. Drozdov, A.; Sanporean, C.-G. Modeling the effects of temperature and ph on swelling of stimuli-responsive gels. *European Polymer Journal* **2015**, *73*, 278-296.
24. Irie, M. Stimuli-responsive poly (n-isopropylacrylamide). Photo-and chemical-induced phase transitions. *Responsive Gels: Volume Transitions II* **1993**, 49-65.
25. Po, R. Water-absorbent polymers: A patent survey. *Journal of Macromolecular Science, Part C: Polymer Reviews* **1994**, *34*, 607-662.
26. Suzuki, H. Stimulus-responsive gels: Promising materials for the construction of micro actuators and sensors. *Journal of intelligent material systems and structures* **2006**, *17*, 1091-1097.
27. Sugiura, S.; Sumaru, K.; Ohi, K.; Hiroki, K.; Takagi, T.; Kanamori, T. Photoresponsive polymer gel microvalves controlled by local light irradiation. *Sensors and Actuators A: Physical* **2007**, *140*, 176-184.
28. Ziółkowski, B.; Czugała, M.; Diamond, D. Integrating stimulus responsive materials and microfluidics: The key to next-generation chemical sensors. *Journal of Intelligent Material Systems and Structures* **2013**, *24*, 2221-2238.
29. Benito-Lopez, F.; Byrne, R.; Răduță, A.M.; Vrana, N.E.; McGuinness, G.; Diamond, D. Ionogel-based light-actuated valves for controlling liquid flow in micro-fluidic manifolds. *Lab on a Chip* **2010**, *10*, 195-201.
30. Benito-Lopez, F.; Antoñana-Díez, M.; Curto, V.F.; Diamond, D.; Castro-López, V. Modular microfluidic valve structures based on reversible thermoresponsive ionogel actuators. *Lab on a Chip* **2014**, *14*, 3530-3538.
31. Czugała, M.; O'Connell, C.; Blin, C.; Fischer, P.; Fraser, K.J.; Benito-Lopez, F.; Diamond, D. Swelling and shrinking behaviour of photoresponsive phosphonium-based ionogel microstructures. *Sensors and Actuators B: Chemical* **2014**, *194*, 105-113.

32. Le Bideau, J.; Viau, L.; Vioux, A. Ionogels, ionic liquid based hybrid materials. *Chemical Society Reviews* **2011**, *40*, 907-925.
33. Kavanagh, A.; Byrne, R.; Diamond, D.; Fraser, K.J. Stimuli responsive ionogels for sensing applications—an overview. *Membranes* **2012**, *2*, 16-39.
34. Akyazi, T.; Saez, J.; Elizalde, J.; Benito-Lopez, F. Fluidic flow delay by ionogel passive pumps in microfluidic paper-based analytical devices. *Sensors and Actuators B: Chemical* **2016**, *233*, 402-408.
35. Akyazi, T.; Gil-González, N.; Basabe-Desmots, L.; Castaño, E.; Morant-Miñana, M.; Benito-Lopez, F. Manipulation of fluid flow direction in microfluidic paper-based analytical devices with an ionogel negative passive pump. *Sensors and Actuators B: Chemical* **2017**, *247*, 114-123.
36. Deive, F.J.; Ruivo, D.; Rodrigues, J.V.; Gomes, C.M.; Sanromán, M.Á.; Rebelo, L.P.N.; Esperança, J.M.; Rodríguez, A. On the hunt for truly biocompatible ionic liquids for lipase-catalyzed reactions. *RSC Advances* **2015**, *5*, 3386-3389.
37. Dias, A.; Cortez, A.; Barsan, M.; Santos, J.; Brett, C.; De Sousa, H. Development of greener multi-responsive chitosan biomaterials doped with biocompatible ammonium ionic liquids. *ACS Sustainable Chemistry & Engineering* **2013**, *1*, 1480-1492.
38. Gouveia, W.; Jorge, T.; Martins, S.; Meireles, M.; Carolino, M.; Cruz, C.; Almeida, T.; Araújo, M. Toxicity of ionic liquids prepared from biomaterials. *Chemosphere* **2014**, *104*, 51-56.
39. Kong, W.; Cheng, L.; He, X.; Xu, Z.; Ma, X.; He, Y.; Lu, L.; Zhang, X.; Deng, Y. Electret-based microfluidic power generator for harvesting vibrational energy by using ionic liquids. *Microfluidics and Nanofluidics* **2015**, *18*, 1299-1307.
40. Petkovic, M.; Ferguson, J.L.; Gunaratne, H.N.; Ferreira, R.; Leitao, M.C.; Seddon, K.R.; Rebelo, L.P.N.; Pereira, C.S. Novel biocompatible cholinium-based ionic liquids—toxicity and biodegradability. *Green Chemistry* **2010**, *12*, 643-649.
41. Rebros, M.; Gunaratne, H.Q.; Ferguson, J.; Seddon, K.R.; Stephens, G. A high throughput screen to test the biocompatibility of water-miscible ionic liquids. *Green Chemistry* **2009**, *11*, 402-408.
42. Rengstl, D.; Kraus, B.; Van Vorst, M.; Elliott, G.D.; Kunz, W. Effect of choline carboxylate ionic liquids on biological membranes. *Colloids and Surfaces B: Biointerfaces* **2014**, *123*, 575-581.
43. Taha, M.; Almeida, M.R.; Domingues, P.; Ventura, S.P.; Coutinho, J.A.; Freire, M.G. Novel biocompatible and self-buffering ionic liquids for biopharmaceutical applications. *Chemistry-A European Journal* **2015**, *21*, 4781-4788.
44. Tao, D.-J.; Cheng, Z.; Chen, F.-F.; Li, Z.-M.; Hu, N.; Chen, X.-S. Synthesis and thermophysical properties of biocompatible cholinium-based amino acid ionic liquids. *Journal of Chemical & Engineering Data* **2013**, *58*, 1542-1548.
45. Vrikkis, R.M.; Fraser, K.J.; Fujita, K.; MacFarlane, D.R.; Elliott, G.D. Biocompatible ionic liquids: A new approach for stabilizing proteins in liquid formulation. *Journal of biomechanical engineering* **2009**, *131*, 074514.
46. Weaver, K.D.; Kim, H.J.; Sun, J.; MacFarlane, D.R.; Elliott, G.D. Cyto-toxicity and biocompatibility of a family of choline phosphate ionic liquids designed for pharmaceutical applications. *Green Chemistry* **2010**, *12*, 507-513.
47. Isik, M.; Lonjaret, T.; Sardon, H.; Marcilla, R.; Herve, T.; Malliaras, G.G.; Ismailova, E.; Mecerreyes, D. Cholinium-based ion gels as solid electrolytes for long-term cutaneous electrophysiology. *Journal of Materials Chemistry C* **2015**, *3*, 8942-8948.
48. Isik, M.; Sardon, H.; Saenz, M.; Mecerreyes, D. New amphiphilic block copolymers from lactic acid and cholinium building units. *RSC Advances* **2014**, *4*, 53407-53410.

49. Mecerreyes, D. Polymeric ionic liquids: Broadening the properties and applications of polyelectrolytes. *Progress in Polymer Science* **2011**, *36*, 1629-1648.
50. Yuan, J.; Antonietti, M. Poly (ionic liquid) s: Polymers expanding classical property profiles. *Polymer* **2011**, *52*, 1469-1482.
51. Yuan, J.; Mecerreyes, D.; Antonietti, M. Poly (ionic liquid) s: An update. *Progress in Polymer Science* **2013**, *38*, 1009-1036.
52. Soleimani, F.; Sadeghi, M. Synthesis of ph-sensitive hydrogel based on starch-polyacrylate superabsorbent. *Journal of Biomaterials and Nanobiotechnology* **2012**, *3*, 310.

Appendix Chapter 7

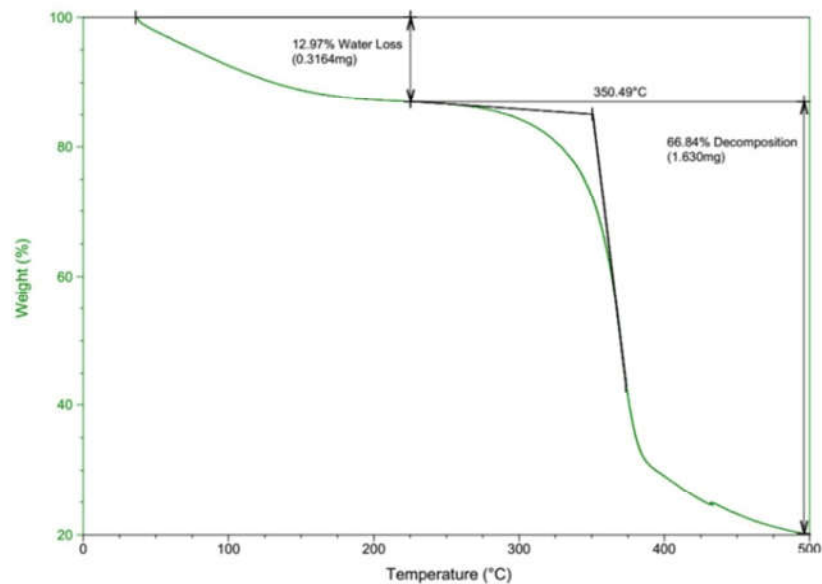


Figure A.7.1. Thermogravimetric curve showing the behaviour of the hydrogel 1 (right after polymerisation) from a 2.44 mg disc, initial weight.

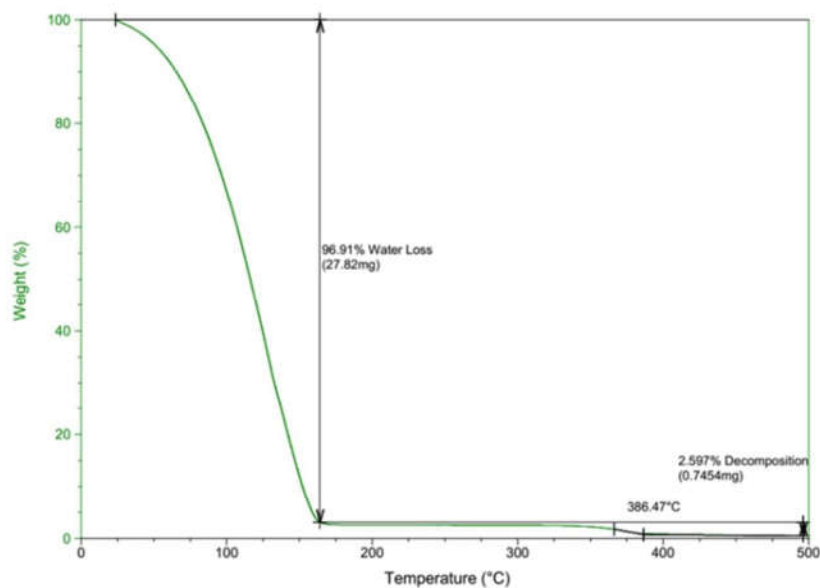


Figure A.7. 2: Thermogravimetric curve showing the behaviour of the hydrogel 2 (after hydration in DI water for 12h) from a 28.71 mg disc, initial weight.

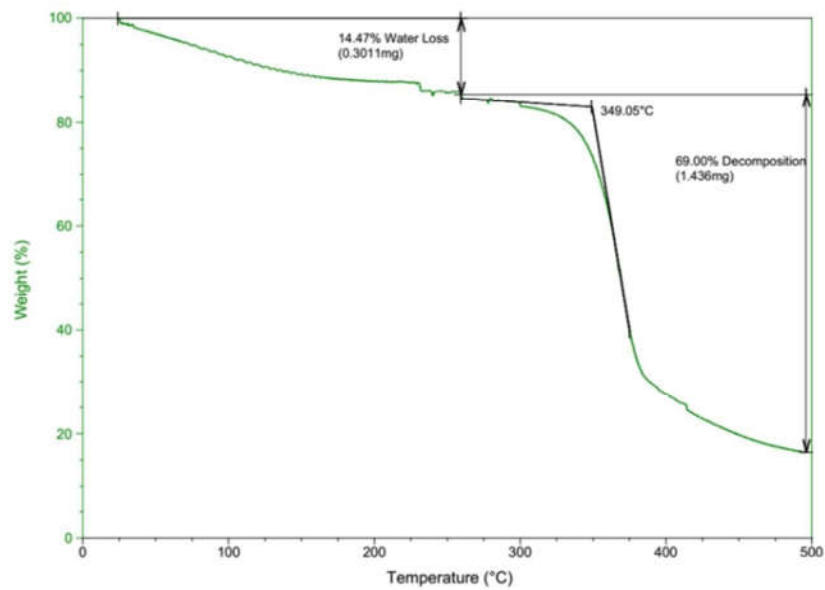


Figure A.7.3: Thermogravimetric curve showing the behaviour of hydrogel 3 (dehydrated) from a 3.08 mg disc, initial weight.

Chapter 8: Future Work - Expanding the Application Profile of Crosslinked Poly(Ionic Liquid)s.

Fluorescent Ionogels and Biocompatible Hydrogels

8.1 The synthesis and spectrophotometric characterization of crosslinked poly(ionic liquid) – fluorescein ionogels

8.1.1 Introduction

8.1.2 Materials

8.1.3 Tetrabutyl phosphonium sulfopropyl methacrylate synthesis

8.1.4 Di(Trihexyltetradecyl phosphonium) fluorescein ionic liquid synthesis

8.1.5 Synthesis of the crosslinked poly(ionic liquid)(PIL) ionogels

*8.1.6 UV-Vis and Fluorescence Spectroscopy characterization of the PIL
ionogels*

8.2 Ionic liquid monomers as photocurable media for 3D printing conductive polymer semi-interpenetrating networks

8.2.1 Introduction

8.2.2 Materials

8.2.3 Synthesis of the cholinium sulfopropyl acrylate ionic liquid monomer

8.2.4 Synthesis of the cholinium PIL hydrogels

8.2.5 Thermal characterization of the cholinium hydrogels

8.3 Conclusion

8.4 References

Chapter 8

Future Work

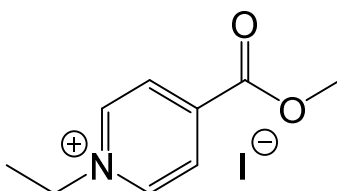
**Expanding the Application Profile of Crosslinked
Poly(Ionic Liquid)s: Fluorescent Ionogels and
Photocurable Monomeric Mixtures for 3D Printing
Conductive Polymer Composites**

8.1 The synthesis of crosslinked poly(ionic liquid) – fluorescein ionogels

8.1.1 Introduction

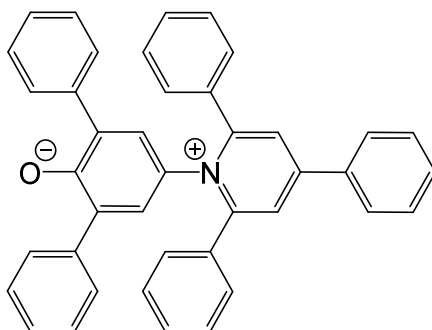
Solvatochromism can be defined as the change in the wavelength of a molecule's maximum absorbance peak when dissolved in different solvents [1-8]. This concept was attempted to be explained by simple electrostatic concepts such as dielectric constant, dipole moment, refractive index or other properties of the solvent, because it was considered that solvents are a non-structured continuum [2,6]. Due to the fact that solvents interact with their solutes at a molecular level, there are other interactions that need to be taken into account, such as hydrogen bonding, electron pair donor/electron pair acceptor, and solvophobic interactions, respectively [6]. Thus the definition of solvent polarity becomes more complicated, and its measurement cannot be performed by using existing macroscopic, physical parameters [1,2,4-7]. Based on these assumptions, there has been extensive research performed in trying to use solvatochromic molecules to define empiric parameters of solvent polarity [2,4,6].

Several methods were developed starting from Kosower, who in 1958 created the first spectroscopic polarity scale [9,10]. It was named the Z scale and it used 1-ethyl-4-(methoxy-carbonyl) pyridinium iodide (Scheme 8.1) as the solvent sensing molecule.



Scheme 8.1. Structure of 1-ethyl-4-(methoxy-carbonyl) pyridinium iodide.

Following this, several other scales have been developed including the χ_R and χ_B scale developed by Brooker *et. al.* in 1964 [11], the π scale by Kamlet, Abboud & Taft in 1977 [12] and the ET(30) scale developed by Dimroth & Reichardt in 1963, respectively [4]. This last method uses a betaine dye, known as Reichardt's dye (Scheme 8.2), as the sensing molecule. This compound exhibits a significant shift in the position of its maximum absorbance peak – it changes from 453 nm to 810 nm with decreasing solvent polarity [6].

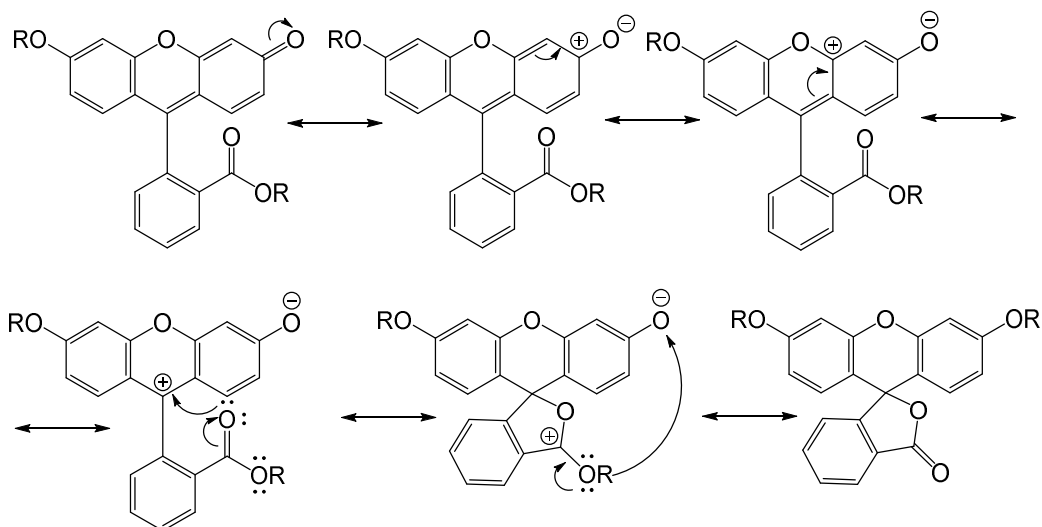


Scheme 8.2. Structure of 2,6-diphenyl-4-(2,4,6-triphenyl-1-pyridinio)phenolate, which is commonly known as Reichardt's dye.

This type of solvatochromism in which there is a hypsochromic shift with increasing polarity is known as negative solvatochromism, while positive solvatochromism is described by a bathochromic shift with increasing solvent polarity[1,2,4,6,9-11].

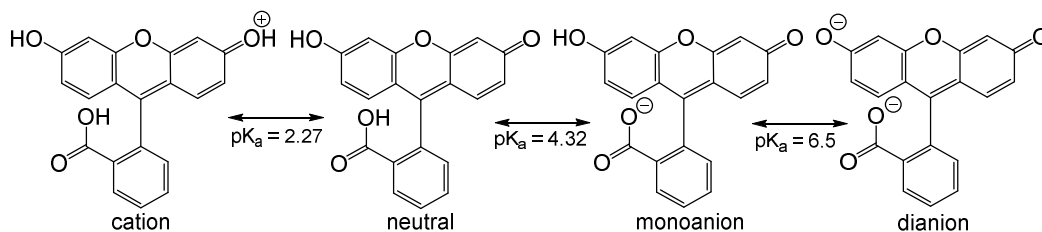
If a molecule that displays solvatochromism is also fluorescent, its emission is affected by the type of solvent used in the analysis [6].

One of the most studied and widely used fluorescent molecules is fluorescein [13-15]. This molecule has a xanthene backbone coupled to a benzoic acid moiety (Scheme 8.3).



Scheme 8.3. Resonance structures of fluorescein.

Due to the presence of the benzoic acid moiety, fluorescein has two acidic hydrogens in its structure, and therefore can also be used as a pH indicator dye (Scheme 8.4) [14].



Scheme 8.4. Chemical structures showing the different ionization states of fluorescein.

The solvatochromism of fluorescein has been thoroughly studied in different solvents and solvent mixtures[15]. More recently, fluorescein was also studied in solutions containing an ionic liquid or as the anion of an ionic liquid, in an ionic liquid mixture [16-20].

This study aims to synthesize a fluorescein-based ionic liquid that would be further added to a poly(ionic liquid) matrix, and determine the solvatochromic properties of the resulting ionogel in different solvent media. For this purpose, a tetrabutyl phosphonium sulfopropyl methacrylate ionic liquid monomer was synthesized and copolymerised with a long chain crosslinker, in order to synthesize a crosslinked poly(ionic liquid) (PILc) ionogel. A small amount of trihexyltetradecyl phosphonium fluorescein ionic liquid was added to the cocktail mixture to obtain a fluorescent ionogel. For characterization of the solvatochromic properties, the ionogels were swollen in different solvents and were characterized using UV-Vis & Fluorescence spectroscopy.

8.1.2 Materials

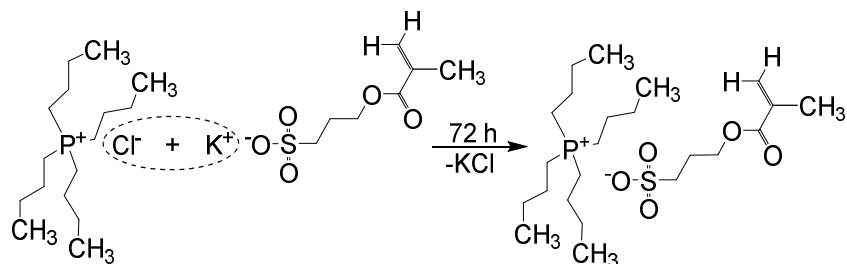
Tetrabutylphosphonium chloride ($P_{4,4,4,4}Cl$) was kindly donated by Cytec[®] Industries. Trihexyltetradecyl phosphonium chloride 95% ($P_{6,6,6,14}Cl$), Potassium 3-sulfopropyl methacrylate 98% (KSPMA), polypropylene glycol diacrylate ($M_w \sim 920$, 100 ppm MEHQ and 100 ppm BHT used as inhibitors) (PPG800), sodium fluorescein (Na_2Fl), 4-(Dimethylamino)benzophenone 98% (DMPA), dichloromethane (DCM, Chormasolv[®] Plus, HPLC grade, $\geq 99.9\%$, contains 50-150 ppm amylene as stabilizer), hexane, methanol (MeOH, Chormasolv[®], HPLC grade, $\geq 99.9\%$) and acetonitrile (ACN, Chormasolv[®], HPLC grade, $\geq 99.9\%$) were purchased from Sigma Aldrich[®] and used as received. Acetone was distilled over anhydrous $MgSO_4$ and stored over

3Å molecular sieves. Deionized water ($18.2 \text{ M}\Omega \cdot \text{cm}^{-1}$) (DI water) was made using a Merck Millipore Milli-Q Water Purification System.

8.1.3 Tetrabutylphosphonium sulfopropyl methacrylate synthesis

The tetrabutyl phosphonium sulfopropyl methacrylate (PSPMA) was synthesised by a metathesis reaction between $\text{P}_{4,4,4,4}\text{Cl}$ and KSPMA (Scheme 8.5). In a typical reaction, 10g of $\text{P}_{4,4,4,4}\text{Cl}$ and 10.02g KSPMA (1.2 molar equivalents) were dissolved in 50ml of DI water and left to react for 3 days under constant stirring. The reaction product was extracted three times with 40 ml of dichloromethane (DCM). The resulting organic phase was concentrated using a rotary evaporator until a viscous transparent liquid was obtained. Following this, the resulting liquid was dried overnight using a high vacuum pump (0.5 mBar). The final yield was ~65%.

PSPMA – $^1\text{H-NMR}$, δ_{H} (400 MHz): 0.89-0.94 (t, 12H, CH_3), 1.46-1.48 (m, 16H, CH_2), 1.85-1.86 (s, 3H, CH_3), 2.12-2.19 (m, 2H, CH_2), 2.23-2.30 (m, 8H, CH_2), 2.81-2.85 (m, 2H, CH_2), 4.17-4.20 (t, 2H, CH_2), 5.46-5.47 (p, 1H, CH), 6.01-6.02 (dd, 1H, CH) (Figure A.8.1).



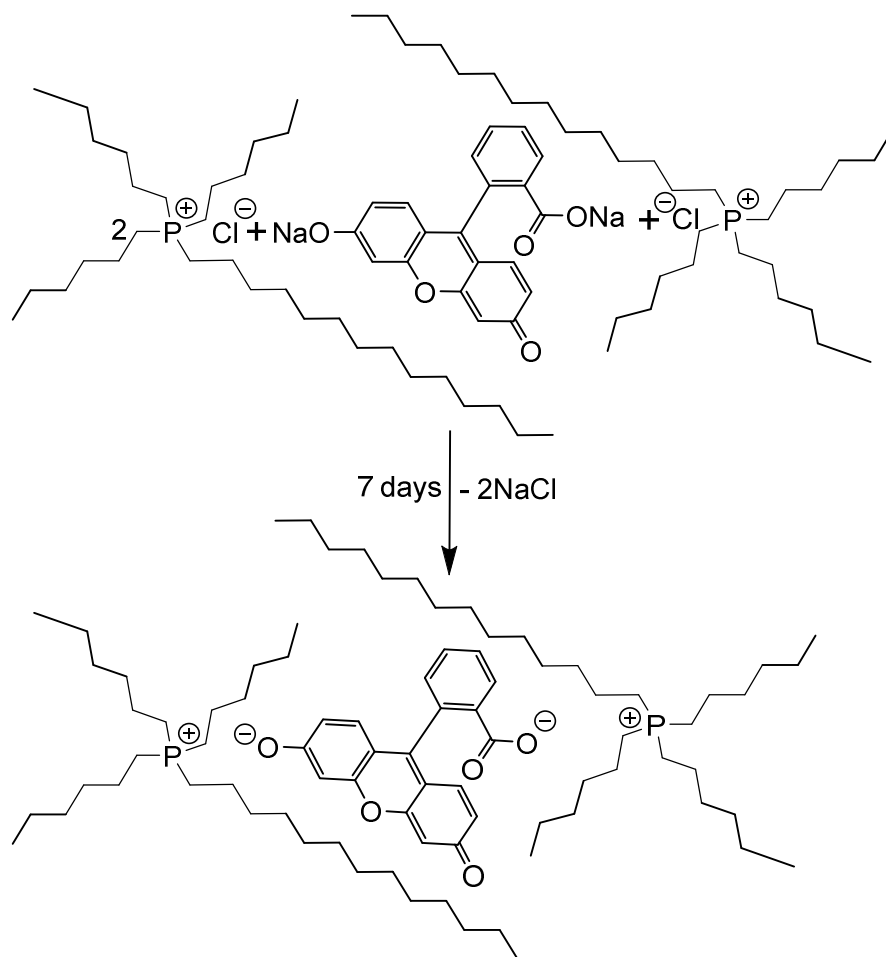
Scheme 8.5. Synthesis reaction of PSPMA.

8.1.4 Di(Trihexyltetradecyl phosphonium) fluorescein synthesis

The di(trihexyltetradecyl) phosphonium fluorescein (PFI) was synthesised in a similar way to the PSPMA. The metathesis reaction was performed by dissolving 3.1g of $\text{P}_{6,6,6,14}\text{Cl}$ in 60 ml of DCM and 3.38g Na_2FI (3 molar equivalents) in 200ml of DI water (Scheme 8.6). The reaction was left for 7 days under constant and vigorous stirring. In this case, the reaction was taking place at the boundary of the two immiscible solvents; hence the need for vigorous stirring to ensure the surface area between the two liquids was maximized. Following this, a separation funnel was used

to isolate the two solvents. The organic phase was washed 3 times with 50ml of DI water, to ensure that all Na_2FI was removed. After the washing was complete, the organic phase was concentrated using a rotary evaporator until a deep red and viscous liquid was obtained. The final purification step consisted in drying the liquid overnight using a high vacuum pump (0.5 mBar). The result was a deep red, tar-like liquid. The final yield was ~40%. Based on the NMR measurements, it can be observed that the ratio between the protons from the fluorescein moiety and the ones from the phosphonium moiety differ from the theoretical values – 1:11.8, instead of 1:13.6. This can be explained by the presence of disodium fluorescein impurities that remained in the IL phase during purification.

PFI – $^1\text{H-NMR}$, δ_{H} (400 MHz): 0.75-0.85 (m, 21H, CH_3), 0.85-1.60 (m, 83, CH_2), 1.90-2.55 (m, 14H, CH_2), 5.23-5.26(s, 1H, CH), 6.25-6.60 (m, 4H, CH), 6.60-6.70 (m, 1H, CH), 6.70-6.85 (s, 1H, CH), 6.90-7.10 (m, 1H, CH), 7.40-7.80 (m, 2H, CH), 7.85-8.40 (m, 1H, CH) (Figure A.8.2).



Scheme 8.6. Synthesis reaction of PFI.

8.1.5 Synthesis of the crosslinked PSPMA - PFl poly(ionic liquid)(PIL) ionogels

For the synthesis of PIL-PFl ionogel, the monomer cocktail contained 0.188 g of PSPMA (400 μmols), 3.3 mg (2.54 μmols) of PFl, 2.55 mg of DMPA (10 μmols), 20.1 mg of PPO800 (20 μmols) and 0.100 g of MeOH. The resulting monomer mixture was mechanically stirred until every component was completely dissolved. Following this, 6 μL aliquots of monomer mixture were pipetted in circular poly(dimethylsiloxane) moulds with a diameter of 3 mm and a depth of 1 mm. The polymerization was performed in a UVP CL-1000 Ultraviolet Crosslinker curing chamber at a wavelength of 365nm and a power level of $3.5 \text{ mW}\cdot\text{cm}^2$ for 30 minutes.

8.1.6 UV-Vis and Fluorescence spectroscopy characterization of the PILc ionogels and their hydration media

The swelling solvents chosen for this study were: hexane, toluene, acetone, acetonitrile, dichloromethane, methanol, and DI water, respectively. As the PFl ionic liquid is not covalently bound in the ionogel, leaching occurs as the ionogel is left to swell in its hydration media. In order to determine the degree of leaching of the PFl in the different solvents and probe the overall stability of the ionogels, UV-Vis and Fluorescence spectroscopy was used to analyse the swelling media before and after ionogel swelling. Three sets of solvents were used, and each set was used to swell the ionogels for 48h. The UV-Vis spectroscopy was performed using a BioTeK μQuant 96 well plate reader, while the Fluorescence spectroscopy was performed using a Jasco FP-8300 Fluorescence Spectrometer. When doing the UV-Vis measurements, a 96 well plate was used and for each series of measurements the wells were filled with 200 μL of solvent. Absorbance measurements were taken from 200 nm to 800 nm with a 2 nm resolution.

Figure 8.1 shows the UV-Vis absorbance spectra of the solvents used in this study (hexane, toluene, acetone, acetonitrile, dichloromethane, methanol, and DI water, respectively). The solvent cut-off points for acetone can be observed at 340 nm and at 315 nm for toluene. In these conditions, any absorption peak related to PFl at lower wavelengths will not be detectable in these solvents. In the case of all the other solvents, the cut-off points are situated around 250 nm, permitting visualisation of any PFl absorption bands situated above 250nm.

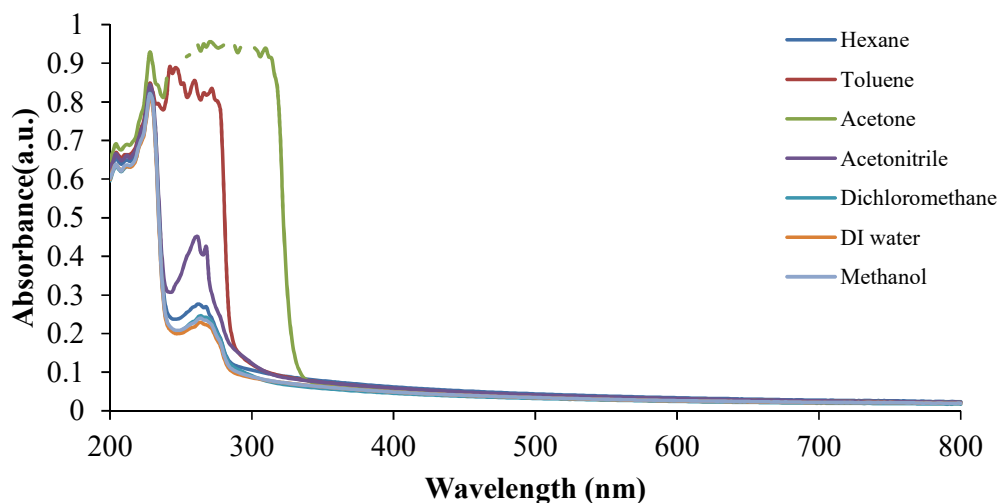


Figure 8.1 Absorption spectra of the solvents used to swell the ionogels.

Figure 8.2 shows the absorbance spectra of the 1st swelling media of the ionogels. The absorption spectra illustrate two new absorbance bands that can be observed in the case of MeOH and DCM. These bands are centred at 430nm, 456 nm, and 484 nm in the case of MeOH, indicating the presence of dissolved PFI ionic liquid, with its peaks exhibiting a hypsochromic shift [19]. In the case of DCM, at 450nm, the corresponding peak suggests the presence of just the dissolved form of the fluorescein dianion [21].

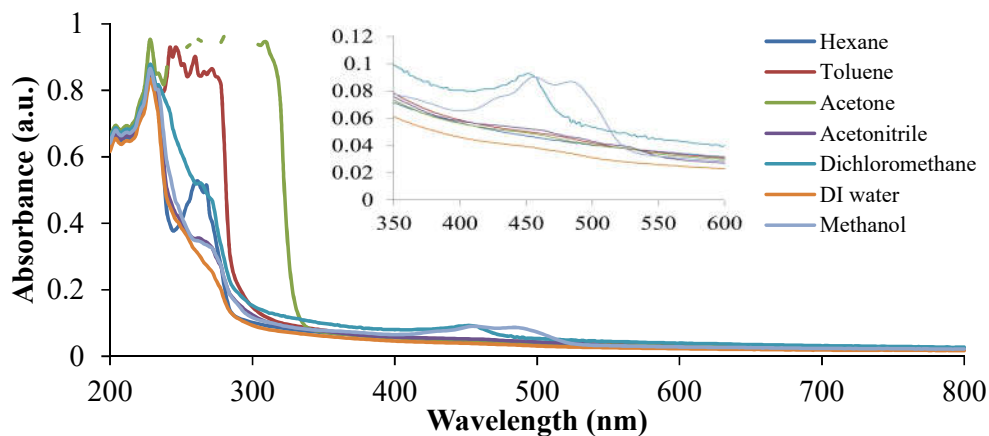


Figure 8.2. Absorption spectra of the different solvents used for the swelling of the ionogels after the 1st swelling process. Insert shows a zoom in of the 350-600nm region.

In the case of the second and third sets of solvents (Figure A.8.3 and Figure A.8.4 in Appendix Chapter 8) used as the solvation media, there is no significant difference when compared to the pure solvents (Figure 8.1), indicating that the leaching of the PFI components was negligible after the first swelling process.

Figure 8.3 shows the absorbance spectra of the ionogels when placed in different solvents. Three distinct absorbance bands can be distinguished centred at 430 nm, 458 nm and 490 nm, in the case of the ionogels hydrated in acetone, ACN, DCM and MeOH, respectively. DI water features only two peaks: one at 464 nm and one at 490 nm. The three peaks that appear in the case of acetone, ACN, DCM and MeOH, can be explained by the presence of a trimer aggregated form of fluorescein, that exhibits a hypsochromic shift in all of its peaks, compared to the absorption spectrum of neat PFI [19]. If compared to the absorbance spectrum of the sodium fluorescein salt, the two higher wavelength absorption peaks appear at similar wavelengths with the dianionic form of fluorescein when dissolved in a basic solution, featuring an absorption λ_{max} at 475 nm and 490 nm [21]. In case of the hydrogels swollen in DI water, there are two absorption peaks centred at 460 nm and 490 nm, respectively. They overlap the three peaks seen for PFI ionogels in the other solvents. The first peak that appears at 460 nm features a small shoulder centred at \sim 434 nm. Based on this, it is reasonable to assume that the first peak is actually an overlap of the first two absorption peaks (430 nm and 458 nm) that appear in the case of the other solvents. Therefore, it is expected that when hydrated in DI water, the PFI ionogels show a trimeric form of the fluorescein dianion [19].

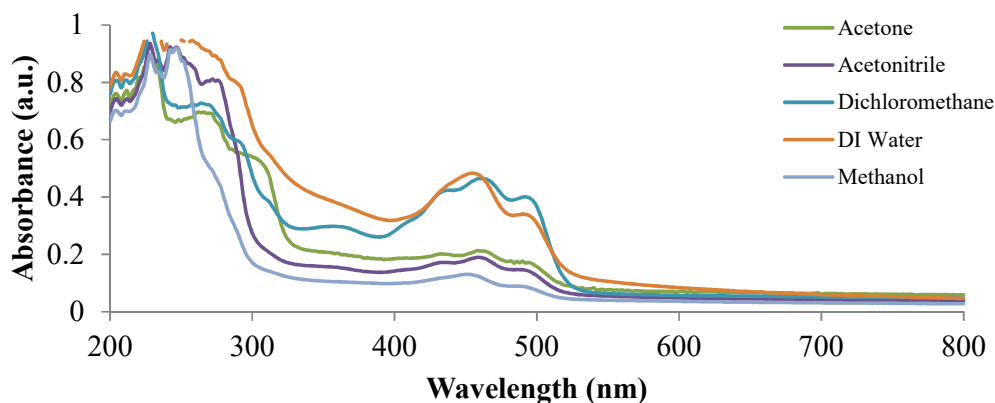


Figure 8.3. Absorption spectra of PIL ionogels after being swollen in different solvents.

The spectra of the gels swollen in toluene and hexane, respectively, were removed from the graph due to the saturation of the detector in the region 450-550 nm. In order to avoid this problem in the future, thinner gels will be employed in order to decrease the absorption path length.

Following the UV-Vis study, fluorescence spectra of the same solvent set used for ionogel swelling were collected at 1 nm intervals, using a scan speed of $500 \text{ nm} \cdot \text{min}^{-1}$ and 2.5 nm slit widths. The results obtained in DI water were excluded, because the PFI formed a suspension, which led to the results varying by a great amount. In the case of DCM, the results varied widely due to the fact that DCM is very volatile and the amount that evaporated in the time interval when the measurements were taken skewed the final results. Because of these reasons, both DI Water and DCM were excluded from the solvent sets, due to highly varying results.

The excitation wavelengths used were: 530 nm for toluene, acetone and ACN, and 500 nm for MeOH and hexane, respectively. These excitation wavelengths were chosen because they provide the highest emission intensity. When testing the fluorescence emission at all the excitation wavelengths for each different solvent, it was determined that in every case the emission peak remained at the same wavelength. This result is in accordance to results published by Sanderson *et al.* [19]. In the case of the first swelling mediums (Figure 8.4), the highest leaching was measured in MeOH, followed by acetone and ACN, respectively. Hexane and toluene exhibited insignificant leaching.

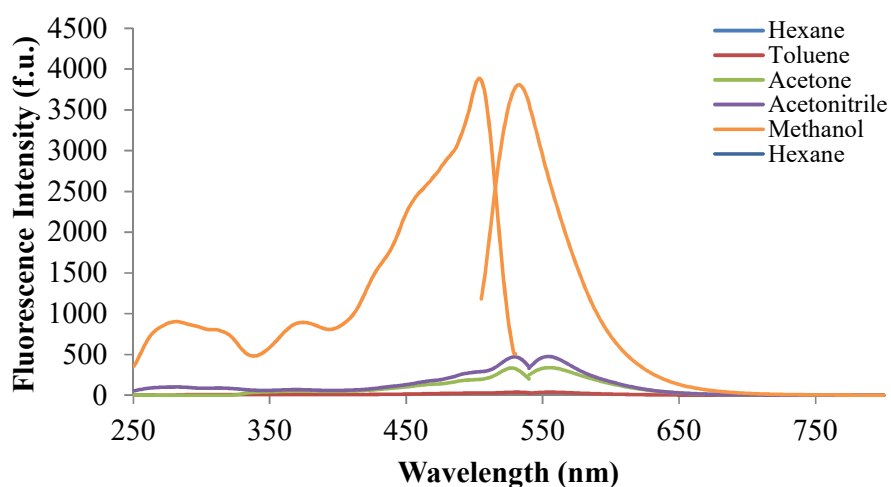


Figure 8.4. Excitation (left) and emission (right) spectra of the different solvents used for the swelling of the ionogels after the 1st swelling process.

Considerably lower fluorescence intensity values were obtained in the case of the solvents used for the second wash (Figure 8.5), indicating minimal leaching.

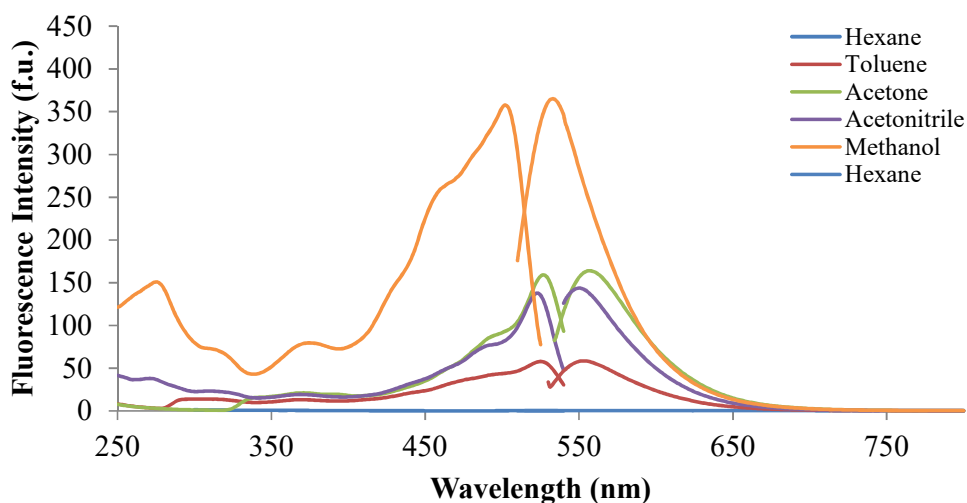


Figure 8.5. Excitation (left) and emission (right) spectra of the different solvents used for the swelling of the ionogels after the 2nd swelling process.

The results from the fluorescence measurements correlate with the results obtained from the UV-Vis measurements for the solvent sets used to swell the ionogels (Figure 8.2). It can be concluded that although leaching of the PFI dye occurs after the first swelling cycle, it becomes minimal for the second and third, irrespective of the solvent used, indicating that after a first washing step, these ionogels are stable and can be used for further characterisation and sensing. Based on the data collected from both experiments, a leaching quantification method will be developed. Furthermore, the fluorescence studies will continue on the ionogels to determine their ability to distinguish between different solvents and investigate how the solvent environment affects the fluorescent properties of the ionogels. For this purpose, a custom made polydimethylsiloxane cell was fabricated. Preliminary data obtained in the case when the hydrogels are immersed in PBS buffer (pH 7.4) are shown in Figure 8.6. The excitation wavelength is 497 nm and emission is centred at 550 nm. This corresponds to the dianionic form of fluorescein ionic liquid (PFI), however it exhibits a bathochromic shift compared to the excitation and emission wavelengths of the sodium fluorescein dianionic form in basic solutions, which has an excitation

wavelength at 490nm and an emission wavelength at 511 nm [15,21,22]. Similar studies will be performed for all the solvents mentioned above.

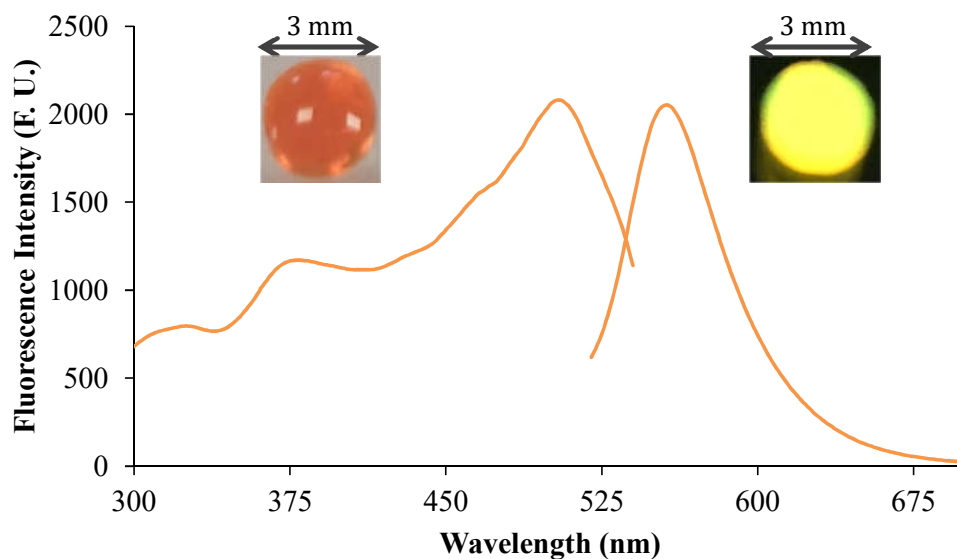


Figure 8.6 Excitation (left) and emission (right) spectra of the PFl ionogels when hydrated in PBS buffer (pH 7.4).

Moreover, digital microscopy will be used to determine the effect of the solvents on the swelling of the ionogels by measuring their increase in area compared to the freshly polymerized ionogels. Scanning Electron Microscopy studies will also be performed in order to determine the morphology and porosity of the ionogels.

8.2 Ionic liquid monomers as photocurable media for 3D printing conductive polymer semi-interpenetrating networks

8.2.1 Introduction

Additive manufacturing technologies have started being researched at the beginning of the 1980's. Hideo Kodama demonstrated, in his 1981 paper, how the use of motorized stages and UV lamps can be used together with photocurable monomer mixtures to create three-dimensional shapes. This was performed by polymerizing the photocurable monomer mixtures as a series of successive layers. This ended up representing the starting point for what today are known as 3D printing [23]. Following this innovation, several other research groups patented different methods

for additive manufacturing in the subsequent years. The first such patent was filed in the US by Charles W. Hull in 1984 and it was entitled “Apparatus for production of three-dimensional objects by stereolithography” [24]. This method would end up being known as “stereolithography” and would become one of the most widely used methods for additive manufacturing. In 1989 S. Scott Crump patented a new additive manufacturing method, “Apparatus and method for creating three-dimensional objects”[25]. Compared to the work performed by Kodama, and Hull, this method does not rely on a photocurable monomer mixture, but works by melting thermoplastic polymers and layering them on top of each other with the help of a computer controlled motorized stage. This method is today known as ‘fused filament fabrication’ or ‘fused deposition modelling’. In recent years this has become the most common commercially available additive manufacturing method and has become synonymous with “3D printing”. Pico- and femto- second pulsed lasers were also investigated as a way to initiate polymerization processes [26,27]. This method of polymerization was first demonstrated in 1965 by Pao and Rentzepis [28], but it was mostly ignored until the 1990’s [27]. Today, this technique is known as direct laser writing (DLW) by multiphoton polymerization and has found applicability in a range of different fields [26,27,29-32]. DLW takes advantage of the high probability of non-linear absorption of photons happening when the light emitted by an ultra-fast laser is focused in a very small volume. Due to the polymerization reaction being dependent on the non-linear absorption of photons, the resolution of this method is very high, because the chances of such absorption happening outside of the laser focus point are greatly decreased. This leads to the ability of this method to be used to print structures with a resolution in the range of hundreds of nanometres [26,31]. In most commercial systems that make use of this method, such those manufactured by Nanoscribe GmbH, the photocurable resins contain a photoinitiator that absorbs light closer to the ultraviolet region of the spectrum, while the laser used has a wavelength closer to the near-infrared region of the spectrum (e.g. 780 nm). The monomers used in the resin formulations tend to have at least two polymerizable groups in their structure [31]. This ensures high reactivity during polymerization and produce final structures that are able to preserve high amount of detail. One of the downsides to using this type of resins is that the final structures are hydrophobic and rigid. Therefore, there is an interest in producing novel monomeric cocktails compatible with DLW to fabricate

much softer, hydrophilic 3D structures that could incorporate additional stimuli-responsive units.

Recently, a new class of materials has emerged that could be used as monomers in creating a new class of photocurable resists. These materials are known as monomeric ionic liquids, and they are a subgroup of ionic liquids that feature polymerizable groups in either of their constituent ions, or in both [33-36]. Ionic liquid monomers (ILMs) possess several properties that would make them suitable for the production of monomeric cocktails suitable for DLW. These properties include: high thermal stability, high transparency, very low vapour pressure, ionic conductivity, biocompatibility and easily tunable chemical and physical properties, such as hydrophilicity and reactivity[36]. Moreover, due to their versatile nature, they could be used in tandem with other well-known conductive polymers, which would lead to the possibility of printing micro-structured electrodes using electrically conductive photo-curable resists, such as 3,4-ethylenedioxythiophene (EDOT) [37]. EDOT polymers (PEDOT) usually doped by poly(styrene sulfonate) (PSS) represent one of the most well-known conductive polymers, PEDOT:PSS. PEDOT:PSS is usually processed as an aqueous dispersion and has found applicability in the fabrication of a wide range of products, such as antistatic coatings for the photographic film industry, or as a semiconductor used in the fabrication of organic field effect or electrochemical transistors. Furthermore, PEDOT:PSS is biocompatible, which makes it an attractive material for interfacing with living cells or tissues[38]. This aspect would make EDOT a suitable material to be included in the formulation of a photocurable resin to construct 3D microscale structures for applications in biological sensing.

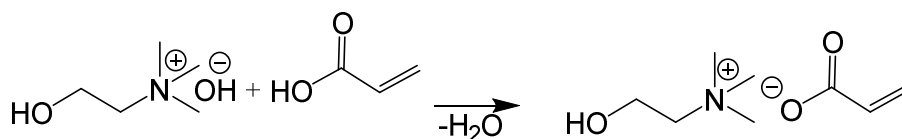
The aim of this study is to develop a method for the synthesis of novel DLW monomeric mixtures that contain a biocompatible ionic liquid monomer, a photoinitiator, a polyethylene-based crosslinker and EDOT, respectively. Following this, the resulting monomeric mixture will be used as a photocurable resin for DLW of 3D microstructure electrode arrays. These structures will then be treated with an oxidizing agent to convert the EDOT present in the microstructures to PEDOT by oxidative polymerization. The final step proposed in this study is the electrochemical characterization of the 3D printed PEDOT – poly(ionic liquid) microstructures in order to determine their usefulness in applications such as monitoring cell activity.

8.2.2 Materials

Choline hydroxide 46% w/w solution in H₂O, Acrylic Acid 99% (200 ppm MEHQ as inhibitor), 3,4-Ethylenedioxythiophene, polyethylene glycol diacrylate (M_w ~ 320, 100 ppm MEHQ as inhibitor) (PEG256), 3-(Trimethoxysilyl)propyl methacrylate 98%, 2-Hydroxyethyl Acrylate 98% (HEA), dimethylsulfoxide, (HPLC grade, ≥99.8%) were purchased from Sigma Aldrich® and used as received. 7-Diethylamino-3-thenoylcoumarin was purchased from Exciton and used as received. Deionized water (18.2 MΩ·cm⁻¹) (DI water) was purified using a Merck Millipore Milli-Q Water Purification System.

8.2.3 Synthesis of the cholinium acrylate ionic liquid monomer

To synthesize the cholinium acrylate ionic liquid monomer, 1 g of acrylic acid (1 molar equivalent) was added to a beaker. Following this, 3.66 g of cholinium hydroxide 46% w/w solution (1 molar equivalent) was slowly added dropwise under constant magnetic stirring (Scheme 8.7). This was needed as the neutralization reaction between the two reagents is exothermic, and the increased temperature of the mixture could have led to the polymerization of the acrylic acid and the reaction product. After leaving the mixture to stir for 2 h, the beaker was transferred to a vacuum oven where it was held for the next 48 h under vacuum, at a temperature of 40 °C. This was performed to eliminate the remaining water in the reaction medium. The resulting product was a viscous liquid with a dark brown appearance.



Scheme 8.7 Reaction scheme for the synthesis of cholinium acrylate.

8.2.4 Ionic liquid monomer mixtures to be used as photoresists

A series of monomer cocktails composed of the ILM cholinium acrylate and hydroxyethyl acrylate in different weight ratios (1:0, 3:1, 3:2, 1:1 and 0:1, respectively) will be screened in order to determine their suitability for DLW. The recipes proposed for the monomeric mixtures are shown below (Table 8.2.1):

Table 8.1 Cholinium acrylate monomer mixtures.

Mix	1	2	3	4	5
ChoAc (mg)	300	300	300	300	0
HEA (mg)	0	100	200	300	300
DEATC (mg)	3	3	3	3	3
PEG258 (mg)	15	15	15	15	15
DMSO (mg)	150	150	150	150	150
EDOT (mg)	30	30	30	30	30

8.2.5 2-Photon polymerization of the monomer mixtures

The 2-photon 3D printing of the PIL structures will be performed using a nanoscribe Photonic Professional GT direct laser writing system. To determine the optimum scanning speed and laser power combination, a calibration programme will be run which will print a matrix of simple geometrical shapes, such as cylinders. The printing algorithm will vary the scan speed on each new line, while the laser power will change on each column. By running an algorithm of this type, the influence of scan speed and laser power can be determined. Moreover, a proportionality relationship between scan speed and laser power can be determined, which would help if there is a need to increase the speed of printing. After the writing parameters are determined, the next step will be to print the final design for the electrodes. These will consist of an array of cone structures with different aspect ratios: an undersquared structure, in which the height of the cone is half of its diameter, a squared structure, in which the height has the same value as the diameter of the cone, and an oversquared structure which will have a height equal to double its diameter (Figure 8.7). By printing cone arrays with different aspect ratios, a conclusion can be drawn about which structure would be the best suited to grow the cells on, while also showing which would have the highest sensitivity when the cells would be further tested.

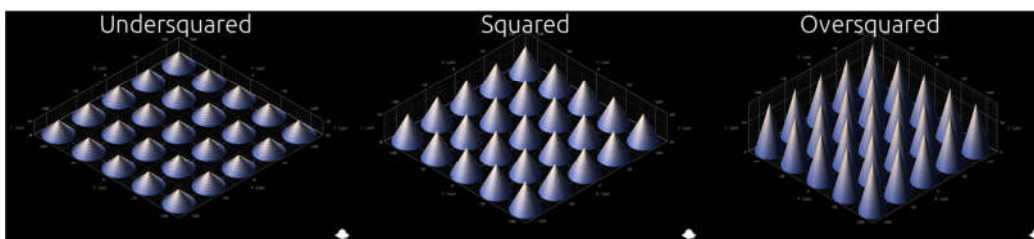


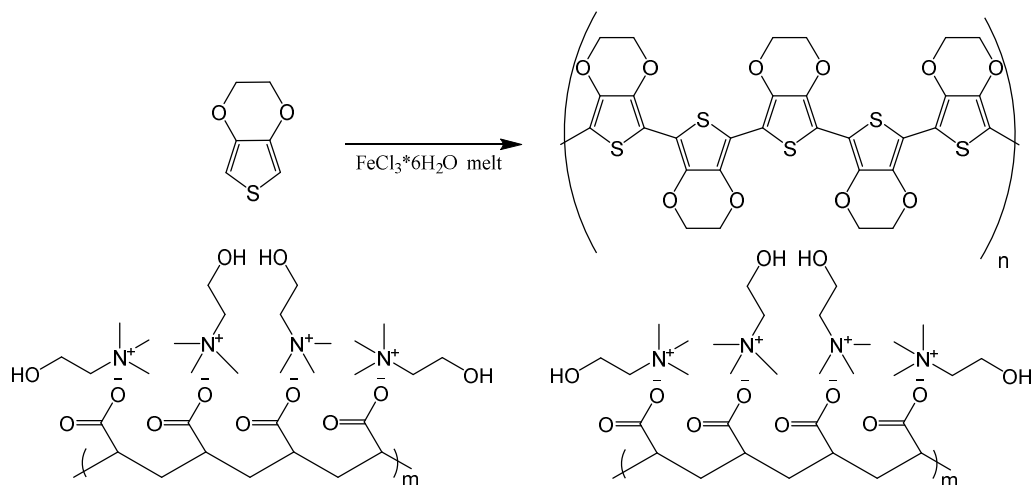
Figure 8.7. The different types of cone matrixes that will be used as templates for the PIL - PEDOT structures.

8.2.6 Silanisation of the glass substrates

To silanise the high precision glass slides (1.5H, 0.17 ± 0.005 mm thick, Fisher Scientific), they will be cleaned using acetone, isopropanol, ethanol, methanol and DI water, dried, and exposed to oxygen plasma for 2 min (Harrick Plasma). Following this, the slides will be immersed in a solution of 3-(trimethoxysilyl)propyl methacrylate (Sigma Aldrich; 3vol% in ethanol with 0.1vol% acetic acid) for 1 h, rinsed in ethanol, and dried under nitrogen.

8.2.7 Fabrication of the electrode arrays

Using the silanised glass substrates and the optimized printing conditions previously determined, the electrode arrays will be printed on the top part of the slides, using the oil immersion configuration. The first step in the fabrication of the microstructured electrode arrays will be the printing of a thin hydrogel base on which the cones are printed with a length of 3 mm, a width of 1 mm and a height of $100 \mu\text{m}$. The conical electrode array will be printed on top of the hydrogel base, occupying its central part (Figure 8.8). After the structures are printed and cleaned, the next step of the process will be to polymerize the EDOT within the PIL structures by using a chemical oxidant, such as a melt of $\text{FeCl}_3 \cdot 6\text{H}_2\text{O}$. As the melting point for this compound is 37°C , it will not damage the structure of the PIL matrix. By immersing the printed structures in the melted salt, the EDOT should begin to polymerise (Scheme 8.8). Due to very small dimensionality of the structures, this process should be complete in a matter of minutes.



Scheme 8.8: The polymerization of EDOT by immersion in molten iron chloride hexahydrate.

The subsequent step will be to sputter coat the glass slide with gold for the purpose of fabricating the electrical contacts needed to connect the PIL-PEDOT array to an electrical circuit. This will be performed by covering the electrode array area with an inert material, such as paraffin wax, while leaving the exposed sides of the elongated platform uncovered. The final step will be the removal of the paraffin wax from the electrode array by washing it away with a non-polar solvent, such as hexane (Figure 8.8). By using a non-polar solvent, the PIL structures should not be affected. Once this step is complete, the final platform will have an electrode surface upon which cells can be grown, while the rest of the slide is covered in gold to facilitate its connection to an electrical circuit.

Another way of fabricating these electrodes is to use indium tin oxide (ITO) covered glass slides. This removes the need for the gold sputter coating step, but there an etching step is required before printing of the microelectrodes. In order to divide the ITO into two distinct conducting areas. The bridge between the two conducting areas will be made by the microprinted electrodes. The etching can be performed using a mixture of hydrochloric acid:nitric acid:DI water in a ratio of 1:1:5 [39] (Figure 8.9).

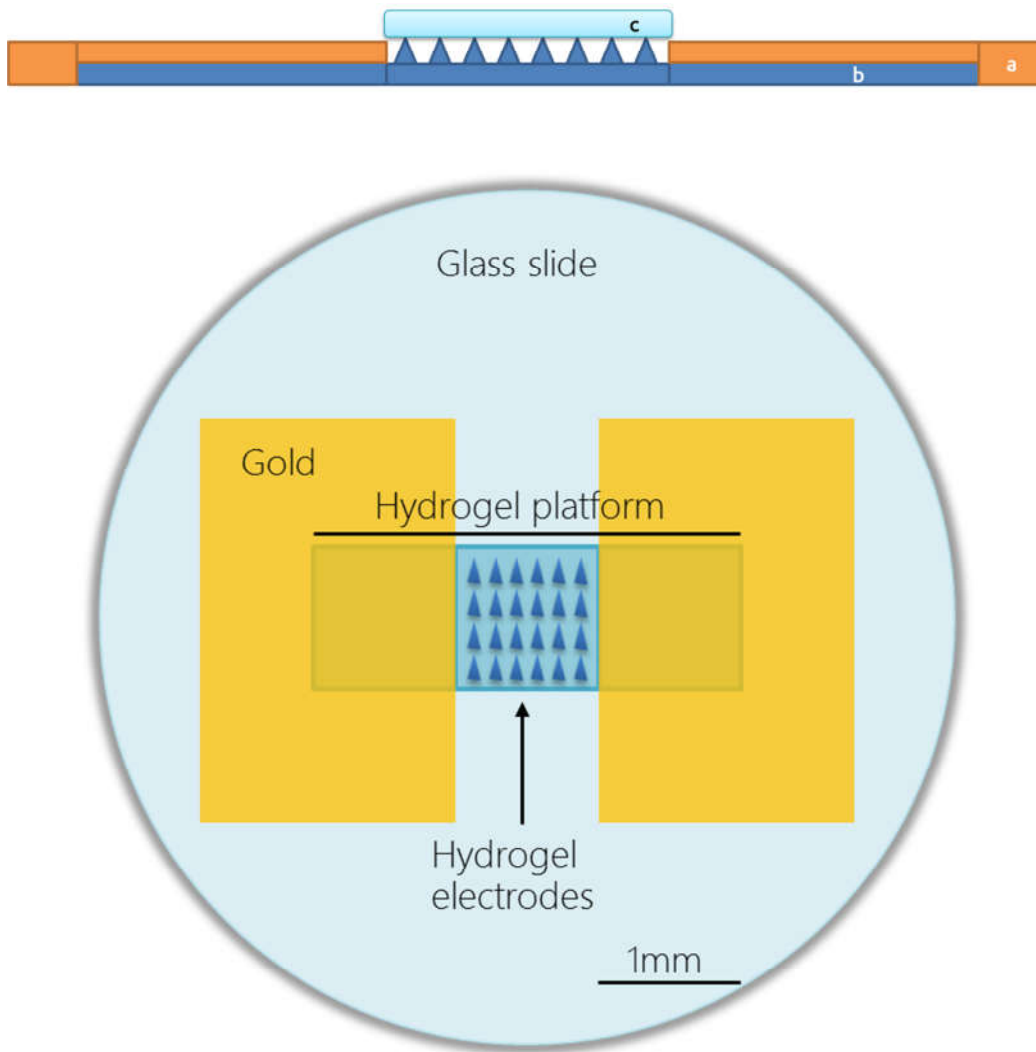


Figure 8.8 (Top) Side view of the glass slide showing: (a) the sputter-coated gold layer, (b) the printed flat square with the conical structures, and (c) the area which will be used to grow cells on; (Bottom) Top view of the final micro-electrode array platform after 3D printing, showing the gold sputter coated areas, and the hydrogel platform featuring the conical microelectrode array.

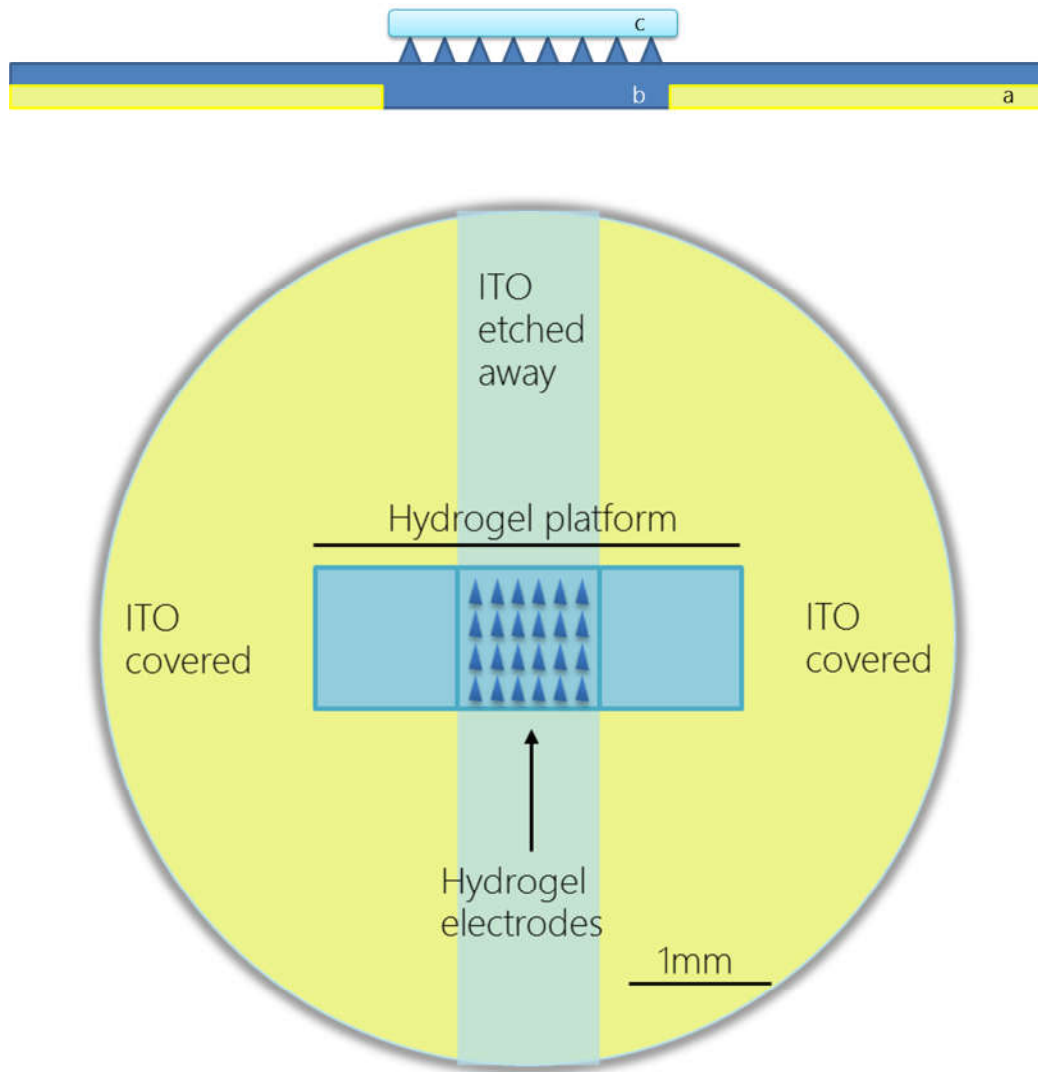


Figure 8.9 (Top) Side view of the ITO glass slide showing: (a) the ITO layer, (b) the printed hydrogel platform with the conical microstructured electrodes printed on top, also showing the channel where the ITO was etched away, and (c) which is the exposed space that will be used to grow cells on; (Bottom) Top view of the final 3D printed micro-electrode array platform, showing the region where the ITO covered areas, the area where the ITO was stripped away, and the hydrogel platform featuring the microstructured cone array.

8.3 Conclusion

The research presented in this thesis focuses on expanding the application profile of crosslinked PIL materials. In this context, in depth analysis of the physical and chemical properties of two different types of PILs based on phosphonium and ammonium ionic liquid monomers are presented.

Temperature responsive xPIL hydrogels based on the phosphonium PILs were synthesized and characterized in Chapter 3. Moreover, sIPNs were prepared by adding a linear photoresponsive polymer based on p(NiPAAm-BSP-AA) to the xPIL, which led to the development of hydrogels showing volume changes in response to multiple stimuli, such as: light, temperature, the presence of ionic charges in the sIPN polymer chain, and the presence of dissolved foreign salts in the hydration medium. This work presented in Chapter 3 demonstrated that crosslinked PILs can form smart polymer materials and act as host matrixes for other smart polymers through which the range of stimuli to which the resulting materials respond can be increased.

Following this, based on the xPIL's temperature response presented in Chapter 3, research continued by integrating the phosphonium xPIL hydrogels into microfluidic devices as temperature controlled actuators for flow control. This application demonstrated that the PIL hydrogel materials can be used as multiple-use actuators in microfluidic devices with actuation times in the range of 6 to 8 s for both opening and closing cycles, without suffering any degradation in performance. Further improvements can be made for this application field by optimizing the design of the microfluidic device, specifically the shape and size of the channel and the positioning, size and geometry of the hydrogel actuator.

The next application developed for the phosphonium ILMs consisted of creating a photopolymerizable monomer mixture capable of being used as a photoresist in a multiphoton 3D printing process known as direct laser writing (DLW). Due to the excellent solvation properties of the ILM, the photoinitiator and the crosslinker dissolved in it without the need to add any additional organic solvents. This represents an important advantage of the ILMs, because it increases the operating window of the photoresist by permitting the use of a wider range of combinations between writing speed and laser power when printing, while also avoiding important issues associated with DLW such as solvent evaporation, or bubbling of the photoresist due to localised heating caused by the laser. This offers the possibility of tuning the mechanical

properties of the printed structures during the printing phase by having the option to print different parts of the design at multiple writing speeds and laser power values. The resulting photoresist was successfully used to 3D print simple geometric shapes such as cylinders and hexagonal pillars, and more complex shapes such as twisted vase-shaped cylinders. All of these structures exhibited a temperature response similar to that presented in the previous chapters, coupled with very fast shrinking and reswelling times, due to their small dimensions.

The next part of the thesis presents the work done on the ammonium ionic liquid monomer. In Chapter 6, the focus shifts towards a novel ILM, namely cholinium sulfopropylacrylate (ChoSPA). This material, when polymerized, is capable of absorbing ~32 times its own weight in DI water, without exhibiting any degradation in its mechanical stability. Its ability to absorb water was measured using thermogravimetric analysis. Based on its superabsorbent properties, an application was developed for this cholinium-based ILM, which is further presented in Chapter 7. The application consists of using ChoSPA hydrogel as passive pumps in paper microfluidic devices as, due to their tremendous absorbent capabilities, they can successfully direct flow while also increasing the wicking capabilities of the device. This protocol could offer the possibility of performing more complex microfluidic operations with these devices, as opposed to traditional paper microfluidic devices.

The final chapter of the thesis presents two further directions that can be pursued using the aforementioned PIL materials, namely: solvatochromic PIL ionogels and 3D printed microelectrode arrays for electrochemical sensing. The solvatochromic materials were synthesized by adding a solvatochromic fluorescent ionic liquid dye to the monomer mixture in a very low concentration. After polymerization, the addition of the hydrogels in different solvents made them swell according to the polarity of the solvent, while also changing their absorbance wavelength in the visible spectrum and their fluorescence emission wavelength. The presence of all these changes allows a multiple input – single output type sensor system to be devised which could be used to differentiate between different solvents. This type of sensor system could also be developed for other analytes, such as glucose or lactose. The main criterion to be taken into account when developing such ionogel sensors is to ensure that there is a similarity between the xPIL matrix used and the IL dye used as the sensing component. In the second part of the chapter, 3D structured electrode arrays printed in an ILM photoresist are designed for cell activity measurements. To ensure that the

cells will be able to grow and develop on top of the microstructured arrays, the photoresist proposed is based on a cholinium ILM, that was shown to be biocompatible.

In conclusion, PIL materials can be used for a wide range of applications, due to their inherently attractive physical and chemical properties. This thesis focused mainly on two monomers, with an anionic polymerisable group, their application in microfluidic devices as sensors and actuators, and their compatibility with 3D printing. If their polymerisable group is changed, polymers with very different and properties can be synthesized or complex 3D structures created using DLW. Moreover, the addition of IL additives to the ILM mixture, as demonstrated in Chapter 8, can further increase the application profile of these materials by adding different functionalities.

In my opinion, niche applications in industry of manufacturing and microfluidics are likely to emerge in the coming years. The prime problem with their adoption is the typical high prices of most ILs, leading to difficult adoption in industrial processes that need large quantities of ILs. This main inconvenience is however avoided if the amount of material needed is small, which is valid in microfluidics or in multiphoton 3D printing. A standalone application that could benefit greatly from the synthetic versatility of ILs and ILMs would definitely be the multiphoton 3D printing industry, by using ILs and ILMs to create photoresists for specific applications. Continuous development of targeted photoresists, would greatly expand the real-world applications of multiphoton 3D printing.

In conclusion, the versatility of both physical properties and chemical properties of ILMs leads to the ability to synthesize a great number of specific xPIL materials that can be integrated in many high-impact applications.

8.4 References

1. Buncel, E.; Rajagopal, S. Solvatochromism and solvent polarity scales. *Accounts of Chemical Research* **1990**, *23*, 226-231.
2. Kiprianov, A.I. Influence of the solvent on the colour of dyes (solvatochromism). *Russian Chemical Reviews* **1960**.
3. Nigam, S.; Rutan, S.C. Principles and applications of solvatochromism. *Applied Spectroscopy* **2001**.
4. Reichardt, C. Empirical parameters of the polarity of solvents. *Angewandte Chemie International Edition in English* **1965**, *4*, 29-40.

5. Reichardt, C. Solvatochromism, thermochromism, piezochromism, halochromism, and chiro-solvatochromism of pyridinium n-phenoxide betaine dyes. *Chemical Society Reviews* **1992**.
6. Reichardt, C. Solvatochromic dyes as solvent polarity indicators. *Chemical Reviews* **1994**, *94*, 2319-2358.
7. Reichardt, C.; Asharin-Fard, S.; Blum, A.; Eschner, M.; Mehranpour, M.A.; Milart, P.; Neim, T.; Schafer, G.; Wilk, M. Solute/solvent interactions and their empirical determination by means of solvatochromic dyes. *Pure and Applied Chemistry* **1993**, *65*, 2593-2601.
8. Johnson, B.P.; Gabrielsen, B.; Matulenko, M.; Dorsey, J.G.; Reichardt, C. Solvatochromic solvent polarity measurements in analytical chemistry: Synthesis and applications of et-30. *Analytical Letters* **1986**, *19*, 939-962.
9. Kosower, E.M. The effect of solvent on spectra. I. A new empirical measure of solvent polarity: Z-values. *Journal of the American Chemical Society* **1958**.
10. Kosower, E.M. The effect of solvent on spectra. II. Correlation of spectral absorption data with z-values. *Journal of the American Chemical Society* **1958**.
11. Brooker, L.G.S.; Craig, A.C.; Heseltine, D.W. Color and constitution. Xiii. Merocyanines as solvent property indicators. *Journal of the ...* **1965**.
12. Kamlet, M.J.; Abboud, J.L.; Taft, R.W. The solvatochromic comparison method. 6. The. Pi.* scale of solvent polarities. *Journal of the American ...* **1977**.
13. Schauenstein, K.; Schauenstein, E. Fluorescence properties of free and protein bound fluorescein dyes. I. Macrospectrofluorometric measurements. *Journal of Histochemistry ...* **1978**.
14. Mota, M.C.; Carvalho, P.; Ramalho, J.; Leite, E. Spectrophotometric analysis of sodium fluorescein aqueous solutions. Determination of molar absorption coefficient. *International Ophthalmology* **1991**, *15*, 321-326.
15. Klonis, N.; Clayton, A.H.A.; Voss, E.W.; Sawyer, W.H. Spectral properties of fluorescein in solvent-water mixtures: Applications as a probe of hydrogen bonding environments in biological systems. *Photochemistry and Photobiology* **1998**, *67*, 500-510.
16. Nicol, E.; Moussa, A.; Habib-Jiwan, J.L.; Jonas, A.M. Layer-by-layer self-assembly of polyelectrolyte and the divalent salt of fluorescein. *Journal of Photochemistry and Photobiology A: Chemistry* **2004**, *167*, 31-35.
17. Das, S.; Chattopadhyay, A.P.; De, S. Controlling j aggregation in fluorescein by bile salt hydrogels. *Journal of Photochemistry and Photobiology A: Chemistry* **2008**, *197*, 402-414.
18. Ali, M.; Kumar, V.; Pandey, S. Unusual fluorescein prototropism within aqueous acidic 1-butyl-3-methylimidazolium tetrafluoroborate solution. *Chemical Communications* **2010**, *46*, 5112-5114.
19. Sanderson, W.M.; Johnson, D.R. Spectroscopic behavior of fluorescein as a constituent anion in a phosphonium-based ionic liquid material. *Materials Chemistry and Physics* **2012**, *132*, 239-243.
20. Das, S.; Magut, P.K.S.; de Rooy, S.L.; Hasan, F.; Warner, I.M. Ionic liquid-based fluorescein colorimetric ph nanosensors. *RSC Advances* **2013**, *3*, 21054-21061.
21. Margulies, D.; Melman, G.; Shanzer, A. Fluorescein as a model molecular calculator with reset capability. *Nature Materials* **2005**, *4*, 768-771.

22. Klonis, N.; Sawyer, W.H. Spectral properties of the prototropic forms of fluorescein in aqueous solution. *Journal of Fluorescence* **1996**, *6*, 147-157.
23. Kodama, H. Automatic method for fabricating a three-dimensional plastic model with photo-hardening polymer. *Review of Scientific Instruments* **1981**, *52*, 1770-1773.
24. Hull, C.W. Apparatus for production of three-dimensional objects by stereolithography. Google Patents: 1986.
25. Crump, S.S. Apparatus and method for creating three-dimensional objects. Google Patents: 1992.
26. Malinauskas, M.; Farsari, M.; Piskarskas, A.; Juodkazis, S. Ultrafast laser nanostructuring of photopolymers: A decade of advances. *Physics Reports* **2013**, *533*, 1-31.
27. Sugioka, K. Progress in ultrafast laser processing and future prospects. *Nanophotonics* **2017**, *6*.
28. Pao, Y.H.; Rentzepis, P.M. Laser-induced production of free radicals in organic compounds. *Applied Physics Letters* **1965**, *6*, 93-95.
29. Ambrosi, A.; Pumera, M. 3d-printing technologies for electrochemical applications. *Chemical Society Reviews* **2016**, *45*, 2740-2755.
30. Bhattacharjee, N.; Urrios, A.; Kang, S.; Folch, A. The upcoming 3d-printing revolution in microfluidics. *Lab Chip* **2016**, *16*, 1720-1742.
31. Fischer, J.; Wegener, M. Three-dimensional optical laser lithography beyond the diffraction limit. *Laser & Photonics Reviews* **2013**, *7*, 22-44.
32. Vaezi, M.; Seitz, H.; Yang, S. A review on 3d micro-additive manufacturing technologies. *The International Journal of Advanced Manufacturing Technology* **2013**, *67*, 1721-1754.
33. Yuan, J.; Mecerreyes, D.; Antonietti, M. Poly(ionic liquid)s: An update. *Progress in Polymer Science* **2013**, *38*, 1009-1036.
34. Yuan, J.; Antonietti, M. Poly(ionic liquid)s: Polymers expanding classical property profiles. *Polymer* **2011**, *52*, 1459-1482.
35. Mecerreyes, D. Polymeric ionic liquids: Broadening the properties and applications of polyelectrolytes. *Progress in Polymer Science* **2011**, *36*, 1629-1648.
36. Qian, W.; Texter, J.; Yan, F. Frontiers in poly(ionic liquid)s: Syntheses and applications. *Chem. Soc. Rev.* **2017**, *46*, 1124-1159.
37. del Agua, I.; Mantione, D.; Casado, N.; Sanchez-Sanchez, A.; Malliaras, G.G.; Mecerreyes, D. Conducting polymer iongels based on pedot and guar gum. *ACS Macro Letters* **2017**, 473-478.
38. Leleux, P.; Rivnay, J.; Lonjaret, T.; Badier, J.M.; Bénar, C.; Hervé, T.; Chauvel, P.; Malliaras, G.G. Organic electrochemical transistors for clinical applications. *Advanced Healthcare Materials* **2015**, *4*, 142-147.
39. Gwamuri, J.; Vora, A.; Mayandi, J.; Güney, D.; Bergstrom, P.L.; Pearce, J.M. A new method of preparing highly conductive ultra-thin indium tin oxide for plasmonic-enhanced thin film solar photovoltaic devices. *Solar Energy Materials and Solar Cells* **2016**, *149*, 250-257.

Appendix Chapter 8

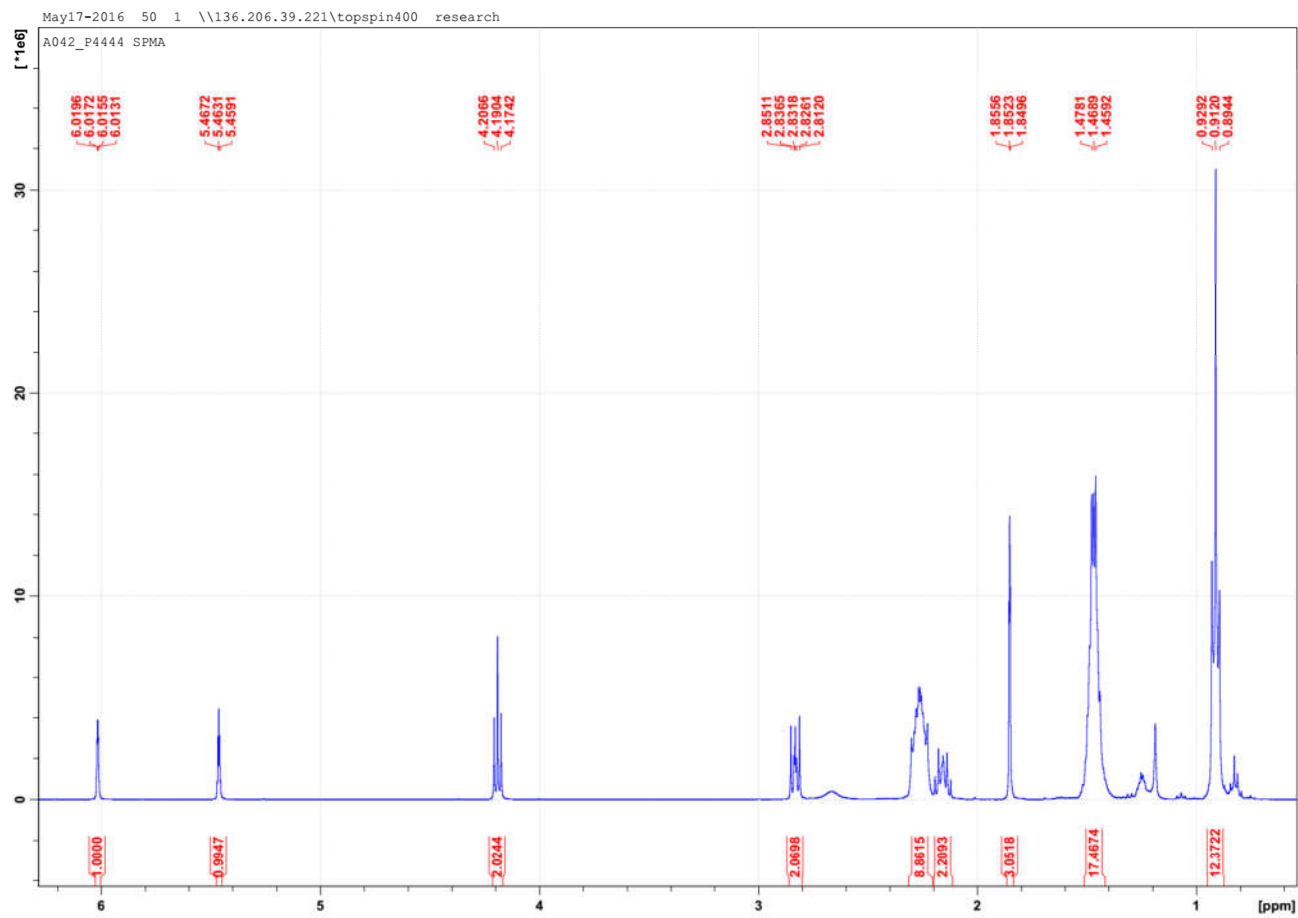


Figure A.8.1 The NMR spectra of the tetrabutylphosphonium sulfopropylmethacrylate

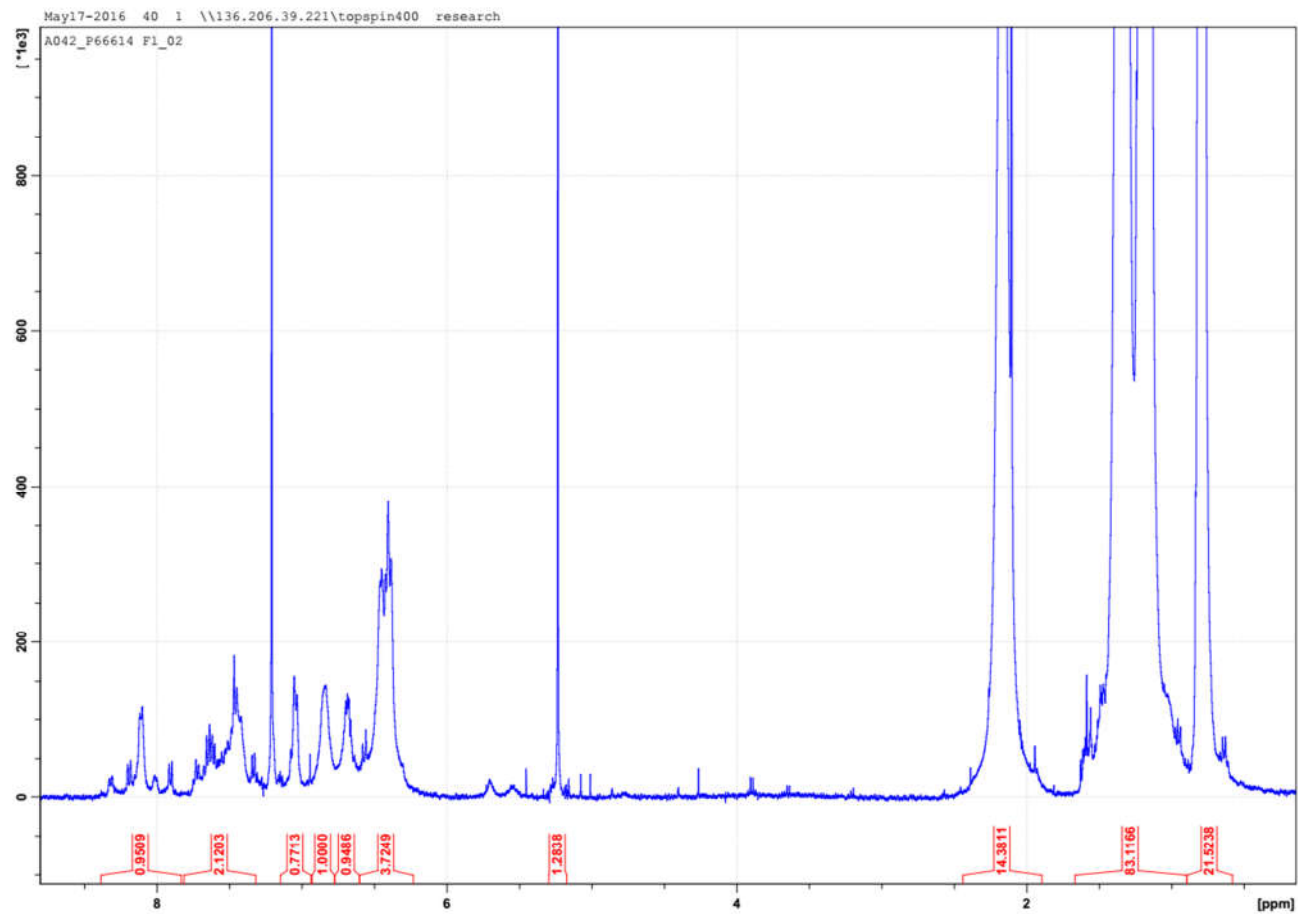


Figure A.8.2 The NMR spectrum of the fluorescein salt of trihexyltetradecylphosphonium

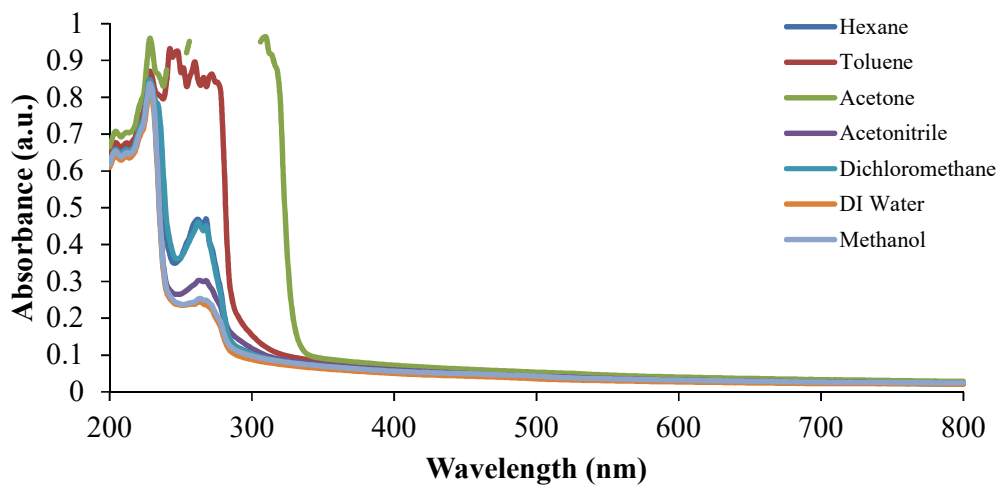


Figure A.8.3. Absorption spectra of the different solvents used for the swelling of the ionogels after the 2nd swelling process.

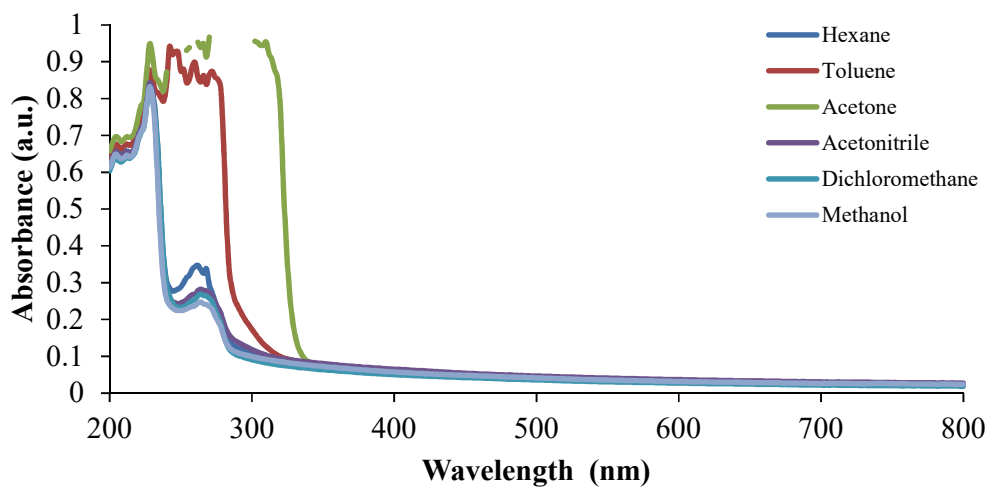


Figure A.8.4. Absorption spectra of the different solvents used for the swelling of the ionogels after the 3rd swelling process.